

**Tissue-Specific Roles for Hedgehog Co-Receptors During Vertebrate Embryogenesis**

by

Martha L. Echevarria Andino

A dissertation submitted in partial fulfillment  
of the requirements for the degree of  
Doctor of Philosophy  
(Cell and Developmental Biology)  
in the University of Michigan  
2020

Doctoral Committee:

Associate Professor Jason Spence, Co-Chair  
Professor Deneen Wellik, Co-Chair  
Associate Professor Benjamin Allen  
Professor Vesa Kaartinen  
Professor Marina Pasca Di Magliano

Martha L. Echevarria Andino

mechevar@umich.edu

ORCID iD: 0000-0002-9052-4339

© Martha L. Echevarria Andino 2020

## **Dedication**

To my family.

To all the students from small places with big dreams.

## **Acknowledgements**

I would like to acknowledge many individuals who made this work possible helping me professionally and personally.

First, I would like to thank my undergraduate mentors Edu Suárez-Martinez and Abigail Ruiz, who gave me my first opportunity to do research. Thank you both for believing in my potential, sparking my interest in science and for showing me all the opportunities that were available for me.

Also, I want to acknowledge my mentor Ben Allen, I cannot thank you enough for all the things that you have taught me over all these years. You are an amazing scientist. Your excitement for science, creativity to design experiments, collaborative skills, skepticism, strong ethics and morals have taught me how to do high quality science. Thank you for teaching me how to do great science and for making me a scientist. Being your trainee has been a privilege. Thanks for your endless patience and for always making time to talk, even when you did not have time. I really appreciate all the time that you spent teaching me concepts, discussing experiments, analyzing data, reviewing my written work and improving my presentation skills. You have also provided me with numerous opportunities to present my research, learn new techniques, and endless resources to do every experiment that I wanted. Thanks for providing me encouragement and unconditional support professionally and personally. Your integrity, kindness, wisdom, and characteristic humor has positively impacted my personality and has made me a better person. Thanks for being so nice, sometimes way too nice! You are an

outstanding mentor and scientist and I will be eternally grateful for the having had the opportunity of being your trainee. Gracias Ben!

Thank you to all the former and current members of the Allen lab: Jane, Irene, Justine, Brandon, Alex, Arielle, Nicole, Mike, Bridget, Anna, Tyler, Nina, Haeyoung and Hannah. Thanks for creating an amazing, collaborative and productive lab environment. We spend so much time together that I consider you my family, I will never forget all of our adventures in and outside the lab. Also, I would like to thank the Allen lab undergraduates, Katarina, Sam, Allie, Melissa, Rajko, Philip, Christa, Ahmad, Nayanna, Justine, Anna, Olivia, and Savannah for their continuous support to keep the lab running. I also want to acknowledge the technical assistance of Nicole and Savannah, which helped me move my research project forward.

I would also like to thank my thesis committee, Deneen Wellik, Marina Pasca Di Magliano, Jason Spence, and Vesa Kaartinen. Thanks for all the helpful discussions to improve my research project and the professional advice to move my career forward. Especially, I would like to thank Deneen. Thanks for your professional and personal support. Thanks for challenging me to be a better scientist, to do great science, and for setting the example of a fearless woman in science.

Thanks to the staff of the Cell and Developmental Biology department for their help in all the administrative aspects of graduate school. Specifically, Karen Lang, Brittney Longeway, Rebecca Rennells, Lori Mirabatur, Kristen Hug, Deontae Hooks, Annette Klomparens and Mohi Shakibafar and Brooke Lorigan. Thanks for all the things that you do to make CDB a great place for students! I also want to thank the Giger, Wellik, Engel, Spence, O'Shea and Schipani laboratories for providing equipment, reagents and mouse models to make my research possible. I want to extend my gratitude to Ben Allen, Deb Gumucio, Deneen Wellik and Scott Barolo and

the CDB department staff for supporting the initiation and development of the outreach program Developing Future Biologists. Furthermore, thanks to all the students, postdocs and professors that kept this program running. To the CDB students and my peers, Seth, Emily, Rafi for interesting science discussions and always be willing to make fun of all the ups and downs of graduate school. I would also give special thanks to the BSRB building employee, David Jones, who always checked in on my well-being and made sure to make me laugh to keep the stress away.

Additionally, I want to express my gratitude to the Microscopy and Image Analysis Laboratory and the MicroCT Core at the University of Michigan. Especially, to Sasha Meshinchi and Michelle Lynch for their assistance. Also, I want to acknowledge Yang Chai and Thach Vu Ho at the University of Southern California and Christopher Panaretos at the University of Michigan for teaching me how to do three dimensional reconstructions in different software. I am also grateful for our collaborator Robert Krauss at Icahn School of Medicine at Mount Sinai for providing mouse models for my research. This work would not have been possible with the funding from, the NSF Graduate Research Fellowship Program, Rackham Merit Fellowship (DGE1256260), Bradley Merrill Patten Fellowship, Rackham Pre-Candidate Graduate Student Research Grant, Rackham Travel Grants and the Travel Award from the American Association of Anatomists (AAA). Also, I want to acknowledge the funding support from the Organogenesis Training Grant (T32 HD00705) from the Center of Organogenesis, and to its former director Linda Samuelson and current administrator Tamika Mohr.

I want to thank my Ann Arbor family, Barbara, Leilani, Jorge, titi Nilda, Luna, Yanaira, Andrea, Elliot, Robinson; thanks for always make me feel like I was at home. To my friends,

Jane and Molly for all the fun adventures during this journey and for always being there. All of you helped to me to get through this and made it more bearable.

Thanks to my family for their continuous support even in the distance and unconditional love. To my parents William and Marta, for believing in me and always saying yes to support me, and for saying no if I wanted to give up. To my siblings Analyd and William, for showing me how hard work and perseverance achieves dreams. To my nephews, William Alexander, Angel Gabriel and Dylan for your contagious joy and all the nerf gun battles that relieved my stress from graduate school. Also, I want to acknowledge my godparents César and Liper who have always supported me in all my academic and personal aspirations. Finally, to my significant other, Andy. Thanks for your support, love and for making me laugh during every stressful situation. I am excited to see where we go next!

## Table of Contents

Dedication	ii
Acknowledgements	iii
List of Tables	x
List of Figures	xi
Abstract	xiv
Chapter 1 Cell Surface Regulation of the Hedgehog Signaling Pathway During Vertebrate Embryogenesis	1
1.1 Abstract.....	1
1.2 Hedgehog signaling from its discovery to its role in development and disease.....	2
1.2.1 Discovery of the Hedgehog gene and core pathway components in Drosophila .....	2
1.2.2 Hedgehog pathway functions during vertebrate embryogenesis .....	4
1.2.3 SHH signaling in birth defects and disease.....	12
1.3 Cell surface regulation of HH signaling.....	13
1.3.1 HH ligand synthesis .....	13
1.3.2 HH ligand release and trafficking mediated by cell surface proteins .....	14
1.3.3 HH ligand reception and trafficking .....	18



1.3.3 HH ligand trafficking independent of cell surface proteins.....	23
1.3.4 HH ligand reception.....	25
1.3.6 HH ligand-independent cell surface regulators.....	42
1.4 Tissue specific roles for GAS1, CDON and BOC.....	53
1.5 Conclusion.....	55
1.6 Figures.....	57
 Chapter 2 The Hedgehog Co-Receptor BOC Differentially Regulates SHH Signaling During Craniofacial Development	
	85
2.1 Abstract.....	85
2.2 Introduction.....	86
2.3 Results.....	89
2.4 Discussion.....	99
2.4.1 Genetic background-dependent phenotypic differences in HH co-receptor mutants .	100
2.4.2 Tissue-specific functions of Boc in HH signal transduction.....	103
2.4.3 Boc as a multi-functional regulator of HH signaling.....	103
2.5 Materials and methods.....	105
2.6 Acknowledgements.....	115
2.7 Author contributions.....	116
2.8 Tables.....	117
2.10 References.....	139

Chapter 3 <i>Cdon</i> is Required for Proper HH-Dependent Patterning of the Developing Limb	144
3.1 Abstract.....	144
3.2 Introduction .....	145
3.3 Results .....	148
3.4 Discussion.....	152
3.4.1 Novel role for CDON during digit specification and limb development.....	153
3.4.2 Forelimb and hindlimb phenotypic differences .....	154
3.4.3 Role of Gas1, Cdon and Boc in SHH-dependent digit specification.....	155
3.5 Materials and methods.....	156
3.6 Acknowledgments .....	160
3.7 Author contributions.....	160
3.8 Tables.....	161
3.9 Figures .....	163
3.10 References .....	170
Chapter 4 Discussion and Future Directions	174
4.1 Summary of findings .....	174
4.2 Future directions .....	176
4.3 Figures .....	188
4.4 References .....	189

### **List of Tables**

Table 2.1 General reagents.....	117
Table 2.2 Primary and secondary antibodies used for immunofluorescence.....	119
Table 2.3 Western blot antibodies.....	120
Table 2.4 qRT-PCR primers.....	121
Table 3.1 General reagents II.....	161
Table 3.2 Primary antibodies used for immunofluorescence II.....	162

## List of Figures

Figure 1.1 Summary of vertebrate HH signal transduction .....	57
Figure 1.2 Shh expression and function in E10.5 mouse tissues. ....	57
Figure 1.3 Cell surface regulation of HH signaling. ....	58
Figure 2.1 The HH co-receptors <i>Gas1</i> , <i>Cdon</i> and <i>Boc</i> are expressed throughout early craniofacial development. ....	122
Figure 2.2 <i>Gas1</i> , <i>Cdon</i> and <i>Boc</i> are differentially expressed across multiple HH-responsive tissues. ....	123
Figure 2.3 Loss of <i>Boc</i> results in midface widening and increased <i>Gli1</i> expression on a congenic C57BL/6J background.....	124
Figure 2.4 Telencephalic vesicle division and MNP separation in <i>Gas1</i> , <i>Cdon</i> and <i>Boc</i> mutants. ....	125
Figure 2.5 <i>Gas1</i> , but not <i>Cdon</i> or <i>Boc</i> , mutant embryos exhibit decreased embryo size at E10.5. ....	126
Figure 2.6 The Spectrum of HPE phenotypes correlates with changes in <i>Gli1</i> expression.....	127
Figure 2.7 Tissue-specific rescue of HH signaling in E10.5 <i>Gas1</i> ; <i>Boc</i> double mutant embryos. ....	128
Figure 2.8 Reduced Crown-Rump Length in E10.5 <i>Gas1</i> ; <i>Boc</i> double mutant embryos.....	129
Figure 2.9 Reduced <i>Gli1</i> mRNA and protein levels in E10.5 <i>Gas1</i> mutant forelimb buds.....	130

Figure 2.10 Selective contribution of <i>Boc</i> to patterning of the neural tube, but not the forebrain neuroepithelium.....	131
Figure 2.11 <i>Boc</i> promotes HH-dependent neural patterning in the developing chicken .....	132
Figure 2.12 Partial rescue of HPE phenotypes persists through E18.5 in <i>Gas1;Boc</i> mutant embryos. ....	133
Figure 2.13 HPE phenotypes and digit specification defects in E18.5 <i>Gas1;Boc</i> mutant embryos. ....	134
Figure 2.14 E18.5 <i>Gas1;Boc</i> mutants display partially ameliorated midfacial defects. ....	135
Figure 2.15 <i>Boc</i> selectively inhibits mesenchymal proliferation during craniofacial development. ....	136
Figure 2.16 <i>Boc</i> does not contribute to neural tube or forelimb mesenchyme proliferation. ....	137
Figure 2.17 <i>BOC</i> is a multi-functional regulator of HH signaling.....	138
Figure 3.1 Analysis of HH-coreceptor expression and function in the developing forelimb bud. ....	163
Figure 3.2 <i>Gas1;Boc</i> and <i>Gas1;Cdon</i> but not <i>Cdon;Boc</i> mutant embryos exhibit significant reduction of <i>Gli1</i> in the developing forelimb bud.....	164
Figure 3.3 Analysis of limb development in single and double HH co-receptors mutants.....	165
Figure 3.4 Conditional <i>Cdon</i> knockout allele. ....	166
Figure 3.5 <i>Prx1-Cre</i> recombination activity in E10.5 embryos.....	167
Figure 3.6 Tissue-specific expression of Cre recombinase in the developing forelimb bud and spinal cord of <i>Prx1-Cre;tdTomato</i> E10.5 embryos. ....	168
Figure 3.7 Digit specification and long bone defects in E18.5 <i>Prx1-Cre;Gas1<sup>-/-</sup>;Cdon<sup>fl/fl</sup>;Boc<sup>-/-</sup></i> . ....	169

Figure 4.1 Summary of the tissue-specific roles of the HH co-receptors ..... 188

## Abstract

The Hedgehog (HH) signaling pathway is essential for the proper patterning of multiple tissues during vertebrate embryogenesis, including the spinal cord, craniofacial structures, and limbs. At the cell surface, secreted HH ligands signal through the canonical receptor Patched 1 (PTCH1) and three co-receptors– GAS1, CDON and BOC. Interestingly, these proteins share similar expression patterns throughout development, bind to HH ligands, and interact with PTCH1. Together, these HH co-receptors are essential to transduce HH signaling in multiple tissues during embryogenesis.

Recent studies suggest that, in addition to their combined, essential role in HH signal transduction, these co-receptors also play individual, tissue-specific roles in the regulation of HH signaling. However, the tissue-specific contributions of these co-receptors remain largely unexplored during vertebrate embryogenesis. The goals of this dissertation are to: 1) investigate novel tissue-specific roles for the HH co-receptors and 2) elucidate the mechanism of HH co-receptor function during vertebrate embryogenesis.

During craniofacial development, the individual deletion of HH co-receptors results in variable craniofacial defects, in which the severity of the phenotype is dependent on the genetic background. To investigate the individual and combined contributions of the HH co-receptors to craniofacial development, I analyzed *Gas1*, *Cdon* and *Boc* mutant embryos on a congenic C57BL/6J background. The deletion of *Gas1* and *Cdon* result in variable degrees of holoprosencephaly; a birth defect characterized by the complete or partial failure of the forebrain

and the midface structures. In contrast, *Boc* deletion results in midface widening. Increasing severity of the craniofacial defects in *Gas1* and *Cdon* mutants correlated with decreased levels of HH pathway activity, while *Boc* mutants display increased levels of HH pathway function. These data suggest that the HH co-receptors differentially contribute to craniofacial development. Further, *Boc* deletion in a *Gas1* null background partially ameliorates the phenotypes observed in *Gas1* single mutants. However, the rescue of the craniofacial defects observed in *Gas1;Boc* mutants is restricted to the craniofacial structures, while other tissues patterned by HH are more severely affected. Mechanistically, BOC can also selectively restrict proliferation in the cranial neural crest-derived mesenchyme. These data suggest that *Boc* functions as a tissue-specific HH pathway antagonist during craniofacial development.

In this thesis, I also investigated the contribution of HH co-receptors to digit specification and limb patterning. Notably, previous studies have demonstrated roles for both *Gas1* and *Boc* in HH-dependent digit specification, but not for *Cdon*. However, the known redundant functions of these HH co-receptors, combined with the early (embryonic day 9.5) lethality of *Gas1;Cdon;Boc* triple mutants has hindered efforts to definitively examine a potential contribution of *Cdon* to limb development. To dissect the function of CDON during HH-dependent digit specification, I performed limb-specific deletion of *Cdon* in a *Gas1;Boc* null background. Embryos lacking *Gas1*, *Cdon* and *Boc* display both severe digit specification defects in the radius, ulna, tibia and fibula. These experiments demonstrate that CDON does indeed contribute to digit specification and limb patterning. Overall, the data presented in this dissertation demonstrate that HH co-receptors contribute in both a redundant and tissue-specific fashion to HH signal transduction, and that these co-receptors are multi-functional regulators of HH signaling during vertebrate embryogenesis.



## **Chapter 1 Cell Surface Regulation of the Hedgehog Signaling Pathway During Vertebrate Embryogenesis**

### **1.1 Abstract**

The Hedgehog (HH) signaling pathway is evolutionarily conserved across many organisms. HH signaling is essential for proper tissue and organ formation during embryonic and postnatal development and tissue homeostasis during adulthood. Secreted HH ligands act as classic morphogens, eliciting different cellular responses in a time- and concentration-dependent manner. Interestingly, HH ligands are employed iteratively across different organisms to establish different body plans and also within an organism to specify different tissues and organs with disparate functions. An outstanding question is: How does a single pathway elicit a multitude of distinct cellular responses necessary to achieve such diversity within and across organisms? One potential explanation is found in the plethora of cell surface-associated proteins and extracellular matrix components that regulate the release, trafficking and signal reception of HH ligands. Recently, three proteins— GAS1, CDON and BOC have been identified as essential HH co-receptors. Together these proteins are required for HH signal transduction in multiple tissues at different developmental stages. However, the mechanisms by which these co-receptors regulate HH signaling remain poorly understood. Further, genetic evidence suggests that these co-receptors are differentially employed in a tissue-specific manner to mediate distinct HH signaling outcomes. Thus, elucidating how different cell surface proteins regulate HH signaling in a tissue-specific manner will be critical to understand how HH patterns different tissues during

development. Additionally, understanding the cell surface regulation of HH signaling can provide significant insight into how mutations in the genes that encode these factors contribute to HH-driven diseases, including a variety of birth defects, developmental disorders and various pediatric and adult cancers. In this chapter, I review the HH pathway components that control the release, trafficking, and reception of HH ligands with an emphasis on the HH co-receptors GAS1, CDON and BOC.

## **1.2 Hedgehog signaling from its discovery to its role in development and disease**

### *1.2.1 Discovery of the Hedgehog gene and core pathway components in Drosophila*

The *Hedgehog* (*Hh*) gene was originally identified in *Drosophila* genetic screens to identify mutations that affected the segmental pattern of the larvae (Nusslein-Volhard and Wieschaus, 1980). *Drosophila* larvae with mutations in *Hh* displayed patterning defects in segmental units containing denticles that were reminiscent of hedgehog spines, leading to the assignment of the *Hh* gene name (Nusslein-Volhard and Wieschaus, 1980). However, its cloning and molecular characterization occurred over a decade later, where HH was described as a secreted protein that provided patterning information to neighboring cells (Lee et al., 1992; Mohler and Vani, 1992; Tabata et al., 1992; Taylor et al., 1993).

The HH gene is evolutionarily conserved across the animal kingdom including sea urchin, planaria, zebrafish, chicken, mouse and human (Ingham et al., 2011). In mammals, the HH gene has three homologs, *Sonic Hedgehog* (*Shh*), *Indian Hedgehog* (*Ihh*) and *Desert Hedgehog* (*Dhh*) (Echelard et al., 1993; Krauss et al., 1993; Riddle et al., 1993). Their distinct expression patterns suggested that these vertebrate homologs had both overlapping and unique functions during development (Bitgood and McMahon, 1995). *Shh*, is the most studied of the

three HH genes in vertebrates. Its expressed in major organizing signaling centers including the zone of polarizing activity in the limb bud (Riddle et al., 1993), the notochord and floor plate of the neural tube (Echelard et al., 1993; Roelink et al., 1994; Roelink et al., 1995) and the pre-chordal plate in the craniofacial structures (Aoto et al., 2009; Rubenstein and Beachy, 1998). In these tissues *Shh* is required for patterning, differentiation, proliferation and cell survival (described in more detail below) (Briscoe and Therond, 2013; McMahon et al., 2003). *Ihh* plays a more limited role, regulating chondrogenesis and osteogenesis during endochondral ossification (Chung et al., 2001) (Vortkamp et al., 1996), while *Dhh* is required for the development of germ cells in the testis (Bitgood et al., 1996; Clark et al., 2000) and ensheathment of peripheral nerves (Parmantier et al., 1999).

HH genes encode secreted proteins that are regulated at the cell surface by core HH pathway components that are also conserved across organisms. The primary receptor in *Drosophila* is *Patched* (*Ptc*), or *Patched1* (*Ptch1*) in mammals, which encodes a twelve pass transmembrane protein (Hooper and Scott, 1989; Marigo et al., 1996; Nakano et al., 1989). Different biochemical studies demonstrated that *Ptc/Ptch1* directly bind HH ligands and that in absence of HH ligands Patched constitutively inhibits the activity of a second receptor, Smoothed (SMO) a G protein-coupled receptor (Figure 1.1, left panel) (Chen and Struhl, 1996; Marigo and Tabin, 1996; Stone et al., 1996). Although, SMO exhibits structural divergence from invertebrate to vertebrates and does not bind to HH ligands, it is an essential transducer of the HH signaling pathway (van den Heuvel and Ingham, 1996; Zhang et al., 2001). Upon HH ligand binding to Patched, the inhibition of SMO is released, resulting in the modulation of the zinc finger transcription factors, Cubitus interruptus (Ci) or the -glioma-associated oncogene (GLI) transcription family– in mammals (Figure1.1, right panel) (Alexandre et al., 1996; Chen and

Struhl, 1996; Taipale et al., 2002). Ci contains three paralogues in mammals, GLI1, GLI2 and GLI3 (Huangfu and Anderson, 2006; Hui and Angers, 2011). The HH transcription factors can function to activate or inhibit HH transcriptional targets (Aberger and Ruiz, 2014; Falkenstein and Vokes, 2014; Hui and Angers, 2011). Even though most of the core HH pathway components are conserved across organisms there are several differences between vertebrates and invertebrates. For example, in vertebrates the HH signaling pathway utilizes the primary cilium, a microtubule structure in which the GLI transcriptional effectors are processed (Goetz and Anderson, 2010; Huangfu et al., 2003). Additionally, several core HH pathway components have undergone duplication events, and recently novel receptors with different contributions to HH signaling have been identified in vertebrates (Allen et al., 2011; Allen et al., 2007; Cole and Krauss, 2003; Izzi et al., 2011; Lum et al., 2003; Tenzen et al., 2006; Zhang et al., 2011). Below I will focus on the cell surface regulation of SHH ligand and the contributions of different cell surface proteins to the control of HH pathway activity during mammalian embryogenesis and disease.

### *1.2.2 Hedgehog pathway functions during vertebrate embryogenesis*

The HH signaling pathway is essential during vertebrate embryogenesis, regulating diverse processes that pattern nearly all the tissues and organs in an embryo (McMahon et al., 2003). Primarily, SHH pathway function has been explored during the development and patterning of the neural tube, the limb and the craniofacial structures (Chiang et al., 1996). At mid-gestation (approximately embryonic day (E) 10.5) in mice, SHH ligands are expressed and secreted to pattern these different structures (Figure 1.2, top panel; (Echelard et al., 1993; Riddle et al., 1993; Xavier et al., 2016) Notably in these structures SHH is not only required for

patterning, it also regulates cell survival and proliferation (Figure 1.2, bottom panel; (Ahlgren and Bronner-Fraser, 1999; Bastida et al., 2004; Cayuso et al., 2006; Jeong et al., 2004; Towers et al., 2008)). The investigation of the contribution of SHH to the formation of these structures has provided great insight into our understanding of HH pathway function. In this section I will discuss the roles of SHH in the context of the development of the neural tube, the limb and the craniofacial structures.

### SHH signaling in patterning of the ventral neural tube

The neural tube is a structure derived from the ectoderm and is formed by a process called neurulation that ultimately give rise to the central nervous system (Gilbert, 2013). During this process, the ectoderm originates as a flat plate of epithelial cells that fold and elevate, subsequently converging and fusing to form a neural tube (Gilbert, 2013). The neural tube contains three different types of neurons including, motor neurons, interneurons and sensory neurons (Gilbert, 2013) that are specified during development. As evidenced by different embryological studies, the rostrocaudal and dorsoventral patterning of the neural tube is regulated by different extrinsic signals derived from the somites and the notochord, mesoderm-derived structures (Wilson and Maden, 2005). Prior to neurulation and before neural tube closure these signals induce all neuronal subtypes in the neural tube (Wilson and Maden, 2005). Specifically, SHH is initially expressed in the notochord, which induces a secondary site of SHH expression in the ventral midline of the neural tube, the floor plate (Echelard et al., 1993; Roelink et al., 1994; Roelink et al., 1995). In these structures SHH functions as a morphogen, specifying the identity of five distinct ventral neuronal progenitors including ventral interneuron progenitors (V0-V3) and motor neurons (Ericson et al., 1997a; Ericson et al., 1997b; Marti et al.,

1995b; Roelink et al., 1995; Wijgerde et al., 2002). These distinct neuronal progenitors are specified by the induction and repression of transcription factors by distinct levels of HH pathway activity (Dessaud et al., 2008). The transcription factors that are repressed by SHH are classified as Class I genes (e.g., *Pax3*, *Pax6*, *Pax7*), which are expressed in the dorsal to intermediate domains of the neural tube (Briscoe et al., 2000). In contrast, transcription factors that are activated by SHH are classified as Class II genes (e.g., *Foxa2*, *Nkx2.2*, *Olig2*, *Nkx6.1*), which are expressed in the ventral neural tube (Briscoe et al., 2000). These transcription factors interpret the gradient of HH pathway activity to establish boundaries between their respective domains, maintaining their integrity and subsequently regulating their neuronal differentiation (Briscoe and Ericson, 1999).

The levels of HH pathway activity that each neuronal progenitor receive are determined by their localization in the neural tube. Neuronal progenitors that are closer to the SHH source will receive the highest levels of HH pathway activity, inducing the expression of Class II genes and repressing Class I genes (Briscoe et al., 2000). While neuronal progenitors located further from the SHH source will receive reduced levels of HH pathway activity, resulting in the expression of Class I genes and the repression of Class II genes (Briscoe et al., 2000). The specification of these different neuronal progenitors is highly regulated not only by SHH concentration, but also by the duration of the exposure to SHH (Dessaud et al., 2007; Ericson et al., 1997b). Several studies have demonstrated this by utilizing naive neural plate explants from chicken embryos and exposing them to different concentrations of SHH over different periods of time (Dessaud et al., 2007; Ericson et al., 1997b; Marti et al., 1995a). These neuronal progenitors respond to ongoing SHH exposure through an adaptation mechanism in which cells become desensitized to SHH, mediated by the upregulation of PTCH1 (Dessaud et al., 2007; Goodrich et

al., 1999; Marigo and Tabin, 1996). Further, the specification of these neuronal progenitor populations also relies on cross-repressive interactions between the Class I and Class II transcription factors to define the final boundaries of these domains (Briscoe and Ericson, 1999; Briscoe et al., 2000; Ericson et al., 1997b; Novitch et al., 2001). Finally, the SHH morphogen gradient in the neural tube can be also influenced by the induction of different cell surface proteins that bind to HH ligands and antagonize signaling, creating a negative feedback loop that maintains the proper levels of HH signaling to specify neuronal progenitor identity (Goodrich et al., 1999; Jeong and McMahon, 2005) (Holtz et al., 2013; Marigo et al., 1996) SHH/GLI signaling also regulates the proliferation and survival of neural progenitors in the neural tube. Overexpression experiments via chicken *in ovo* electroporations demonstrated that blockage of SHH or inhibition of GLI activity decreases the proliferation and survival of the neuronal progenitor cells (Cayuso et al., 2006). Further, GLI transcriptional activation promotes proliferation and rescues the effects mediated by the inhibition (Cayuso et al., 2006). These cellular responses are also influenced by other signals like Wingless-type MMTV related integration site (Wnt), and Bone morphogenetic proteins (Bmp) which also regulate the cell cycle progression and cell cycle exit in the dorsal neural tube (Le Dreau and Marti, 2013; Megason and McMahon, 2002).

### SHH Signaling During Craniofacial Development

Formation of the face is a complex process that is highly coordinated by the activity of multiple developmental signaling pathways. Craniofacial structures are formed by the interactions of multiple tissues including, cranial neural crest cells, ectoderm, endoderm and mesenchyme (Chai and Maxson, 2006). The patterning and growth of craniofacial structures

depends on facial prominences, which grow symmetrically and asymmetrically to properly pattern the face (Feng et al., 2009; Rossant and Tam, 2002). Primarily, the facial prominences are comprised of mesenchymal swellings that are covered by an overlying epithelium (Feng et al., 2009). There are three main paired prominences in mouse and humans, the frontonasal prominence (which will give rise to the medial and lateral nasal processes), the maxillary prominence and the mandibular prominence. The interactions between all these different tissues allow for the proper development of the facial skeleton, connective tissue and muscle.

In these structures, SHH ligands are expressed sequentially, establishing multiple critical points in which HH pathway activity is required. In early craniofacial structures the expression of *Shh* is first detected in the prechordal plate (Aoto et al., 2009; Cordero et al., 2004; Rubenstein and Beachy, 1998; Zhang et al., 2006), a mesendoderm-derived structure (Kaufman, 1992). Even though the prechordal plate and the notochord are morphologically similar structures that express *Shh*, these structures differentially express genes (e.g., *goosecoid-1*) during early development (Belo et al., 1998). SHH is required to differentiate prechordal cells into ventral cranial mesoderm, which is necessary for midline development of the forebrain (Aoto et al., 2009). After its expression at the prechordal plate, SHH is expressed in different ectodermal domains in early craniofacial structures [reviewed by (Xavier et al., 2016)]. First, SHH is expressed in the ventral forebrain neuroepithelium, specifically, in the diencephalon and telencephalon [reviewed by (Xavier et al., 2016)]. Subsequently, this expression in the neuroepithelium, establishes the bilateral expression of SHH in the surface ectoderm of the medial nasal processes, establishing polarity and growth of the facial processes [reviewed by (Xavier et al., 2016)]. Finally, SHH is expressed in the pharyngeal endoderm of the first branchial arch, which is critical for survival of cranial neural crest cells and formation of Meckel's cartilage [reviewed by (Xavier et al., 2016)].



This highly coordinated developmental sequence of SHH expression regulates growth and patterning of the craniofacial structures.

Genetic analysis in mice have demonstrated that targeted deletion of *Shh* results in severe craniofacial defects, in which the eyes, nose and oral structures are not recognizable (Chiang et al., 1996). Instead, *Shh* mutants display cyclopia, a proboscis (a nose-like structure) and holoprosencephaly (HPE) (Chiang et al., 1996). HPE is a birth defect that is characterized by the complete or partial failure of the division of the forebrain and a wide spectrum of midline defects (Schachter and Krauss, 2008). The function of SHH was also explored in the developing craniofacial structures of chicken embryos. Loss of function studies utilizing function-blocking anti-SHH antibody and gain-of function studies by ectopic expression of SHH in the craniofacial structures of developing chicken embryos demonstrated that SHH signaling is essential for proliferation and survival of neural crest cells (Ahlgren and Bronner-Fraser, 1999; Hu and Helms, 1999). These studies were supported by the removal of HH-responsiveness in craniofacial structures by the conditional deletion of *Smo* in neural crest cells using *Wnt1Cre* (Jeong et al., 2004). This conditional deletion leads to increased apoptosis, decreased cell proliferation and truncation of the facial skeleton and connective tissue (Jeong et al., 2004). Thus, in craniofacial structures HH signaling is required to establish the patterning and growth of the face primordia (Chiang et al., 1996; Jeong et al., 2004).

#### SHH signaling in the developing limb

The mammalian limbs arise from a combination of mesenchymal cells from the lateral plate mesoderm and the somites (Gilbert, 2013). After migration from the lateral plate mesoderm and the somites to the limb field, these mesenchymal cells accumulate under an ectodermal

tissue pocket to create a condensation of tissue called the limb bud (Gilbert, 2013; Tabin and Wolpert, 2007). In each vertebrate embryo there are up to four limb buds that are paired opposite to each other along the right and left axis (Gilbert, 2013). Positioning of the limb buds is established by a combinatorial code of *Hox* gene expression, which patterns the limb skeleton along the proximodistal axis [reviewed by (Capdevila and Izpisua Belmonte, 2001; Pineault and Wellik, 2014)]. The patterning of the limb bud is mediated by several specialized structures that function as signaling centers including the apical ectodermal ridge (AER), the zone of polarizing activity (ZPA) and the non-ridge ectoderm [reviewed by (Capdevila and Izpisua Belmonte, 2001; Gilbert, 2013)]. These structures coordinate patterning along the different axes of the limb: dorsal-ventral, anterior-posterior and proximo-distal [reviewed by (Capdevila and Izpisua Belmonte, 2001)]. Each one of these signaling centers establish different molecular domains that will give rise to the skeletal elements, muscles and connective tissues of the mature limb. During this process SHH is secreted from the ZPA, which determines the anterior-posterior axis and specifies digit identity (Echelard et al., 1993; Riddle et al., 1993; Saunders, 1968).

Experiments in chicken embryos provided the first evidence that *Shh* transcripts were expressed in the ZPA of the chicken wing bud and were capable of polarizing limbs in grafting experiments (Riddle et al., 1993). Moreover, the activity mediated by SHH in the ZPA also has effects in the apical ectodermal ridge, linking anterior-posterior and proximo distal pattern formation. This was demonstrated by grafting experiments in which the grafted ZPA was placed in the most anterior part of the chicken wing bud resulting in a wider chicken bud (Smith and Wolpert, 1981; Tickle et al., 1975). The role of the ZPA initially identified in chicken embryos, was also explored and confirmed in mice. Mouse embryos lacking the *Shh* gene display severe defects in limb patterning. Even though, *Shh* mutants develop limbs, these are severely truncated,

and they only exhibit one digit in the hindlimbs (Chiang et al., 1996). In mice, the limb is comprised of five digits (1-5 through the anterior-posterior axis). The remaining digit observed in *Shh* mutant embryos is considered to be digit 1, and its patterning is independent of HH signaling. Although these studies demonstrate an essential role for SHH in digit specification in the limb, there are discrepancies regarding how HH specifies digit identity in the limbs.

Different studies have proposed several mechanisms of HH function in digit specification. The first model was reported by (Harfe et al., 2004), and proposed that digit identity was determined by the concentration and time of exposure to SHH in both mouse and chicken embryos. This model establishes that digits 5, 4 and the posterior part of digit 3 receive the highest levels of HH activity by autocrine signaling. While digit 2 receives very low levels of HH activity by paracrine signaling. Furthermore, this model was supported by (Scherz et al., 2007), which performed a series of experiments utilizing genetic and pharmacological approaches to limit the time of exposure or the concentration of SHH in the bud mesenchyme of chicken and mouse embryos. (Scherz et al., 2007) demonstrated that both exposure and dose of SHH contribute to specification of digit identity and that the time of exposure for the most posterior digits is critical. This classical model was further extended by (Towers et al., 2008), which integrated a growth component. Suggesting that SHH regulates proliferation through the control of cell cycle regulators and (Towers et al., 2008). A second model for digit specification was proposed by (Zhu et al., 2008), which conditionally deleted *Shh* at different time points using *Hoxb6CreER*, revealing that *Shh* is required in two phases. According to this model SHH is first required during a transient early phase that regulates digit identity, and then in a second expansion growth phase where it maintains sufficient cell numbers for digit condensation (Zhu et al., 2008). The cell survival component has not been as integrated as the growth component in

these models. Experiments in which SHH was increased or inhibited by grafting or SHH protein beads, demonstrated that SHH can selectively regulate cell death and survival in a position-dependent manner (Sanz-Ezquerro and Tickle, 2000). Additionally, (Bastida et al., 2004) suggested that GLI-dependent transcription can mediate cell survival and apoptosis. However, is still unclear how SHH regulates cell survival in the developing limb.

### *1.2.3 SHH signaling in birth defects and disease*

Given the essential roles of SHH signaling during vertebrate embryogenesis, it is not surprising that aberrant SHH pathway activity results in a wide variety of birth defects and diseases. Mutations in different HH pathway components result in gain-of-function phenotypes or loss-of-function phenotypes that contribute to disease. For example, loss-of-function mutations in *SHH* have been identified in human holoprosencephaly (HPE) patients, a birth defect in which the forebrain and midfacial structures are not properly developed (Belloni et al., 1996; Roessler et al., 1996). HPE mutations in other HH pathway components will be described in greater detail below. In the context of cancer, mutations have been identified in basal cell carcinoma, the most common skin cancer. Specifically, loss-of-function mutations in *PCTHI* and/or gain-of function mutations in *SMO* (Hahn et al., 1996; Johnson et al., 1996; Xie et al., 1998). Moreover, overactive HH signaling has been implicated in other cancers including, medulloblastoma, pancreatic cancer and ovarian cancer (Barakat et al., 2010; Teglund and Toftgard, 2010; Thayer et al., 2003; Theunissen and de Sauvage, 2009). However, these different types of cancers caused by defective HH signaling do not emerge in the same manner. There are several mechanisms by which defects in HH activity can lead to cancer. Specifically, these mechanisms are classified according the type of mutation, HH ligand requirement, and the type

of cell communication between cancer cells and the neighboring cells in the tumor microenvironment [reviewed by (Scales and de Sauvage, 2009)]. Understanding the mechanisms by which HH signaling is regulated during embryogenesis and disease will be essential to develop novel therapeutic approaches.

### **1.3 Cell surface regulation of HH signaling**

The HH signaling pathway regulates the patterning, morphogenesis, and homeostasis of multiple tissues during development and adulthood. However, it is unclear how the same pathway can be utilized iteratively within the same organism to form such different structures. The HH signaling pathway is regulated by an array of different proteins at the cell surface. These proteins regulate the release, trafficking, reception, and signal transduction of the HH ligands. Also, this multitude of proteins allow the complex regulation of the HH gradient by creating multiple feedback loops to maintain the proper levels of HH and further extend the role of the HH pathway by performing non-canonical functions. The following section will be focused on describing the function of cell surface proteins that regulate HH ligand release, trafficking, reception and signal transduction (Figure 1.3).

#### *1.3.1 HH ligand synthesis*

HH ligands are secreted proteins that are synthesized as an approximately 45kDa immature precursor (Bumcrot et al., 1995; Lee et al., 1994). During biosynthesis this precursor undergoes signal sequence cleavage and enters the secretory pathway, followed by autocatalytic cleavage performed by its carboxyl-terminal (C-terminal) (Bumcrot et al., 1995; Lee et al., 1994; Porter et al., 1995). Simultaneously, a cholesterol moiety is attached to the amino terminal (N-

terminal) of the peptide (Porter et al., 1996). This results in a 19 kDa peptide that performs all signaling activities; however, this peptide is subjected to additional post-translational modifications. Specifically, HH ligands are palmitoylated at an N-terminal cysteine residue by the acyltransferase skinny hedgehog (SKI) (Chamoun et al., 2001; Lee and Treisman, 2001; Micchelli et al., 2002; Taylor et al., 2001). Both lipid modifications are critical for the stabilization and distribution of HH ligands. The cholesterol moiety limits the spread of HH ligands by anchoring them to the plasma membrane and limiting their diffusion (Lewis et al., 2001; Li et al., 2006; Peters et al., 2004). In contrast, palmitoylation enhances the potency of HH ligand, presumably by mediating oligomerization (Chen et al., 2004; Kohtz et al., 2001; Lee et al., 2001b). Defects in the lipidation or processing of HH precursors result in loss of SHH function and subsequently in developmental defects (Belloni et al., 1996; Maity et al., 2005; Roessler et al., 1996). After HH ligands are dually lipidated they are tethered to the lipid bilayer of the plasma membrane where they can be released by several different mechanisms to employ their morphogen functions.

### *1.3.2 HH ligand release and trafficking mediated by cell surface proteins*

#### Dispatched (DISP)

DISP is a twelve-pass transmembrane protein, from the resistance-nodulation division (RND) transporter family originally identified in *Drosophila* genetic screens; which mediates the secretion of cholesterol-modified HH ligands (Burke et al., 1999; Caspary et al., 2002; Ma et al., 2002; Tian et al., 2005). The DISP proteins display structurally similar multi-spanning transmembrane domains and sterol sensing domains to the HH ligand receptor, PTCH1 (Burke et al., 1999; Caspary et al., 2002; Kawakami et al., 2002). As observed in *Drosophila* HH mutants,

*Disp* null larvae also display strong defects in segment polarity (Burke et al., 1999). Early studies in *Drosophila* demonstrated that *Disp* mutant ligand producing cells retain cholesterol modified HH ligands, but not HH ligands without cholesterol (Burke et al., 1999). Despite the structural similarity between DISP and PTCH1 these experiments demonstrated that these proteins play essential distinct functions in HH signal transduction. DISP is conserved across organisms and its role in HH signaling has also been reported in vertebrates which possess two homologs, DISP1 and DISP2 (Caspary et al., 2002; Kawakami et al., 2002; Ma et al., 2002). Interestingly, DISP1 is ubiquitously expressed during early mouse embryogenesis and overlaps with SHH and IHH expression, while DISP2 is undetectable (Kawakami et al., 2002; Ma et al., 2002). Furthermore, overexpression of DISP2 in HH ligand export assays demonstrated that it has no effect in the release of soluble HH processed ligands, indicating that DISP1 is the main regulator of ligand release (Ma et al., 2002). *Disp* mutant mouse embryos display a severe loss of HH function, phenocopying *Smo* mutant embryos (Caspary et al., 2002; Kawakami et al., 2002; Ma et al., 2002). These embryos display severe defects in the forebrain, neural tube patterning defects and disrupted left/ right asymmetry, resulting in abnormal embryonic turning and heart looping defects (Caspary et al., 2002; Kawakami et al., 2002; Ma et al., 2002). The mechanism by which DISP releases HH ligands is still unknown. Based on biochemical data it is thought that DISP mediates HH ligand release by binding to cholesterol through its sterol sensing domain (Creanga et al., 2012; Tukachinsky et al., 2012). More recently, mechanistic analyses have revealed that DISP is cleaved in its predicted first extracellular loop by the proprotein convertase Furin; which influences its ability to release HH ligands from producing cells (Stewart et al., 2018). However, DISP alone is not sufficient to mediate the release of HH ligands. DISP functions synergistically with the vertebrate-specific secreted glycoprotein, SCUBE2, which

differentially binds the cholesterol moiety and releases HH ligands from the cell surface (Creanga et al., 2012; Hollway et al., 2006; Kawakami et al., 2005; Tukachinsky et al., 2012; Woods and Talbot, 2005). These data have led to a model in which DISP transfers the cholesterol modified HH ligand to SCUBE2 which subsequently increase its solubility in the extracellular space.

#### Signal sequence-CUB domain epidermal growth factor like-related 2 (SCUBE2)

SCUBE2 is a secreted glycoprotein from the EGF-CUB family (Grimmond et al., 2001; Wu et al., 2004; Yang et al., 2002). This protein was originally identified as the *you* gene in zebrafish genetic screens as part of the *you*-class mutations (Hollway et al., 2006; Kawakami et al., 2005; van Eeden et al., 1996; Woods and Talbot, 2005). The molecular cloning of the *you* gene was reported simultaneously by several groups, which also demonstrated that this gene encodes the SCUBE2 protein, and that it was conserved from zebrafish to mouse and humans (Grimmond et al., 2000; Grimmond et al., 2001; Hollway et al., 2006; Kawakami et al., 2005; Woods and Talbot, 2005). Interestingly, the *you* gene has no homologue in *Drosophila*. SCUBE2 is part of a protein family that is comprised by three members, SCBUBE1, SCUBE2 and SCUBE3 (Grimmond et al., 2000; Grimmond et al., 2001; Wu et al., 2004; Yang et al., 2002). The SCUBE2 protein structure is characterized by a single peptide, followed by nine EGF repeats, a spacer region, three cysteine-rich motifs and a CUB domain at the C-terminus (Hollway et al., 2006; Kawakami et al., 2005; Tsai et al., 2009). Structure-function analyses of SCUBE2 indicate that the spacer region and/or the cysteine rich repeats are critical for membrane attachment (Tsai et al., 2009). The expression profile of *Scube2* has previously been examined in zebrafish, and in mouse embryos where is widely expressed (Grimmond et al.,



2001; Kawakami et al., 2005; Woods and Talbot, 2005). Primarily, *Scube2* is expressed during mouse embryogenesis in the neuroectoderm, craniofacial structures, heart, multiple regions of the endochondral skeleton (Grimmond et al., 2001; Xavier and Cobourne, 2011). Zebrafish *you* mutants display weak cyclopia, curled tails, and defects in slow muscle and ventral neural patterning; defects associated with aberrant HH signaling (Hollway et al., 2006; Kawakami et al., 2005; Woods and Talbot, 2005). The combined loss of the SCUBE family of proteins results in complete loss of HH signaling in zebrafish (Johnson et al., 2012). Several studies in zebrafish have demonstrated that the primary function of SCUBE2 is to mediate long range HH signaling, by releasing HH ligands into the extracellular environment (Hollway et al., 2006; Kawakami et al., 2005; Woods and Talbot, 2005). Specifically, SCUBE2 binds to the cholesterol moiety in HH ligands, increasing its solubility and enhancing its potency (Creanga et al., 2012; Tukachinsky et al., 2012). There is some conflicting evidence from (Creanga et al., 2012) suggesting that SCUBE2 can also mediate the release of palmitoylated HH ligands, however this is unclear. Additional biochemical analyses and functional reporter assays showed that human SCUBE2 interacts with SHH and PTCH1 and promote HH signaling within the cholesterol-rich raft microdomains in the plasma membrane (Tsai et al., 2009). Recent studies have also examined the function of SCUBE2 on mammalian embryos. Mouse mutants lacking *Scube2* have been examined in the context of bone development, where its deletion impairs IHH function resulting in defective endochondral bone formation (Lin et al., 2015). However, despite SCUBE2 function in HH signaling, other HH-responsive tissues seem to remain unaffected in *Scube* mutants (Lin et al., 2015).

### 1.3.3 HH ligand reception and trafficking

#### Low-density lipoprotein receptor- related protein 2 (LRP2)

LRP2 is a multi-ligand glycoprotein receptor from the low density lipoprotein (LDL) receptor gene family, originally identified as the major autoantigen in induced glomerular nephritis model in rats (Kerjaschki and Farquhar, 1983; Kerjaschki et al., 1992; Saito et al., 1994). LRP2 is a single-spanning protein comprised of an N-terminal signal peptide sequence, an extracellular region, a transmembrane domain and a C-terminal cytoplasmic domain (Christensen and Birn, 2002; Saito et al., 1994). The extracellular portion contains four cysteine-rich clusters of LDL receptor type A repeats (putative ligand binding regions), which are separated by seventeen epidermal growth factor (EGF)-like repeats and eight cysteine spacer regions that contain YWTD repeats (Christensen and Birn, 2002; Saito et al., 1994). The cytoplasmic domain has an NPXY sequence, which mediate clathrin coated endocytosis (Christensen and Birn, 2002; Saito et al., 1994). In mice, throughout gastrulation the expression of LRP2 is distributed in the apical side of the neural plate; this expression persists during development and becomes restricted to the midline of the ventral forebrain neuroepithelium (Christ et al., 2012). LRP2 is also expressed in the kidney anlage in the mesonephric tubules; while in the adult kidney it is expressed in glomerular and proximal tubule cells (Kerjaschki et al., 1984; Sahali et al., 1993). Consistent with its expression in the kidney, the main function of LRP2 was initially described in kidney proximal-tubule epithelium, where it functions as a clearance (or endocytic) receptor, mediating the nonspecific uptake of proteins (Kerjaschki et al., 1984). The function of LRP2 was further explored *Lrp2*<sup>-/-</sup> mice, which primarily display defects in the forebrain, lungs and kidneys; notably these mutants die from respiratory insufficiency

(Spoelgen et al., 2005; Willnow et al., 1996). The forebrain defects in *Lrp2* mutants, are in fact HPE defects (Willnow et al., 1996). Specifically, *Lrp2* mutants display forebrain fusion, a protusion in the midline of the head, shortened nose, occasional microphthalmia and absence of olfactory bulbs (Willnow et al., 1996). Notably, human mutations in *Lrp2* result in Donnai-Barrow syndrome, which is characterized by HPE-like phenotypes (Kantarci et al., 2007). The requirement of LRP2 in forebrain development was further explored by (Spoelgen et al., 2005) (Christ et al., 2012) which revealed that disruption of LRP2 leads to loss of *Shh* in the ventral forebrain; preventing the formation of the SHH signaling center in the prechordal plate. Mechanistic studies using whole embryo culture, immunofluorescence and cell culture experiments demonstrated that LRP2 co-localizes with SHH and PTCH1 in the neuroepithelial cell surface of E8.5 embryos (Christ et al., 2012). These data suggested that LRP2 forms a co-receptor complex with PTCH1 that is internalized upon HH ligand binding, which is mediated by clathrin (Christ et al., 2012). Immunofluorescence analysis with markers of different endocytic compartments suggested that the LRP2/SHH/PTCH1 complex undergoes recycling rather than degradation; allowing the re-secretion of the complex (Christ et al., 2012). Moreover, (McCarthy et al., 2002) and (Morales et al., 2006) showed that SHH ligand can be internalized in cell lines and efferent duct epithelial cells, respectively, and trafficked to the lysosome for potential degradation. Blockage of LRP2 via the antagonist RAP or anti-LRP2 antibody disrupts the internalization of SHH ligands (McCarthy et al., 2002; Morales et al., 2006). These studies demonstrated that LRP2 functions as endocytic receptor in certain epithelial cells to traffic SHH ligands. LRP2 function in SHH signaling has been further explored in other contexts; however, the data suggest that this co-receptor has tissue-specific functions that could also determine the fate of the internalized molecule [reviewed by (Christ et al., 2016)]. For example, in the optic

nerve where LRP2 is expressed in astrocytes, it mediates the transcytosis of SHH ligand from the apical to the basolateral side of the cells (Ortega et al., 2012). In contrast, in the murine retinal margin LRP2 functions as a HH antagonist, by sequestering SHH ligand and trafficked for lysosomal degradation (Christ et al., 2015). Overall these data indicate that LRP2 regulates HH signaling in a context-dependent manner. Even though these studies provide direct evidence that LRP2 functions as a clearance receptor in SHH signaling, it is unclear the mechanism by which this protein internalizes SHH ligand and how it selectively determines its fate in a tissue-specific manner.

#### Glypicans (GPCs)

GPCs are glycoproteins from the heparan sulfate proteoglycan family, which can positively or negatively regulate HH signaling (Filmus and Capurro, 2014). These proteins are characterized by carrying glycosaminoglycan (GAG) chains, including heparan sulfate and chondroitin sulfate. Structurally, GPC are comprised of core protein with an N-terminal secretory signal peptide and a GPI anchor (Filmus and Selleck, 2001). These proteins also contain fourteen highly conserved cysteine residues, and the GAG sites which are localized close to the C-terminus (Filmus and Capurro, 2014; Filmus and Selleck, 2001). The number of GAG insertion sites vary among glypicans and this could have an effect on their mechanistic function (Filmus and Capurro, 2014). Additionally, GPCs can be secreted via cleavage of the GPI anchor from the plasma membrane by the notum enzyme or by the furin-like convertase (Filmus and Capurro, 2014; Traister et al., 2008). One function of GPCs is to mediate interactions between cells and the extracellular matrix, primarily through their GAG side chains (Filmus and Capurro, 2014). Importantly, another key function for GPCs is to regulate signaling pathways such as Wnt, HH,

Fibroblast growth factor (FGF) and transforming growth factor-beta (Lin, 2004). GPCs are expressed throughout development in a tissue- and stage-specific manner (Filmus and Capurro, 2014).

The requirement for GPCs in HH signaling was first described in *Drosophila* (Lum et al., 2003). Specifically, the GPC homologues Dally and Dally-like are required for HH ligand release and oligomerization (Eugster et al., 2007; Han et al., 2004). GPCs have also been demonstrated to function in vertebrate HH signaling. There are a total of six glypicans in mammals (GPC1-6) (Filmus and Selleck, 2001), which have been implicated in the regulation of Wnt, HH, FGF and BMP signaling. The first glypican to be implicated in SHH signaling was GPC3, which is expressed in a wide variety of endodermal, ectodermal and mesodermal tissues (Pellegrini et al., 1998). Additionally, GPC3 was the first GPC to be associated with Simpson-Golabi-Behmel syndrome, which is characterized by a variable spectrum of developmental abnormalities including, distinctive craniofacial structures, skeletal abnormalities, heart defects and kidney defects (Li et al., 2001). Mice lacking *Gpc3* display increased levels of HH signaling in the neural tube, the hindgut, and the limb, developmental overgrowth and cystic dysplastic kidneys (Capurro et al., 2008). *In vitro* and experiments also demonstrated that GPC3 binds to SHH ligand and competes with PTCH1 binding at the cell surface. HH ligand binding to GPC3 results in endocytosis and degradation of this complex (Capurro et al., 2008). Moreover, (Capurro et al., 2008) showed that GPC3 membrane attachment is required to mediate SHH inhibition, while the heparan sulfate chains are not required to perform its regulatory effect, but they are optimal for its function. GPC3 also interacts with LRP1, which mediates the endocytosis of GPC3 and SHH through interactions with heparan sulfate (Capurro et al., 2012). GPC5 has also been implicated in HH signaling, by its upregulation in rhabdomyosarcoma, a tumor that

arise from abnormal HH signaling (Li et al., 2011a). GPC5 is expressed in the developing kidney, limb and brain; it also binds to SHH (Li et al., 2011a; Saunders et al., 1997). In contrast to GPC3, coimmunoprecipitation experiments in HEK293T cells revealed that PTCH1 can bind GPC5, which significantly stimulates the SHH binding to PTCH1 (Li et al., 2011a). Importantly, GPC5 with mutations in the GAG binding sites cannot stimulate HH signaling or SHH ligand binding to PTCH1 (Li et al., 2011a). These data suggest that GAG interactions are critical for GPC5 function in HH signaling, while they are dispensable for GPC3 function. In addition, GPC5 also functions in the reception of SHH ligands in cerebellar granule neural progenitor cells, where SHH signaling promotes proliferation and differentiation (Witt et al., 2013). Another GPC implicated in SHH signaling is GPC1. This GPC has been associated with SHH in two different contexts. In commissural neurons where SHH is required for axon guidance, GPC1 acts as a SHH co-receptor (Wilson and Stoeckli, 2013). Deletion of GPC1 in commissural axons disrupts axon guidance at the midline (Wilson and Stoeckli, 2013). GPC1 also regulates HH signaling in biliary atresia, a progressive proinflammatory disease in children involving the extrahepatic and intrahepatic biliary tree, where high HH activity has been reported in patients (Cui et al., 2013). Examination of copy number variants revealed that deletions at the 2q37.3 locus results in a deletion of one copy of GPC1 (Cui et al., 2013). Studies in zebrafish that indicate that the downregulation of GPC1 results in developmental biliary defects (Cui et al., 2013). Interestingly, injection of SHH lead to similar biliary defects in GPC1 zebrafish mutants (Cui et al., 2013). These data suggest that GPC1 can antagonize HH signaling; however, this has yet to be investigated in mice. The function of mammalian GPCs in HH signaling has also been compared to the function of the *Drosophila* glypicans Dally and Dally-like (Williams et al., 2010). Specifically, (Williams et al., 2010) tested if the mammalian glypicans could enhance or

inhibit the HH response in a *Drosophila* cell culture assay. This study revealed that GPC4 and GPC6, enhanced the HH response in a dosage dependent manner (Williams et al., 2010). In contrast, GPC3, GPC2, GPC5 have trans-dominant negative activities (Williams et al., 2010). These data suggested that the activity of the mammalian GPCs is conserved from insects to mammals and that the GPCs could mediate stimulatory and inhibitory effects on HH signaling. However, this data contradicts the more recently described role for GPC5 in the reception of SHH ligands in cerebellar granule neural progenitor cells, where it positively regulates HH signaling (Witt et al., 2013). These differences could be explained by their tissue-specific functions.

### *1.3.3 HH ligand trafficking independent of cell surface proteins*

HH ligands can also be transported by additional mechanisms that do not require cell surface proteins. Multiple studies have identified that HH ligands can be trafficked with different carriers that are associated to the cell surface (Therond, 2012). For example, HH ligands can be released as soluble multimers, associated with lipoproteins or vesicles (Briscoe and Therond, 2013; Therond, 2012). These carriers are essential for the spread of HH ligands in the hydrophilic environment of the extracellular matrix and to mediate long-range HH signaling. Most of these types of carriers have been described in invertebrates. However, there are some examples described in vertebrates, which will be briefly described below.

#### Soluble oligomeric complexes

Soluble lipid modified HH ligands can self-assemble and form monomeric and/or oligomeric complexes that are released from the plasma membrane. Importantly, the assembly of

HH ligands on these structures is dependent on lipid modifications, heparan sulfate proteoglycans interactions and specific regions of the SHH ligand (Chen et al., 2004; Goetz and Anderson, 2010; Therond, 2012; Zeng et al., 2001). In vertebrates these oligomeric complexes have been reported by purification and biochemical analyses in different cell lines. Some of the vertebrate cell lines that form these complexes include, C3H10T1/2 cells, HEK, primary chicken chondrocyte cells, HeLa, CHO, and C17 cells (Chen et al., 2004; Dierker et al., 2009; Goetz et al., 2006; Therond, 2012; Zeng et al., 2001). Interestingly, SHH oligomeric complexes of different molecular weight oligomers have been detected and these can enhance HH signaling activity (Chen et al., 2004; Zeng et al., 2001).

#### Exovesicles

SHH ligands also are transported in exovesicles during vertebrate embryogenesis. Specifically, SHH ligands have been observed in exovesicles or “nodal vesicle particles” during symmetry breaking in mammalian embryos in the node (Tanaka et al., 2005). The nodal vesicle particles are comprised of a membrane sheath and a lipid core, allowing the lipophilic morphogens to be transported without being solubilized in water (Tanaka et al., 2005). These vesicles originate from the apical microvilli at the surface of the mouse ventral node, enabling a left to right gradient (Tanaka et al., 2005). This type of carrier also has been found to carry other important developmental signal molecules including, Notch and Wnt, indicating that is a common mechanism to transport signals (Therond, 2012).

#### Specialized filopodia



SHH ligands and HH pathway components have been also reported to be transported in long and dynamic cytoplasmic extensions, called filopodia. Recent studies in *Drosophila* and vertebrates suggest that SHH ligands are transported through these extensions, without the need for cell surface proteins (Bischoff et al., 2013; Rojas-Rios et al., 2012; Sanders et al., 2013). The only study that have observed this in vertebrates, demonstrated that chicken wing buds have specialized actin based filopodia that direct long-range transport of SHH (Sanders et al., 2013). This specialized filopodia are also capable of transporting HH pathway components, specifically the HH co-receptors CDON and BOC, in HH-responding cells (Sanders et al., 2013). These results suggested that SHH-producing cells can distribute SHH ligand and create stabilized interactions with SHH-receiving cells (Sanders et al., 2013). Notably, this mechanism of HH trafficking could have been ignored before due to the technical challenges to detect filopodial extensions (Kornberg and Roy, 2014). However, further studies will be required to determine whether these filopodia can mediate long-range HH signaling, since only *in vitro* studies have provided evidence that these structures mediate signaling in other contexts (Kornberg and Roy, 2014).

#### 1.3.4 HH ligand reception

The cell surface regulators of the HH signaling pathway have significantly expanded in vertebrates since its discovery in *Drosophila*. A multitude of cell surface proteins that interact and bind to the HH ligands have been identified. These cell surface regulators can promote or antagonize HH signaling, creating signaling feedback loops to maintain the right level of HH function during embryogenesis and tissue homeostasis during adulthood. In this section I will

focus on the description of the function of these proteins through the interactions with SHH, and how they regulate HH signaling during vertebrate embryogenesis.

### Patched1 (PTCH1)

SHH ligands are primarily received at the cell surface by the multi-spanning transmembrane protein PCTH1, which resembles the RND family and Nieman-Pick type C1 (NPC1) cholesterol transporter (Marigo et al., 1996; Qi et al., 2018b; Stone et al., 1996; Taipale et al., 2002; Yang et al., 2015; Zhang et al., 2018). PTCH1 possesses twelve transmembrane domains, two large extracellular domains, a C-terminal cytoplasmic domain and a conserved sterol sensing domain involved in cholesterol regulation (Carstea et al., 1997; Stone et al., 1996). During embryogenesis *Ptch1* is expressed in the floor plate of the neural tube, the somites (cells closer to the notochord), the posterior limb bud, the diencephalon, the ventral telencephalon, the medial nasal process and the mandibular process of the craniofacial structures (Goodrich et al., 1996; Kurosaka et al., 2014). Loss of *Ptch1* in mouse embryos results in embryonic lethality around E9.5, possibly due to heart defects (Goodrich et al., 1997). Phenotypically, *Ptch1*<sup>-/-</sup> embryos fail to properly close the neural tube and exhibit overgrowth in the head folds, hindbrain and spinal cord (Goodrich et al., 1997). The expression of HH transcriptional targets in *Ptch* mutants, including *Gli1* and *Ptch1* itself are aberrantly expanded, demonstrating that PTCH1 is essential to repress genes activated by SHH (Goodrich et al., 1997). Mutations in the human *PTCH1* locus have been identified in several cancers and birth defects associated to HH signaling. In cancer PTCH1 is the main driving mutation in Gorlin's syndrome or basal cell nevus syndrome, which is characterized by a predisposition to develop basal cell carcinoma and medulloblastoma (Hahn et al., 1996; Johnson et al., 1996). Additionally, four mutations in

human holoprosencephaly patients with variable phenotypes have been identified in *Ptch1* (Ribeiro et al., 2006). These data demonstrate that PTCH1 is an essential regulator of HH signaling in development and disease.

Functionally, PTCH1 plays dual roles in the regulation of HH pathway activity (Chen and Struhl, 1996). In absence of HH ligands, PTCH1 represses SMO resulting in the repression of HH transcriptional targets (ligand-independent antagonism) (Chen and Struhl, 1996; Jeong and McMahon, 2005). HH ligand binding to PTCH1 results in the de-repression of SMO and activation of HH transcriptional targets. *Ptch1* itself is a HH transcriptional target (Agren et al., 2004); *Ptch1* upregulation leads to PTCH1-mediated sequestration of HH ligands that restrains HH signaling in responding tissues (ligand-dependent antagonism) (Hooper and Scott, 1989; Jeong and McMahon, 2005; Nakano et al., 1989). Notably, these dual activities of PTCH1 are conserved across organisms (Goodrich et al., 1996). However, as discussed in greater detail below there are additional, vertebrate-specific HH pathway antagonists that also contribute to both of these functions to maintain the proper levels of HH signaling (see PTCH2 and HHIP sections) (Holtz et al., 2013).

Although PTCH1 is required for proper HH signal transduction, the mechanism by which HH ligands bind to PTCH1 and the mechanism of PTCH1-mediated SMO inhibition remain unclear. Recently, cryo-electron microscopy studies have revealed important structural information about PTCH1 and its interactions with SHH ligand (Gong et al., 2018; Qi et al., 2018a; Qi et al., 2018b; Zhang et al., 2018). Specifically, (Qi et al., 2018a) and (Zhang et al., 2018) reported that PTCH1 can form a dimer at the plasma membrane. Additionally, the structure of PTCH1 exhibits cholesterol-like densities in a central hydrophobic conduit or “tunnel” across the transmembrane domain of PTCH1 and the plasma membrane, that resembles

the structures used by RND proteins to transport substrates (Gong et al., 2018; Qi et al., 2018a; Zhang et al., 2018). Presumably, this tunnel is required to transport sterol-like molecules, such as cholesterol from the membrane and/or to the extracellular space (Gong et al., 2018; Qi et al., 2018a; Zhang et al., 2018). Interestingly, *Ptch1* overexpression in *Ptch1*<sup>-/-</sup> mouse embryonic fibroblasts reduces cholesterol activity in the inner leaflet of the plasma membrane; this reduction is rapidly restored by HH stimulation (Zhang et al., 2018). These data are supported by previous studies in the *Drosophila* wing imaginal disc, which showed that *Ptc* overexpression increases sterol mobilization from endosomal compartments (Khaliullina et al., 2009). Moreover, (Bidet et al., 2011) reported that *Ptch1* overexpression in yeast (*S. cerevisiae*) increases the efflux of a cholesterol derivative. These data indicate that PTCH1 can directly transport cholesterol; however, further experiments will be required to determine whether (and how) this transport regulates SMO activity.

These studies also showed that SHH ligands bind to PTCH1 through distinct interfaces that dependent on SHH lipid modifications. Dually-lipidated SHH ligand bind to the cavity between the extracellular domains I and II of PTCH1 via palmitate modification of SHH (Qi et al., 2018a; Qi et al., 2018b). This is the predominant interface for SHH ligand binding and it results in the obstruction of the tunnel of PTCH1(Qi et al., 2018a). In contrast, SHH ligand lacking the palmitate modification uses the opposite site of the ligand to bind the extracellular domain I of PTCH1(Gong et al., 2018; Qi et al., 2018b). Interestingly, this second interface is calcium-dependent and is where the ligand can interact with HH co-receptors (Beachy et al., 2010; Gong et al., 2018; Izzi et al., 2011; Qi et al., 2018b). These discrepancies observed in the binding interfaces of the SHH ligand were clarified in (Qi et al., 2018a), where they demonstrated that a single SHH ligand molecule is capable of binding to both interfaces in a

PTCH1 dimer complex. Functional analyses indicate that point mutations on the palmitate or the calcium PTCH1 interfaces decreases HH signaling activity, demonstrating that they are essential for HH signal transduction (Izzi et al., 2011; Qi et al., 2018b). Based on these data, a model has been proposed (discussed in (Sommer and Lemmon, 2018)) where, in the absence of HH ligand, PTCH1 exports cholesterol (which is necessary for SMO activation) from the membrane. Depletion of cholesterol maintains SMO in an inactive state that is unable to transduce HH signaling. In the presence of SHH ligands, one molecule of SHH binds the PTCH1 dimer complex, resulting in the inhibition of cholesterol transport. The cholesterol available in the plasma membrane activates SMO, initiating a signal transduction cascade that culminates in the activation of HH transcriptional targets. It remains unclear how other cell surface regulators of HH pathway activity (discussed below) fit into this model.

#### Patched 2 (PTCH2)

Patched 2 (PTCH2) is a homologue of PTCH1, that was discovered in the newt eye and is conserved in zebrafish, chicken and mouse (Carpenter et al., 1998; Motoyama et al., 1998b; Takabatake et al., 1997). Human PTCH1 and PTCH2 share 54% amino acid identity (Carpenter et al., 1998; Kawamura et al., 2008). Despite the structural homology between PCTH1 and PTCH2, these proteins exhibit some differences in their domains. Specifically, PTCH2 possess a truncated C-terminal cytoplasmic domain which confers more stability to the protein and lacks one of the glycosylation sites observed in PTCH1(Carpenter et al., 1998). All three mammalian HH ligands, SHH, IHH and DHH, bind to PTCH2 with similar affinity to PTCH1(Carpenter et al., 1998). Interestingly, *Ptch2* expression is similar but not identical to *Ptch1*. During early embryogenesis *Ptch2* exhibits overlapping expression patterns with *Ptch1* in the developing

central nervous system, the embryonic lung, stomach and intestine (Motoyama et al., 1998a). The highest levels of *Ptch2* are detected in the skin (Carpenter et al., 1998). Another unique characteristic of *Ptch2* is that it is co-expressed with *Shh* in different tissues during mouse embryogenesis (Motoyama et al., 1998a). This distinct expression profile suggests that PTCH2 could function differently from PTCH1. *Ptch2*<sup>-/-</sup> mutant embryos develop normally and do not display any defects in the patterning of the neural tube, limbs, hair follicles or testis (Nieuwenhuis et al., 2006). However, they exhibit a subtle increase of HH transcriptional targets in the limb bud and hair follicle (Nieuwenhuis et al., 2006). Adult *Ptch2*<sup>-/-</sup> mice display skin lesions that are characterized by alopecia, ulceration and epidermal hyperplasia (Nieuwenhuis et al., 2006). These defects are consistent with *Ptch2* expression in the skin and indicates that PTCH2 plays an important role in maintaining skin homeostasis. Even though *Ptch2* mutants do not have a predisposition to develop tumors, rare mutations have been identified in several cases of basal cell carcinoma and medulloblastoma (Lee et al., 2006; Smyth et al., 1999; Zaphiropoulos et al., 1999). Moreover, the deletion of *Ptch2* in a *Ptch1*<sup>+/-</sup> background enhances tumor formation (basal cell carcinoma and medulloblastoma), indicating that both PTCH1 and PTCH2 can function as tumor suppressor genes (Lee et al., 2006).

Genomic analysis of GLI binding sites, cell based assays, and overexpression studies in the chicken spinal cord demonstrated that *Ptch2* is a direct transcriptional target of HH signaling (Holtz et al., 2013; Peterson et al., 2012; Vokes et al., 2007; Vokes et al., 2008). However, the lack of phenotype in *Ptch2* mutants indicated that it is dispensable for HH signaling during development (Goodrich et al., 1997; Nieuwenhuis et al., 2006). Thus, it was unclear if PTCH2 had a role in HH signaling and if it was capable of antagonizing HH signaling as its homologue PTCH1. This was clarified by (Holtz et al., 2013), who demonstrated that PTCH2 is a HH

pathway antagonist that functions redundantly with *Ptch1* and *Hhip* to restrict HH-dependent specification of ventral neural progenitors (Holtz et al., 2013). Further, PTCH2 antagonizes HH signaling in the developing chicken neural tube and in HH-responsive NIH/3T3 fibroblasts (Holtz et al., 2013). These results demonstrate that PTCH2 does play a role in ligand dependent antagonism of HH signaling. *In vitro* studies also have demonstrated that PTCH2 can mediate ligand independent antagonism (Alfaro et al., 2014). This was demonstrated in *Ptch1*<sup>-/-</sup> cells where *Ptch2* mediates the residual responsiveness to SHH retained in these cells (Alfaro et al., 2014). Genetic evidence also supports that PTCH2 could mediate this mechanism, however to a lesser extent than PTCH1.

#### Hedgehog-Interacting Protein 1 (*Hhip*)

HHIP is a secreted glycoprotein that was identified in a biochemical screen from E10.0 mouse limb buds (Chuang and McMahon, 1999). Sequence comparisons showed that HHIP is conserved across organisms including zebrafish, chicken and mice, but not in *Xenopus* (Chuang and McMahon, 1999). HHIP is comprised of multiple functional domains: an N-terminal cysteine rich domain, a 6-bladed  $\beta$  propeller domain, two proximal EGF repeats, a C-terminal hydrophobic region, and 4 N-linked glycosylation sites (Chuang and McMahon, 1999).

Examination of *Hhip* expression in mouse embryos revealed that this protein is closely expressed to *Shh* (Chuang and McMahon, 1999). First, *Hhip* is detected at E8.75 in the ventral midline of the neural tube and the ventral medial somites, next to *Shh* expressing cells (Chuang and McMahon, 1999). *Hhip* is also expressed next to *Shh* expressing cells in the midbrain, gut mesenchyme and in the posterior half of the limb bud (Chuang and McMahon, 1999). At later stages of development *Shh* is expressed in multiple epithelial tissues, like the lung, hair, whiskers

and the gut, in which *Hhip* is expressed in the adjacent mesenchyme (Bitgood and McMahon, 1995). Interestingly, this expression profile near the ligand sources, indicated that *Hhip* was a HH transcriptional target; this was later confirmed by the genomic characterization of *Gli* activator targets performed by (Chuang and McMahon, 1999) and (Vokes et al., 2007). This novel protein binds to all three mammalian HH ligands with similar affinity as PTCH1 (Chuang and McMahon, 1999). Crystal structures revealed that the site of HH ligand binding in HHIP was localized in the  $\beta$  propeller domain (Bishop et al., 2009; Bosanac et al., 2009). Subsequent biochemical analyses provided more insights about HHIP function in HH signaling. Initially HHIP was described by (Chuang and McMahon, 1999) as a membrane anchored protein in COS-7 cells. In contrast (Coulombe et al., 2004) detected a secreted version of HHIP in HEK293T cells. More recently, a series of biochemical and overexpression experiments in the chick neural tube demonstrated that HHIP1 is a secreted protein that can be attached to the plasma membrane through cell type-specific interactions with heparan sulfate via its cysteine rich domain, which localizes HHIP to the basement membrane (Holtz et al., 2015). This was the first description of a secreted HH pathway antagonist that inhibits HH signaling in a non-cell autonomous manner (Holtz et al., 2015). Notably, this mechanism is not only restricted to the neural tube; HHIP is also secreted in the embryonic lung and in the developing diencephalon (Holtz et al., 2015).

*Hhip* mutant mice die shortly after birth due to respiratory defects (Chuang et al., 2003). These mutants display developmental defects in lung branching morphogenesis, with a reduced number of lobes, and defects in the endochondral skeleton (Chuang et al., 2003). Other HH-responsive tissues such as the craniofacial structures, limbs and the neural tube are phenotypically normal in these mutants (Chuang et al., 2003). The developing lungs of *Hhip* mutants display a slight upregulation and expansion of *Ptch1* expression in the lung mesenchyme



(Chuang et al., 2003), suggesting that HHIP is a HH pathway antagonist. Further analyses indicated that the branching defects in *Hhip* mutants arise from loss of *Fgf10* in the mesenchyme. SHH signaling is required in the mesenchyme to suppress *Fgf10* and mediate proper branching morphogenesis (Litingtung et al., 1998; Pepicelli et al., 1998). Additionally, (Kawahira et al., 2003) reported that *Hhip* mutants display defects in the pancreas, stomach and duodenum. Interestingly, in *Hhip* mutant pancreata display decreased levels of *Fgf10* in the mesenchyme; the pancreas also requires SHH suppression for proper development (Kawahira et al., 2003). These data indicate that HHIP is required in certain tissues to inhibit HH signaling and maintain the proper levels of *Fgf10*. As an important regulator of lung development, HHIP also has been involved in a number of human lung diseases such as asthma, chronic obstructive pulmonary disease lung cancer and emphysema (Pillai et al., 2009) (Castaldi et al., 2014; Li et al., 2011b; Young et al., 2010; Zhou et al., 2012).

The lack of defects observed in a variety of HH responsive tissues in *Hhip* mutants, suggested that HHIP antagonistic function was functionally redundant with PTCH1. Different genetic studies tested this possibility by simultaneously deleting *Hhip* in a *Ptch*<sup>+/-</sup>, *Ptch1*<sup>-/-</sup> background or in combination with the *MtPtch1* transgene (which expresses *Ptch1* at low levels from a metallothionein promoter) and subsequently analyzing HH transcriptional targets (Jeong and McMahon, 2005; Milenkovic et al., 1999). These compound mutants displayed variable phenotypes that ranged from increased overall embryo size to exencephaly, spina bifida, hyperplastic first branchial arches and subtle expansion of the ventral progenitor domains (Jeong and McMahon, 2005). The phenotypes were more severe in *MtPtch1;Ptch1*<sup>-/-</sup>;*Hhip*<sup>-/-</sup> embryos, where the entire brain was open, the branchial arches were expanded and the eyes were absent. Strikingly, *MtPtch1;Ptch1*<sup>-/-</sup>;*Hhip1*<sup>-/-</sup> mutants displayed the largest expansion of ventral neural

progenitors and the reduction of intermediate and dorsal progenitor domains (Jeong and McMahon, 2005). These phenotypes are consistent with increased HH activity and suggested that both HHIP and PTCH1 are redundant pathway components of the feedback control that regulate SHH signaling in the neural tube. The redundancy of HHIP and PTCH1 during neural tube patterning was further explored by (Holtz et al., 2013), which integrated into the analysis another HH pathway antagonist, PTCH2. First, this study addressed the possible redundancy between HHIP and PTCH2; these double mutant embryos do not display any apparent defects and display normal neural patterning at E10.5 (Holtz et al., 2013). However, the combined deletion of *Ptch1* and *Ptch2* (*MtPtch1;Ptch1<sup>-/-</sup>;Ptch2<sup>-/-</sup>* embryos) results in midbrain and hindbrain exencephaly and significant expansion of SHH-dependent ventral neural progenitors; indicative of increased HH signaling (Holtz et al., 2013). Furthermore, (Holtz et al., 2013) also examined *MtPtch1;Ptch1<sup>-/-</sup>;Ptch2<sup>-/-</sup>;Hhip<sup>-/-</sup>* embryos which display a neural tube with only ventral neural progenitors, significant defects in size and neuro-epithelial outgrowths; the most striking phenotype among these compound mutants (Holtz et al., 2013). These experiments demonstrated that PTCH1, PTCH2, and HHIP are collectively required to mediate HH ligand-dependent inhibition in the neural tube to properly specify all the neuronal progenitors in the neural tube.

#### Growth arrest-specific 1 (GAS1)

GAS1 is a GPI-anchored cell surface protein related to the glial cell-derived neurotrophic factor (GDNF) (Cabrera et al., 2006). GAS1 is composed of an N-terminal signal sequence peptide, two cysteine rich domains and a GPI anchor (Cabrera et al., 2006). Originally *Gas1* was identified as a negative regulator of growth and mediator of cell death, however this function has

not been demonstrated in an animal model (Schneider et al., 1988). GAS1 is broadly expressed during mouse and chicken embryogenesis and its expression is first detected at E6.5 (Lee and Fan, 2001). Specifically, *Gas1* is expressed in the neural tube, craniofacial structures, limbs, somites, optic and otic vesicles, among other structures (Lee and Fan, 2001). This protein was first implicated in SHH signaling as an antagonist by overexpression in presomitic cells and tooth explants (Cobourne et al., 2004; Lee et al., 2001a). Additionally, (Lee et al., 2001a) and (Martinelli and Fan, 2007) demonstrated that GAS1 binds SHH ligand. Later, multiple transcriptional profiling experiments from *Smo* and *Ptch1* embryos at several embryonic stages identified *Gas1* as a gene that is downregulated in response to SHH (Allen et al., 2007; Tenzen et al., 2006). Despite the antagonistic roles previously described for GAS1 in HH signaling, the examination of *Gas1* null embryos revealed roles that are consistent with a role of GAS1 in the promotion of HH signaling. Specifically, *Gas1* mutants display severe HPE defects, microphthalmia, cerebellar, limb and axon guidance defects (Allen et al., 2007; Martinelli and Fan, 2007; Seppala et al., 2007) (Liu et al., 2002; Liu et al., 2001). Examination of *Gas1* expression revealed that during early stages of development *Gas1* is expressed within HH-responsive cells, but as the levels of HH signaling increase, *Gas1* becomes dorsally restricted, consistent with the idea that *Gas1* is a negative target of SHH signaling (Allen et al., 2007; Martinelli and Fan, 2007). Analysis of HH-dependent patterning in *Gas1* null embryos, showed a significant decrease of *Nkx2.1*, a direct transcriptional target of HH signaling, in the craniofacial structures and decreased expression of the HH targets FOXA2, NKX2.2 and OLIG2 in ventral neuronal progenitors (Allen et al., 2007). Conversely, ectopic expression of *Gas1* by chicken *in ovo* electroporations drives the ectopic expression of these genes in the developing chicken forebrain and neural tube (Allen et al., 2007). Further, reducing the dosage of *Shh* in a

*Gas1* null background exacerbates the developmental defects in these mutants (Allen et al., 2007; Seppala et al., 2007). In other HH-dependent tissues like the cerebellum, *Gas1* is required to promote proliferation of cerebellar granule neuron progenitors (CGNPs) that reside in the proliferative external germinal layer (Izzi et al., 2011). These data demonstrated that *Gas1* positively regulates HH signaling during vertebrate embryogenesis.

The requirement of *Gas1* in SHH signal transduction was further elucidated by deleting it in combination with two other HH pathway components, the Cell adhesion molecule–related/down-regulated by oncogenes (*Cdon*) and Brother of *Cdon* (*Boc*; discussed below). The simultaneous deletion of *Gas1* with either *Cdon* or *Boc* also enhances the severity of the phenotypes observed in *Gas1* null embryos in the craniofacial structures, the limbs, the cerebellum, and the neural tube (Allen et al., 2007; Izzi et al., 2011). These data demonstrate that GAS1 is part of a HH receptor complex essential for proper HH signal transduction. However, the variability in the severity of the of the phenotypes observed in *Gas1*<sup>-/-</sup> embryos, has made it difficult to interpret its individual contribution to HH signaling. For example, in the craniofacial structures the HPE phenotypes are dependent on the genetic background. In a 129Sv-C57BL/6J mixed genetic background, the craniofacial defects are mild, characterized by fused premaxillary incisor, synostic premaxilla, cleft secondary palate and defects in the basisphenoid bone (Seppala et al., 2007). When *Gas1*<sup>-/-</sup> mutants are maintained predominantly in a BL/6J background they display truncated maxilla, reduced parietal bone and disrupted tympanic bone (Allen et al., 2007). In addition, there is some variability in the limbs defects of *Gas1* null mutants, which lack digit 2 or 3 both in the forelimb and in the hindlimb (Allen et al., 2011). However, the variability in the limb defects has not been attributed to genetic background. Is still unclear why *Gas* mutants display highly variable phenotypes. These phenotypes suggest that the *Gas1* locus can

be influenced by other unknown epigenetic and or environmental factors that affect its function. In the context of disease *Gas1* has been involved in HPE, where patients with mutations in the *Gas1* gene display highly variable clinical manifestations (Ribeiro et al., 2010). *Gas1* is also implicated in pancreatic cancer, where it regulates the levels of HH signaling in a dosage dependent manner to regulate growth and angiogenesis (Mathew et al., 2014).

The mechanism by which GAS1 regulates HH signaling is still unclear. However, different studies have elucidated important insights about GAS1 function. Co-immunoprecipitation experiments have demonstrated that GAS1 interacts with PTCH1 and with PTCH2 (Holtz et al., 2013; Izzi et al., 2011). This interaction suggests that GAS1 can present the SHH ligand to PTCH1 or provide more stability to the receptor complex. Additionally, based on the digit specification defects (digits 2 and 3 which require low levels of HH activity) of *Gas1*<sup>-/-</sup> embryos and the expression of GAS1 in the limb bud, it is thought that GAS1 functions in areas of long range and low levels of SHH signaling (Allen et al., 2011; Martinelli and Fan, 2007). However, this type of regulation mediated by GAS1 might be restricted to specific tissues and be dependent on the levels of SHH. More recently, *Gas1* also was implicated in primordial germ cell migration in mouse, where is suggested to form a complex with PTCH2 to induce the activity of GLI and the parallel activation of cAMP-responsive element binding protein and the Src tyrosine kinase (Kim et al., 2020). This study suggests that GAS1 could differentially regulate SHH signaling by interacting with other cell surface proteins.

Cell adhesion molecule – related/down-regulated by oncogenes (CDON) and Brother of CDON (BOC)

CDON and BOC are two structurally similar related proteins from the immunoglobulin (Ig) superfamily (Kang et al., 1997; Kang et al., 2002). CDON and BOC were initially described as cell adhesion molecules, which form complexes in a cis manner to enhance myogenic differentiation by a positive feedback loop with MyoD in myogenic precursors (Kang et al., 1997; Kang et al., 2002). These proteins are comprised of an N-terminal signal peptide, four (BOC) or five (CDON) Ig domains followed by three fibronectin type III domains (FNIII), a single pass transmembrane domain and a cytoplasmic domain (Kang et al., 2002). The arrangement of Ig and FNIII domains of CDON and BOC resemble the Robo family of proteins, which are axon guidance receptors (Simpson et al., 2000). Despite the significant structural similarity between CDON and BOC, the amino acid identity of the single domains is variable ranging from 38% to 80% of homology (Kang et al., 2002). They also differ in the number of Ig domains (CDON (5) vs. BOC (4)) and their unique cytoplasmic domains that are not related to each other, and do not resemble any other known proteins (Kang et al., 2002). CDON was first associated with HH in an siRNA screen in cultured *Drosophila* cells, which identified CG2911, a fly homologue for CDON with unknown function in HH signaling (Lum et al., 2003; Yao et al., 2006). In flies this gene was denominated as *interference hedgehog* (ihog). Additionally, another *ihog* family member CG32796 or *brother of ihog* (boi), a BOC homologue, was also linked to HH signaling (Lum et al., 2003; Yao et al., 2006). Genetic studies in *Drosophila* and in vitro biochemical studies elucidated that both ihog and boi are proteins that bind to SHH through their first FNIII domain and that they function at the level of PTC to collectively enhance the HH signaling (Camp et al., 2010; Camp et al., 2014; McLellan et al., 2008; Yao et al., 2006; Zheng et al., 2010). In addition, overexpression of boi in cells lacking ihog rescued the HH activity,

suggesting that *ihog* and *boi* act in a redundant manner to mediate the promotion of HH signaling in flies (Yao et al., 2006).

The role of *Cdon* and *Boc* in HH signal transduction is conserved from flies to vertebrates. These proteins were also identified in transcriptional profiling experiments from *Smo* and *Ptch1* mouse mutants, with the aim of identifying novel cell surface proteins that could regulate HH signaling (Tenzen et al., 2006). Extensive expression characterization by *in situ* hybridization in the mouse and chicken embryo showed that *Cdon* and *Boc* are broadly and similarly expressed throughout development (Mulieri et al., 2002; Mulieri et al., 2000). *Cdon* and *Boc* are expressed in the neural tube, craniofacial structures, limbs, somites, urogenital system, among other tissues (Mulieri et al., 2002; Mulieri et al., 2000; Tenzen et al., 2006). Notably, in HH-responsive tissues they are expressed in opposition to the *Shh* ligand, consistent with the notion that they are negatively regulated by HH signaling. This was also confirmed by examining *Cdon* and *Boc* expression in *Shh*<sup>-/-</sup> and *Smo*<sup>-/-</sup> mutants, where their expression is enhanced and expanded closer to the SHH ligand source (Tenzen et al., 2006). In contrast, in *Ptch1*<sup>-/-</sup> mutants, their expression is lost or downregulated (Tenzen et al., 2006). These data suggest that *Cdon* and *Boc* are general negative targets of HH signaling. Interestingly, *Boc* was also identified as a positive target of *Gli1* in a genome wide screen in medulloblastoma; indicating that *Boc* expression is regulated by SHH signaling (Lee et al., 2010). Analysis of *Cdon*<sup>-/-</sup> and *Boc*<sup>-/-</sup> mouse embryos revealed subtle defects in certain HH responsive tissues; interestingly the defects are not similar between these mutants. *Cdon*<sup>-/-</sup> embryos are embryonically lethal at E18.5 and display variable strain-specific HPE defects, as observed in *Gas1* null mutants (Cole and Krauss, 2003; Zhang et al., 2006). In a mixed 129/Sv background *Cdon*<sup>-/-</sup> embryos display microrforms of HPE, displaying single median maxillary incisor, and

defects in certain bones; while in a congenic BL/6J background the defects are enhanced resulting in midface hypoplasia, a single nostril and ocular hypotelorism (Cole and Krauss, 2003; Zhang et al., 2006). In contrast, *Boc* mutants are viable and fertile, and are phenotypically normal with no overt craniofacial defects regardless of the genetic background. Notably and different from *Cdon* mutants, *Boc*<sup>-/-</sup> embryos display defects in commissural axon guidance and have a smaller cerebellum with proliferation defects (Izzi et al., 2011; Okada et al., 2006). Interestingly, *Cdon*<sup>-/-</sup> and *Boc*<sup>-/-</sup> embryos do not display any limb patterning defects (Allen et al., 2011; Cole and Krauss, 2003). Detailed examination of ventral neural patterning of E10.5 single *Cdon* and *Boc* mutants revealed that only *Cdon*<sup>-/-</sup> embryos have neural patterning defects. Specifically, these mutants display decreased numbers of FOXA2 positive cells resulting in defects in floor plate specification (Allen et al., 2011; Tenzen et al., 2006). The absence of phenotypes in *Boc* null mutants suggested that as observed in *Drosophila*, *Cdon* and *Boc* have redundant roles in vertebrate HH signaling. To further elucidate this possibility in vertebrates, several groups examined the defects observed in different tissues of *Cdon*<sup>-/-</sup>;*Boc*<sup>-/-</sup> embryos. In the absence of both *Cdon* and *Boc*, the patterning defects in the craniofacial structures and in the neural tube are exacerbated, while the limbs are unaffected; demonstrating that these proteins display overlapping roles in certain tissues (Allen et al., 2011; Zhang et al., 2011). Based on their similar expression patterns and transcriptional signatures, the genetic interactions of *Gas1*, *Cdon* and *Boc* were analyzed as compound mutants. *Gas1*;*Cdon* mutants display a striking reduction in SHH signaling, resulting in severe HPE with fusion of the forebrain, a single nostril and near complete loss of HH-dependent ventral neural patterning (Allen et al., 2007). Similarly, *Gas1*;*Boc* mutants display loss of ventral neural patterning, however the craniofacial defects are not as severe as the ones observed in *Gas1*;*Cdon* mutants (Allen et al., 2011; Seppala et al.,



2014). Surprisingly, severe digit specification defects are only observed in the *Gas1;Boc* double mutants, lacking digit 2 and showing fusion of digits 3 and 4 (Allen et al., 2011). Despite *Cdon* expression in the developing limb, the deletion of *Cdon* in a *Boc* or *Gas1* null background does not result in any defects in digit specification (Allen et al., 2011). These data suggest that CDON does not play a role in HH-dependent limb patterning, in comparison to GAS1 and BOC.

Further, the simultaneous deletion of *Gas1*, *Cdon* and *Boc* resulted in even more striking defects, with embryonic lethality at E10.5, complete loss of ventral neural patterning, cyclopia, HPE, and heart looping defects (Allen et al., 2011). The phenotypes observed in single, compound and triple mutants demonstrate that GAS1, CDON and BOC are essential during development by collectively regulating HH signaling. Given their essential requirement during development, mutations in *Cdon* and *Boc* have been identified in human HPE patients (Bae et al., 2011; Hong et al., 2017). CDON and BOC are not only active during development. Their expression has also been detected in the stroma of pancreatic lesions, where their deletion affects the levels of HH signaling (Mathew et al., 2014). In addition, *Boc* expression is upregulated in a subset of human medulloblastoma tumors in which it regulates their proliferation rate (Mille et al., 2014).

Even though CDON and BOC are essential during development to mediate HH signal transduction, the mechanisms by which they regulate HH signaling are poorly understood. Similar to their fly homologues, CDON and BOC also bind to SHH ligand; however, the interaction occurs in a different manner. Biochemical, biophysical, X-ray structural studies and cell culture binding assays demonstrated that SHH binds directly to the third FNIII domain of CDON and BOC, and that this interaction requires calcium (McLellan et al., 2008; Tenzen et al., 2006; Yao et al., 2006). Furthermore, other studies have performed structure function analysis to determine which domains of CDON and BOC are necessary to promote HH signaling activity.

Biochemical experiments showed that CDON and BOC establish interactions with PTCH1 through their first and second fibronectin domains, and they also bind to PTCH2 (Bae et al., 2011; Izzi et al., 2011) (Holtz et al., 2013). Recently, *in vivo* gain-of-function experiments in the chicken neural tube dissected novel and distinct requirements for CDON and BOC in HH signal transduction (Song et al., 2015). Specifically, both proteins require membrane attachment, the third FNIII domain, and the first or second FNIII domain to promote HH signaling in the spinal cord (Song et al., 2015). Additionally, BOC exhibits some unique requirements like the Ig-FNIII linker region and an extracellular cleavage event at the linker that connects the FNIII and integral membrane attachment (Song et al., 2015). Conversely, CDON does not require the Ig-FNIII linker, does not undergo extracellular cleavage, and just requires peripheral membrane attachment (Song et al., 2015). Interestingly, in both proteins the cytoplasmic domain is dispensable. Notably, this domain is required in CDON but not in BOC during myogenesis (Kang et al., 2002; Song et al., 2015). In contrast, this domain in BOC is required for interactions with specific proteins in axon guidance and neuronal differentiation (Makihara et al., 2018; Vuong et al., 2017). Overall, these studies demonstrate that CDON and BOC utilize different domains to promote HH signaling.

### *1.3.6 HH ligand-independent cell surface regulators*

While HH ligand-binding proteins comprise the largest class of cell surface regulators, a second class of cell surface HH pathway components exists that functions independently of HH ligands. These proteins transduce HH signaling through the modulation of downstream HH pathway components. In this section I discuss HH ligand-independent cell surface regulators of

the pathway, how they regulate HH signaling, how they are influenced by HH ligand-dependent cell surface regulators, and their role in HH-driven disease.

### Smoothened (SMO)

The *Smoothened (smo)* gene was identified in a *Drosophila* genetic screen, where it was described as a segment polarity gene, originally named *Smooth* (Nusslein-Volhard et al., 1984). However, the name *Smooth* was already used to name another locus, and the new gene was renamed *Smoothened* (Lindsley and Zimm, 2012). *Drosophila* larvae lacking *smo* display variable segment polarity cuticle phenotypes resembling *Hh* mutant larvae, suggesting a role in HH signaling (Nusslein-Volhard et al., 1984; van den Heuvel and Ingham, 1996). SMO was identified and characterized as a HH transducer by two different studies, (Alcedo et al., 1996) and (van den Heuvel and Ingham, 1996), which demonstrated that *smo* was necessary for the response of cells to HH signaling by performing molecular and genetic experiments in *Drosophila*. Due to the relevance of SMO in HH signal transduction in *Drosophila*, the role of *Smo* was also explored during vertebrate embryogenesis.

Deletion of *Smo* in mice results in embryonic lethality at E9.5— *Smo* mutants display severe developmental defects including cyclopia and HPE, similar to phenotypes observed in *Shh* mouse mutants (Chiang et al., 1996; Zhang et al., 2001). *Smo* homozygous mutants also fail to undergo embryonic turning, closure of the ventral midgut and normal heart looping (Zhang et al., 2001). Additionally, (Zhang et al., 2001) performed genetic experiments that demonstrated that *Smo* is epistatic to *Ptch1* and that SMO is essential to transduce both SHH and IHH ligands. Specifically, in absence of HH ligands, SMO is constitutively inhibited by PTCH1. HH ligand binding to PTCH1 releases SMO inhibition in a catalytic manner that does not require the

interaction of these proteins (Taipale et al., 2002). The mechanism of SMO inhibition by PTCH1 remains unclear. Various studies suggest that this inhibition occurs through an indirect mechanism, potentially by regulating the availability of small molecules that bind to SMO (Ingham et al., 2000; Taipale et al., 2002). Recent cryo-electron microscopy studies revealed the structures of PTCH1, which displayed a “tunnel” that could transport cholesterol from within the membrane to the extracellular space (Qi et al., 2018a). These data suggest a model in which PTCH1 inhibits SMO by depleting cholesterol, which is required for SMO signaling; ligand binding to PTCH1 occludes cholesterol transport and allows for SMO activation [reviewed by (Sommer and Lemmon, 2018)]. These data demonstrate a potential mechanism that directly links ligand reception to downstream signaling.

The *Smo* gene encodes a protein that display typical characteristics of the G-protein coupled receptors (GPCR) superfamily, which are closely related to the Frizzled family of Wnt receptors (Alcedo et al., 1996; Dann et al., 2001; Fredriksson et al., 2003; van den Heuvel and Ingham, 1996). The GPCR-like structure of SMO suggests that this protein could be functioning through heterotrimeric G proteins to transduce HH signaling. Several studies have demonstrated that SMO utilizes the G $\alpha$ i heterotrimeric G proteins to regulate HH pathway activity (DeCamp et al., 2000; Kasai et al., 2004; Ogden et al., 2008; Riobo et al., 2006). However, there is limited evidence in how SMO directly binds to these proteins and how they influence HH activity. Moreover, recent studies have suggested that vertebrate SMO can regulate HH signaling in a G protein-independent manner [reviewed by (Arensdorf et al., 2016)], suggesting that SMO could be regulating HH signaling through multiple mechanisms.

Structurally, SMO contains a cysteine rich (CRD) domain in the extracellular N-terminal region, three extracellular and three intracellular loops, seven transmembrane domains, and a

intracellular carboxyl-terminal tail (Alcedo et al., 1996; van den Heuvel and Ingham, 1996; Zhang et al., 2001). This receptor is conserved across organisms, but there is structural divergence in some of the SMO domains (Huangfu and Anderson, 2006). Comparisons of invertebrate and vertebrate SMO sequences indicate that the transmembrane domains are relatively conserved, while the major differences are in the intracellular carboxyl-terminal tail [reviewed by (Huangfu and Anderson, 2006)]. Over the years, different studies have focused on elucidating the functions of the different structural domains of SMO that serve as binding sites for different small molecules or domains, which can undergo posttranslational modifications that alter HH pathway activity [reviewed by (Arensdorf et al., 2016)].

Recently, (Nachtergaele et al., 2013) solved the crystal structure of the zebrafish SMO CRD domain, identifying a conserved hydrophobic groove rich in cysteine amino acids that is analogous to the Frizzled and Frizzled-like CRDs that bind to the palmityl modification of Wnt ligands and small hydrophobic ligands. This hydrophobic groove serves as binding site for oxysterols, which can activate SMO in the absence of HH ligands in certain tissues (Corcoran and Scott, 2006; Dwyer et al., 2007; Nachtergaele et al., 2013). Other studies have focused on the seven transmembrane domains of SMO, which foster stabilizing interactions with the amino-terminal linker domain and the first and third extracellular loops to ensure proper positioning of the CRD domain (Wang et al., 2013). Additionally, the seven transmembrane domains possess a binding site for cyclopamine, a plant alkaloid that inhibits HH signaling (Chen et al., 2002a). This specific binding site also binds to a variety of small molecules that modulate HH activity, including SMO agonists (SAG) and antagonists (SANT-1 and Vismodegib) (Chen et al., 2002b; Frank-Kamenetsky et al., 2002; Robarge et al., 2009). Finally, the carboxyl-terminal tail of SMO also regulates HH pathway function. This domain is hyperphosphorylated upon HH pathway

activation by Protein kinase A (PKA), Casein kinase I (CK1 $\alpha$ ) and the G protein coupled receptor kinase 2 (GRK2) (Chen et al., 2011; Jia et al., 2004). Subsequently, this causes a conformational change in SMO that in *Drosophila* results in the translocation of SMO to cell membrane, while in vertebrates it goes to the primary cilium to initiate a signaling transduction cascade that results in differential processing of the Ci/GLI transcription family (Denef et al., 2000; Hui and Angers, 2011; Zhao et al., 2007). The levels of these phosphorylation events positively correlate with the levels of SMO at the cell surface and at the primary cilia and HH pathway activity. The SMO carboxyl-terminal domain can also be ubiquitinated in *Drosophila* and in MEFs, preventing the accumulation of SMO at the cell surface and primary cilia respectively, negatively impacting the activation of HH transduction by SMO (Desai et al., 2020; Xia et al., 2012).

Given the implications of HH signaling in cancer, mutations in signal transduction components like SMO can lead to the hyperactivation of the pathway and consequently tumorigenesis. Activating mutations in the human *SMO* gene have been identified in sporadic basal cell carcinoma, where *SMO* functions as an oncogene (Xie et al., 1998). The identified mutations affect multiple domains of *SMO* including the carboxyl-terminal tail, transmembrane domains of SMO, and the binding pocket of the transmembrane domains [reviewed by (Arensdorf et al., 2016)]. SMO is an attractive therapeutic target of HH signaling due to its multiple binding sites, which could be targeted to regulate aberrant activity in HH-dependent cancers. Taking advantage of this, pharmacological treatments like GDC-0449 (Vismodegib) targeting SMO have been developed (Robarge et al., 2009). Vismodegib is the first targeted inhibitor of the HH signaling pathway approved by the United States Food and Drug Administration [reviewed by (Rudin, 2012)]. This treatment produced promising anti-tumor responses, causing tumor

regression in different cancers like basal cell carcinoma and medulloblastoma (Von Hoff et al., 2009; Yauch et al., 2009). However, certain tumors become drug resistant after treatment with Vismodegib, due to a point mutation that disrupted the binding of the drug (Rudin et al., 2009; Yauch et al., 2009). This resistance results from outgrowth of drug-resistant clones from the original tumor or from *de novo* mutations (Sharpe et al., 2015). New therapies are being developed to avoid this drug-resistance by developing other drugs that bind SMO at sites distinct from Vismodegib, or by targeting HH signaling downstream of SMO (Long et al., 2014).

#### G-protein coupled receptor 161 (GPR161)

GPR161 is an orphan class A conserved GPCR, identified in a screen of cultured IMCD3 cells, with the purpose of identifying novel receptors that negatively regulated SHH signaling (Mukhopadhyay et al., 2013). This receptor was previously implicated as a locus that encodes the vacuolated lens mutation, which causes congenital cataracts and neural tube defects (Matteson et al., 2008). GPCRs are part of large superfamily of proteins that contain seven transmembrane spanning domains, and the capacity to modulate intracellular metabolism through the activation of heterotrimeric GTP-binding proteins (Gainetdinov et al., 2004). At early stages of mouse development, *Gpr161* is ubiquitously expressed (Matteson et al., 2008; Mukhopadhyay et al., 2013). At mid-gestation *Gpr161* is restricted to the brain, spinal cord, dorsal ganglia, and at lower levels in the hindlimb (Mukhopadhyay et al., 2013). In a variety of ciliated cell types, GPR161 localization is confined to the primary cilium (Mukhopadhyay et al., 2013), a structure required for proper HH signal transduction (Goetz and Anderson, 2010). Homozygous *Gpr161* mutant mouse embryos are embryonically lethal at E10.5 (Mukhopadhyay et al., 2013). Phenotypically, these embryos exhibit extensive craniofacial abnormalities, open

forebrain/midbrain region, a ventralized neural tube and lack of limbs buds (Mukhopadhyay et al., 2013). *Gpr161* mutants resemble embryos lacking TULP3 (Tubby-like protein)/Intraflagellar transport-A mutants (IFT-A), which mediate the trafficking of GPCR proteins to the primary cilium and also regulate GPR161 (Mukhopadhyay et al., 2010; Svard et al., 2006). Additionally, GPR161 has been implicated in the restriction of the medulloblastoma pathogenesis, a cancer that originates in the cerebellum from dysregulation of SHH signaling (Shimada et al., 2018). All these characteristic phenotypes and expression patterns of *Gpr161* suggested that this protein could negatively regulate HH signaling during vertebrate embryogenesis. This was further confirmed by the upregulated levels of *Gli1* and *Ptch1* detected in E9.5 and E10.5 *Gpr161* mutant embryos by in situ hybridization and qPCR (Mukhopadhyay et al., 2013). Additionally, these embryos display a striking expansion of HH-dependent ventral neuronal progenitors in the neural tube, and defects in the processing of GLI2 and GLI3 (Mukhopadhyay et al., 2013). Overexpression of GPR161 results in increased levels of cyclic adenosine monophosphate (cAMP), which in turn activates protein kinase A (PKA), which regulates GLI processing (Mukhopadhyay et al., 2013; Tuson et al., 2011). Specifically, GPR161 regulates the levels of GLI3 by processing it into its repressor form (Mukhopadhyay et al., 2013). Recently, other studies have also reported GPR161 can repress HH signaling in other tissues like the forebrain and limb, where it is required for proper patterning (Hwang et al., 2018; Shimada et al., 2019). Overall, these studies demonstrate that GPR161 is a negative regulator of the SHH signaling pathway that acts through the regulation of GLI transcription factors.

Neuropilins (NRPs)



NRPs are transmembrane glycoproteins from the semaphorin family, initially identified in *Xenopus* tadpoles neuronal screens as targets of monoclonal antibodies against the optic tectum (Takagi et al., 1987). Based on the name of the monoclonal antibody that identified this novel protein, originally it was named A5. Subsequent studies identified that the target recognized by the A5 monoclonal antibody, encoded a 140kDa protein that was highly conserved among organisms, including chicken and mouse (Kawakami et al., 1996) (Takagi et al., 1991; Takagi et al., 1995). However, later it was renamed NRP1 due to its characteristic expression in the nerve terminals, or neuropils of the optic nerve and other specific regions of the nervous system [reviewed by (Fujisawa et al., 1997)]. Mammals possess two NRP genes, *NRP1* and *NRP2*, which share 44 % amino acid identity homology and possess similar structural domains (Chen et al., 1997; Kolodkin et al., 1997). Structurally NRPs are comprised of a large extracellular domain that contains five sub domains known as a1/a2, b1/b2 and c, a transmembrane domain and a short cytoplasmic domain (Takagi et al., 1991). The extracellular domain of NRPs consist of two CUB motifs (a1/a2), which share sequence homology to C1r and C1s proteins, two domains that are homologous coagulation factors V and VIII (b1/b2), and a membrane-proximal meprin MAM domain (c) (Kawakami et al., 1996; Takagi et al., 1991). The extracellular domains a1/a2 and b1/b2 serve as binding sites for two unrelated families of ligands; class 3 Semaphorin (SEMA) ligands and vascular endothelial growth factor (VEGF), which bind to NRP1 and NRP2 with different specificity (Chen et al., 1997; Giger et al., 1998; Gluzman-Poltorak et al., 2000; He and Tessier-Lavigne, 1997; Kolodkin et al., 1997; Makinen et al., 1999; Migdal et al., 1998; Soker et al., 1998; Takahashi et al., 1998). The NRP transmembrane domain is responsible for mediating dimerization and oligomerization through a double GXXXG motif, which stabilizes the formation of signaling complexes (Roth et al., 2008).

While the NRP cytoplasmic domain does not resemble any other protein motif and does not perform any catalytic activity, this domain does possess a C-terminal SEA (serine-glutamine-alanine) motif that interacts with intracellular proteins containing a PSD-95/Dlg/ZO-1 (PDZ)-domain.

The major function ascribed to NRPs has been a central role in axon guidance as part of the SEMA signaling pathway. In this context, NRPs function as co-receptors with the plexin (PLXN) family of proteins to mediate SEMA signal transduction [reviewed by (Zhou et al., 2008)]. These proteins can preferentially form different complexes, which function in a specific manner during axonal growth cone, regulating attraction and repulsion during axon guidance, [reviewed by (Tata, 2015) (Zhou et al., 2008)].

NRPs also function as co-receptors, along with VEGF receptors (VEGFR), for VEGF ligands. VEGF interactions with NRP VEGFR induce angiogenesis by forming distinct receptor complexes that enhance VEGF ligand binding and subsequently activate downstream signaling [reviewed by (Klagsbrun et al., 2002)].

During mouse embryogenesis NRPs are expressed in the axons of actively growing neurons of specific neuronal populations, the cardiovascular and skeletal system, and in the limb at different developmental stages (Kawakami et al., 1996; Kitsukawa et al., 1995; Kolodkin et al., 1997). Notably, despite the structural similarity between NRP1 and NRP2, their expression patterns are not completely overlapping. Multiple studies have shown that there are various transmembrane and truncated isoforms of NRPs that are generated from alternative splicing, which exhibit tissue-specific expression, suggesting distinct roles for these isoforms (Cackowski et al., 2004; Gagnon et al., 2000; Rossignol et al., 2000). Deletion of *Nrp1* in mice results in embryonic lethality around E12.5-E13.5 due to cardiovascular defects (Kawasaki et al., 1999).

Specifically, *Nrp1* mutants embryos display severe disruption in the vasculature of the yolk sac, the CNS and the peripheral nervous system, heart outflow tracts defects and disorganized branchial arch arteries and great vessels (Kawasaki et al., 1999). Additionally, these mutants exhibit defects in the trajectory of the cranial and spinal efferent fibers which express NRP1 (Kitsukawa et al., 1997). In contrast, *Nrp2* mutants are viable, with normal vascular phenotypes; but they display defects in axonal projections in CNS and peripheral nervous system (Chen et al., 2000; Giger et al., 2000). Mouse embryos lacking both NRPs die in utero at E8.5 with some mutants that die at even earlier embryonic stages (Takashima et al., 2002). E8.5 *Nrp1*<sup>-/-</sup>;*Nrp2*<sup>-/-</sup> embryos display severe growth defects, abnormal blood vessel development and totally avascular yolk sacs (Takashima et al., 2002). Together, NRP1 and NRP2 are important regulators of axon guidance and angiogenesis; nonetheless, their function is not limited to these biological processes.

NRPs also regulate mammalian HH signaling. An RNAi screen in HH-responsive fibroblasts revealed a requirement for *Nrp1* and *Nrp2* in HH pathway activation (Hillman et al., 2011). Further, morpholino knockdown of *Nrp1a* in zebrafish embryos resulted in ventral body curvature and U-shaped somites, a phenotype consistent with HH pathway loss-of-function (Hillman et al., 2011). More recently, the tissue-specific deletion of *Nrp1* in cerebellar granular progenitors (CGNP), a HH-responsive cell type, in a *Nrp2* null background, results in decreased levels of *Gli1* transcript and protein, and reduced CGNP proliferation (Ge et al., 2015).

Conversely overexpression of NRP1 and NRP2 in NIH3T3 fibroblasts increased HH pathway activity after stimulation with HH ligand (Hillman et al., 2011; Pinsky et al., 2017). However, combined stimulation of SHH with SEMA3A or SEMA3F in NIH3T3 fibroblasts, significantly enhanced the SHH-induced transcription of *Gli1* (Ge et al., 2015). Although, SEMA

ligands do not induce *Gli1* expression by themselves, disruption of the NRP-SEMA3 interaction with function-blocking NRP antibodies in the presence of HH ligand, decreases the levels of *Gli1* in NIH3T3 cells (Ge et al., 2015). These data suggest that NRPs can enhance HH signal transduction in presence of HH ligands, and through SEMA3 ligands. However, more studies will be necessary to understand the requirement of the SEMA3 ligands in HH signal transduction, since there are some contradictory results regarding the NRPs domains that promote HH activity. (Ge et al., 2015) demonstrated that the a1/a2 domains and the cytoplasmic domains of NRP1 are required to promote HH signaling, while the b1/b2 domains are dispensable. In contrast, (Pinskey et al., 2017) demonstrated that the cytoplasmic domain and transmembrane domain are necessary and sufficient to activate HH pathway function. Moreover, (Pinskey et al., 2017) identified a novel 12-amino acid motif within the membrane-proximal half of the NRP-1 cytoplasmic domain that is critical for HH activity promotion. Despite the discrepancies in the requirements for the SEMA 3 ligands, several studies suggest that NRPs regulate HH signaling through the modulation of GLI activity. Initially, (Hillman et al., 2011) suggested that *Nrps* regulate HH signaling at the level of Suppressor of Fused (SUFU); a negative regulator of the pathway. (Ge et al., 2015) proposed a model where NRPs function downstream of SUFU by regulating GLI phosphorylation through interactions with phosphodiesterase 4D (PDE4D), which inhibits PKA, a negative regulator of HH signaling. In contrast, (Pinskey et al., 2017) suggested that NRPs promote HH signaling selectively at the level of GLI and independently of PKA phosphorylation. Based on these results, the cytoplasmic domain of NRP is critical to mediate HH signaling transduction, but additional mechanistic experiments will be required to understand the how the cytoplasmic domain interacts and recruits different proteins and how they regulate HH signaling collectively.

NRPs have been also implicated in various HH driven cancers including human medulloblastoma (Ge et al., 2015; Hayden Gephart et al., 2013; Snuderl et al., 2013), where both *Nrp1* and *Nrp2* are highly expressed (Snuderl et al., 2013). In medulloblastoma (Snuderl et al., 2013), suggested that tumor-secreted SHH stimulates the stromal production of the Placental Growth Factor (PlGF), a VEGF family member, which promotes the growth and spread of medulloblastoma. Additionally, pharmacological inhibition of the PDE4D enzyme inhibited tumor growth in mouse medulloblastoma tumors resistant to SMO inhibitors (Ge et al., 2015). These data establish NRPs as positive regulators of HH signaling during development and identify NRPs as potential novel therapeutic targets for HH-driven cancers.

#### **1.4 Tissue specific roles for GAS1, CDON and BOC**

GAS, CDON and BOC are generally known as HH co-receptors based on their collective requirement to promote HH signaling, similar expression profiles during development and their capability to bind to HH ligands (Allen et al., 2011; Bae et al., 2011; Izzi et al., 2011; Lee et al., 2001a; Lee and Fan, 2001; McLellan et al., 2008; Mulieri et al., 2002; Mulieri et al., 2000). Genetic evidence in mice and *Drosophila* demonstrate that these proteins are essential to mediate HH signal transduction and in some cases function redundantly (Allen et al., 2011; Allen et al., 2007; Yao et al., 2006; Zheng et al., 2010). However, there are several lines of evidence that indicate that these proteins could regulate HH signaling in a tissue-specific manner. First, even though these co-receptors are expressed similarly throughout development, there are differences in their spatiotemporal expression (Lee and Fan, 2001; Mulieri et al., 2002; Mulieri et al., 2000). In mice, their expression is first detected during different early embryonic stages, *Gas1* at E6.5, *Cdon* at E7.0 and *Boc* at E.7.5 (Lee and Fan, 2001; Mulieri et al., 2002; Mulieri et al., 2000).

Throughout development their expression patterns are mostly restricted to the same structures. However, the extent of their expression domains and their expression in relation to HH ligand source varies among tissues. GAS1 is broadly expressed in the neural tube, craniofacial structures, limbs (Figure 2.2). In contrast, CDON expression domains in these same tissues are more restricted; while BOC expression is similar to GAS1, however it extends closer to the HH ligand source (Figure 2.2). These subtle expression differences will provide critical information to understand how these proteins regulate HH signaling and how they could interact with other proteins. The differential expression of GAS1, CDON and BOC during development suggest that these proteins could mediate distinct functions in certain tissues.

The HH co-receptors can also interact with PTCH1 and PTCH2 and form distinct SHH receptor complexes; suggesting that they could function independently of each other (Bae et al., 2011; Holtz et al., 2013; Izzi et al., 2011). This is also supported by non-overlapping functions of GAS1, CDON and BOC in different tissues. For example, some unique roles for the HH co-receptors include: GAS1 as a regulator of enteric axon projections, CDON as a dependence receptor to promote apoptosis in absence of SHH, and BOC as regulator of SHH-dependent axon guidance (Jin et al., 2015; Kang et al., 2002; Okada et al., 2006). Additionally, CDON and BOC can form complexes in a *cis* fashion through the interactions of their extracellular and intracellular domains; the significance of this interaction for HH signaling has yet to be determined (Kang et al., 2002). The interactions of the HH co-receptors with other cell surface regulators could provide different combinations of SHH receptor complexes that could differentially regulate HH signaling in different tissues.

GAS1, CDON and BOC have been extensively analyzed as positive regulators of HH signaling. However, there is evidence that in certain tissues HH co-receptors can function as HH

pathway antagonists. Initially the first co-receptor described to antagonize HH signaling was GAS1, in presomitic mesoderm and tooth bud explants in mice (Cobourne et al., 2004; Lee et al., 2001a; Ohazama et al., 2009). Additionally, it has been shown that *Cdon* can antagonize HH signaling in the optic vesicle of chicken and zebrafish embryos (Cardozo et al., 2014). Lastly, recent studies suggest that *Boc* can antagonize HH signaling in the zebrafish lower jaw (Bergeron et al., 2011). However, this study does not show direct evidence that *Boc* is a HH pathway antagonist (Bergeron et al., 2011). Their analysis is limited to the description of a phenotype and does not examine the levels of the HH transcriptional targets. It is still unknown how the HH co-receptors can differentially regulate HH signaling across different tissues and organisms. These dual (promotion/inhibition) functions of the HH co-receptors could explain how the HH signaling pathway patterns different structures during vertebrate embryogenesis.

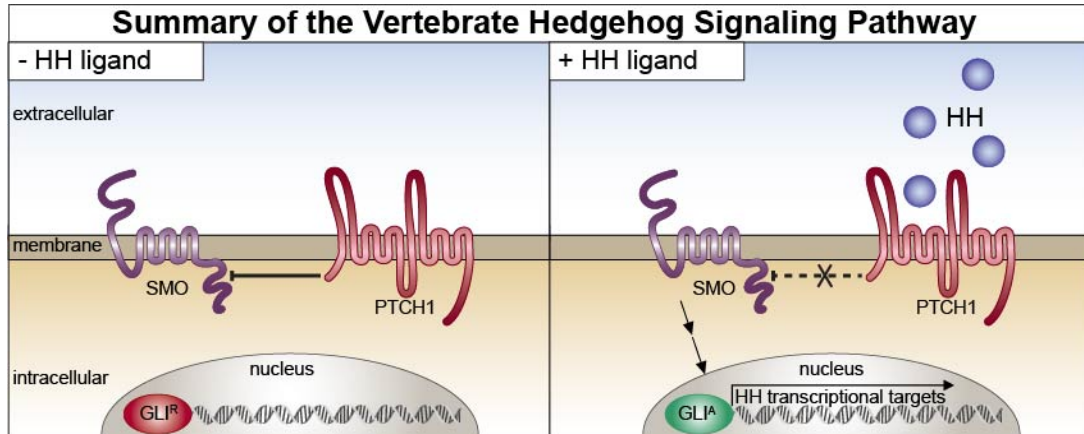
## **1.5 Conclusion**

The expression patterns of the HH co-receptors, their different phenotypes in HH responsive tissues, and their identified dual roles, suggest that these proteins are not functionally redundant. This raises the possibility that the HH co-receptors function in a tissue-specific manner to differentially regulate HH signaling. In this dissertation, my main objectives were to: 1) investigate novel tissue-specific roles for the HH co-receptors and 2) elucidate HH co-receptor function during vertebrate embryogenesis. Chapter two will focus on exploring HH co-receptor function in craniofacial development. In this chapter I provide evidence that indicates that BOC works in opposition to GAS1 and CDON during craniofacial development, by antagonizing HH signaling. Also, I demonstrate that this novel antagonistic role mediated by BOC is restricted to the craniofacial structures. Further, I show that the deletion of *Boc* in a *Gas1* null mutant

background ameliorates the HPE phenotype observed in *Gas1* single mutants. Chapter 3 provides evidence for a novel role for CDON during HH-dependent digit specification. In this chapter, I utilize a novel *Cdon* conditional allele to simultaneously delete *Gas1*, *Cdon* and *Boc*, specifically in the limb. In Chapter 4, I discuss the interpretation of my data and propose future directions for my work. Overall the data presented here demonstrates that HH co-receptors are multi-functional, tissue-specific regulators of HH signaling during vertebrate embryogenesis.



## 1.6 Figures



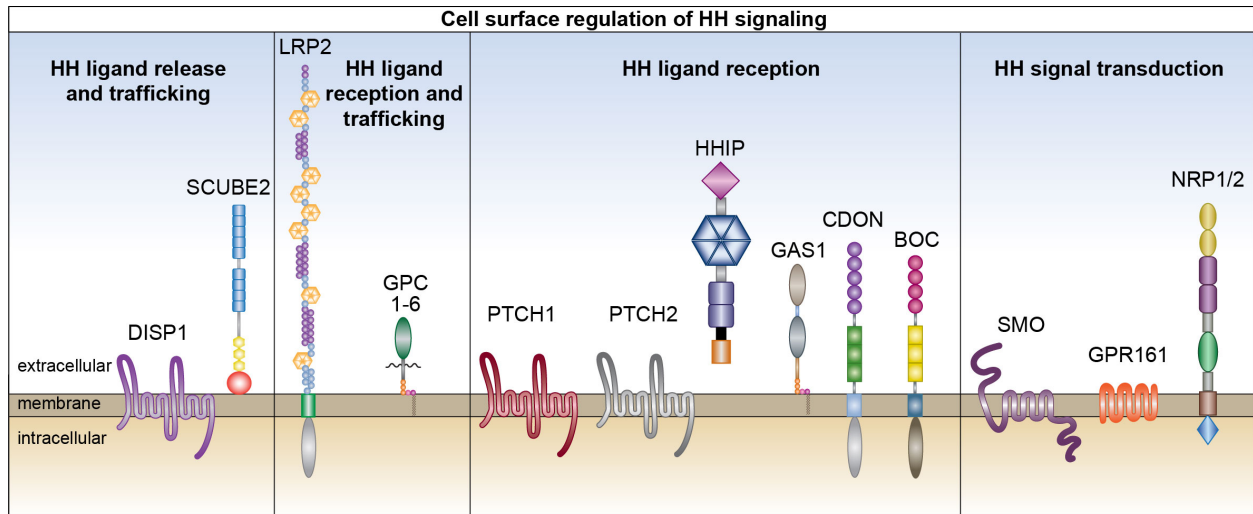
**Figure 1.1 Summary of vertebrate HH signal transduction**

(Left panel) In the absence of HH ligand, PTCH1 inhibits SMO, resulting in the processing of GLI transcription factors into repressors that inhibit HH target gene expression. (Right panel) In the presence of HH ligand, HH binds to PTCH1, leading to de-repression of SMO and subsequent processing of GLI transcription factors into activators that induce HH target gene expression. Abbreviations: repressor (R) and activator (A).

E10.5 HH-responsive tissues	Forebrain	Neural tube	Limb bud
<div style="display: flex; flex-direction: column; gap: 5px;"> <div><span style="display: inline-block; width: 15px; height: 10px; background-color: yellow; border: 1px solid black;"></span> Mesenchyme</div> <div><span style="display: inline-block; width: 15px; height: 10px; background-color: purple; border: 1px solid black;"></span> Neuroepithelium</div> <div><span style="display: inline-block; width: 15px; height: 10px; background-color: teal; border: 1px solid black;"></span> Surface ectoderm</div> <div><span style="display: inline-block; width: 15px; height: 10px; background-color: red; border: 1px solid black;"></span> <i>Shh</i> expression</div> </div>			
<b>HH-mediated cellular responses</b>			
<b>Patterning</b>	Yes	Yes	Yes
<b>Proliferation</b>	Yes	Yes	Yes
<b>Survival</b>	Yes	Yes	Yes

**Figure 1.2 *Shh* expression and function in E10.5 mouse tissues.**

(Top panel) *Shh* expression in E10.5 mouse forebrain, neural tube, and limb bud. Colors denote mesenchyme (yellow), neuroepithelium (purple), surface ectoderm (green) and *Shh* expression domain (red). At E10.5 *Shh* is expressed in the following structures: in the forebrain is expressed the ventral telencephalon and the medial nasal process; in the neural tube is expressed in the notochord and floorplate and in the limb bud in the posterior mesenchyme (zone of polarizing activity). (Bottom panel) Summary of SHH-mediated cellular responses in the forebrain, neural tube and limb bud.



**Figure 1.3 Cell surface regulation of HH signaling.**

(First panel) Cell surface proteins that regulate HH ligand release and trafficking, Dispatched (DISP1) and Signal sequence-CUB domain-epidermal growth factor like-related 2 (SCUBE2). (Second panel) Cell surface proteins that regulate HH ligand reception and trafficking, Low-density lipoprotein receptor- related protein 2 (LRP2) and Glypicans (GPC1-6). (Third panel) Cell surface proteins that regulate HH ligand reception, Patched 1 (PTCH1), Patched 2 (PTCH2), HH-interacting protein (HHIP), Growth arrest-specific 1 (GAS1), Cell adhesion molecule – related /down-regulated by oncogenes (CDON) and Brother of Cdon (BOC). (Fourth panel) Cell surface proteins that regulate HH signal transduction, Smoothened (SMO), G-protein couple receptor 161 (GPR161) and Neuropilin1/2 (NRP1/2). Note that common domains of these proteins are not represented by the same shape across the different proteins. This figure was adapted from (Beachy et al., 2010; Christ et al., 2016)

## 1.7 References

- Aberger, F. and Ruiz, I. A. A.** (2014). Context-dependent signal integration by the GLI code: the oncogenic load, pathways, modifiers and implications for cancer therapy. *Semin Cell Dev Biol* **33**, 93-104.
- Agren, M., Kogerman, P., Kleman, M. I., Wessling, M. and Toftgard, R.** (2004). Expression of the PTCH1 tumor suppressor gene is regulated by alternative promoters and a single functional Gli-binding site. *Gene* **330**, 101-114.
- Ahlgren, S. C. and Bronner-Fraser, M.** (1999). Inhibition of sonic hedgehog signaling in vivo results in craniofacial neural crest cell death. *Curr Biol* **9**, 1304-1314.
- Alcedo, J., Ayzenzon, M., Von Ohlen, T., Noll, M. and Hooper, J. E.** (1996). The Drosophila smoothed gene encodes a seven-pass membrane protein, a putative receptor for the hedgehog signal. *Cell* **86**, 221-232.
- Alexandre, C., Jacinto, A. and Ingham, P. W.** (1996). Transcriptional activation of hedgehog target genes in Drosophila is mediated directly by the cubitus interruptus protein, a member of the GLI family of zinc finger DNA-binding proteins. *Genes Dev* **10**, 2003-2013.
- Alfaro, A. C., Roberts, B., Kwong, L., Bijlsma, M. F. and Roelink, H.** (2014). Ptch2 mediates the Shh response in Ptch1<sup>-/-</sup> cells. *Development* **141**, 3331-3339.
- Allen, B. L., Song, J. Y., Izzi, L., Althaus, I. W., Kang, J. S., Charron, F., Krauss, R. S. and McMahon, A. P.** (2011). Overlapping roles and collective requirement for the coreceptors GAS1, CDO, and BOC in SHH pathway function. *Dev Cell* **20**, 775-787.
- Allen, B. L., Tenzen, T. and McMahon, A. P.** (2007). The Hedgehog-binding proteins Gas1 and Cdo cooperate to positively regulate Shh signaling during mouse development. *Genes Dev* **21**, 1244-1257.
- Aoto, K., Shikata, Y., Imai, H., Matsumaru, D., Tokunaga, T., Shioda, S., Yamada, G. and Motoyama, J.** (2009). Mouse Shh is required for prechordal plate maintenance during brain and craniofacial morphogenesis. *Dev Biol* **327**, 106-120.
- Arendorf, A. M., Marada, S. and Ogden, S. K.** (2016). Smoothed Regulation: A Tale of Two Signals. *Trends Pharmacol Sci* **37**, 62-72.
- Bae, G. U., Domene, S., Roessler, E., Schachter, K., Kang, J. S., Muenke, M. and Krauss, R. S.** (2011). Mutations in CDON, encoding a hedgehog receptor, result in holoprosencephaly and defective interactions with other hedgehog receptors. *Am J Hum Genet* **89**, 231-240.
- Barakat, M. T., Humke, E. W. and Scott, M. P.** (2010). Learning from Jekyll to control Hyde: Hedgehog signaling in development and cancer. *Trends Mol Med* **16**, 337-348.

**Bastida, M. F., Delgado, M. D., Wang, B., Fallon, J. F., Fernandez-Teran, M. and Ros, M. A.** (2004). Levels of Gli3 repressor correlate with Bmp4 expression and apoptosis during limb development. *Dev Dyn* **231**, 148-160.

**Beachy, P. A., Hymowitz, S. G., Lazarus, R. A., Leahy, D. J. and Siebold, C.** (2010). Interactions between Hedgehog proteins and their binding partners come into view. *Genes Dev* **24**, 2001-2012.

**Belloni, E., Muenke, M., Roessler, E., Traverso, G., Siegel-Bartelt, J., Frumkin, A., Mitchell, H. F., Donis-Keller, H., Helms, C., Hing, A. V., et al.** (1996). Identification of Sonic hedgehog as a candidate gene responsible for holoprosencephaly. *Nat Genet* **14**, 353-356.

**Belo, J. A., Leyns, L., Yamada, G. and De Robertis, E. M.** (1998). The prechordal midline of the chondrocranium is defective in Goosecoid-1 mouse mutants. *Mech Dev* **72**, 15-25.

**Bergeron, S. A., Tyurina, O. V., Miller, E., Bagas, A. and Karlstrom, R. O.** (2011). Brother of cdo (umleitung) is cell-autonomously required for Hedgehog-mediated ventral CNS patterning in the zebrafish. *Development* **138**, 75-85.

**Bidet, M., Joubert, O., Lacombe, B., Ciantar, M., Nehme, R., Mollat, P., Bretillon, L., Faure, H., Bittman, R., Ruat, M., et al.** (2011). The hedgehog receptor patched is involved in cholesterol transport. *PLoS One* **6**, e23834.

**Bischoff, M., Gradilla, A. C., Seijo, I., Andres, G., Rodriguez-Navas, C., Gonzalez-Mendez, L. and Guerrero, I.** (2013). Cytonemes are required for the establishment of a normal Hedgehog morphogen gradient in *Drosophila* epithelia. *Nat Cell Biol* **15**, 1269-1281.

**Bishop, B., Aricescu, A. R., Harlos, K., O'Callaghan, C. A., Jones, E. Y. and Siebold, C.** (2009). Structural insights into hedgehog ligand sequestration by the human hedgehog-interacting protein HHIP. *Nat Struct Mol Biol* **16**, 698-703.

**Bitgood, M. J. and McMahon, A. P.** (1995). Hedgehog and Bmp genes are coexpressed at many diverse sites of cell-cell interaction in the mouse embryo. *Dev Biol* **172**, 126-138.

**Bitgood, M. J., Shen, L. and McMahon, A. P.** (1996). Sertoli cell signaling by Desert hedgehog regulates the male germline. *Curr Biol* **6**, 298-304.

**Bosanac, I., Maun, H. R., Scales, S. J., Wen, X., Lingel, A., Bazan, J. F., de Sauvage, F. J., Hymowitz, S. G. and Lazarus, R. A.** (2009). The structure of SHH in complex with HHIP reveals a recognition role for the Shh pseudo active site in signaling. *Nat Struct Mol Biol* **16**, 691-697.

**Briscoe, J. and Ericson, J.** (1999). The specification of neuronal identity by graded Sonic Hedgehog signalling. *Semin Cell Dev Biol* **10**, 353-362.

**Briscoe, J., Pierani, A., Jessell, T. M. and Ericson, J.** (2000). A homeodomain protein code specifies progenitor cell identity and neuronal fate in the ventral neural tube. *Cell* **101**, 435-445.

- Briscoe, J. and Therond, P. P.** (2013). The mechanisms of Hedgehog signalling and its roles in development and disease. *Nat Rev Mol Cell Biol* **14**, 416-429.
- Bumcrot, D. A., Takada, R. and McMahon, A. P.** (1995). Proteolytic processing yields two secreted forms of sonic hedgehog. *Mol Cell Biol* **15**, 2294-2303.
- Burke, R., Nellen, D., Bellotto, M., Hafen, E., Senti, K. A., Dickson, B. J. and Basler, K.** (1999). Dispatched, a novel sterol-sensing domain protein dedicated to the release of cholesterol-modified hedgehog from signaling cells. *Cell* **99**, 803-815.
- Cabrera, J. R., Sanchez-Pulido, L., Rojas, A. M., Valencia, A., Manes, S., Naranjo, J. R. and Mellstrom, B.** (2006). Gas1 is related to the glial cell-derived neurotrophic factor family receptors alpha and regulates Ret signaling. *J Biol Chem* **281**, 14330-14339.
- Cackowski, F. C., Xu, L., Hu, B. and Cheng, S. Y.** (2004). Identification of two novel alternatively spliced Neuropilin-1 isoforms. *Genomics* **84**, 82-94.
- Camp, D., Currie, K., Labbe, A., van Meyel, D. J. and Charron, F.** (2010). Ihog and Boi are essential for Hedgehog signaling in Drosophila. *Neural Dev* **5**, 28.
- Camp, D., Haitian He, B., Li, S., Althaus, I. W., Holtz, A. M., Allen, B. L., Charron, F. and van Meyel, D. J.** (2014). Ihog and Boi elicit Hh signaling via Ptc but do not aid Ptc in sequestering the Hh ligand. *Development* **141**, 3879-3888.
- Capdevila, J. and Izpisua Belmonte, J. C.** (2001). Patterning mechanisms controlling vertebrate limb development. *Annu Rev Cell Dev Biol* **17**, 87-132.
- Capurro, M. I., Shi, W. and Filmus, J.** (2012). LRP1 mediates Hedgehog-induced endocytosis of the GPC3-Hedgehog complex. *J Cell Sci* **125**, 3380-3389.
- Capurro, M. I., Xu, P., Shi, W., Li, F., Jia, A. and Filmus, J.** (2008). Glypican-3 inhibits Hedgehog signaling during development by competing with patched for Hedgehog binding. *Dev Cell* **14**, 700-711.
- Cardozo, M. J., Sanchez-Arrones, L., Sandonis, A., Sanchez-Camacho, C., Gestri, G., Wilson, S. W., Guerrero, I. and Bovolenta, P.** (2014). Cdon acts as a Hedgehog decoy receptor during proximal-distal patterning of the optic vesicle. *Nat Commun* **5**, 4272.
- Carpenter, D., Stone, D. M., Brush, J., Ryan, A., Armanini, M., Frantz, G., Rosenthal, A. and de Sauvage, F. J.** (1998). Characterization of two patched receptors for the vertebrate hedgehog protein family. *Proc Natl Acad Sci U S A* **95**, 13630-13634.
- Carstea, E. D., Morris, J. A., Coleman, K. G., Loftus, S. K., Zhang, D., Cummings, C., Gu, J., Rosenfeld, M. A., Pavan, W. J., Krizman, D. B., et al.** (1997). Niemann-Pick C1 disease gene: homology to mediators of cholesterol homeostasis. *Science* **277**, 228-231.

- Caspary, T., Garcia-Garcia, M. J., Huangfu, D., Eggenchwiler, J. T., Wyler, M. R., Rakeman, A. S., Alcorn, H. L. and Anderson, K. V.** (2002). Mouse Dispatched homolog1 is required for long-range, but not juxtacrine, Hh signaling. *Curr Biol* **12**, 1628-1632.
- Castaldi, P. J., Cho, M. H., San Jose Estepar, R., McDonald, M. L., Laird, N., Beaty, T. H., Washko, G., Crapo, J. D., Silverman, E. K. and Investigators, C. O.** (2014). Genome-wide association identifies regulatory Loci associated with distinct local histogram emphysema patterns. *Am J Respir Crit Care Med* **190**, 399-409.
- Cayuso, J., Ulloa, F., Cox, B., Briscoe, J. and Martí, E.** (2006). The Sonic hedgehog pathway independently controls the patterning, proliferation and survival of neuroepithelial cells by regulating Gli activity. *Development* **133**, 517-528.
- Chai, Y. and Maxson, R. E., Jr.** (2006). Recent advances in craniofacial morphogenesis. *Dev Dyn* **235**, 2353-2375.
- Chamoun, Z., Mann, R. K., Nellen, D., von Kessler, D. P., Bellotto, M., Beachy, P. A. and Basler, K.** (2001). Skinny hedgehog, an acyltransferase required for palmitoylation and activity of the hedgehog signal. *Science* **293**, 2080-2084.
- Chen, H., Bagri, A., Zupicich, J. A., Zou, Y., Stoeckli, E., Pleasure, S. J., Lowenstein, D. H., Skarnes, W. C., Chedotal, A. and Tessier-Lavigne, M.** (2000). Neuropilin-2 regulates the development of selective cranial and sensory nerves and hippocampal mossy fiber projections. *Neuron* **25**, 43-56.
- Chen, H., Chedotal, A., He, Z., Goodman, C. S. and Tessier-Lavigne, M.** (1997). Neuropilin-2, a novel member of the neuropilin family, is a high affinity receptor for the semaphorins Sema E and Sema IV but not Sema III. *Neuron* **19**, 547-559.
- Chen, J. K., Taipale, J., Cooper, M. K. and Beachy, P. A.** (2002a). Inhibition of Hedgehog signaling by direct binding of cyclopamine to Smoothed. *Genes Dev* **16**, 2743-2748.
- Chen, J. K., Taipale, J., Young, K. E., Maiti, T. and Beachy, P. A.** (2002b). Small molecule modulation of Smoothed activity. *Proc Natl Acad Sci U S A* **99**, 14071-14076.
- Chen, M. H., Li, Y. J., Kawakami, T., Xu, S. M. and Chuang, P. T.** (2004). Palmitoylation is required for the production of a soluble multimeric Hedgehog protein complex and long-range signaling in vertebrates. *Genes Dev* **18**, 641-659.
- Chen, Y., Sasai, N., Ma, G., Yue, T., Jia, J., Briscoe, J. and Jiang, J.** (2011). Sonic Hedgehog dependent phosphorylation by CK1alpha and GRK2 is required for ciliary accumulation and activation of smoothed. *PLoS Biol* **9**, e1001083.
- Chen, Y. and Struhl, G.** (1996). Dual roles for patched in sequestering and transducing Hedgehog. *Cell* **87**, 553-563.

**Chiang, C., Litington, Y., Lee, E., Young, K. E., Corden, J. L., Westphal, H. and Beachy, P. A.** (1996). Cyclopia and defective axial patterning in mice lacking Sonic hedgehog gene function. *Nature* **383**, 407-413.

**Christ, A., Christa, A., Klippert, J., Eule, J. C., Bachmann, S., Wallace, V. A., Hammes, A. and Willnow, T. E.** (2015). LRP2 Acts as SHH Clearance Receptor to Protect the Retinal Margin from Mitogenic Stimuli. *Dev Cell* **35**, 36-48.

**Christ, A., Christa, A., Kur, E., Lioubinski, O., Bachmann, S., Willnow, T. E. and Hammes, A.** (2012). LRP2 is an auxiliary SHH receptor required to condition the forebrain ventral midline for inductive signals. *Dev Cell* **22**, 268-278.

**Christ, A., Herzog, K. and Willnow, T. E.** (2016). LRP2, an auxiliary receptor that controls sonic hedgehog signaling in development and disease. *Dev Dyn* **245**, 569-579.

**Christensen, E. I. and Birn, H.** (2002). Megalin and cubilin: multifunctional endocytic receptors. *Nat Rev Mol Cell Biol* **3**, 256-266.

**Chuang, P. T., Kawcak, T. and McMahon, A. P.** (2003). Feedback control of mammalian Hedgehog signaling by the Hedgehog-binding protein, Hip1, modulates Fgf signaling during branching morphogenesis of the lung. *Genes Dev* **17**, 342-347.

**Chuang, P. T. and McMahon, A. P.** (1999). Vertebrate Hedgehog signalling modulated by induction of a Hedgehog-binding protein. *Nature* **397**, 617-621.

**Chung, U. I., Schipani, E., McMahon, A. P. and Kronenberg, H. M.** (2001). Indian hedgehog couples chondrogenesis to osteogenesis in endochondral bone development. *J Clin Invest* **107**, 295-304.

**Clark, A. M., Garland, K. K. and Russell, L. D.** (2000). Desert hedgehog (Dhh) gene is required in the mouse testis for formation of adult-type Leydig cells and normal development of peritubular cells and seminiferous tubules. *Biol Reprod* **63**, 1825-1838.

**Cobourne, M. T., Miletich, I. and Sharpe, P. T.** (2004). Restriction of sonic hedgehog signalling during early tooth development. *Development* **131**, 2875-2885.

**Cole, F. and Krauss, R. S.** (2003). Microform holoprosencephaly in mice that lack the Ig superfamily member Cdon. *Curr Biol* **13**, 411-415.

**Corcoran, R. B. and Scott, M. P.** (2006). Oxysterols stimulate Sonic hedgehog signal transduction and proliferation of medulloblastoma cells. *Proc Natl Acad Sci U S A* **103**, 8408-8413.

**Cordero, D., Marcucio, R., Hu, D., Gaffield, W., Tapadia, M. and Helms, J. A.** (2004). Temporal perturbations in sonic hedgehog signaling elicit the spectrum of holoprosencephaly phenotypes. *J Clin Invest* **114**, 485-494.

- Coulombe, J., Traiffort, E., Loulier, K., Faure, H. and Ruat, M.** (2004). Hedgehog interacting protein in the mature brain: membrane-associated and soluble forms. *Mol Cell Neurosci* **25**, 323-333.
- Creanga, A., Glenn, T. D., Mann, R. K., Saunders, A. M., Talbot, W. S. and Beachy, P. A.** (2012). Scube/You activity mediates release of dually lipid-modified Hedgehog signal in soluble form. *Genes Dev* **26**, 1312-1325.
- Cui, S., Leyva-Vega, M., Tsai, E. A., EauClaire, S. F., Glessner, J. T., Hakonarson, H., Devoto, M., Haber, B. A., Spinner, N. B. and Matthews, R. P.** (2013). Evidence from human and zebrafish that GPC1 is a biliary atresia susceptibility gene. *Gastroenterology* **144**, 1107-1115 e1103.
- Dann, C. E., Hsieh, J. C., Rattner, A., Sharma, D., Nathans, J. and Leahy, D. J.** (2001). Insights into Wnt binding and signalling from the structures of two Frizzled cysteine-rich domains. *Nature* **412**, 86-90.
- DeCamp, D. L., Thompson, T. M., de Sauvage, F. J. and Lerner, M. R.** (2000). Smoothened activates Galphai-mediated signaling in frog melanophores. *J Biol Chem* **275**, 26322-26327.
- Denef, N., Neubuser, D., Perez, L. and Cohen, S. M.** (2000). Hedgehog induces opposite changes in turnover and subcellular localization of patched and smoothened. *Cell* **102**, 521-531.
- Desai, P. B., Stuck, M. W., Lv, B. and Pazour, G. J.** (2020). Ubiquitin links smoothened to intraflagellar transport to regulate Hedgehog signaling. *J Cell Biol* **219**.
- Dessaud, E., McMahon, A. P. and Briscoe, J.** (2008). Pattern formation in the vertebrate neural tube: a sonic hedgehog morphogen-regulated transcriptional network. *Development* **135**, 2489-2503.
- Dessaud, E., Yang, L. L., Hill, K., Cox, B., Ulloa, F., Ribeiro, A., Mynett, A., Novitch, B. G. and Briscoe, J.** (2007). Interpretation of the sonic hedgehog morphogen gradient by a temporal adaptation mechanism. *Nature* **450**, 717-720.
- Dierker, T., Dreier, R., Migone, M., Hamer, S. and Grobe, K.** (2009). Heparan sulfate and transglutaminase activity are required for the formation of covalently cross-linked hedgehog oligomers. *J Biol Chem* **284**, 32562-32571.
- Dwyer, J. R., Sever, N., Carlson, M., Nelson, S. F., Beachy, P. A. and Parhami, F.** (2007). Oxysterols are novel activators of the hedgehog signaling pathway in pluripotent mesenchymal cells. *J Biol Chem* **282**, 8959-8968.
- Echelard, Y., Epstein, D. J., St-Jacques, B., Shen, L., Mohler, J., McMahon, J. A. and McMahon, A. P.** (1993). Sonic hedgehog, a member of a family of putative signaling molecules, is implicated in the regulation of CNS polarity. *Cell* **75**, 1417-1430.



**Ericson, J., Briscoe, J., Rashbass, P., van Heyningen, V. and Jessell, T. M. (1997a).** Graded sonic hedgehog signaling and the specification of cell fate in the ventral neural tube. *Cold Spring Harb Symp Quant Biol* **62**, 451-466.

**Ericson, J., Rashbass, P., Schedl, A., Brenner-Morton, S., Kawakami, A., van Heyningen, V., Jessell, T. M. and Briscoe, J. (1997b).** Pax6 controls progenitor cell identity and neuronal fate in response to graded Shh signaling. *Cell* **90**, 169-180.

**Eugster, C., Panakova, D., Mahmoud, A. and Eaton, S. (2007).** Lipoprotein-heparan sulfate interactions in the Hh pathway. *Dev Cell* **13**, 57-71.

**Falkenstein, K. N. and Vokes, S. A. (2014).** Transcriptional regulation of graded Hedgehog signaling. *Semin Cell Dev Biol* **33**, 73-80.

**Feng, W., Leach, S. M., Tipney, H., Phang, T., Geraci, M., Spritz, R. A., Hunter, L. E. and Williams, T. (2009).** Spatial and temporal analysis of gene expression during growth and fusion of the mouse facial prominences. *PLoS One* **4**, e8066.

**Filmus, J. and Capurro, M. (2014).** The role of glypicans in Hedgehog signaling. *Matrix Biol* **35**, 248-252.

**Filmus, J. and Selleck, S. B. (2001).** Glypicans: proteoglycans with a surprise. *J Clin Invest* **108**, 497-501.

**Frank-Kamenetsky, M., Zhang, X. M., Bottega, S., Guicherit, O., Wichterle, H., Dudek, H., Bumcrot, D., Wang, F. Y., Jones, S., Shulok, J., et al. (2002).** Small-molecule modulators of Hedgehog signaling: identification and characterization of Smoothed agonists and antagonists. *J Biol* **1**, 10.

**Fredriksson, R., Lagerstrom, M. C., Lundin, L. G. and Schioth, H. B. (2003).** The G-protein-coupled receptors in the human genome form five main families. Phylogenetic analysis, paralogon groups, and fingerprints. *Mol Pharmacol* **63**, 1256-1272.

**Fujisawa, H., Kitsukawa, T., Kawakami, A., Takagi, S., Shimizu, M. and Hirata, T. (1997).** Roles of a neuronal cell-surface molecule, neuropilin, in nerve fiber fasciculation and guidance. *Cell Tissue Res* **290**, 465-470.

**Gagnon, M. L., Bielenberg, D. R., Gechtman, Z., Miao, H. Q., Takashima, S., Soker, S. and Klagsbrun, M. (2000).** Identification of a natural soluble neuropilin-1 that binds vascular endothelial growth factor: In vivo expression and antitumor activity. *Proc Natl Acad Sci U S A* **97**, 2573-2578.

**Gainetdinov, R. R., Premont, R. T., Bohn, L. M., Lefkowitz, R. J. and Caron, M. G. (2004).** Desensitization of G protein-coupled receptors and neuronal functions. *Annu Rev Neurosci* **27**, 107-144.

**Ge, X., Milenkovic, L., Suyama, K., Hartl, T., Purzner, T., Winans, A., Meyer, T. and Scott, M. P.** (2015). Phosphodiesterase 4D acts downstream of Neuropilin to control Hedgehog signal transduction and the growth of medulloblastoma. *Elife* **4**.

**Giger, R. J., Cloutier, J. F., Sahay, A., Prinjha, R. K., Levengood, D. V., Moore, S. E., Pickering, S., Simmons, D., Rastan, S., Walsh, F. S., et al.** (2000). Neuropilin-2 is required in vivo for selective axon guidance responses to secreted semaphorins. *Neuron* **25**, 29-41.

**Giger, R. J., Urquhart, E. R., Gillespie, S. K., Levengood, D. V., Ginty, D. D. and Kolodkin, A. L.** (1998). Neuropilin-2 is a receptor for semaphorin IV: insight into the structural basis of receptor function and specificity. *Neuron* **21**, 1079-1092.

**Gilbert, S. F.** (2013). *Developmental Biology, 10th Ed.*: Sinauer Associates Incorporated.

**Gluzman-Poltorak, Z., Cohen, T., Herzog, Y. and Neufeld, G.** (2000). Neuropilin-2 is a receptor for the vascular endothelial growth factor (VEGF) forms VEGF-145 and VEGF-165 [corrected]. *J Biol Chem* **275**, 18040-18045.

**Goetz, J. A., Singh, S., Suber, L. M., Kull, F. J. and Robbins, D. J.** (2006). A highly conserved amino-terminal region of sonic hedgehog is required for the formation of its freely diffusible multimeric form. *J Biol Chem* **281**, 4087-4093.

**Goetz, S. C. and Anderson, K. V.** (2010). The primary cilium: a signalling centre during vertebrate development. *Nat Rev Genet* **11**, 331-344.

**Gong, X., Qian, H., Cao, P., Zhao, X., Zhou, Q., Lei, J. and Yan, N.** (2018). Structural basis for the recognition of Sonic Hedgehog by human Patched1. *Science* **361**.

**Goodrich, L. V., Johnson, R. L., Milenkovic, L., McMahon, J. A. and Scott, M. P.** (1996). Conservation of the hedgehog/patched signaling pathway from flies to mice: induction of a mouse patched gene by Hedgehog. *Genes Dev* **10**, 301-312.

**Goodrich, L. V., Jung, D., Higgins, K. M. and Scott, M. P.** (1999). Overexpression of ptcl inhibits induction of Shh target genes and prevents normal patterning in the neural tube. *Dev Biol* **211**, 323-334.

**Goodrich, L. V., Milenkovic, L., Higgins, K. M. and Scott, M. P.** (1997). Altered neural cell fates and medulloblastoma in mouse patched mutants. *Science* **277**, 1109-1113.

**Grimmond, S., Larder, R., Van Hateren, N., Siggers, P., Hulsebos, T. J., Arkell, R. and Greenfield, A.** (2000). Cloning, mapping, and expression analysis of a gene encoding a novel mammalian EGF-related protein (SCUBE1). *Genomics* **70**, 74-81.

**Grimmond, S., Larder, R., Van Hateren, N., Siggers, P., Morse, S., Hacker, T., Arkell, R. and Greenfield, A.** (2001). Expression of a novel mammalian epidermal growth factor-related gene during mouse neural development. *Mech Dev* **102**, 209-211.

**Hahn, H., Wicking, C., Zaphiropoulous, P. G., Gailani, M. R., Shanley, S., Chidambaram, A., Vorechovsky, I., Holmberg, E., Unden, A. B., Gillies, S., et al.** (1996). Mutations of the human homolog of *Drosophila* patched in the nevoid basal cell carcinoma syndrome. *Cell* **85**, 841-851.

**Han, C., Belenkaya, T. Y., Wang, B. and Lin, X.** (2004). *Drosophila* glypicans control the cell-to-cell movement of Hedgehog by a dynamin-independent process. *Development* **131**, 601-611.

**Harfe, B. D., Scherz, P. J., Nissim, S., Tian, H., McMahon, A. P. and Tabin, C. J.** (2004). Evidence for an expansion-based temporal Shh gradient in specifying vertebrate digit identities. *Cell* **118**, 517-528.

**Hayden Gephart, M. G., Su, Y. S., Bandara, S., Tsai, F. C., Hong, J., Conley, N., Rayburn, H., Milenkovic, L., Meyer, T. and Scott, M. P.** (2013). Neuropilin-2 contributes to tumorigenicity in a mouse model of Hedgehog pathway medulloblastoma. *J Neurooncol* **115**, 161-168.

**He, Z. and Tessier-Lavigne, M.** (1997). Neuropilin is a receptor for the axonal chemorepellent Semaphorin III. *Cell* **90**, 739-751.

**Hillman, R. T., Feng, B. Y., Ni, J., Woo, W. M., Milenkovic, L., Hayden Gephart, M. G., Teruel, M. N., Oro, A. E., Chen, J. K. and Scott, M. P.** (2011). Neuropilins are positive regulators of Hedgehog signal transduction. *Genes Dev* **25**, 2333-2346.

**Hollway, G. E., Maule, J., Gautier, P., Evans, T. M., Keenan, D. G., Lohs, C., Fischer, D., Wicking, C. and Currie, P. D.** (2006). Scube2 mediates Hedgehog signalling in the zebrafish embryo. *Dev Biol* **294**, 104-118.

**Holtz, A. M., Griffiths, S. C., Davis, S. J., Bishop, B., Siebold, C. and Allen, B. L.** (2015). Secreted HHIP1 interacts with heparan sulfate and regulates Hedgehog ligand localization and function. *J Cell Biol* **209**, 739-757.

**Holtz, A. M., Peterson, K. A., Nishi, Y., Morin, S., Song, J. Y., Charron, F., McMahon, A. P. and Allen, B. L.** (2013). Essential role for ligand-dependent feedback antagonism of vertebrate hedgehog signaling by PTCH1, PTCH2 and HHIP1 during neural patterning. *Development* **140**, 3423-3434.

**Hong, M., Srivastava, K., Kim, S., Allen, B. L., Leahy, D. J., Hu, P., Roessler, E., Krauss, R. S. and Muenke, M.** (2017). BOC is a modifier gene in holoprosencephaly. *Hum Mutat* **38**, 1464-1470.

**Hooper, J. E. and Scott, M. P.** (1989). The *Drosophila* patched gene encodes a putative membrane protein required for segmental patterning. *Cell* **59**, 751-765.

**Hu, D. and Helms, J. A.** (1999). The role of sonic hedgehog in normal and abnormal craniofacial morphogenesis. *Development* **126**, 4873-4884.

- Huangfu, D. and Anderson, K. V.** (2006). Signaling from Smo to Ci/Gli: conservation and divergence of Hedgehog pathways from *Drosophila* to vertebrates. *Development* **133**, 3-14.
- Huangfu, D., Liu, A., Rakeman, A. S., Murcia, N. S., Niswander, L. and Anderson, K. V.** (2003). Hedgehog signalling in the mouse requires intraflagellar transport proteins. *Nature* **426**, 83-87.
- Hui, C. C. and Angers, S.** (2011). Gli proteins in development and disease. *Annu Rev Cell Dev Biol* **27**, 513-537.
- Hwang, S. H., White, K. A., Somatilaka, B. N., Shelton, J. M., Richardson, J. A. and Mukhopadhyay, S.** (2018). The G protein-coupled receptor Gpr161 regulates forelimb formation, limb patterning and skeletal morphogenesis in a primary cilium-dependent manner. *Development* **145**.
- Ingham, P. W., Nakano, Y. and Seger, C.** (2011). Mechanisms and functions of Hedgehog signalling across the metazoa. *Nat Rev Genet* **12**, 393-406.
- Ingham, P. W., Nystedt, S., Nakano, Y., Brown, W., Stark, D., van den Heuvel, M. and Taylor, A. M.** (2000). Patched represses the Hedgehog signalling pathway by promoting modification of the Smoothed protein. *Curr Biol* **10**, 1315-1318.
- Izzi, L., Levesque, M., Morin, S., Laniel, D., Wilkes, B. C., Mille, F., Krauss, R. S., McMahon, A. P., Allen, B. L. and Charron, F.** (2011). Boc and Gas1 each form distinct Shh receptor complexes with Ptch1 and are required for Shh-mediated cell proliferation. *Dev Cell* **20**, 788-801.
- Jeong, J., Mao, J., Tenzen, T., Kottmann, A. H. and McMahon, A. P.** (2004). Hedgehog signaling in the neural crest cells regulates the patterning and growth of facial primordia. *Genes Dev* **18**, 937-951.
- Jeong, J. and McMahon, A. P.** (2005). Growth and pattern of the mammalian neural tube are governed by partially overlapping feedback activities of the hedgehog antagonists patched 1 and Hhip1. *Development* **132**, 143-154.
- Jia, J., Tong, C., Wang, B., Luo, L. and Jiang, J.** (2004). Hedgehog signalling activity of Smoothed requires phosphorylation by protein kinase A and casein kinase I. *Nature* **432**, 1045-1050.
- Jin, S., Martinelli, D. C., Zheng, X., Tessier-Lavigne, M. and Fan, C. M.** (2015). Gas1 is a receptor for sonic hedgehog to repel enteric axons. *Proc Natl Acad Sci U S A* **112**, E73-80.
- Johnson, J. L., Hall, T. E., Dyson, J. M., Sonntag, C., Ayers, K., Berger, S., Gautier, P., Mitchell, C., Hollway, G. E. and Currie, P. D.** (2012). Scube activity is necessary for Hedgehog signal transduction in vivo. *Dev Biol* **368**, 193-202.

- Johnson, R. L., Rothman, A. L., Xie, J., Goodrich, L. V., Bare, J. W., Bonifas, J. M., Quinn, A. G., Myers, R. M., Cox, D. R., Epstein, E. H., Jr., et al.** (1996). Human homolog of patched, a candidate gene for the basal cell nevus syndrome. *Science* **272**, 1668-1671.
- Kang, J. S., Gao, M., Feinleib, J. L., Cotter, P. D., Guadagno, S. N. and Krauss, R. S.** (1997). CDO: an oncogene-, serum-, and anchorage-regulated member of the Ig/fibronectin type III repeat family. *J Cell Biol* **138**, 203-213.
- Kang, J. S., Mulieri, P. J., Hu, Y., Taliana, L. and Krauss, R. S.** (2002). BOC, an Ig superfamily member, associates with CDO to positively regulate myogenic differentiation. *EMBO J* **21**, 114-124.
- Kantarci, S., Al-Gazali, L., Hill, R. S., Donnai, D., Black, G. C., Bieth, E., Chassaing, N., Lacombe, D., Devriendt, K., Teebi, A., et al.** (2007). Mutations in LRP2, which encodes the multiligand receptor megalin, cause Donnai-Barrow and facio-oculo-acoustico-renal syndromes. *Nat Genet* **39**, 957-959.
- Kasai, K., Takahashi, M., Osumi, N., Sinnarajah, S., Takeo, T., Ikeda, H., Kehrl, J. H., Itoh, G. and Arnheiter, H.** (2004). The G12 family of heterotrimeric G proteins and Rho GTPase mediate Sonic hedgehog signalling. *Genes Cells* **9**, 49-58.
- Kaufman, M. H.** (1992). *The Atlas of Mouse Development*: Elsevier Science.
- Kawahira, H., Ma, N. H., Tzanakakis, E. S., McMahon, A. P., Chuang, P. T. and Hebrok, M.** (2003). Combined activities of hedgehog signaling inhibitors regulate pancreas development. *Development* **130**, 4871-4879.
- Kawakami, A., Kitsukawa, T., Takagi, S. and Fujisawa, H.** (1996). Developmentally regulated expression of a cell surface protein, neuropilin, in the mouse nervous system. *J Neurobiol* **29**, 1-17.
- Kawakami, A., Nojima, Y., Toyoda, A., Takahoko, M., Satoh, M., Tanaka, H., Wada, H., Masai, I., Terasaki, H., Sakaki, Y., et al.** (2005). The zebrafish-secreted matrix protein you/scube2 is implicated in long-range regulation of hedgehog signaling. *Curr Biol* **15**, 480-488.
- Kawakami, T., Kawcak, T., Li, Y. J., Zhang, W., Hu, Y. and Chuang, P. T.** (2002). Mouse dispatched mutants fail to distribute hedgehog proteins and are defective in hedgehog signaling. *Development* **129**, 5753-5765.
- Kawamura, S., Hervold, K., Ramirez-Weber, F. A. and Kornberg, T. B.** (2008). Two patched protein subtypes and a conserved domain of group I proteins that regulates turnover. *J Biol Chem* **283**, 30964-30969.
- Kawasaki, T., Kitsukawa, T., Bekku, Y., Matsuda, Y., Sanbo, M., Yagi, T. and Fujisawa, H.** (1999). A requirement for neuropilin-1 in embryonic vessel formation. *Development* **126**, 4895-4902.

- Kerjaschki, D. and Farquhar, M. G.** (1983). Immunocytochemical localization of the Heymann nephritis antigen (GP330) in glomerular epithelial cells of normal Lewis rats. *J Exp Med* **157**, 667-686.
- Kerjaschki, D., Noronha-Blob, L., Sacktor, B. and Farquhar, M. G.** (1984). Microdomains of distinctive glycoprotein composition in the kidney proximal tubule brush border. *J Cell Biol* **98**, 1505-1513.
- Kerjaschki, D., Ullrich, R., Diem, K., Pietromonaco, S., Orlando, R. A. and Farquhar, M. G.** (1992). Identification of a pathogenic epitope involved in initiation of Heymann nephritis. *Proc Natl Acad Sci U S A* **89**, 11179-11183.
- Khaliullina, H., Panakova, D., Eugster, C., Riedel, F., Carvalho, M. and Eaton, S.** (2009). Patched regulates Smoothed trafficking using lipoprotein-derived lipids. *Development* **136**, 4111-4121.
- Kim, Y., Lee, J., Seppala, M., Cobourne, M. T. and Kim, S. H.** (2020). Author Correction: Ptch2/Gas1 and Ptch1/Boc differentially regulate Hedgehog signalling in murine primordial germ cell migration. *Nat Commun* **11**, 2275.
- Kitsukawa, T., Shimizu, M., Sanbo, M., Hirata, T., Taniguchi, M., Bekku, Y., Yagi, T. and Fujisawa, H.** (1997). Neuropilin-semaphorin III/D-mediated chemorepulsive signals play a crucial role in peripheral nerve projection in mice. *Neuron* **19**, 995-1005.
- Kitsukawa, T., Shiono, A., Kawakami, A., Kondoh, H. and Fujisawa, H.** (1995). Overexpression of a membrane protein, neuropilin, in chimeric mice causes anomalies in the cardiovascular system, nervous system and limbs. *Development* **121**, 4309-4318.
- Klagsbrun, M., Takashima, S. and Mamluk, R.** (2002). The role of neuropilin in vascular and tumor biology. *Adv Exp Med Biol* **515**, 33-48.
- Kohtz, J. D., Lee, H. Y., Gaiano, N., Segal, J., Ng, E., Larson, T., Baker, D. P., Garber, E. A., Williams, K. P. and Fishell, G.** (2001). N-terminal fatty-acylation of sonic hedgehog enhances the induction of rodent ventral forebrain neurons. *Development* **128**, 2351-2363.
- Kolodkin, A. L., Levengood, D. V., Rowe, E. G., Tai, Y. T., Giger, R. J. and Ginty, D. D.** (1997). Neuropilin is a semaphorin III receptor. *Cell* **90**, 753-762.
- Kornberg, T. B. and Roy, S.** (2014). Cytonemes as specialized signaling filopodia. *Development* **141**, 729-736.
- Krauss, S., Concordet, J. P. and Ingham, P. W.** (1993). A functionally conserved homolog of the Drosophila segment polarity gene hh is expressed in tissues with polarizing activity in zebrafish embryos. *Cell* **75**, 1431-1444.
- Kurosaka, H., Iulianella, A., Williams, T. and Trainor, P. A.** (2014). Disrupting hedgehog and WNT signaling interactions promotes cleft lip pathogenesis. *J Clin Invest* **124**, 1660-1671.

- Le Dreau, G. and Marti, E.** (2013). The multiple activities of BMPs during spinal cord development. *Cell Mol Life Sci* **70**, 4293-4305.
- Lee, C. S., Buttitta, L. and Fan, C. M.** (2001a). Evidence that the WNT-inducible growth arrest-specific gene 1 encodes an antagonist of sonic hedgehog signaling in the somite. *Proc Natl Acad Sci U S A* **98**, 11347-11352.
- Lee, C. S. and Fan, C. M.** (2001). Embryonic expression patterns of the mouse and chick Gas1 genes. *Mech Dev* **101**, 293-297.
- Lee, E. Y., Ji, H., Ouyang, Z., Zhou, B., Ma, W., Vokes, S. A., McMahon, A. P., Wong, W. H. and Scott, M. P.** (2010). Hedgehog pathway-regulated gene networks in cerebellum development and tumorigenesis. *Proc Natl Acad Sci U S A* **107**, 9736-9741.
- Lee, J. D., Kraus, P., Gaiano, N., Nery, S., Kohtz, J., Fishell, G., Loomis, C. A. and Treisman, J. E.** (2001b). An acylatable residue of Hedgehog is differentially required in Drosophila and mouse limb development. *Dev Biol* **233**, 122-136.
- Lee, J. D. and Treisman, J. E.** (2001). Sightless has homology to transmembrane acyltransferases and is required to generate active Hedgehog protein. *Curr Biol* **11**, 1147-1152.
- Lee, J. J., Ekker, S. C., von Kessler, D. P., Porter, J. A., Sun, B. I. and Beachy, P. A.** (1994). Autoproteolysis in hedgehog protein biogenesis. *Science* **266**, 1528-1537.
- Lee, J. J., von Kessler, D. P., Parks, S. and Beachy, P. A.** (1992). Secretion and localized transcription suggest a role in positional signaling for products of the segmentation gene hedgehog. *Cell* **71**, 33-50.
- Lee, Y., Miller, H. L., Russell, H. R., Boyd, K., Curran, T. and McKinnon, P. J.** (2006). Patched2 modulates tumorigenesis in patched1 heterozygous mice. *Cancer Res* **66**, 6964-6971.
- Lewis, P. M., Dunn, M. P., McMahon, J. A., Logan, M., Martin, J. F., St-Jacques, B. and McMahon, A. P.** (2001). Cholesterol modification of sonic hedgehog is required for long-range signaling activity and effective modulation of signaling by Ptc1. *Cell* **105**, 599-612.
- Li, F., Shi, W., Capurro, M. and Filmus, J.** (2011a). Glypican-5 stimulates rhabdomyosarcoma cell proliferation by activating Hedgehog signaling. *J Cell Biol* **192**, 691-704.
- Li, M., Shuman, C., Fei, Y. L., Cutiongco, E., Bender, H. A., Stevens, C., Wilkins-Haug, L., Day-Salvatore, D., Yong, S. L., Geraghty, M. T., et al.** (2001). GPC3 mutation analysis in a spectrum of patients with overgrowth expands the phenotype of Simpson-Golabi-Behmel syndrome. *Am J Med Genet* **102**, 161-168.
- Li, X., Howard, T. D., Moore, W. C., Ampleford, E. J., Li, H., Busse, W. W., Calhoun, W. J., Castro, M., Chung, K. F., Erzurum, S. C., et al.** (2011b). Importance of hedgehog interacting protein and other lung function genes in asthma. *J Allergy Clin Immunol* **127**, 1457-1465.

- Li, Y., Zhang, H., Litingtung, Y. and Chiang, C.** (2006). Cholesterol modification restricts the spread of Shh gradient in the limb bud. *Proceedings of the National Academy of Sciences* **103**, 6548-6553.
- Lin, X.** (2004). Functions of heparan sulfate proteoglycans in cell signaling during development. *Development* **131**, 6009-6021.
- Lin, Y. C., Roffler, S. R., Yan, Y. T. and Yang, R. B.** (2015). Disruption of Scube2 Impairs Endochondral Bone Formation. *J Bone Miner Res* **30**, 1255-1267.
- Lindsley, D. L. and Zimm, G. G.** (2012). *The Genome of Drosophila Melanogaster*: Elsevier Science.
- Litingtung, Y., Lei, L., Westphal, H. and Chiang, C.** (1998). Sonic hedgehog is essential to foregut development. *Nat Genet* **20**, 58-61.
- Liu, Y., Liu, C., Yamada, Y. and Fan, C. M.** (2002). Growth arrest specific gene 1 acts as a region-specific mediator of the Fgf10/Fgf8 regulatory loop in the limb. *Development* **129**, 5289-5300.
- Liu, Y., May, N. R. and Fan, C. M.** (2001). Growth arrest specific gene 1 is a positive growth regulator for the cerebellum. *Dev Biol* **236**, 30-45.
- Long, J., Li, B., Rodriguez-Blanco, J., Pastori, C., Volmar, C. H., Wahlestedt, C., Capobianco, A., Bai, F., Pei, X. H., Ayad, N. G., et al.** (2014). The BET bromodomain inhibitor I-BET151 acts downstream of smoothed protein to abrogate the growth of hedgehog protein-driven cancers. *J Biol Chem* **289**, 35494-35502.
- Lum, L., Yao, S., Mozer, B., Rovescalli, A., Von Kessler, D., Nirenberg, M. and Beachy, P. A.** (2003). Identification of Hedgehog pathway components by RNAi in Drosophila cultured cells. *Science* **299**, 2039-2045.
- Ma, Y., Erkner, A., Gong, R., Yao, S., Taipale, J., Basler, K. and Beachy, P. A.** (2002). Hedgehog-mediated patterning of the mammalian embryo requires transporter-like function of dispatched. *Cell* **111**, 63-75.
- Maity, T., Fuse, N. and Beachy, P. A.** (2005). Molecular mechanisms of Sonic hedgehog mutant effects in holoprosencephaly. *Proc Natl Acad Sci U S A* **102**, 17026-17031.
- Makihara, S., Morin, S., Ferent, J., Cote, J. F., Yam, P. T. and Charron, F.** (2018). Polarized Dock Activity Drives Shh-Mediated Axon Guidance. *Dev Cell* **46**, 410-425 e417.
- Makinen, T., Olofsson, B., Karpanen, T., Hellman, U., Soker, S., Klagsbrun, M., Eriksson, U. and Alitalo, K.** (1999). Differential binding of vascular endothelial growth factor B splice and proteolytic isoforms to neuropilin-1. *J Biol Chem* **274**, 21217-21222.
- Marigo, V., Davey, R. A., Zuo, Y., Cunningham, J. M. and Tabin, C. J.** (1996). Biochemical evidence that patched is the Hedgehog receptor. *Nature* **384**, 176-179.



- Marigo, V. and Tabin, C. J.** (1996). Regulation of patched by sonic hedgehog in the developing neural tube. *Proc Natl Acad Sci U S A* **93**, 9346-9351.
- Marti, E., Bumcrot, D. A., Takada, R. and McMahon, A. P.** (1995a). Requirement of 19K form of Sonic hedgehog for induction of distinct ventral cell types in CNS explants. *Nature* **375**, 322-325.
- Marti, E., Takada, R., Bumcrot, D. A., Sasaki, H. and McMahon, A. P.** (1995b). Distribution of Sonic hedgehog peptides in the developing chick and mouse embryo. *Development* **121**, 2537-2547.
- Martinelli, D. C. and Fan, C. M.** (2007). Gas1 extends the range of Hedgehog action by facilitating its signaling. *Genes Dev* **21**, 1231-1243.
- Mathew, E., Zhang, Y., Holtz, A. M., Kane, K. T., Song, J. Y., Allen, B. L. and Pasca di Magliano, M.** (2014). Dosage-dependent regulation of pancreatic cancer growth and angiogenesis by hedgehog signaling. *Cell Rep* **9**, 484-494.
- Matteson, P. G., Desai, J., Korstanje, R., Lazar, G., Borsuk, T. E., Rollins, J., Kadambi, S., Joseph, J., Rahman, T., Wink, J., et al.** (2008). The orphan G protein-coupled receptor, Gpr161, encodes the vacuolated lens locus and controls neurulation and lens development. *Proc Natl Acad Sci U S A* **105**, 2088-2093.
- McCarthy, R. A., Barth, J. L., Chintalapudi, M. R., Knaak, C. and Argraves, W. S.** (2002). Megalin functions as an endocytic sonic hedgehog receptor. *J Biol Chem* **277**, 25660-25667.
- McLellan, J. S., Zheng, X., Hauk, G., Ghirlando, R., Beachy, P. A. and Leahy, D. J.** (2008). The mode of Hedgehog binding to Ihog homologues is not conserved across different phyla. *Nature* **455**, 979-983.
- McMahon, A. P., Ingham, P. W. and Tabin, C. J.** (2003). Developmental roles and clinical significance of hedgehog signaling. *Curr Top Dev Biol* **53**, 1-114.
- Megason, S. G. and McMahon, A. P.** (2002). A mitogen gradient of dorsal midline Wnts organizes growth in the CNS. *Development* **129**, 2087-2098.
- Micchelli, C. A., The, I., Selva, E., Mogila, V. and Perrimon, N.** (2002). Rasp, a putative transmembrane acyltransferase, is required for Hedgehog signaling. *Development* **129**, 843-851.
- Migdal, M., Huppertz, B., Tessler, S., Comforti, A., Shibuya, M., Reich, R., Baumann, H. and Neufeld, G.** (1998). Neuropilin-1 is a placenta growth factor-2 receptor. *J Biol Chem* **273**, 22272-22278.
- Milenkovic, L., Goodrich, L. V., Higgins, K. M. and Scott, M. P.** (1999). Mouse patched1 controls body size determination and limb patterning. *Development* **126**, 4431-4440.

- Mille, F., Tamayo-Orrego, L., Levesque, M., Remke, M., Korshunov, A., Cardin, J., Bouchard, N., Izzi, L., Kool, M., Northcott, P. A., et al.** (2014). The Shh receptor Boc promotes progression of early medulloblastoma to advanced tumors. *Dev Cell* **31**, 34-47.
- Mohler, J. and Vani, K.** (1992). Molecular organization and embryonic expression of the hedgehog gene involved in cell-cell communication in segmental patterning of *Drosophila*. *Development* **115**, 957-971.
- Morales, C. R., Zeng, J., El Alfy, M., Barth, J. L., Chintalapudi, M. R., McCarthy, R. A., Incardona, J. P. and Argraves, W. S.** (2006). Epithelial trafficking of Sonic hedgehog by megalin. *J Histochem Cytochem* **54**, 1115-1127.
- Motoyama, J., Heng, H., Crackower, M. A., Takabatake, T., Takeshima, K., Tsui, L. C. and Hui, C.** (1998a). Overlapping and non-overlapping Ptch2 expression with Shh during mouse embryogenesis. *Mech Dev* **78**, 81-84.
- Motoyama, J., Takabatake, T., Takeshima, K. and Hui, C.** (1998b). Ptch2, a second mouse Patched gene is co-expressed with Sonic hedgehog. *Nat Genet* **18**, 104-106.
- Mukhopadhyay, S., Wen, X., Chih, B., Nelson, C. D., Lane, W. S., Scales, S. J. and Jackson, P. K.** (2010). TULP3 bridges the IFT-A complex and membrane phosphoinositides to promote trafficking of G protein-coupled receptors into primary cilia. *Genes Dev* **24**, 2180-2193.
- Mukhopadhyay, S., Wen, X., Ratti, N., Loktev, A., Rangell, L., Scales, S. J. and Jackson, P. K.** (2013). The ciliary G-protein-coupled receptor Gpr161 negatively regulates the Sonic hedgehog pathway via cAMP signaling. *Cell* **152**, 210-223.
- Mulieri, P. J., Kang, J. S., Sassoon, D. A. and Krauss, R. S.** (2002). Expression of the boc gene during murine embryogenesis. *Dev Dyn* **223**, 379-388.
- Mulieri, P. J., Okada, A., Sassoon, D. A., McConnell, S. K. and Krauss, R. S.** (2000). Developmental expression pattern of the cdo gene. *Dev Dyn* **219**, 40-49.
- Nachtergaele, S., Whalen, D. M., Mydock, L. K., Zhao, Z., Malinauskas, T., Krishnan, K., Ingham, P. W., Covey, D. F., Siebold, C. and Rohatgi, R.** (2013). Structure and function of the Smoothed extracellular domain in vertebrate Hedgehog signaling. *Elife* **2**, e01340.
- Nakano, Y., Guerrero, I., Hidalgo, A., Taylor, A., Whittle, J. R. and Ingham, P. W.** (1989). A protein with several possible membrane-spanning domains encoded by the *Drosophila* segment polarity gene patched. *Nature* **341**, 508-513.
- Nieuwenhuis, E., Motoyama, J., Barnfield, P. C., Yoshikawa, Y., Zhang, X., Mo, R., Crackower, M. A. and Hui, C. C.** (2006). Mice with a targeted mutation of patched2 are viable but develop alopecia and epidermal hyperplasia. *Mol Cell Biol* **26**, 6609-6622.
- Novitsch, B. G., Chen, A. I. and Jessell, T. M.** (2001). Coordinate regulation of motor neuron subtype identity and pan-neuronal properties by the bHLH repressor Olig2. *Neuron* **31**, 773-789.

- Nusslein-Volhard, C. and Wieschaus, E.** (1980). Mutations affecting segment number and polarity in *Drosophila*. *Nature* **287**, 795-801.
- Nusslein-Volhard, C., Wieschaus, E. and Kluding, H.** (1984). Mutations affecting the pattern of the larval cuticle in *Drosophila melanogaster* : I. Zygotic loci on the second chromosome. *Wilehm Roux Arch Dev Biol* **193**, 267-282.
- Ogden, S. K., Fei, D. L., Schilling, N. S., Ahmed, Y. F., Hwa, J. and Robbins, D. J.** (2008). G protein Galphai functions immediately downstream of Smoothed in Hedgehog signalling. *Nature* **456**, 967-970.
- Ohazama, A., Haycraft, C. J., Seppala, M., Blackburn, J., Ghafoor, S., Cobourne, M., Martinelli, D. C., Fan, C. M., Peterkova, R., Lesot, H., et al.** (2009). Primary cilia regulate Shh activity in the control of molar tooth number. *Development* **136**, 897-903.
- Okada, A., Charron, F., Morin, S., Shin, D. S., Wong, K., Fabre, P. J., Tessier-Lavigne, M. and McConnell, S. K.** (2006). Boc is a receptor for sonic hedgehog in the guidance of commissural axons. *Nature* **444**, 369-373.
- Ortega, M. C., Cases, O., Merchan, P., Kozyraki, R., Clemente, D. and de Castro, F.** (2012). Megalin mediates the influence of sonic hedgehog on oligodendrocyte precursor cell migration and proliferation during development. *Glia* **60**, 851-866.
- Parmantier, E., Lynn, B., Lawson, D., Turmaine, M., Namini, S. S., Chakrabarti, L., McMahan, A. P., Jessen, K. R. and Mirsky, R.** (1999). Schwann cell-derived Desert hedgehog controls the development of peripheral nerve sheaths. *Neuron* **23**, 713-724.
- Pellegrini, M., Pilia, G., Pantano, S., Lucchini, F., Uda, M., Fumi, M., Cao, A., Schlessinger, D. and Forabosco, A.** (1998). Gpc3 expression correlates with the phenotype of the Simpson-Golabi-Behmel syndrome. *Dev Dyn* **213**, 431-439.
- Pepicelli, C. V., Lewis, P. M. and McMahan, A. P.** (1998). Sonic hedgehog regulates branching morphogenesis in the mammalian lung. *Curr Biol* **8**, 1083-1086.
- Peters, C., Wolf, A., Wagner, M., Kuhlmann, J. and Waldmann, H.** (2004). The cholesterol membrane anchor of the Hedgehog protein confers stable membrane association to lipid-modified proteins. *Proc Natl Acad Sci U S A* **101**, 8531-8536.
- Peterson, K. A., Nishi, Y., Ma, W., Vedenko, A., Shokri, L., Zhang, X., McFarlane, M., Baizabal, J. M., Junker, J. P., van Oudenaarden, A., et al.** (2012). Neural-specific Sox2 input and differential Gli-binding affinity provide context and positional information in Shh-directed neural patterning. *Genes Dev* **26**, 2802-2816.
- Pillai, S. G., Ge, D., Zhu, G., Kong, X., Shianna, K. V., Need, A. C., Feng, S., Hersh, C. P., Bakke, P., Gulsvik, A., et al.** (2009). A genome-wide association study in chronic obstructive pulmonary disease (COPD): identification of two major susceptibility loci. *PLoS Genet* **5**, e1000421.

- Pineault, K. M. and Wellik, D. M.** (2014). Hox genes and limb musculoskeletal development. *Curr Osteoporos Rep* **12**, 420-427.
- Pinsky, J. M., Franks, N. E., McMellen, A. N., Giger, R. J. and Allen, B. L.** (2017). Neuropilin-1 promotes Hedgehog signaling through a novel cytoplasmic motif. *J Biol Chem* **292**, 15192-15204.
- Porter, J. A., von Kessler, D. P., Ekker, S. C., Young, K. E., Lee, J. J., Moses, K. and Beachy, P. A.** (1995). The product of hedgehog autoproteolytic cleavage active in local and long-range signalling. *Nature* **374**, 363-366.
- Porter, J. A., Young, K. E. and Beachy, P. A.** (1996). Cholesterol modification of hedgehog signaling proteins in animal development. *Science* **274**, 255-259.
- Qi, X., Schmiede, P., Coutavas, E. and Li, X.** (2018a). Two Patched molecules engage distinct sites on Hedgehog yielding a signaling-competent complex. *Science* **362**.
- Qi, X., Schmiede, P., Coutavas, E., Wang, J. and Li, X.** (2018b). Structures of human Patched and its complex with native palmitoylated sonic hedgehog. *Nature* **560**, 128-132.
- Ribeiro, L. A., Murray, J. C. and Richieri-Costa, A.** (2006). PTCH mutations in four Brazilian patients with holoprosencephaly and in one with holoprosencephaly-like features and normal MRI. *Am J Med Genet A* **140**, 2584-2586.
- Ribeiro, L. A., Queizi, R. G., Nascimento, A., Bertolacini, C. P. and Richieri-Costa, A.** (2010). Holoprosencephaly and holoprosencephaly-like phenotype and GAS1 DNA sequence changes: Report of four Brazilian patients. *Am J Med Genet A* **152A**, 1688-1694.
- Riddle, R. D., Johnson, R. L., Laufer, E. and Tabin, C.** (1993). Sonic hedgehog mediates the polarizing activity of the ZPA. *Cell* **75**, 1401-1416.
- Riobo, N. A., Saucy, B., Dilizio, C. and Manning, D. R.** (2006). Activation of heterotrimeric G proteins by Smoothed. *Proc Natl Acad Sci U S A* **103**, 12607-12612.
- Robarge, K. D., Brunton, S. A., Castanedo, G. M., Cui, Y., Dina, M. S., Goldsmith, R., Gould, S. E., Guichert, O., Gunzner, J. L., Halladay, J., et al.** (2009). GDC-0449-a potent inhibitor of the hedgehog pathway. *Bioorg Med Chem Lett* **19**, 5576-5581.
- Roelink, H., Augsburger, A., Heemskerk, J., Korzh, V., Norlin, S., Ruiz i Altaba, A., Tanabe, Y., Placzek, M., Edlund, T., Jessell, T. M., et al.** (1994). Floor plate and motor neuron induction by vhh-1, a vertebrate homolog of hedgehog expressed by the notochord. *Cell* **76**, 761-775.
- Roelink, H., Porter, J. A., Chiang, C., Tanabe, Y., Chang, D. T., Beachy, P. A. and Jessell, T. M.** (1995). Floor plate and motor neuron induction by different concentrations of the amino-terminal cleavage product of sonic hedgehog autoproteolysis. *Cell* **81**, 445-455.

- Roessler, E., Belloni, E., Gaudenz, K., Jay, P., Berta, P., Scherer, S. W., Tsui, L. C. and Muenke, M.** (1996). Mutations in the human Sonic Hedgehog gene cause holoprosencephaly. *Nat Genet* **14**, 357-360.
- Rojas-Rios, P., Guerrero, I. and Gonzalez-Reyes, A.** (2012). Cytoneme-mediated delivery of hedgehog regulates the expression of bone morphogenetic proteins to maintain germline stem cells in *Drosophila*. *PLoS Biol* **10**, e1001298.
- Rossant, J. and Tam, P. T.** (2002). *Mouse Development: Patterning, Morphogenesis, and Organogenesis*: Elsevier Science.
- Rossignol, M., Gagnon, M. L. and Klagsbrun, M.** (2000). Genomic organization of human neuropilin-1 and neuropilin-2 genes: identification and distribution of splice variants and soluble isoforms. *Genomics* **70**, 211-222.
- Roth, L., Nasarre, C., Dirrig-Grosch, S., Aunis, D., Cremel, G., Hubert, P. and Bagnard, D.** (2008). Transmembrane domain interactions control biological functions of neuropilin-1. *Mol Biol Cell* **19**, 646-654.
- Rubenstein, J. L. and Beachy, P. A.** (1998). Patterning of the embryonic forebrain. *Curr Opin Neurobiol* **8**, 18-26.
- Rudin, C. M.** (2012). Vismodegib. *Clin Cancer Res* **18**, 3218-3222.
- Rudin, C. M., Hann, C. L., Laterra, J., Yauch, R. L., Callahan, C. A., Fu, L., Holcomb, T., Stinson, J., Gould, S. E., Coleman, B., et al.** (2009). Treatment of medulloblastoma with hedgehog pathway inhibitor GDC-0449. *N Engl J Med* **361**, 1173-1178.
- Sahali, D., Mulliez, N., Chatelet, F., Laurent-Winter, C., Citadelle, D., Sabourin, J. C., Roux, C., Ronco, P. and Verroust, P.** (1993). Comparative immunochemistry and ontogeny of two closely related coated pit proteins. The 280-kd target of teratogenic antibodies and the 330-kd target of nephritogenic antibodies. *Am J Pathol* **142**, 1654-1667.
- Saito, A., Pietromonaco, S., Loo, A. K. and Farquhar, M. G.** (1994). Complete cloning and sequencing of rat gp330/"megalin," a distinctive member of the low density lipoprotein receptor gene family. *Proc Natl Acad Sci U S A* **91**, 9725-9729.
- Sanders, T. A., Llagostera, E. and Barna, M.** (2013). Specialized filopodia direct long-range transport of SHH during vertebrate tissue patterning. *Nature* **497**, 628-632.
- Sanz-Ezquerro, J. J. and Tickle, C.** (2000). Autoregulation of Shh expression and Shh induction of cell death suggest a mechanism for modulating polarising activity during chick limb development. *Development* **127**, 4811-4823.
- Saunders, J. W., Jr. and M. T. Gasseling** (1968). *Ectodermal-mesodermal interactions in the origin of limb symmetry*. Baltimore: Williams & Wilkins.

- Saunders, S., Paine-Saunders, S. and Lander, A. D.** (1997). Expression of the cell surface proteoglycan glypican-5 is developmentally regulated in kidney, limb, and brain. *Dev Biol* **190**, 78-93.
- Scales, S. J. and de Sauvage, F. J.** (2009). Mechanisms of Hedgehog pathway activation in cancer and implications for therapy. *Trends Pharmacol Sci* **30**, 303-312.
- Schachter, K. A. and Krauss, R. S.** (2008). Murine models of holoprosencephaly. In *Curr Top Dev Biol*, pp. 139-170.
- Scherz, P. J., McGlinn, E., Nissim, S. and Tabin, C. J.** (2007). Extended exposure to Sonic hedgehog is required for patterning the posterior digits of the vertebrate limb. *Dev Biol* **308**, 343-354.
- Schneider, C., King, R. M. and Philipson, L.** (1988). Genes specifically expressed at growth arrest of mammalian cells. *Cell* **54**, 787-793.
- Seppala, M., Depew, M. J., Martinelli, D. C., Fan, C. M., Sharpe, P. T. and Cobourne, M. T.** (2007). Gas1 is a modifier for holoprosencephaly and genetically interacts with sonic hedgehog. *J Clin Invest* **117**, 1575-1584.
- Seppala, M., Xavier, G. M., Fan, C. M. and Cobourne, M. T.** (2014). Boc modifies the spectrum of holoprosencephaly in the absence of Gas1 function. *Biol Open* **3**, 728-740.
- Sharpe, H. J., Pau, G., Dijkgraaf, G. J., Basset-Seguín, N., Modrusan, Z., Januario, T., Tsui, V., Durham, A. B., Dlugosz, A. A., Haverty, P. M., et al.** (2015). Genomic analysis of smoothed inhibitor resistance in basal cell carcinoma. *Cancer Cell* **27**, 327-341.
- Shimada, I. S., Hwang, S. H., Somatilaka, B. N., Wang, X., Skowron, P., Kim, J., Kim, M., Shelton, J. M., Rajaram, V., Xuan, Z., et al.** (2018). Basal Suppression of the Sonic Hedgehog Pathway by the G-Protein-Coupled Receptor Gpr161 Restricts Medulloblastoma Pathogenesis. *Cell Rep* **22**, 1169-1184.
- Shimada, I. S., Somatilaka, B. N., Hwang, S. H., Anderson, A. G., Shelton, J. M., Rajaram, V., Konopka, G. and Mukhopadhyay, S.** (2019). Derepression of sonic hedgehog signaling upon Gpr161 deletion unravels forebrain and ventricular abnormalities. *Dev Biol* **450**, 47-62.
- Simpson, J. H., Kidd, T., Bland, K. S. and Goodman, C. S.** (2000). Short-range and long-range guidance by slit and its Robo receptors. Robo and Robo2 play distinct roles in midline guidance. *Neuron* **28**, 753-766.
- Smith, J. C. and Wolpert, L.** (1981). Pattern formation along the anteroposterior axis of the chick wing: the increase in width following a polarizing region graft and the effect of X-irradiation. *J Embryol Exp Morphol* **63**, 127-144.
- Smyth, I., Narang, M. A., Evans, T., Heimann, C., Nakamura, Y., Chenevix-Trench, G., Pietsch, T., Wicking, C. and Wainwright, B. J.** (1999). Isolation and characterization of

human patched 2 (PTCH2), a putative tumour suppressor gene in basal cell carcinoma and medulloblastoma on chromosome 1p32. *Hum Mol Genet* **8**, 291-297.

**Snuderl, M., Batista, A., Kirkpatrick, N. D., Ruiz de Almodovar, C., Riedemann, L., Walsh, E. C., Anolik, R., Huang, Y., Martin, J. D., Kamoun, W., et al.** (2013). Targeting placental growth factor/neuropilin 1 pathway inhibits growth and spread of medulloblastoma. *Cell* **152**, 1065-1076.

**Soker, S., Takashima, S., Miao, H. Q., Neufeld, G. and Klagsbrun, M.** (1998). Neuropilin-1 is expressed by endothelial and tumor cells as an isoform-specific receptor for vascular endothelial growth factor. *Cell* **92**, 735-745.

**Sommer, A. and Lemmon, M. A.** (2018). Smoothing out the patches. *Science* **362**, 26-27.

**Song, J. Y., Holtz, A. M., Pinsky, J. M. and Allen, B. L.** (2015). Distinct structural requirements for CDON and BOC in the promotion of Hedgehog signaling. *Dev Biol* **402**, 239-252.

**Spoelgen, R., Hammes, A., Anzenberger, U., Zechner, D., Andersen, O. M., Jerchow, B. and Willnow, T. E.** (2005). LRP2/megalin is required for patterning of the ventral telencephalon. *Development* **132**, 405-414.

**Stewart, D. P., Marada, S., Bodeen, W. J., Truong, A., Sakurada, S. M., Pandit, T., Pruett-Miller, S. M. and Ogden, S. K.** (2018). Cleavage activates dispatched for Sonic Hedgehog ligand release. *Elife* **7**.

**Stone, D. M., Hynes, M., Armanini, M., Swanson, T. A., Gu, Q., Johnson, R. L., Scott, M. P., Pennica, D., Goddard, A., Phillips, H., et al.** (1996). The tumour-suppressor gene patched encodes a candidate receptor for Sonic hedgehog. *Nature* **384**, 129-134.

**Svard, J., Heby-Henricson, K., Persson-Lek, M., Rozell, B., Lauth, M., Bergstrom, A., Ericson, J., Toftgard, R. and Teglund, S.** (2006). Genetic elimination of Suppressor of fused reveals an essential repressor function in the mammalian Hedgehog signaling pathway. *Dev Cell* **10**, 187-197.

**Tabata, T., Eaton, S. and Kornberg, T. B.** (1992). The Drosophila hedgehog gene is expressed specifically in posterior compartment cells and is a target of engrailed regulation. *Genes Dev* **6**, 2635-2645.

**Tabin, C. and Wolpert, L.** (2007). Rethinking the proximodistal axis of the vertebrate limb in the molecular era. *Genes Dev* **21**, 1433-1442.

**Taipale, J., Cooper, M. K., Maiti, T. and Beachy, P. A.** (2002). Patched acts catalytically to suppress the activity of Smoothed. *Nature* **418**, 892-897.

**Takabatake, T., Ogawa, M., Takahashi, T. C., Mizuno, M., Okamoto, M. and Takeshima, K.** (1997). Hedgehog and patched gene expression in adult ocular tissues. *FEBS Lett* **410**, 485-489.

**Takagi, S., Hirata, T., Agata, K., Mochii, M., Eguchi, G. and Fujisawa, H.** (1991). The A5 antigen, a candidate for the neuronal recognition molecule, has homologies to complement components and coagulation factors. *Neuron* **7**, 295-307.

**Takagi, S., Kasuya, Y., Shimizu, M., Matsuura, T., Tsuboi, M., Kawakami, A. and Fujisawa, H.** (1995). Expression of a cell adhesion molecule, neuropilin, in the developing chick nervous system. *Dev Biol* **170**, 207-222.

**Takagi, S., Tsuji, T., Amagai, T., Takamatsu, T. and Fujisawa, H.** (1987). Specific cell surface labels in the visual centers of *Xenopus laevis* tadpole identified using monoclonal antibodies. *Dev Biol* **122**, 90-100.

**Takahashi, T., Nakamura, F., Jin, Z., Kalb, R. G. and Strittmatter, S. M.** (1998). Semaphorins A and E act as antagonists of neuropilin-1 and agonists of neuropilin-2 receptors. *Nat Neurosci* **1**, 487-493.

**Takashima, S., Kitakaze, M., Asakura, M., Asanuma, H., Sanada, S., Tashiro, F., Niwa, H., Miyazaki Ji, J., Hirota, S., Kitamura, Y., et al.** (2002). Targeting of both mouse neuropilin-1 and neuropilin-2 genes severely impairs developmental yolk sac and embryonic angiogenesis. *Proc Natl Acad Sci U S A* **99**, 3657-3662.

**Tanaka, Y., Okada, Y. and Hirokawa, N.** (2005). FGF-induced vesicular release of Sonic hedgehog and retinoic acid in leftward nodal flow is critical for left-right determination. *Nature* **435**, 172-177.

**Tata, M., Tillo, M., Ruhrberg, C.** (2015). Chapter 6 - Neuropilins in Development and Disease of the Nervous System. In *Neural Surface Antigens* (ed. J. Pruszek), pp. 65-75: Academic Press.

**Taylor, A. M., Nakano, Y., Mohler, J. and Ingham, P. W.** (1993). Contrasting distributions of patched and hedgehog proteins in the *Drosophila* embryo. *Mech Dev* **42**, 89-96.

**Taylor, F. R., Wen, D., Garber, E. A., Carmillo, A. N., Baker, D. P., Arduini, R. M., Williams, K. P., Weinreb, P. H., Rayhorn, P., Hronowski, X., et al.** (2001). Enhanced potency of human Sonic hedgehog by hydrophobic modification. *Biochemistry* **40**, 4359-4371.

**Teglund, S. and Toftgard, R.** (2010). Hedgehog beyond medulloblastoma and basal cell carcinoma. *Biochim Biophys Acta* **1805**, 181-208.

**Tenzen, T., Allen, B. L., Cole, F., Kang, J. S., Krauss, R. S. and McMahon, A. P.** (2006). The cell surface membrane proteins Cdo and Boc are components and targets of the Hedgehog signaling pathway and feedback network in mice. *Dev Cell* **10**, 647-656.

**Thayer, S. P., di Magliano, M. P., Heiser, P. W., Nielsen, C. M., Roberts, D. J., Lauwers, G. Y., Qi, Y. P., Gysin, S., Fernandez-del Castillo, C., Yajnik, V., et al.** (2003). Hedgehog is an early and late mediator of pancreatic cancer tumorigenesis. *Nature* **425**, 851-856.

**Therond, P. P.** (2012). Release and transportation of Hedgehog molecules. *Curr Opin Cell Biol* **24**, 173-180.



- Theunissen, J. W. and de Sauvage, F. J.** (2009). Paracrine Hedgehog signaling in cancer. *Cancer Res* **69**, 6007-6010.
- Tian, H., Jeong, J., Harfe, B. D., Tabin, C. J. and McMahon, A. P.** (2005). Mouse *Disp1* is required in sonic hedgehog-expressing cells for paracrine activity of the cholesterol-modified ligand. *Development* **132**, 133-142.
- Tickle, C., Summerbell, D. and Wolpert, L.** (1975). Positional signalling and specification of digits in chick limb morphogenesis. *Nature* **254**, 199-202.
- Towers, M., Mahood, R., Yin, Y. and Tickle, C.** (2008). Integration of growth and specification in chick wing digit-patterning. *Nature* **452**, 882-886.
- Traister, A., Shi, W. and Filmus, J.** (2008). Mammalian Notum induces the release of glypicans and other GPI-anchored proteins from the cell surface. *Biochem J* **410**, 503-511.
- Tsai, M. T., Cheng, C. J., Lin, Y. C., Chen, C. C., Wu, A. R., Wu, M. T., Hsu, C. C. and Yang, R. B.** (2009). Isolation and characterization of a secreted, cell-surface glycoprotein SCUBE2 from humans. *Biochem J* **422**, 119-128.
- Tukachinsky, H., Kuzmickas, R. P., Jao, C. Y., Liu, J. and Salic, A.** (2012). Dispatched and *scube* mediate the efficient secretion of the cholesterol-modified hedgehog ligand. *Cell Rep* **2**, 308-320.
- Tuson, M., He, M. and Anderson, K. V.** (2011). Protein kinase A acts at the basal body of the primary cilium to prevent *Gli2* activation and ventralization of the mouse neural tube. *Development* **138**, 4921-4930.
- van den Heuvel, M. and Ingham, P. W.** (1996). *smoothed* encodes a receptor-like serpentine protein required for hedgehog signalling. *Nature* **382**, 547-551.
- van Eeden, F. J., Granato, M., Schach, U., Brand, M., Furutani-Seiki, M., Haffter, P., Hammerschmidt, M., Heisenberg, C. P., Jiang, Y. J., Kane, D. A., et al.** (1996). Mutations affecting somite formation and patterning in the zebrafish, *Danio rerio*. *Development* **123**, 153-164.
- Vokes, S. A., Ji, H., McCuine, S., Tenzen, T., Giles, S., Zhong, S., Longabaugh, W. J., Davidson, E. H., Wong, W. H. and McMahon, A. P.** (2007). Genomic characterization of *Gli*-activator targets in sonic hedgehog-mediated neural patterning. *Development* **134**, 1977-1989.
- Vokes, S. A., Ji, H., Wong, W. H. and McMahon, A. P.** (2008). A genome-scale analysis of the cis-regulatory circuitry underlying sonic hedgehog-mediated patterning of the mammalian limb. *Genes Dev* **22**, 2651-2663.
- Von Hoff, D. D., LoRusso, P. M., Rudin, C. M., Reddy, J. C., Yauch, R. L., Tibes, R., Weiss, G. J., Borad, M. J., Hann, C. L., Brahmer, J. R., et al.** (2009). Inhibition of the hedgehog pathway in advanced basal-cell carcinoma. *N Engl J Med* **361**, 1164-1172.

**Vortkamp, A., Lee, K., Lanske, B., Segre, G. V., Kronenberg, H. M. and Tabin, C. J.** (1996). Regulation of rate of cartilage differentiation by Indian hedgehog and PTH-related protein. *Science* **273**, 613-622.

**Vuong, T. A., Leem, Y. E., Kim, B. G., Cho, H., Lee, S. J., Bae, G. U. and Kang, J. S.** (2017). A Sonic hedgehog coreceptor, BOC regulates neuronal differentiation and neurite outgrowth via interaction with ABL and JNK activation. *Cell Signal* **30**, 30-40.

**Wang, C., Wu, H., Katritch, V., Han, G. W., Huang, X. P., Liu, W., Siu, F. Y., Roth, B. L., Cherezov, V. and Stevens, R. C.** (2013). Structure of the human smoothed receptor bound to an antitumour agent. *Nature* **497**, 338-343.

**Wijgerde, M., McMahon, J. A., Rule, M. and McMahon, A. P.** (2002). A direct requirement for Hedgehog signaling for normal specification of all ventral progenitor domains in the presumptive mammalian spinal cord. *Genes Dev* **16**, 2849-2864.

**Williams, E. H., Pappano, W. N., Saunders, A. M., Kim, M. S., Leahy, D. J. and Beachy, P. A.** (2010). Dally-like core protein and its mammalian homologues mediate stimulatory and inhibitory effects on Hedgehog signal response. *Proc Natl Acad Sci U S A* **107**, 5869-5874.

**Willnow, T. E., Hilpert, J., Armstrong, S. A., Rohlmann, A., Hammer, R. E., Burns, D. K. and Herz, J.** (1996). Defective forebrain development in mice lacking gp330/megalin. *Proc Natl Acad Sci U S A* **93**, 8460-8464.

**Wilson, L. and Maden, M.** (2005). The mechanisms of dorsoventral patterning in the vertebrate neural tube. *Dev Biol* **282**, 1-13.

**Wilson, N. H. and Stoeckli, E. T.** (2013). Sonic hedgehog regulates its own receptor on postcrossing commissural axons in a glypican1-dependent manner. *Neuron* **79**, 478-491.

**Witt, R. M., Hecht, M. L., Pazyra-Murphy, M. F., Cohen, S. M., Noti, C., van Kuppevelt, T. H., Fuller, M., Chan, J. A., Hopwood, J. J., Seeberger, P. H., et al.** (2013). Heparan sulfate proteoglycans containing a glypican 5 core and 2-O-sulfo-iduronic acid function as Sonic Hedgehog co-receptors to promote proliferation. *J Biol Chem* **288**, 26275-26288.

**Woods, I. G. and Talbot, W. S.** (2005). The you gene encodes an EGF-CUB protein essential for Hedgehog signaling in zebrafish. *PLoS Biol* **3**, e66.

**Wu, B. T., Su, Y. H., Tsai, M. T., Wasserman, S. M., Topper, J. N. and Yang, R. B.** (2004). A novel secreted, cell-surface glycoprotein containing multiple epidermal growth factor-like repeats and one CUB domain is highly expressed in primary osteoblasts and bones. *J Biol Chem* **279**, 37485-37490.

**Xavier, G. M. and Cobourne, M. T.** (2011). Scube2 expression extends beyond the central nervous system during mouse development. *J Mol Histol* **42**, 383-391.

**Xavier, G. M., Seppala, M., Barrell, W., Birjandi, A. A., Geoghegan, F. and Cobourne, M. T.** (2016). Hedgehog receptor function during craniofacial development. *Dev Biol* **415**, 198-215.

- Xia, R., Jia, H., Fan, J., Liu, Y. and Jia, J.** (2012). USP8 promotes smoothed signaling by preventing its ubiquitination and changing its subcellular localization. *PLoS Biol* **10**, e1001238.
- Xie, J., Murone, M., Luoh, S. M., Ryan, A., Gu, Q., Zhang, C., Bonifas, J. M., Lam, C. W., Hynes, M., Goddard, A., et al.** (1998). Activating Smoothed mutations in sporadic basal-cell carcinoma. *Nature* **391**, 90-92.
- Yang, J., Li, W., He, X., Zhang, G., Yue, L. and Chai, Y.** (2015). VEGF overexpression is a valuable prognostic factor for non-Hodgkin's lymphoma evidence from a systemic meta-analysis. *Dis Markers* **2015**, 786790.
- Yang, R. B., Ng, C. K., Wasserman, S. M., Colman, S. D., Shenoy, S., Mehraban, F., Komuves, L. G., Tomlinson, J. E. and Topper, J. N.** (2002). Identification of a novel family of cell-surface proteins expressed in human vascular endothelium. *J Biol Chem* **277**, 46364-46373.
- Yao, S., Lum, L. and Beachy, P.** (2006). The ihog cell-surface proteins bind Hedgehog and mediate pathway activation. *Cell* **125**, 343-357.
- Yauch, R. L., Dijkgraaf, G. J., Alicke, B., Januario, T., Ahn, C. P., Holcomb, T., Pujara, K., Stinson, J., Callahan, C. A., Tang, T., et al.** (2009). Smoothed mutation confers resistance to a Hedgehog pathway inhibitor in medulloblastoma. *Science* **326**, 572-574.
- Young, R. P., Whittington, C. F., Hopkins, R. J., Hay, B. A., Epton, M. J., Black, P. N. and Gamble, G. D.** (2010). Chromosome 4q31 locus in COPD is also associated with lung cancer. *Eur Respir J* **36**, 1375-1382.
- Zaphiropoulos, P. G., Unden, A. B., Rahnema, F., Hollingsworth, R. E. and Toftgard, R.** (1999). PTCH2, a novel human patched gene, undergoing alternative splicing and up-regulated in basal cell carcinomas. *Cancer Res* **59**, 787-792.
- Zeng, X., Goetz, J. A., Suber, L. M., Scott, W. J., Jr., Schreiner, C. M. and Robbins, D. J.** (2001). A freely diffusible form of Sonic hedgehog mediates long-range signalling. *Nature* **411**, 716-720.
- Zhang, W., Hong, M., Bae, G. U., Kang, J. S. and Krauss, R. S.** (2011). Boc modifies the holoprosencephaly spectrum of Cdo mutant mice. *Dis Model Mech* **4**, 368-380.
- Zhang, W., Kang, J. S., Cole, F., Yi, M. J. and Krauss, R. S.** (2006). Cdo functions at multiple points in the Sonic Hedgehog pathway, and Cdo-deficient mice accurately model human holoprosencephaly. *Dev Cell* **10**, 657-665.
- Zhang, X. M., Ramalho-Santos, M. and McMahon, A. P.** (2001). Smoothed mutants reveal redundant roles for Shh and Ihh signaling including regulation of L/R asymmetry by the mouse node. *Cell* **105**, 781-792.
- Zhang, Y., Bulkley, D. P., Xin, Y., Roberts, K. J., Asarnow, D. E., Sharma, A., Myers, B. R., Cho, W., Cheng, Y. and Beachy, P. A.** (2018). Structural Basis for Cholesterol Transport-like Activity of the Hedgehog Receptor Patched. *Cell* **175**, 1352-1364 e1314.

**Zhao, Y., Tong, C. and Jiang, J.** (2007). Hedgehog regulates smoothened activity by inducing a conformational switch. *Nature* **450**, 252-258.

**Zheng, X., Mann, R. K., Sever, N. and Beachy, P. A.** (2010). Genetic and biochemical definition of the Hedgehog receptor. *Genes Dev* **24**, 57-71.

**Zhou, X., Baron, R. M., Hardin, M., Cho, M. H., Zielinski, J., Hawrylkiewicz, I., Sliwinski, P., Hersh, C. P., Mancini, J. D., Lu, K., et al.** (2012). Identification of a chronic obstructive pulmonary disease genetic determinant that regulates HHIP. *Hum Mol Genet* **21**, 1325-1335.

**Zhou, Y., Gunput, R. A. and Pasterkamp, R. J.** (2008). Semaphorin signaling: progress made and promises ahead. *Trends Biochem Sci* **33**, 161-170.

**Zhu, J., Nakamura, E., Nguyen, M. T., Bao, X., Akiyama, H. and Mackem, S.** (2008). Uncoupling Sonic hedgehog control of pattern and expansion of the developing limb bud. *Dev Cell* **14**, 624-632.

## Chapter 2 The Hedgehog Co-Receptor BOC Differentially Regulates SHH Signaling During Craniofacial Development

### 2.1 Abstract

The Hedgehog (HH) pathway controls multiple aspects of craniofacial development. HH ligands signal through the canonical receptor PTCH1, and three co-receptors: GAS1, CDON and BOC. Together, these co-receptors are required during embryogenesis to mediate proper HH signaling. Here we investigated the individual and combined contributions of GAS1, CDON and BOC to HH-dependent mammalian craniofacial development. Notably, individual deletion of either *Gas1* or *Cdon* results in variable holoprosencephaly phenotypes, even on a congenic background. In contrast, we find that *Boc* deletion results in facial widening that correlates with increased HH target gene expression. Additionally, *Boc* deletion in a *Gas1* null background partially ameliorates the craniofacial defects observed in *Gas1* single mutants; a phenotype that persists over developmental time, resulting in significant improvements to a subset of craniofacial structures. This contrasts with HH-dependent phenotypes in other tissues that significantly worsen following combined deletion of *Gas1* and *Boc*. Together, these data indicate that BOC acts as a multi-functional regulator of HH signaling during craniofacial development, alternately promoting or restraining HH pathway activity in a tissue-specific fashion.

## 2.2 Introduction

Hedgehog (HH) signaling regulates the patterning and growth of nearly every tissue in the body (Briscoe and Thérond, 2013; McMahon et al., 2003). Aberrant HH pathway activity results in severe birth defects including Holoprosencephaly (HPE), a defect characterized by the failure of the division of the embryonic forebrain into two cerebral hemispheres (Muenke and Beachy, 2000). HPE is one of the most common birth defects in humans, estimated to affect as many as 1 in 250 embryos (Hong and Krauss, 2018). The clinical manifestations of HPE are highly heterogeneous, consisting of a wide phenotypic spectrum of defects (Schachter and Krauss, 2008). Notably, 80% or more of HPE cases will display facial defects in addition to the forebrain malformations (Schachter and Krauss, 2008).

Multiple mutations associated with developmental signaling pathways such as HH, have been identified in human HPE patients (Roessler and Muenke, 2010). Specifically, mutations in *Sonic Hedgehog* (*SHH*) account for 6%-8% of sporadic HPE (Roessler et al., 2009). During craniofacial development *Shh* regulates the establishment of forebrain identity, and patterns the face primordia (Schachter and Krauss, 2008). Moreover, disruption of *Shh* in mice results in abnormal dorsoventral patterning in the neural tube, defective axial skeleton formation and alobar HPE (Chiang et al., 1996).

SHH ligands signal through the twelve-pass transmembrane receptor Patched (PTCH1) (Marigo et al., 1996). However, SHH also binds three co-receptors, growth arrest-specific 1 (GAS1), CAM-related/downregulated by oncogenes (CDON) and brother of CDON (BOC) (Allen et al., 2011; Allen et al., 2007; Beachy et al., 2010; Izzi et al., 2011; Lee et al., 2001; McLellan et al., 2008; Tenzen et al., 2006; Yao et al., 2006; Zhang et al., 2011; Zhang et al.,

2006). CDON and BOC are structurally similar members of the immunoglobulin superfamily that are conserved from *Drosophila* to mammals (Beachy et al., 2010; Kang et al., 1997; Kang et al., 2002; Lum et al., 2003). GAS1 is a vertebrate-specific, GPI-anchored protein with structural resemblance to GDNF receptors (Cabrera et al., 2006). In the absence of SHH ligand, PTCH1 inhibits the activity of the GPCR-like protein Smoothed (SMO). SHH ligand binding to PTCH1 and GAS1, CDON or BOC releases SMO inhibition leading to a signal transduction cascade that leads to modulation of the GLI family of transcriptional effectors (Hui and Angers, 2011). Together, GAS1, CDON and BOC are required for HH signal transduction during embryogenesis (Allen et al., 2011; Allen et al., 2007; Cole and Krauss, 2003; Izzi et al., 2011; Martinelli and Fan, 2007; Tenzen et al., 2006; Zhang et al., 2011; Zhang et al., 2006)

Similar to *Shh* mutants, simultaneous genetic removal of *Gas1*, *Cdon* and *Boc*, results in alobar HPE (Allen et al., 2011). Further, multiple mutations in these HH co-receptors have been identified in human HPE patients (Bae et al., 2011; Hong et al., 2017; Ribeiro et al., 2010), suggesting that these proteins play key roles in craniofacial development. This is supported by multiple studies in mice demonstrating a role for these genes during HH-dependent craniofacial development (Cole and Krauss, 2003; Seppala et al., 2007; Seppala et al., 2014; Zhang et al., 2011; Zhang et al., 2006). *Gas1* and *Cdon* single mutants display microforms of HPE, in which the severity of the phenotype is dependent on the genetic background of the mouse model (Allen et al., 2007; Cole and Krauss, 2003; Seppala et al., 2007; Zhang et al., 2006). In contrast, in mixed genetic backgrounds *Boc* deletion does not result in any HPE phenotypes, although these animals do display defects in SHH-dependent commissural axon guidance (Okada et al., 2006; Seppala et al., 2014; Zhang et al., 2011). More recently, *Boc* has been demonstrated to function as silent HPE modifier gene that, in the context of other HPE mutations, can modify the severity

of the HPE phenotype (Hong and Krauss, 2018). It has been proposed that modifier genes like *Boc* contribute to the phenotypic differences observed in different genetic backgrounds.

GAS1, CDON and BOC have generally been described as positive regulators of the HH signaling pathway. However, in certain contexts these co-receptors can act to restrain HH signaling. For example, *Gas1* can antagonize HH signaling in presomitic mesoderm explants (Lee et al., 2001), and restricts HH signaling during tooth development in mice (Cobourne et al., 2004; Ohazama et al., 2009). Similarly, *Cdon* negatively regulates HH pathway function in the optic vesicle of zebrafish and chick embryos (Cardozo et al., 2014). It remains unclear how these co-receptors differentially regulate HH signaling in these different contexts.

Here we investigated the contributions of GAS1, CDON and BOC to HH-dependent mammalian craniofacial development. Specifically, we examined the individual and combined deletion of different HH co-receptors on a congenic C57BL/6J background. Surprisingly, we found that *Boc* mutants display facial widening and increased HH target gene expression in the nasal processes. Additionally, deletion of *Boc* in a *Gas1* null background partially ameliorates the craniofacial defects observed in *Gas1* single mutants, while other HH-dependent phenotypes in these mutants are significantly worsened. Interestingly, the rescue of the craniofacial defects in *Gas1;Boc* mutants persists over developmental time, but is restricted to the nostrils and the soft tissues of the craniofacial structures. Finally, we provide evidence that BOC selectively restricts neural crest-derived mesenchymal proliferation. Together, our data indicate that BOC acts as a multi-functional regulator of HH signaling during craniofacial development, alternately promoting or restraining HH pathway activity in a tissue-specific fashion.



## 2.3 Results

To define the expression of the HH pathway co-receptors *Gas1*, *Cdon* and *Boc* during early craniofacial development, we utilized *lacZ* (*Gas1* and *Cdon*) and *Alkaline phosphatase* (*AP*; *Boc*) reporter alleles (Figure 2.1) (Cole and Krauss, 2003; Martinelli and Fan, 2007; Zhang et al., 2011). At E8.5 *Gas1*, *Cdon* and *Boc* are primarily expressed in the cranial neural folds, the somites and the neural tube (Figure 2.1A-D). During this stage *Cdon* is the only co-receptor expressed in the prechordal plate (PCP; see arrowhead in Figure 2.1C inset), a major signaling center during craniofacial development that secretes SHH ligand, which patterns the ventral forebrain (Cordero et al., 2004; Rubenstein and Beachy, 1998; Zhang et al., 2006). As development progresses, these expression patterns are maintained in the somites and neural tube, and expand to additional structures. At E9.5 the HH co-receptors are all expressed in the frontonasal prominence (FNP), maxillary process (MXP) and mandibular process (MP; Figure 2.1E-H). Differences in *Gas1*, *Cdon* and *Boc* expression in craniofacial structures are revealed by analysis of E10.5 embryos (Figure 2.1I-T).

En face views of whole-mount stained E10.5 embryos (Figure 2.1M-P) demonstrate broad expression of *Gas1*, *Cdon* and *Boc* in the forebrain. X-Gal and AP staining in coronal sections of E10.5 embryos reveals that all three co-receptors are present in the surface ectoderm and in the forebrain neuroepithelium (NE) in a dorso-ventral gradient (Figure 2.1Q-T; Figure 2.2A-D). Notably, the ventral extent of *Cdon* expression in the NE is greatly restricted compared to *Gas1* and *Boc*. Similarly, *Gas1* and *Boc* display broad expression in the olfactory epithelium (OE), while *Cdon* expression is limited to a subset of cells in the medial OE of the LNP (see arrowhead in Figure 2.1S, Figure 2.2G).

At E10.5, *Gas1* is the only co-receptor expressed in the MP and in the MXP (Figure 2.1J, N). Further differences in the expression of the HH co-receptors are detected in the medial nasal and lateral nasal processes (MNP and LNP). All three co-receptors are expressed in the LNP (Figure 2.1Q-T). However, *Gas1* and *Boc* are expressed throughout the LNP mesenchyme, while *Cdon* expression is restricted to the most dorsal aspect of the LNP mesenchyme (Figure 2.1S, Figure 2.2G). In the MNP, *Gas1* and *Boc* are broadly expressed at lower levels in the mesenchyme; in contrast, *Cdon* is only expressed in mesenchymal cells that are proximal to the NE (Figure 2.1S, Figure 2.2G). The expression of *Gas1*, *Cdon* and *Boc* in the craniofacial structures is consistent with their general negative transcriptional regulation by the HH signaling pathway (Allen et al., 2007; Tenzen et al., 2006). In addition to the differences in expression of the HH co-receptors in craniofacial structures, their expression in other HH-responsive tissues such as the forelimb bud (Figure 2.2J-L), and the neural tube (Figure 2.2N-P) is also not identical. In particular, the expression domains of *Boc* in the forebrain neuroepithelium (Figure 2.2H) and in the neural tube (Figure 2.2 P) extend further ventrally, and closer to the sources of *Shh* expression in these tissues, namely the ventral telencephalon and the notochord/floor plate, respectively. These data raise the question of whether these co-receptors, and *BOC* in particular, may differentially contribute to HH-dependent craniofacial development.

To address the individual contributions of *Gas1*, *Cdon*, and *Boc* to craniofacial development, we examined single mutant embryos at mid-gestation on a congenic C57BL/6J background (Figure 2.3). At E10.5 *Gas1*<sup>-/-</sup> and *Cdon*<sup>-/-</sup> embryos display a spectrum of HPE phenotypes that range from proper telencephalic vesicle (TV) division with normal MNP separation, to no TV division with no MNP separation (Figure 2.4). Most of these mutants exhibit incomplete TV division (76% of *Gas1*<sup>-/-</sup> embryos, and 50% of *Cdon*<sup>-/-</sup> embryos), while a

smaller portion (12% and 17%, respectively) of these mutants fails to divide the TV (Figure 2.4H). *Gas1*<sup>-/-</sup> and *Cdon*<sup>-/-</sup> embryos predominantly show either incomplete MNP separation (47% of *Gas1*<sup>-/-</sup> embryos, and 33% of *Cdon*<sup>-/-</sup> embryos) or no MNP separation (29% and 42%, respectively; Figure 2.4I). Notably, a minority of *Gas1* and *Cdon* mutants have more mild phenotypes that are characterized by normal TV division (Figure 2.4H) and either normal or reduced MNP separation (Figure 2.4I). In contrast, *Boc*<sup>-/-</sup> embryos do not manifest any gross craniofacial defects (Figure 2.3J-L), with 100% of embryos displaying normal TV division and normal MNP separation (Figure 2.4H-I). Together, these data indicate that even on a congenic C57BL/6J genetic background there remains a spectrum of HPE phenotypes observed in *Gas1* and *Cdon* mutants. Strikingly, and despite the broad expression of *Boc* in multiple HH-responsive cell types in the developing forebrain (Figure 2.1), we do not observe any HPE phenotypes in *Boc* mutants maintained on a C57BL/6J background.

To further characterize the spectrum of HPE phenotypes, we quantified the internasal distance in E10.5 embryos. Consistent with our initial assessment, this quantitation revealed significant reductions in the internasal distance in both *Gas1* and *Cdon* mutant embryos (Figure 2.3M). Surprisingly, this quantitation also revealed an unexpected subtle, but significant increase in the internasal distance in *Boc* mutant embryos compared to wildtype embryos (443µm in wildtype embryos, and 496µm *Boc*<sup>-/-</sup> embryos; Figure 2.3M). These data suggest potentially opposing roles for *Gas1* and *Cdon* compared to *Boc* during mammalian craniofacial development. One explanation for these counterintuitive results is that the increased internasal distance in *Boc* embryos was due to an overall increase in embryo size. Therefore, we measured the crown-rump length (CRL) in E10.5 wildtype and mutant embryos (Figure 2.5A-E). While *Gas1* mutants are significantly smaller than their wildtype littermates, both *Cdon* and *Boc* mutant

embryos have similar CRL as wildtype embryos (Figure 2.5F). These data support the notion that the MNP widening observed in *Boc* mutants at E10.5 reflects differences in the contribution of this HH co-receptor to craniofacial development. Interestingly, widening or duplication of midfacial tissues is associated with increased levels of HH signaling (Brugmann et al., 2010; Hu and Helms, 1999).

To determine if the variable craniofacial defects observed in these HH co-receptor mutant embryos correlates with HH pathway activity, we performed *in situ* hybridization for *Gli1*, a general and direct transcriptional target of HH signaling (Dai et al., 1999). *Gli1* is expressed in multiple craniofacial structures, including the MNP, MXP and MP (Figure 2.6A). *Gas1*<sup>-/-</sup> and *Cdon*<sup>-/-</sup> embryos with less severe HPE phenotypes maintain *Gli1* expression in the MNP, but embryos with increasingly severe HPE phenotypes display a loss of *Gli1* expression in the MNP (Figure 2.6D-F, G-I). In contrast, in *Boc*<sup>-/-</sup> embryos *Gli1* expression is maintained in the MNP across all *Boc* mutant embryos (Figure 2.6J-L). To quantify changes in *Gli1* expression we performed qRT-PCR in E11.5 nasal processes (Figure 2.3N). *Boc*<sup>-/-</sup> embryos display a significant increase in *Gli1* expression, consistent with the internasal distance widening (Figure 2.3M). In contrast, and consistent with the *in situ* hybridization data, *Gas1*<sup>-/-</sup> embryos display a significant decrease in *Gli1* (Figure 2.3N). We also explored if changes in *Gli1* mRNA translated into protein level differences (Figure 2.3O). *Boc* mutants maintain similar levels of GLI1 protein as wildtype embryos, while GLI1 protein is reduced in *Gas1* mutants. While these changes do not reach the level of statistical significance (Figure 2.5G), these results are consistent with both the *Gli1* *in situ* hybridization and qRT-PCR results. Taken together, these data indicate that HPE severity in *Gas1* and *Cdon* mutant embryos correlates with *Gli1* loss in the nasal processes, and demonstrate that, in contrast to *Gas1* and *Cdon*, *Boc* mutants display increased *Gli1* expression

in the nasal processes. These data suggest an antagonistic role for BOC during HH-dependent craniofacial development.

Previous studies have suggested that combinatorial deletion of *Gas1*, *Cdon*, or *Boc* results in more severe HPE phenotypes (Allen et al., 2011; Allen et al., 2007; Seppala et al., 2014; Zhang et al., 2011), suggesting that HH co-receptors positively regulate HH signaling during craniofacial development. In contrast, the midface widening that we observe in *Boc*<sup>-/-</sup> embryos (Figure 2.3M) is consistent with a role for *Boc* as a potential HH antagonist during craniofacial development. To explore this possibility, we deleted *Boc* in combination with *Gas1* deletion on a congenic C57BL/6J background.

Analysis of E10.5 *Gas1*<sup>-/-</sup>;*Boc*<sup>-/-</sup> embryos revealed a spectrum of HPE phenotypes, as observed in *Gas1*<sup>-/-</sup> embryos (Figure 2.7). Importantly, the HPE phenotypes observed in *Gas1*;*Boc* double mutants are less severe than those observed in *Gas1* single mutants (cf. Figure 2.7B and 2.7D). Specifically, we observed an increase in the percentage of *Gas1*;*Boc* double mutants with normal TV division compared to *Gas1* single mutants (31% vs. 12%, respectively; Figure 2.7E). Further, we found that 50% of *Gas1*;*Boc* double mutants display MNP separation compared to 24% of *Gas1* mutants (Figure 2.7F). To investigate whether this rescue was due to increased overall embryo size, we measured the CRL of *Gas1*<sup>-/-</sup>;*Boc*<sup>-/-</sup> embryos (Figure 2.8A-E). We find that *Gas1*<sup>-/-</sup>;*Boc*<sup>-/-</sup> embryos tend to be smaller than *Gas1*<sup>-/-</sup> embryos (Figure 2.8F); while not statistically significant, these data rule out increased embryo size as an explanation for the rescue of the HPE phenotypes. Overall, these data suggest that *Boc* deletion in a *Gas1* mutant background partially rescues TV and MNP separation in E10.5 embryos.

To determine if the phenotypes observed in *Gas1*;*Boc* mutants correlate with changes in HH pathway activity, we performed *in situ* hybridization for the direct HH transcriptional target

*Gli1* in E10.5 wildtype, *Gas1*<sup>-/-</sup>, *Boc*<sup>-/-</sup>, and *Gas1*<sup>-/-</sup>;*Boc*<sup>-/-</sup> embryos (Figure 2.7G-J). *Gas1*<sup>-/-</sup>;*Boc*<sup>-/-</sup> embryos that display increased MNP separation also display increased *Gli1* expression in the MNP (Figure 2.7J), consistent with the notion that *Boc* antagonizes HH pathway activity during craniofacial development. Similarly, *Gas1*;*Boc* mutants that do not display the rescue of the craniofacial defects, exhibit decreased *Gli1* levels, indicating that the rescue is HH-dependent (Figure 2.6M-O). We also examined *Gli1* expression in the forelimb bud from these same embryos (Figure 2.7G'-J'). While we do not observe significant differences in *Gli1* gene expression, or GLI1 protein levels in *Gas1* or *Boc* single mutants (Figure 2.9), we do detect decreased *Gli1* expression in *Gas1*;*Boc* double mutant embryos (cf. Figure 2.7G', H', J'). Together these data suggest that loss of *Boc* partially and selectively rescues HPE phenotypes observed in *Gas1* mutant embryos, through increased HH pathway activity specifically in craniofacial structures.

To examine the consequences of *Boc* deletion on additional targets of the HH pathway, and to begin to dissect possible tissue-specific contributions to craniofacial development, we investigated HH-dependent neural patterning in both the developing forebrain and spinal cord (Figure 2.10). Specifically, we used whole mount immunofluorescence to analyze the expression of NKX2.1, a direct HH transcriptional target in the ventral telencephalon (Pabst et al., 2000) (Figure 2.10E-H,M). In E10.5 *Gas1*<sup>-/-</sup> embryos the expression domain of NKX2.1 is significantly reduced (Figure 2.10F), while NKX2.1 expression in *Boc*<sup>-/-</sup> embryos is unchanged compared to wildtype embryos (cf. Figure 2.10E,G). Notably, compared to *Gas1*<sup>-/-</sup> embryos (Figure 2.10F), *Gas1*<sup>-/-</sup>;*Boc*<sup>-/-</sup> embryos maintain similar levels of NKX2.1 expression (Figure 2.10H). Quantitation confirms that NKX2.1 is not significantly altered in *Gas1*<sup>-/-</sup>;*Boc*<sup>-/-</sup> embryos compared to *Gas1*<sup>-/-</sup> embryos (Figure 2.10M). We also confirmed that NKX2.1 is not

significantly different in *Boc*<sup>-/-</sup> embryos (Figure 2.10M). Together, these data suggest that, despite its broad expression in the forebrain neuroepithelium (Figure 2.1T), *Boc* does not positively contribute to HH-dependent patterning in this tissue. These data do raise the question of whether *Boc* can regulate HH signaling in the developing telencephalon, or whether it may be playing an antagonistic role. To address these possibilities, we used chicken *in ovo* telencephalon electroporations to assess *Boc* function during HH-dependent neural patterning in the forebrain (Figure 2.11). Expression of GFP (pCIG, empty vector) in the chicken telencephalon does not affect NKX2.1 expression (Figure 2.11A-D). In contrast, expression of *SmoM2* (a constitutively active form of SMO) (Xie et al., 1998), which drives high levels of HH pathway activity, induces ectopic NKX2.1 expression (Figure 2.11E-H). Similarly, expression of *Boc* also induces ectopic NKX2.1 expression (Figure 2.11I-L). These data demonstrate that *Boc* can promote HH-dependent patterning in the developing chicken forebrain, and suggests that *Boc* does not play an antagonistic role in the forebrain neuroepithelium.

We also analyzed HH-dependent neural patterning in the spinal cord of wildtype, *Gas1*<sup>-/-</sup>, *Boc*<sup>-/-</sup>, and *Gas1*<sup>-/-</sup>;*Boc*<sup>-/-</sup> embryos (Figure 2.10I-L,N). We examined the expression of NKX2.2 and OLIG2, two direct HH transcriptional targets that are activated in response to high and moderate levels of SHH signaling, respectively (Briscoe et al., 2000; Dessaud et al., 2008). At E10.5, *Gas1*<sup>-/-</sup> embryos display a significant reduction in the number of NKX2.2+ cells compared to wildtype embryos (Figure 2.10J,N). In contrast, the number of NKX2.2+ cells are not significantly reduced in *Boc*<sup>-/-</sup> embryos (Figure 2.10K,N). Strikingly, *Gas1*<sup>-/-</sup>;*Boc*<sup>-/-</sup> embryos have a very severe phenotype— OLIG2 expression is completely absent (Figure 2.10L), and we observe a near complete absence of NKX2.2 expression (Figure 2.10L,N). In some sections from *Gas1*;*Boc* mutants we could detect a few NKX2.2+ cells (Figure 2.10L, inset). Overall, these

data are consistent with previous studies (Allen et al., 2011), and further demonstrate that *Boc* selectively contributes to spinal cord, but not forebrain neural patterning.

Given that E10.5 *Gas1*<sup>-/-</sup>;*Boc*<sup>-/-</sup> mutants manifest a partial rescue of the craniofacial defects observed in *Gas1* single mutants, we investigated whether this rescue is maintained over developmental time. This question is particularly relevant since a prior analysis of *Gas1*<sup>-/-</sup>;*Boc*<sup>-/-</sup> embryos maintained on a mixed 129sv/C57BL/6/CD1 background demonstrated severe craniofacial defects such as clefting of the lip, palate and tongue, and disruption of the maxillary incisor (Seppala et al., 2014). To address this question, we examined craniofacial development in E18.5 wildtype and mutant embryos (Figure 2.12A-D). Consistent with previous work, E18.5 *Gas1*<sup>-/-</sup> embryos display a range of craniofacial defects, while *Boc*<sup>-/-</sup> embryos appear phenotypically normal (Figure 2.12A-C, Figure 2.13A-B, H-I) (Allen et al., 2011; Allen et al., 2007; Martinelli and Fan, 2007; Seppala et al., 2007; Seppala et al., 2014; Zhang et al., 2011). *Gas1*<sup>-/-</sup> and *Gas1*<sup>-/-</sup>;*Boc*<sup>-/-</sup> embryos share defects that include microphthalmia, midface and mandible hypoplasia, and cleft palate (Martinelli and Fan, 2007). Strikingly, and similar to what was observed during earlier developmental stages, E18.5 *Gas1*<sup>-/-</sup>;*Boc*<sup>-/-</sup> mutants display a less severe phenotype in specific craniofacial structures (Figure 2.12D,P). Specifically, *Gas1*<sup>-/-</sup>;*Boc*<sup>-/-</sup> mutants display a wider maxilla and partial separation of the nasal pits; in comparison, *Gas1*<sup>-/-</sup> embryos have a smaller maxilla and no separation of the nasal pits (cf. black and white arrows in Figure 2.12B,D). Skeletal preparations (Figure 2.12E-L) confirm that *Gas1*<sup>-/-</sup>;*Boc*<sup>-/-</sup> mutants exhibit separation of the nasal capsule, while in *Gas1*<sup>-/-</sup> single mutants the nasal capsule is not separated (Figure 2.12F,H). In addition to the nasal capsule, some *Gas1*<sup>-/-</sup>;*Boc*<sup>-/-</sup> embryos exhibit widening of the premaxilla, although in others it is hypoplastic (see red arrow in Figure 2.12H



and inset in Figure 2.13J). These data suggest that the amelioration of the craniofacial defects observed at E10.5 in *Gas1;Boc* mutant embryos persists over developmental time.

In contrast to the nasal capsule and premaxilla, *Gas1<sup>-/-</sup>;Boc<sup>-/-</sup>* embryos exhibit a shortened mandible and truncated meckel's cartilage compared to *Gas1<sup>-/-</sup>* embryos (Figure 2.12J,L). The mandible of *Gas1<sup>-/-</sup>;Boc<sup>-/-</sup>* mutants also exhibit ectopic bone duplications on the posterior inferior side of the mandible (Figure 2.12L). Occasionally, *Gas1<sup>-/-</sup>* mutants with severe HPE phenotypes display a similar phenotype (Figure 2.12J inset). Bone duplications have been associated with loss of HH signaling in the mandibular neural crest derived mesenchyme (Jeong et al., 2004; Xu et al., 2019). *Gas1<sup>-/-</sup>;Boc<sup>-/-</sup>* mutants also display severe defects in the maxilla, palatine bone and the occipital bone (Figure 2.13J). We also evaluated SHH-dependent digit specification in these embryos (Figure 2.13G'-J'). Consistent with previous work (Allen et al., 2011), combined loss of *Gas1* and *Boc* results in severe digit specification defects (Figure 2.13J'). These results suggest opposing and tissue-specific contributions of *Boc* to HH-dependent craniofacial development.

To further investigate these phenotypes, we analyzed three (3D) dimensional reconstructions from micro-computed tomography ( $\mu$ CT) images (Figure 2.12M'-P', Figure 2.13A'-D'). Specifically, we focused on the nasal bone, where we observed the partial rescue in *Gas1;Boc* mutants. The 3D reconstructions indicated that the nasal bone in *Gas1<sup>-/-</sup>;Boc<sup>-/-</sup>* embryos is reduced in size and partially fused when compared to wildtype embryos (Figure 2.12M', P'). As we observed at E10.5 (Figure 2.7), there is a spectrum of HPE phenotypes in *Gas1* mutants, ranging from reduced and fused nasal bone to fragments of nasal bone (Figure 2.12N', Figure 2.13A-D). *Gas1;Boc* mutants display an intermediate nasal bone phenotype when compared to the spectrum of phenotypes in *Gas1* single mutants (Figure 2.12N',P', Figure 2.13A'-D').

Quantitation of head width in E18.5 embryos demonstrates that *Gas1;Boc* mutants display a significantly narrower head compared to *Gas1* mutants (Figure 2.14A-B), consistent with our observations at E10.5 that *Gas1;Boc* mutant embryos trend smaller overall than *Gas1* single mutants (Figure 2.8F). Accounting for this size difference, *Gas1;Boc* mutant embryos exhibit a significant increase in interocular distance when compared to *Gas1* mutant embryos (Figure 2.14A, C). Examination of nostril frequency at E18.5 revealed that 100% (8/8 embryos) of *Gas1<sup>-/-</sup>;Boc<sup>-/-</sup>* embryos display two partially fused nostrils; in contrast only 58% (7/12 embryos) of *Gas1<sup>-/-</sup>* embryos exhibit two partially nostrils, while 42% (5/12 embryos) display a single nostril (Figure 2.14E). Finally, *Gas1;Boc* mutants exhibit a significantly wider medial lip notch distance at E18.5 than *Gas1* mutants (Figure 2.14F). Taken together these data demonstrate that *Boc* deletion in a *Gas1* mutant background significantly ameliorates several craniofacial defects at later developmental stages, consistent with the phenotypes observed at E10.5.

To investigate the mechanisms that could explain the partial rescue observed in *Gas1<sup>-/-</sup>;Boc<sup>-/-</sup>* embryos, we analyzed tissue-specific proliferation in the forebrain of E10.5 wildtype and mutant embryos. Specifically, we performed immunofluorescence for Phospho-Histone H3 (PH3), and co-stained with E-CADHERIN (E-CAD) and PDGFR $\alpha$  to discriminate between the surface ectoderm, forebrain neuroepithelium, and craniofacial mesenchyme (Figure 2.15A-E). Coronal sections of E10.5 *Gas1<sup>-/-</sup>* mutant embryos display normal numbers of PH3+ cells across the surface ectoderm and forebrain neuroepithelium (Figure 2.15B,F-G). In the craniofacial mesenchyme *Gas1* mutant embryos display a subtle increase in PH3+ cells that fails to reach statistical significance (Figure 2.15H). *Cdon<sup>-/-</sup>* embryos do not exhibit any significant changes in proliferation in any of the craniofacial tissues (Figure 2.15F-H). Similarly, *Boc<sup>-/-</sup>* embryos do not

display any apparent changes in proliferation in the surface ectoderm or in the neuroepithelium (Figure 2.15F,G). However, *Boc*<sup>-/-</sup> embryos do display a significant increase in craniofacial mesenchymal proliferation compared to wildtype embryos (Figure 2.15D,H). These results suggest that *Boc* negatively regulates proliferation specifically in craniofacial mesenchyme.

We also investigated tissue-specific proliferation in *Gas1*<sup>-/-</sup>;*Boc*<sup>-/-</sup> mutant embryos. Notably, the levels of proliferation in the surface ectoderm and the forebrain neuroepithelium are not significantly different when compared to wildtype or *Gas1*<sup>-/-</sup> embryos (Figure 2.15F-G). In contrast, proliferation is significantly increased in the craniofacial mesenchyme of *Gas1*;*Boc* mutants when compared to wildtype embryos, although not when compared with *Gas1* mutants. (Figure 2.15H). Surprisingly, this effect on proliferation appears to be quite selective, as there are no significant changes in proliferation in either the neural tube or the forelimb mesenchyme (Figure 2.16). Overall, these data suggest that *Boc* functions in a non-redundant manner to restrict proliferation in the craniofacial mesenchyme.

## 2.4 Discussion

Here we investigated the individual and combined contributions of the HH co-receptors *Gas1*, *Cdon* and *Boc* during HH-dependent craniofacial development. We found that *Boc* displays a significantly broader expression pattern than *Gas1* and *Cdon* in multiple craniofacial structures. Surprisingly, and distinct from *Gas1* and *Cdon*, loss of *Boc* results in facial widening and increased HH pathway activity in the nasal processes (Brugmann et al., 2010; Hu and Helms, 1999). Further, analysis of *Gas1*;*Boc* double mutants revealed an amelioration of the craniofacial phenotype observed in *Gas1* single mutants, corresponding with increased HH pathway activity, and consistent with the notion that loss of *Boc* can counterintuitively drive increased HH

signaling. Notably, this improvement is restricted to a subset of craniofacial structures, but persists throughout embryonic development. Mechanistic analyses suggest that *Boc* selectively restricts proliferation in neural crest-derived mesenchyme and limits HH pathway activity in the nasal processes. Taken together, these data demonstrate that *Boc* regulates HH signaling in a tissue-specific manner, and suggests that, in certain tissues, BOC works in opposition to other HH co-receptors to restrain HH pathway function.

#### 2.4.1 Genetic background-dependent phenotypic differences in HH co-receptor mutants

Understanding the molecular mechanisms that underlie HPE is confounded by the significant phenotypic variability observed in this disease, and the complex genetics that contribute to proper craniofacial development. Our data indicate that, even when maintained on a congenic C57BL/6J background, *Gas1* and *Cdon* mutants display a range of HPE phenotypes. These phenotypes vary from microforms of HPE to semilobar HPE, and their severity correlates with HH pathway activity as assessed by *Gli1* expression. The variability in the HPE phenotypes of our mutants could be explained due to multiple genetic and non-genetic risk factors (Hong and Krauss, 2018). In particular, the variable severity across the phenotypes in our mutants could arise from stochastic changes in the establishment or response to the SHH morphogen gradient in the neuroepithelium, neural crest-derived mesenchyme and/or surface ectoderm. In early craniofacial structures *Shh* is expressed sequentially, initiating in the prechordal plate, followed by the diencephalon and telencephalon, subsequently in the surface ectoderm of the frontonasal prominence, and finally in the pharyngeal endoderm of the first branchial arch (Aoto et al., 2009; Cordero et al., 2004; Marcucio et al., 2005; Rubenstein and Beachy, 1998; Xavier et al., 2016a). This complex developmental expression sequence of *Shh*, which is required to properly pattern

the craniofacial structures (Krauss, 2007), combined with the differential expression of multiple HH receptors could generate an inherent variability that affects the severity of the HPE phenotypes.

The lack of craniofacial defects in *Boc* mutants maintained on different genetic mixed backgrounds (Okada et al., 2006; Seppala et al., 2014; Zhang et al., 2011) suggested a minor, redundant role for *Boc* in HH-dependent craniofacial development. This notion of *Boc* as a silent HPE modifier gene is supported by studies where *Boc* deletion in a *Gas1* or *Cdon* null background enhances HPE severity and decreases the levels of HH pathway targets (Seppala et al., 2014; Zhang et al., 2011). However, our data indicate that *Boc* mutants on a C57BL/6J background exhibit internasal distance widening in E10.5 embryos and increased *Gli1* expression specifically in the nasal processes. These data suggest an antagonistic role for *Boc* in HH signaling during craniofacial development. Previous studies described *Boc* as a potential HH pathway antagonist in the zebrafish lower jaw (Bergeron et al., 2011). However, this study is limited to a brief phenotypic description of the thickening and expansion of the cartilage elements in the lower jaw of *Boc* (*umleitung*) zebrafish mutants, and does not examine the effects of *Boc* deletion on HH pathway activity in this tissue. While we do not observe any mandible phenotypes in *Boc*<sup>-/-</sup> embryos, species-specific differences in craniofacial development between mouse and fish likely limit our ability to draw a direct connection. Alternatively, our analysis of *Boc* in the developing mandible may not be comprehensive enough to reveal this function. Regardless, our data reveal a novel, antagonistic role for *Boc* during aspects of craniofacial development, and raises the question of whether BOC may work in concert with other known redundant HH pathway antagonists, including PTCH1, PTCH2 and HHIP1, to maintain the balance between HH pathway activation and inhibition (Holtz et al., 2013) in the craniofacial

structures. Additionally, our data suggest that HH co-receptors can function to alternately promote or antagonize HH signaling depending on the context. In support of this notion, *Gas1* can antagonize HH signaling in presomitic mesoderm explants (Lee et al., 2001), and restricts HH signaling during tooth development in mice (Cobourne et al., 2004; Ohazama et al., 2009). Similarly, *Cdon* negatively regulates HH pathway function in the optic vesicle of zebrafish and chick embryos (Cardozo et al., 2014).

*Boc* deletion partially rescues the HPE phenotypes of *Gas1* single mutants. Specifically, *Gas1;Boc* double mutants display increased MNP separation at E10.5 and increased interocular distance, partially restored nostril frequency, and broader medial lip notch distance at E18.5. Importantly, these phenotypes correlate with increased *Gli1* levels in the MNP and increased proliferation in the neural crest mesenchyme. While the combination of these tissue-specific effects could mediate the rescue of the craniofacial defects in *Gas1;Boc* mutants, the incomplete penetrance of the rescue indicates that the variable HPE phenotypes observed in *Gas1* single mutants also impacts the degree of rescue. Overall, this suggests a more complex mechanism, where genetic, epigenetic, and environmental cues all contribute to proper craniofacial development. Along these lines, our data partially contrast with previous work (Seppala et al., 2014), in which *Gas1;Boc* mutants on a 129Sv-C57BL/6/CD1 genetic background display more severe phenotypes than those observed in *Gas1* mutants (Seppala et al., 2014). Although *Gas1;Boc* mutants on a C57BL/6J background display severe defects in the majority of the bones of the skull and cleft palate as previously reported (Seppala et al., 2014), we never observe clefting of the lip in these mutants. Given that the lip is formed by the fusion of the MXP and the nasal processes (Jiang et al., 2006), this result is consistent with the partial rescue mediated by *Boc* deletion in the nasal bone and nasal capsule.

#### 2.4.2 Tissue-specific functions of *Boc* in HH signal transduction

Analysis of HH transcriptional targets revealed that *Boc* deletion results in differential changes in HH-dependent gene expression in a tissue-specific fashion (Figure 2.17A). Specifically, our data suggest that BOC promotes the expression of the direct HH transcriptional target, NKX2.2, in the spinal cord neuroepithelium, but does not contribute to expression of NKX2.1 in the telencephalon neuroepithelium. These data suggest that BOC differentially regulates HH-dependent neural patterning at distinct axial levels. In the surface ectoderm, BOC does not impact proliferation; further experiments will be required to determine if BOC contributes to patterning of this tissue (Figure 2.17A). Further, BOC promotes *Gli1* expression in the limb bud mesenchyme, but antagonizes *Gli1* expression in the forebrain mesenchyme. Notably, *Boc* appears to selectively impact HH-dependent patterning, but not proliferation in the developing limb bud; conversely, *Boc* selectively inhibits proliferation in the neural crest-derived mesenchyme of the craniofacial structures (Figure 2.17A). This is consistent with previous work by (Xavier et al., 2016b) suggesting that *Boc* contributes to mesenchymal proliferation in the palatal shelf. Taken together, these data argue that BOC regulates patterning and proliferation in a tissue-specific manner and raises the possibility that BOC performs multiple, and in some cases, opposing roles in HH signal transduction.

#### 2.4.3 *Boc* as a multi-functional regulator of HH signaling

Based on our data, and the work of others, we propose a model whereby BOC acts as a multi-functional receptor to contribute to vertebrate embryogenesis (Figure 2.17B). Specifically, we propose that BOC can act to: 1) promote HH signaling through interactions with HH ligands

and the canonical receptor PTCH1; 2) antagonize HH signaling, either through ligand sequestration, or perhaps through the formation of an inhibitory complex with PTCH1; 3) contribute to HH-dependent signaling via its unique cytoplasmic domain; 4) function independently of the HH pathway.

BOC physically interacts with PTCH1 in a SHH-independent manner (Izzi et al., 2011). In craniofacial structures PTCH1 and BOC are both expressed in the MNP (Seppala et al., 2014). The differential interaction of these proteins could allow the formation of a receptor complex that alternately activates or inhibits HH pathway activity. Alternatively, BOC binding to HH ligands via its extracellular domain (Beachy et al., 2010; McLellan et al., 2008; Yao et al., 2006) raises the possibility that BOC can sequester SHH ligand in areas of low SHH concentration, and subsequently antagonize HH signaling. Consistent with this notion, *Boc* expression in HH-responsive tissues generally extends closer to the source of SHH ligand than either *Gas1* or *Cdon*. In particular, at E10.5 *Boc* is expressed in the surface ectoderm of the MNP, where *Shh* is also expressed (Xavier et al., 2016a). Loss of *Boc* in the MNP could allow for the expansion of SHH protein distribution, resulting in increased pathway function, and subsequently in widening of the midface. This putative increased range of SHH could similarly explain the partial rescue of craniofacial defects in *Gas1;Boc* mutants compared to *Gas1* single mutants.

BOC displays a unique cytoplasmic domain that does not resemble any other protein or motif (Kang et al., 2002). Recently work suggests that the BOC cytoplasmic domain binds to the non-receptor tyrosine kinase ABL (Vuong et al., 2017) and to the adaptor protein ELMO1 (Makihara et al., 2018). Thus, this domain could be critical to mediate tissue-specific, HH-dependent signals, or to perform HH-independent functions through the activation of downstream signaling cascades. Future work will be required to determine potential



contributions of these mechanisms to BOC tissue-specific functions during craniofacial development. Overall, this work identifies multiple and distinct roles for BOC in HH-dependent craniofacial development.

## 2.5 Materials and methods

### Reagents

General reagents (Table 2.1), primary and secondary antibodies for immunofluorescence (Table 2.2), western blot analysis antibodies (Table 2.3) and qRT-PCR Primers (Table 2.4).

### Animal Models

*Gas1<sup>lacZ</sup>* (Martinelli and Fan, 2007), *Cdon<sup>lacZ-2</sup>* (Cole and Krauss, 2003), and *Boc<sup>AP</sup>* (Zhang et al., 2011) mice have been all described previously. *Gas1*, *Cdon*, and *Boc* mutants were backcrossed for at least ten generations to create lines on a congenic C57BL/6J background. *Cdon<sup>lacZ-1</sup>* mice (Cole and Krauss, 2003) were maintained on a mixed 129/Sv/C57BL/6 background for expression analysis. For embryonic dissections, noon of the day on which a vaginal plug was detected was considered as E0.5. For precise staging, somites were counted during the dissection. Embryos with 34-38 somites were considered E10.5 embryos. Fertilized eggs were obtained from the Poultry Teaching & Research Center at Michigan State University. To obtain Hamburger-Hamilton (HH) stage 11 chicken embryos, the fertilized eggs were incubated 39-40 hours at 37°C in a GQF 1550 hatcher incubator with normal humidity settings (45%-55%). All animal procedures were reviewed and approved by the Institutional Animal Care and Use Committee (IACUC) at the University of Michigan.

### X-gal staining

Embryos were dissected in 1X PBS, pH 7.4, and fixed (1% formaldehyde, 0.2% glutaraldehyde, 2mM MgCl<sub>2</sub>, 5mM EGTA, 0.02% NP-40) on ice for 10-60 minutes depending on the embryonic stage. Subsequently, the embryos were washed 3 x 5 minutes with 1X PBS, pH 7.4 + 0.02% NP-40 for permeabilization.  $\beta$ -Galactosidase activity was detected with X-Gal staining solution (5mM K<sub>3</sub>Fe(CN)<sub>6</sub>, 5mM K<sub>4</sub>Fe(CN)<sub>6</sub>, 2mM MgCl<sub>2</sub>, 0.01% Na deoxycholate, 0.02% NP-40, 1mg/mL X-gal). The signal was developed from 25 minutes to 24 hours at 37° C depending on the *lacZ* allele. After staining, the embryos were washed 3 x 5 minutes with 1X PBS, pH 7.4 at 4°C, and post-fixed in 4% paraformaldehyde for 20 minutes at room temperature, followed by 3 x 5 minute washes in 1X PBS, pH 7.4. Finally, embryos were stored and photographed in 1X PBS, pH 7.4 + 50% glycerol. X-gal staining of sections (20 $\mu$ m) was performed as described above for whole mount embryos. After staining, sections were washed 3 x 5 minutes with 1X PBS, pH 7.4, counterstained with nuclear fast red for 5 minutes and dehydrated in an ethanol series (70% ethanol, 95% ethanol, 100% ethanol and 100% Xylenes) followed by application of coverslips with permount mounting media (Thermo Fisher Scientific).

### Alkaline Phosphatase Staining

Embryos were dissected in 1X PBS, pH 7.4, and fixed (1% formaldehyde, 0.2% glutaraldehyde, 2mM MgCl<sub>2</sub>, 5mM EGTA, 0.02% NP-40) on ice for 10-60 minutes depending on the embryonic stage on ice. Subsequently, the embryos were washed 3 x 5 minutes with 1X PBS, pH 7.4. To deactivate endogenous alkaline phosphatases, embryos were incubated in 1X PBS, pH 7.4 at 70°C for 30 minutes. Then the embryos were rinsed with 1X PBS, pH 7.4 and washed for 10 minutes in alkaline phosphatase buffer (100mM NaCl, 100mM Tris-HCl pH9.5, 50mM MgCl<sub>2</sub>,

1% Tween-20) at room temperature. Embryos were stained with BM purple from 2 to 3 hours at 37°C depending on the embryonic stage. After staining, the embryos were washed 3 x 5 minutes with 1X PBS, pH 7.4 at 4°C, and post-fixed in 4% paraformaldehyde for 20 minutes at room temperature, followed by 3 x 5 minute washes with 1X PBS, pH 7.4. Finally, embryos were stored and photographed in 1X PBS, pH 7.4 + 50% glycerol. Alkaline phosphatase staining of sections (20µm) was performed as described above for whole mount embryos. After staining, sections were washed 3 x 5 minutes with 1X PBS, pH7.4, counterstained with nuclear fast red for 5 minutes and dehydrated in an ethanol series (70% ethanol, 95% ethanol, 100% ethanol and 100% xylenes for five minutes each) followed by application of coverslips with permount mounting media.

#### Whole-Mount Digoxigenin *in situ* Hybridization

Whole-mount digoxigenin *in situ* hybridization was performed as previously described in (Allen et al., 2011; Wilkinson, 1992). In brief, embryos were dissected in 1X PBS, pH 7.4 and fixed in 4% paraformaldehyde overnight on a rocking platform. After fixation, embryos were dehydrated in a methanol/PBST (1X PBS, pH 7.4 + 0.1 % Tween) series (25% methanol, 50 %methanol, 75% methanol) and stored in 100% methanol at -20°C until the experiment was performed for up to 6 months. Embryos were digested with 10µg/mL proteinase K at RT for 2 minutes.

Hybridization was performed with the indicated digoxigenin probe with a concentration of 1ng/µL for 16-19 hours at 70°C. The embryos were incubated in alkaline phosphatase-conjugated anti-DIG antibody at a dilution of 1:4,000. AP-anti-DIG was detected with BM purple, and signal was developed for 3.5 hours at room temperature. Embryos were cleared in 50% glycerol in 1XPBST and were photographed using a Nikon SMZ1500 microscope.

## Immunofluorescence

Section immunofluorescence was performed as in (Allen et al., 2011). Embryos were dissected in 1X PBS, pH 7.4 and fixed for 1 hour in 4% paraformaldehyde on ice, followed by 3 x 5 minutes washes with 1X PBS, pH 7.4 and cryoprotected for 24-48 hours in 1X PBS + 30% sucrose. Embryos were embedded in OCT compound and sectioned on a Leica cryostat (CM1950) (12  $\mu$ m thick forebrain and forelimb neural tube sections). Sections were blocked in blocking buffer (3% bovine serum albumin, 1% heat-inactivated sheep serum, 0.1% TritonX-100 in 1X PBS, pH 7.4) for 1 hour. Primary antibodies were diluted in blocking buffer incubated overnight at 4 °C in a humidified chamber. A list of all the primary and secondary antibodies used in this study is provided in (Table 2.2). Secondary antibodies were diluted in blocking solution and incubated for 1 hour at room temperature, followed by 3 x 5 minute washes with 1X PBS, pH 7.4. All Alexa Fluor Dyes secondary antibodies were used at a 1:500 dilution. Nuclei were labeled with DAPI for 10 minutes at room temperature and slides were mounted with coverslips using Immu-mount aqueous mounting medium. Sections were visualized on a Leica upright SP5X confocal microscope.

## Whole-Mount Immunofluorescence

Embryos were dissected in 1X PBS, pH 7.4, fixed with 4% paraformaldehyde for 2 hours at 4°C, and washed 2 x 10 minutes washes with PBTX (1X PBS + 0.1% Triton X-100). Subsequently, embryos were blocked for 1 hour in PBTX + 10% goat serum. Primary antibodies were diluted in PBTX + 10% goat serum and incubated overnight at 4 °C on a rocking platform. A list of all the primary and secondary antibodies used in this study is provided in (Table 2.2). The next day

the embryos were rinsed 2 x 5 minutes with PBTX, followed by 3 x 1 hour washes with PBTX on a rocking platform at 4°C. After the washes, embryos were incubated overnight with secondary antibodies diluted in PBTX+ 10% serum. All Alexa Fluor Dyes secondary antibodies were used at a 1:500 dilution. Next, embryos were washed as described for the primary antibody above, and cleared with *Clear<sup>T2</sup>* (25% Formamide/10%PEG for one hour; 50% Formamide/20%PEG for 72 hours) (Kuwajima et al., 2013). Finally, embryos were visualized on a Nikon SMZ1500 microscope. With the *Clear<sup>T2</sup>* reagent we did not observed any tissue expansion. (Protocol courtesy of Jean-Denis Bénazet, UCSF)

#### Micro Computed Tomography (Micro CT)

E18.5 embryos were skinned and eviscerated. Subsequently, embryos were fixed overnight in 100% ethanol, and maintained in 70% ethanol until ready to scan. The scans were performed using embryos covered with a 1X PBS, pH 7.4-soaked kim wipe and scanned over the entire length of the skull using the  $\mu$ CT100 system (Scanco Medical, Bassersdorf, Switzerland). Scan settings were as follows: 12  $\mu$ m voxel size, 55 kVp, 109  $\mu$ A, 0.5 mm AL filter, and 500 ms integration time. Micro CT scans were analyzed with the Amira software (Thermo Fisher Scientific). The Micro CT scans were uploaded as DICOM files into the software and the three-dimensional reconstructions were generated using the isosurface feature. The individual bones were manually segmented using the extract surface and buffer tools of Amira (Ho et al., 2015). Finally, the individual bones were color coded.

#### Skeletal Preparation

Skeletons were prepared as previously described before in (Allen et al., 2011). E18.5 embryos were skinned and eviscerated. Subsequently, embryos were fixed in 100% ethanol, followed by 100% acetone for 24 hours respectively at room temperature. Cartilage and bone were stained with alcian blue/alizarin red staining solution (5% alcian blue, 5% alizarin red, 5% glacial acetic acid and 70% ethanol) for 4 days at room temperature. The remaining tissue was digested with several washes of 1% potassium hydroxide. The skeletons were cleared by 24 hour washes of a gradient of glycerol (20%, 50%, and 80%) in 1% potassium hydroxide, and photographed in 80% glycerol.

#### In ovo chicken electroporations

Chicken electroporations were performed as previously described in (Allen et al., 2011; Tenzen et al., 2006). The indicated construct (pCIG plasmid -1  $\mu\text{g}/\mu\text{l}$  in 1X PBS, pH7.4, with 50ng/ $\mu\text{l}$  fast green) was injected into the forebrain cavity of Hamburger-Hamilton stage 11 chicken embryos. L-shaped electrodes were made with platinum wire, 8mm long (3mm were bent to form the L shape) and spaced 1mm apart. Electrodes (L-shaped part) were placed in front of the forebrain of the embryo (pulsed five times at 25 V for 50 ms with a BTX electroporator). The electroporated embryos were screened for GFP expression after 48 hours at Hamburger-Hamilton stage 21-22 and processed for immunofluorescence.

#### RNA isolation and qRT-PCR

RNA was isolated from micro-dissected nasal processes (without the forebrain neuroepithelium) and forelimb buds of E11.5 wildtype and mutant embryos. RNA was extracted with a Quick-RNA micro prep (Zymo Research). cDNA was generated from 500ng and 1 $\mu\text{g}$  of total RNA

from the nasal process and forelimb bud mesenchyme, respectively, with a High Capacity cDNA reverse transcription kit (Applied Biosystems). qRT-PCR was performed with PowerUP SYBR Green Master Mix (Applied Biosystems) in a Step One Plus Real-Time PCR System (Applied Biosystems). qRT-PCR primers utilized in this paper are listed in (Table 2.4). Gene expression was normalized to *Gapdh*, and relative expression analyses were performed using the  $2^{(-\Delta\Delta CT)}$  method. For qRT-PCR analysis at least three biological replicates were analyzed in triplicate.

### Western Blot Analysis

E11.5 embryos were dissected in 1X PBS pH7.4. Nasal processes and forelimb buds were micro-dissected and incubated for 15 minutes and lysed in radioimmunoprecipitation assay buffer (50mM Tris-HCl, pH7.2, 150mM NaCl, 0.1% Triton X-100, 1% sodium deoxycholate, 5mM EDTA), containing a protease inhibitor cocktail (Roche). Samples were sonicated using a sonic dismembrator (model 500, Thermo Fisher Scientific) with 10 pulses of 1s at 10 % amplitude. Extracts were cleared by centrifugation at 15,000 rpm (21,130 g) for 20 min at 4C°. Total protein concentration was determined with the Pierce BCA protein assay kit (Thermo Fisher Scientific), utilizing 10µg of each sample. Lysates were mixed with 6X Laemmli buffer, and boiled for 10 minutes at 95C°. Proteins were separated using SDS-PAGE in 5% gels and transferred onto Immuno-Blot PVDF membranes (Bio-Rad). Membranes were blocked for 1hr at room temperature in western blocking buffer [30g/liter bovine serum albumin with 0.2% NaN<sub>3</sub> in TBST (Tris-buffered saline, 0.5% tween-20)]. Blots were probed with the indicated primary antibodies (Table 2.3) diluted in western blocking buffer and incubated overnight. After incubation in primary antibody, the membranes were rinsed 3 x in TBST, followed by 3 x 10 minutes washes in TBST. Peroxidase conjugated secondary antibodies (Table 2.3) were diluted

in western blocking buffer and incubated for 1hr at room temperature and washed as the primary above. Membranes were incubated with Amersham ECL Prime Western Blotting Detecting Reagent GE Healthcare) for 5 minutes, and exposed to HyBlot CL autoradiography film (Denville) and developed using a Konica Minolta SRX-101A medical film processor. Relative expression values were obtained by normalizing the mean gray value of each band in the blot, subtracting the background and normalizing to the mean gray value of VINCULIN. For relative expression analysis at least three biological replicates were analyzed.

#### Quantitation and statistical analysis

All the data are represented as mean  $\pm$  standard deviation. All statistical analyses were performed using GraphPad statistic calculator (GraphPad Software, La Jolla California USA, [www.graphpad.com](http://www.graphpad.com)). Statistical significance was determined using two-tailed Student's *t*-test or the Fisher's Exact test. Bonferroni correction was employed to account for multiple comparisons in each dataset. In brief, to account for multiple comparisons using the Bonferroni correction, the original  $\alpha$ -value (0.05) is divided by the number of comparisons in each dataset, generating a new adjusted  $\alpha$ -value, that will determine the significance of the results. For all the experimental analyses a minimum of 3 embryos of each genotype were examined, each n represents an embryo. All the statistical details (statistical test used, adjusted p-value, statistical significance and exact value of each n) for each experiment are specified in the figure legends.

#### Telencephalic division and medial nasal process classification



Frontal pictures of E10.5 mouse embryos were photographed with a Nikon SMZ1500 microscope. Blind classification of the telencephalic division and media nasal process separation, was performed by a blinded evaluator according the categories showed in (Figure 2.4A-F).

#### Internasal distance and crown-rump length quantitation

Pictures of the nasal processes and whole E10.5 embryos were taken in 1X PBS, pH7.4 with a Nikon SMZ1500 microscope. Internasal distance was defined as the distance between the edges of the medial nasal process. Crown rump length was defined as the top of the crown of the midbrain, bisecting the forelimb bud to the curvature at the bottom c-shaped part of the embryo. Blind quantitation of the interasal distance and crown-rump length was performed manually by a single evaluator using the scale bar tool of the NIS-Elements software (Nikon) annotations and measurements feature.

#### Immunofluorescence quantitation

To quantify immunofluorescence images, we examined a minimum of 3 embryos per genotype and 2 sections from each embryo.

NKX2.1 quantitation: Side view pictures of whole mount immunofluorescent wildtype and mutant embryos were taken in *Clear*<sup>T2</sup> with a Nikon SMZ1500 microscope. The NKX2.1 area of expression was quantified using the area measure plugin of ImageJ (Schneider et al., 2012). Each image was thresholded automatically by ImageJ before the area of expression was quantified.

NKX2.2 quantitation: Pictures of transverse sections of wildtype and mutant neural tubes stained with antibodies directed against NKX2.2 were merged with their respective DAPI images.

NKX2.2 positive cells were quantified with the point tool of ImageJ (Schneider et al., 2012).

Phospho-histone H3 quantitation:

All phospho-histone H3 quantitation was performed with the point tool and analyze particle feature of ImageJ (Schneider et al., 2012). In the forebrain, the phospho-histone H3 positive cells were quantified in different tissue compartments. The phospho-histone H3 images were merged with markers specific to each tissue: E-CADHERIN (surface ectoderm), and PDGFR $\alpha$  (mesenchyme). The neuroepithelium was identified morphologically. The dorsal telencephalic midline was excluded from this analysis. After identifying each tissue compartment with these markers and based on their morphology, we manually isolated the mesenchyme of the lateral and medial nasal process, the surface ectoderm of the olfactory epithelium and the forebrain neuroepithelium with the clear outside tool of ImageJ. Each image was manually thresholded and the analyze particle feature of was used to automatically quantify the phospho-histone H3<sup>+</sup> cells. DAPI<sup>+</sup> cells were also quantified as described above to normalize the number of phospho-histone H3<sup>+</sup> cells. For the neural tube quantitation, the phospho-histone H3 cells were quantified along the entire neural tube with the point tool. Finally, in the forelimb bud, the phospho-histone H3 positive cells were quantified with the point tool, specifically in a selected area of equal size in wildtype and mutant embryos.

MicroCT Nasal Bone width quantitation

To measure the nasal bone width of E18.5 wildtype and mutant embryos, micro CT scans were imported as DICOM files into MicroView (Parallax Innovations). Three-dimensional reconstructions were generated using the Isosurface tool. All the 3D reconstructions were equally thresholded. To measure distance width, we utilized the built-in measure function of Parallax MicroView and measured the widest point of each nasal bone.

#### Quantitation of anatomical landmarks and nostril frequency

Frontal pictures of E18.5 mouse embryos were photographed in 1X PBS, pH7.4 with a Nikon SMZ1500 microscope. Head width was defined as the widest length of the head above the eyes (Figure 2.14A). Interocular distance was defined as the distance between the eyes (Figure 2.14A). Snout width was denoted as the distance between the second line of most ventral vibrissae from left to right (Figure 2.14A). The interocular distance and snout width was normalized to the head width. Quantitation was performed manually by a single evaluator using the scale bar tool of the NIS-Elements software (Nikon) annotations and measurements feature or using the line tool in Adobe Illustrator. The frequency of the nostrils was quantified according to the presence of partially fused nostrils with nasal pigment or a single nostril without pigment (Figure 2.14E, left panel).

## **2.6 Acknowledgements**

We thank all current and past members of the Allen lab for valuable feedback and suggestions throughout the course of this study. In particular, we thank Nicole Franks and Savannah Struble for significant technical assistance. We also thank Michelle Lynch (University of Michigan) for assistance with scanning MicroCT samples, Thach-Vu Ho (University of

Southern California) for assistance with generating the MicroCT 3D reconstructions, Jingwen Yang (University of Michigan) for assistance with nasal processes microdissection and the University of Michigan Consulting for Statistics, Computing and Analytics Research Center for assistance with statistical analyses. We also gratefully acknowledge the Department of Cell and Developmental Biology, including the Engel, Spence, and O'Shea laboratories at the University of Michigan for providing access to research equipment. The NKX2.2 antibody was obtained from the Developmental Studies Hybridoma Bank, created by the NICHD of the NIH and maintained at The University of Iowa, Department of Biology, Iowa City, IA 52242. Finally, we acknowledge the Biomedical Research Core Facilities Microscopy Core for providing access to confocal microscopy equipment, which is supported by the Rogel Cancer Center.

## **2.7 Author contributions**

Conceptualization, M.L.E.A. and B.L.A.; Methodology, M.L.E.A. and B.L.A.; Validation, M.L.E.A. and B.L.A.; Formal Analysis, M.L.E.A.; Investigation, M.L.E.A. Resources, B.L.A.; Writing – Original Draft, M.L.E.A. and B.L.A.; Writing – Review & Editing, M.L.E.A. and B.L.A.; Visualization, M.L.E.A. and B.L.A.; Supervision, B.L.A.; Project Administration, B.L.A.; Funding Acquisition, M.L.E.A. and B.L.A.

## 2.8 Tables

Table 2.1 General reagents

Reagent	Vendor	Catalog number
Alcian Blue	Millipore Sigma	A5268
Alizarin Red	Millipore Sigma	A5533
Amersham ECL Prime Western Blotting Detection Reagent	GE Healthcare	RPN2232
Anti-Digoxigenin-Ap, Fab fragments	Roche	11 093 274 910
BM purple	Roche	11442074001
BSA	Millipore Sigma	A7906
Complete mini Protease Inhibitor Cocktail	Roche	1836153
DAPI	Thermo Fisher Scientific	D1306
EGTA	Millipore Sigma	E3889
EDTA	Thermo Fisher Scientific	<b>S311-500</b>
Fast green	Millipore Sigma	EM-4510
Formaldehyde	VWR	EMD-FX0410-5
Formamide	Millipore Sigma	4650-500ML
Glacial Acetic Acid	Thermo Fisher Scientific	BP2401-500
Glutaraldehyde	Millipore Sigma	G5882
Glycerol	VWR	EMGX0185-5
Goat serum	Thermo Fisher Scientific	16210064
High capacity cDNA reverse transcription kit	Applied Biosystems	4368814
Hyblot CL Autoradiography Film	Denville	E3018
Igepal (NP-40)	Millipore Sigma	I8896
Immu-mount	Thermo Fisher Scientific	9990412
Immuno-Blot PVDF membranes	Bio-Rad	162-0177
K <sub>3</sub> Fe(CN) <sub>6</sub>	Millipore Sigma	PX1455
K <sub>4</sub> Fe(CN) <sub>6</sub>	Millipore Sigma	P9387
MgCl <sub>2</sub>	VWR	0288-500G
NaCl	Millipore Sigma	SX0420-3
Na deoxycholate	VWR	SX0480-2
OCT	Thermo Fisher Scientific	23730571
Paraformaldehyde	Thermo Fisher Scientific	50980489
Permunt	Thermo Fisher Scientific	SP15100
Pierce BCA protein assay kit	Thermo Fisher Scientific	PI23225
Polyethyleneglycol	Millipore Sigma	91893-1L-F
Potassium hydroxide	VWR	PX1490-1
PowerUP SYBR Green Master Mix	Applied Biosystems	A25742
Proteinase K	Roche	03115836001

Quick-RNA micro prep	Zymo Research	R1055
Sheep serum	Bioworld	30611168-1
Tris	VWR	JT4109-2
Triton X-100	VWR	9410
Tween-20	VWR	9480
X-gal	Goldbio	X4281C
Xylenes	VWR	XX00555

**Table 2.2 Primary and secondary antibodies used for immunofluorescence**

Primary antibodies	Vendor	Catalog number	Dilution
NKX2.1 (rabbit IgG)	Abcam	ab76013	1:200
E-CADHERIN (mouseIgG2a)	BD Biosciences	610181	1:500
NKX2.2 (mouseIgG2b)	Developmental Studies Hybridoma Bank	74.5A5	1:20
OLIG2 (rabbit IgG)	Millipore Sigma	AB9610	1:2,000
NKX6.1 (mouseIgG1)	Developmental Studies Hybridoma Bank	F55A10	1:20
Phospho-histone H3 (rabbit IgG)	Millipore Sigma	06-570	1:1,000
Phospho-histone H3 (mouse IgG1)	Cell Signaling Technology	9706S	1:100
PDGFR $\alpha$ (rabbit IgG)	Cell Signaling Technology	3174S	1:100
Secondary antibodies	Vendor	Catalog number	Dilution
Alexa Fluor 488 (Goat anti-Rabbit IgG)	Thermo Fisher Scientific	A-11008	1:500
Alexa Fluor 555 (Goat anti-Mouse IgG2b)		A-21147	
Alexa Fluor 488 (Goat anti-Mouse IgG2a)		A-21131	
Alexa Fluor 555- (Goat anti-Rabbit IgG)		A-21428	
Alexa Fluor 488 (Goat anti-Mouse IgG1)		A-21121	
Alexa Fluor 555 (Goat anti-Mouse IgG2a)		A-21137	
Alexa Fluor 647 (Goat anti-Mouse IgG1)		A-21240	

**Table 2.3 Western blot antibodies**

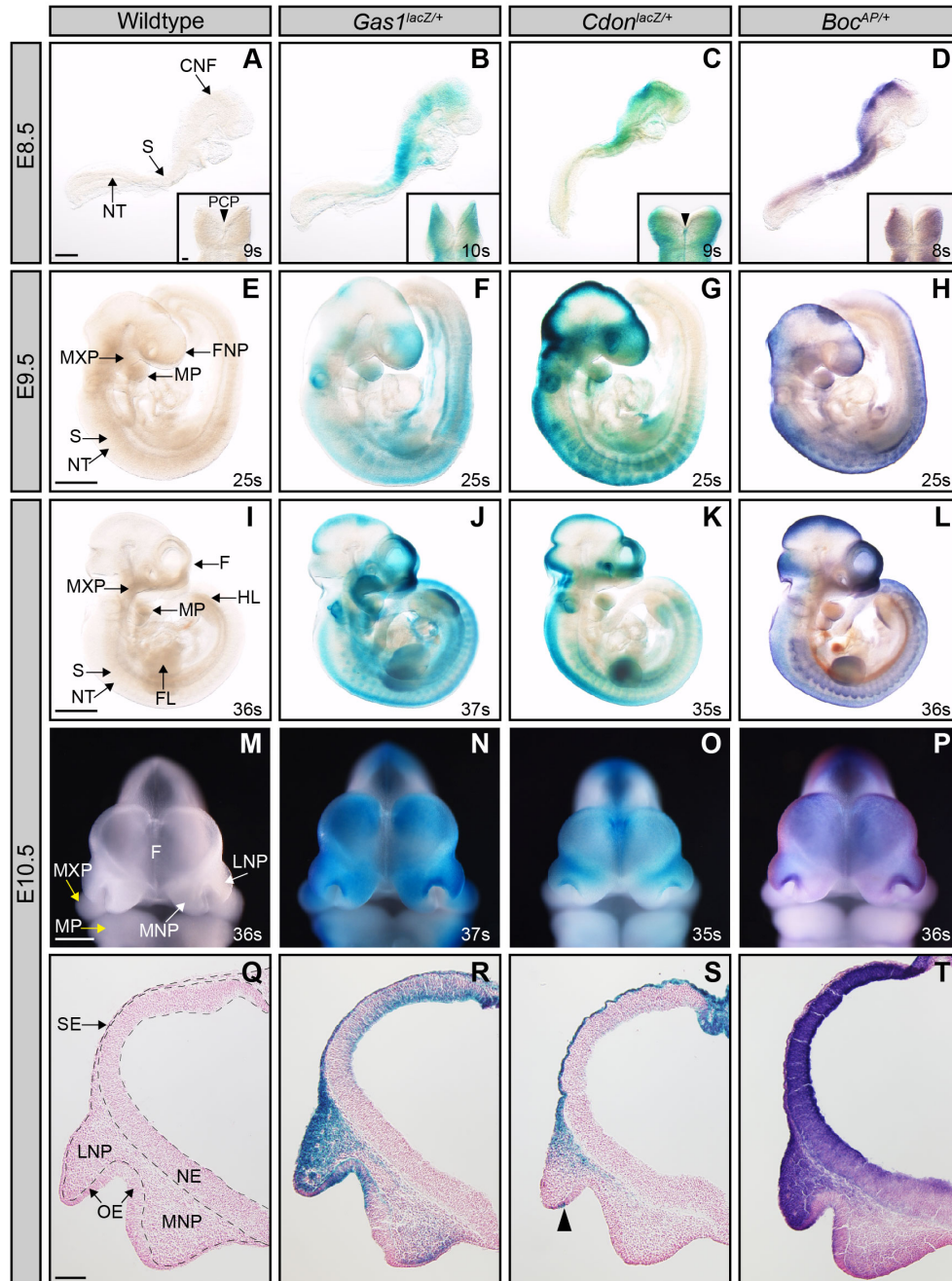
Primary antibodies	Vendor	Catalog number	Dilution
Gli1 (V812) (rabbit IgG)	Cell signaling Technology	#2354	1:1,000
Vinculin (E1E9V) XP (rabbit IgG)	Cell Signaling Technology	#13901	1:1,000
Secondary antibodies	Vendor	Catalog number	Dilution
Peroxidase conjugated AffiniPure F(ab)2 Fragment Donkey Anti-Rabbit IgG	Jackson ImmunoResearch	711-036-152	1:10,000



**Table 2.4 qRT-PCR primers**

Gene	Sequence	Source
<i>Gli1-F</i>	GTGCACGTTTGAAGGCTGTC	(Han et al., 2017)
<i>Gli1-R</i>	GAGTGGGTCCGATTCTGGTG	
<i>Gapdh-F</i>	GGTGAAGGTCGGTGTGAACG	(Lewandowski et al., 2015)
<i>Gapdh-R</i>	CTCGCTCCTGGAAGATGGTG	

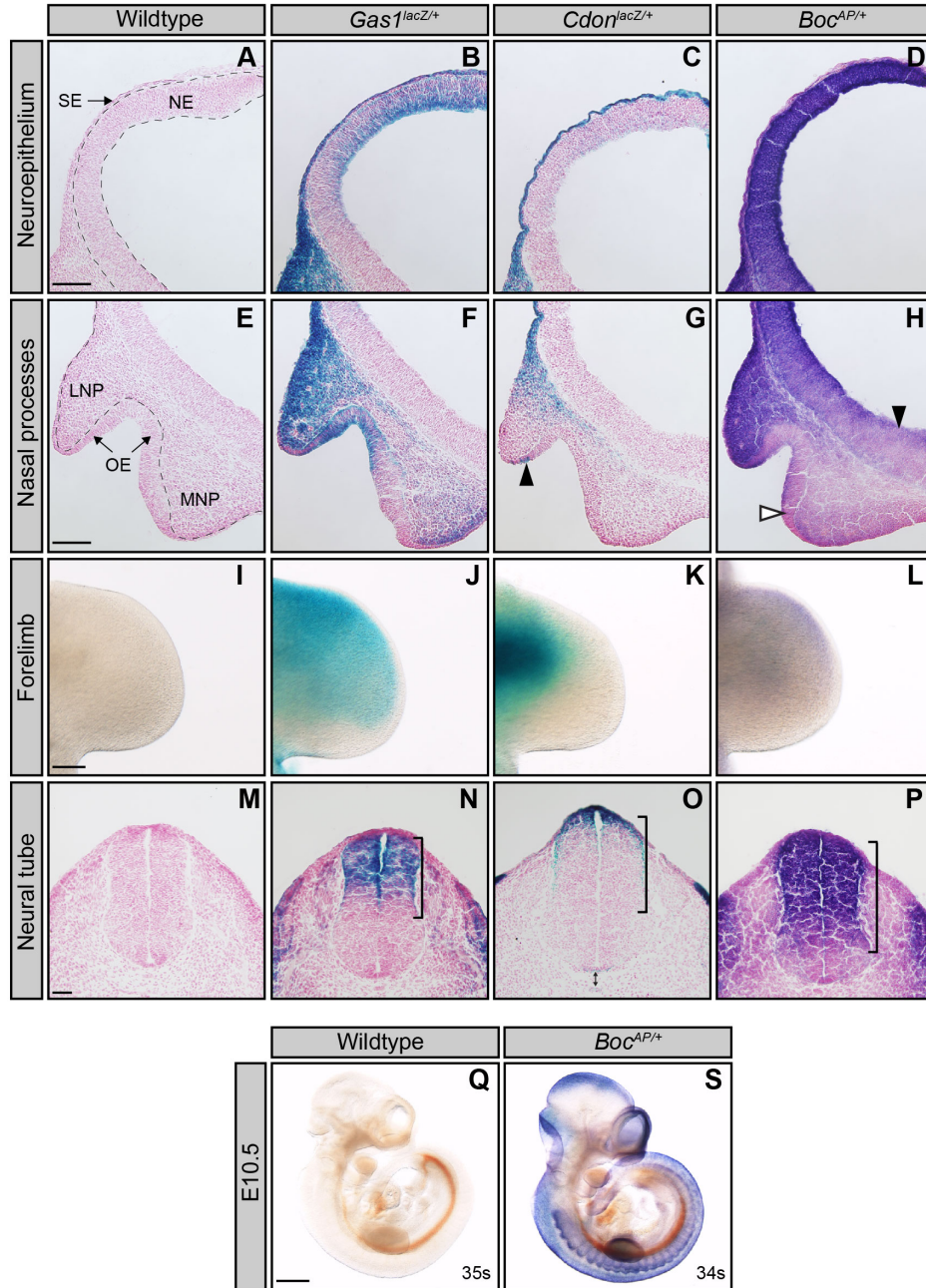
## 2.9 Figures



**Figure 2.1 The HH co-receptors *Gas1*, *Cdon* and *Boc* are expressed throughout early craniofacial development.**

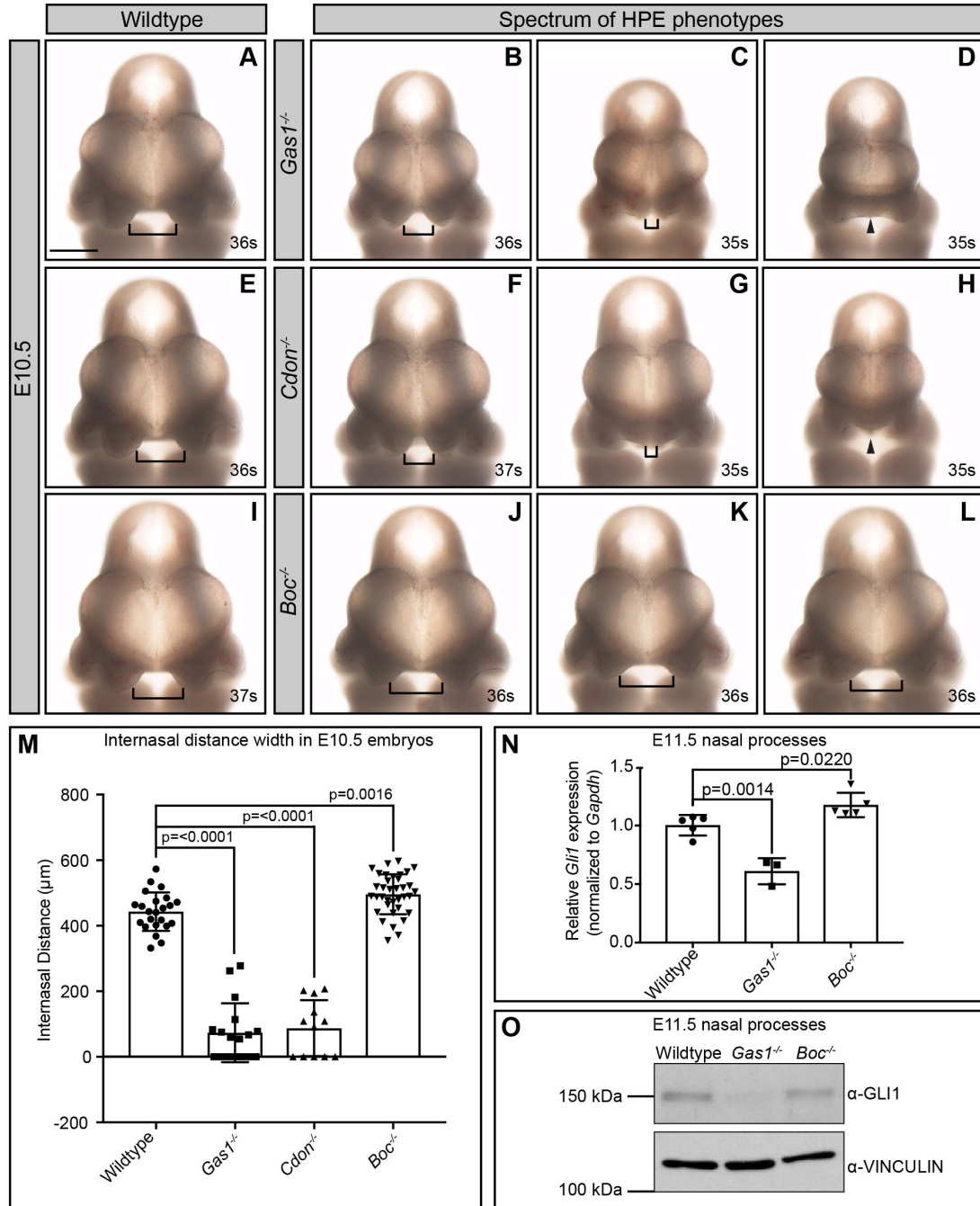
Analysis of HH co-receptor expression using *lacZ* (*Gas1*, *Cdon*) and *hPLAP* (*Boc*) reporter alleles (A-T). Whole mount X-Gal and Alkaline Phosphatase staining of E8.5 (A-D), E9.5 (E-H), and E10.5 (I-L), wildtype (A, E, I, M, Q), *Gas1*<sup>lacZ/+</sup> (B, F, J, N, R), *Cdon*<sup>lacZ/+</sup> (C, G, K, O, S), and *Boc*<sup>AP/+</sup> (D, H, L, P, T) embryos is shown. Somite number (s) is indicated in the lower right corner of each panel. Dorsal views of the cranial neural folds of E8.5 embryos are shown in insets (A-D); black arrowheads denote the prechordal plate (PCP). Frontal view of craniofacial structures of E10.5 embryos (M-P). White arrows denote LNP and MNP and yellow arrows denote MXP and MP (M). Coronal sections of E10.5 forebrains (Q-T); arrowhead denotes a subset of cells expressing *Cdon* in the olfactory epithelium. Scale bars, (A-P) 500  $\mu$ m, insets (A-D) 50  $\mu$ m and (Q-T) 200  $\mu$ m.

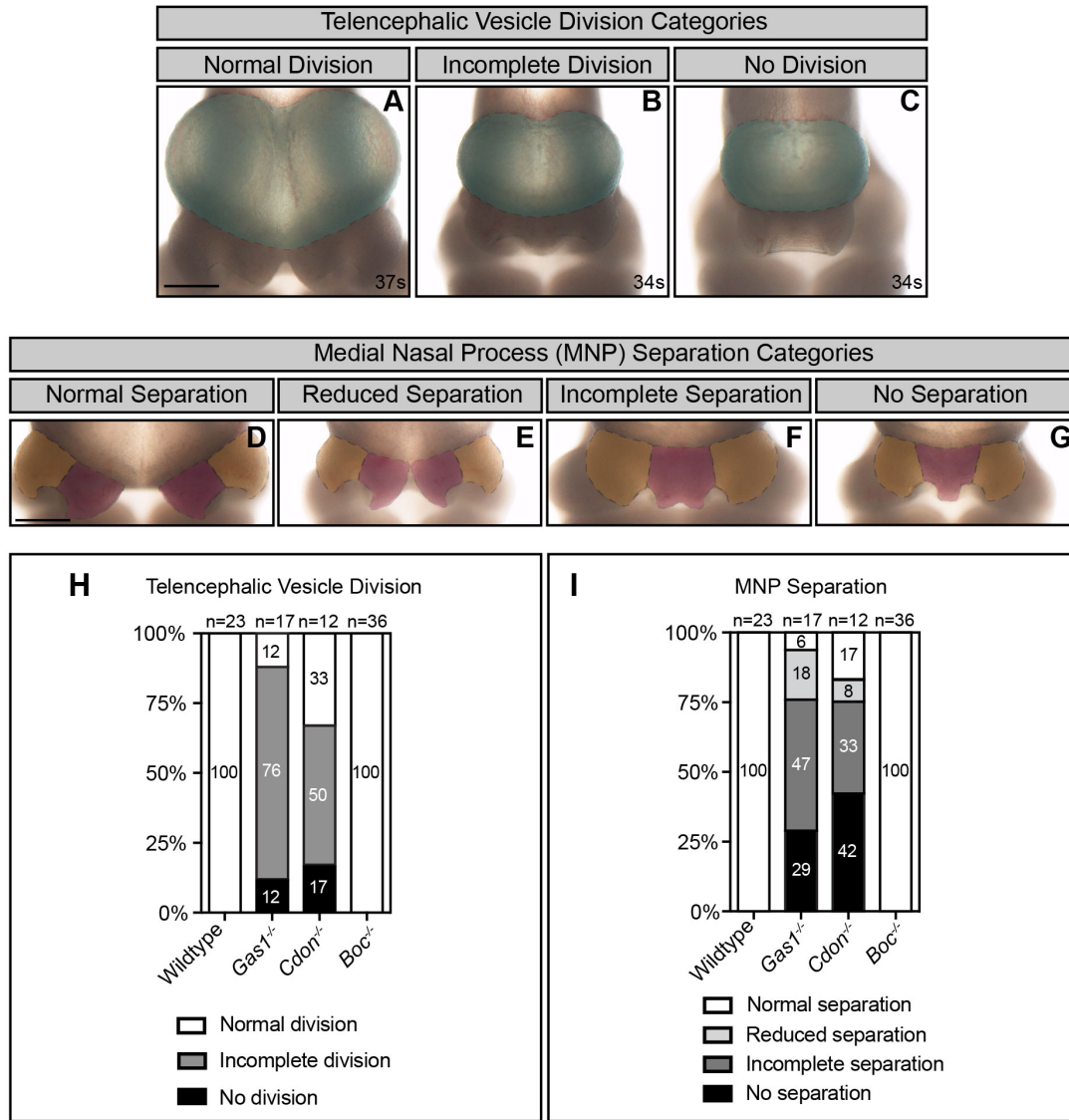
Abbreviations: cranial neural fold (CNF), somites (S), neural tube (NT), pre-chordal plate (PCP), frontonasal prominence (FNP), maxillary process (MXP), mandibular process (MP), forebrain (F), forelimb (FL), hindlimb (HL), medial nasal process (MNP), lateral nasal process (LNP), surface ectoderm (SE), neuroepithelium (NE) and olfactory epithelium (OE).



**Figure 2.2** *Gas1*, *Cdon* and *Boc* are differentially expressed across multiple HH-responsive tissues.

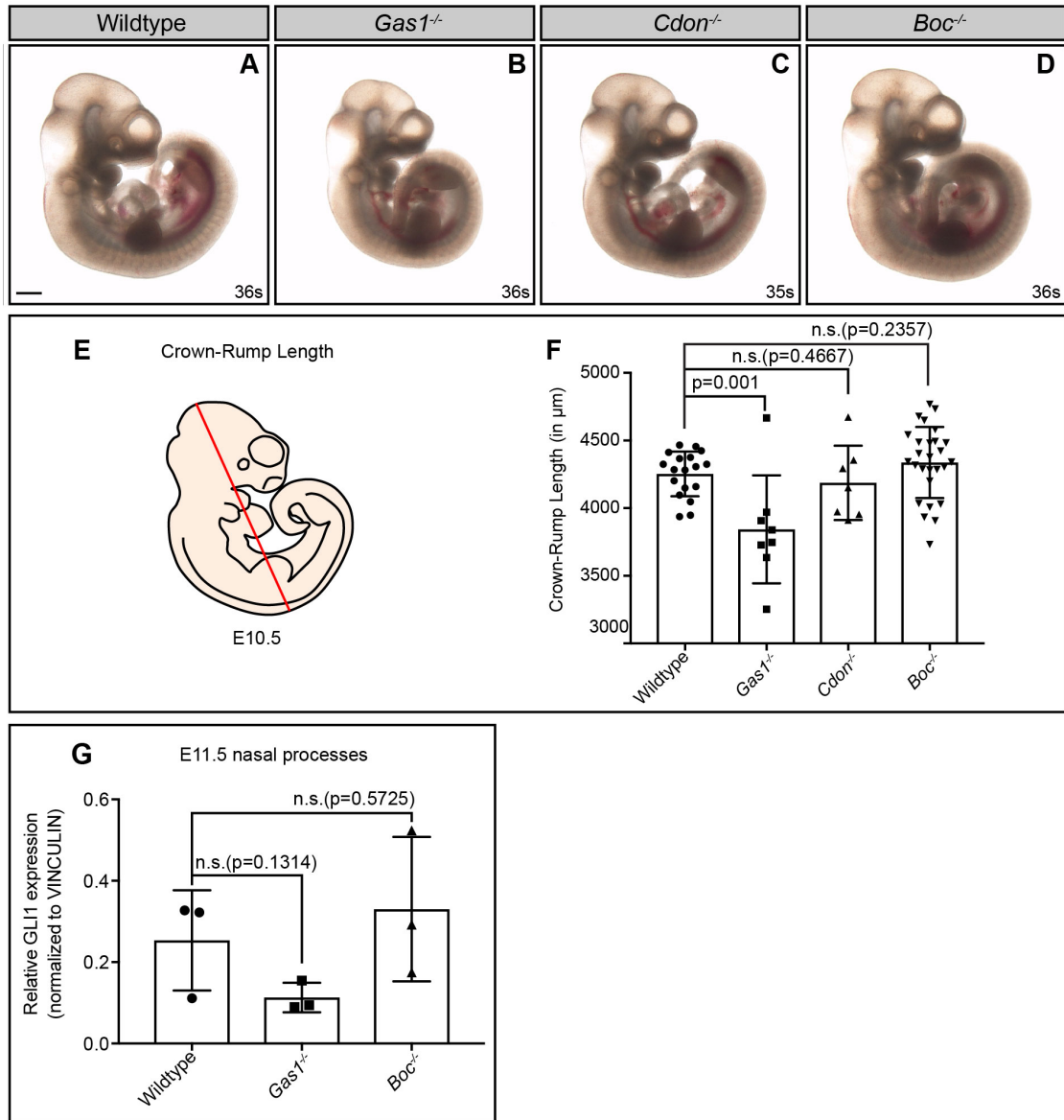
Analysis of HH co-receptor expression using *lacZ* (*Gas1*, *Cdon*) and *hPLAP* (*Boc*) reporter alleles in HH-responsive tissues (A-P). High magnification pictures of coronal sections of E10.5 forebrains, from wildtype (A, E), *Gas1<sup>lacZ/+</sup>* (B, F), *Cdon<sup>lacZ/+</sup>* (C, G), and *Boc<sup>AP/+</sup>* (D, H) embryos are shown. E10.5 forebrain neuroepithelia (A-D) and nasal processes (E-H). Arrowhead in (G) denotes a subset of cells expressing *Cdon* in the olfactory epithelium. Black arrowhead in (H) identifies the extended ventral expression of *Boc* closer to the telencephalon source of *Shh* expression. White arrowhead in (H) denotes *Boc* expression in the olfactory epithelium. Whole mount X-Gal and Alkaline Phosphatase staining of E10.5 forelimb buds (I-L) from wildtype (I), *Gas1<sup>lacZ/+</sup>* (J), *Cdon<sup>lacZ/+</sup>* (K), and *Boc<sup>AP/+</sup>* (L) embryos. Transverse sections of E10.5 neural tubes (M-P) from wildtype (M), *Gas1<sup>lacZ/+</sup>* (N), *Cdon<sup>lacZ/+</sup>* (O), and *Boc<sup>AP/+</sup>* (P) embryos. Black brackets denote the expression domain of the HH co-receptors in the neural tube. Double-headed arrow in (O) indicates *Cdon* expression in the floor plate and notochord. Heat inactivation of endogenous alkaline phosphatase at E10.5 in wildtype (Q) and *Boc<sup>AP/+</sup>* (S) animals demonstrates the specificity of alkaline phosphatase staining. Somite number (s) is indicated in the lower right corner (Q-S). Scale bars, (A-H) 100µm, (I-L) 200µm, (M-P) 50µm, (Q-S) 500µm. Abbreviations: surface ectoderm (SE), neuroepithelium (NE), lateral nasal process (LNP), medial nasal process (MNP), olfactory epithelium (OE).





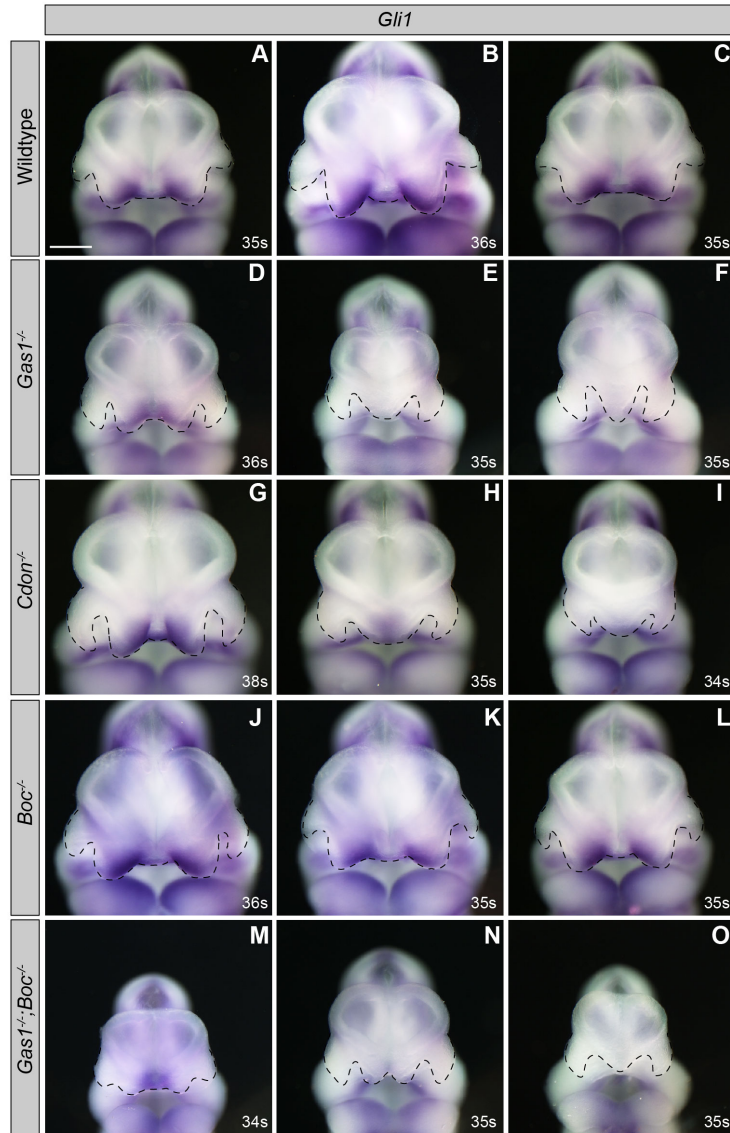
**Figure 2.4 Telencephalic vesicle division and MNP separation in *Gas1*, *Cdon* and *Boc* mutants.**

*En face* view of E10.5 embryos (A-C). The telencephalic vesicles are pseudocolored in green and surrounded by a dotted line. Telencephalic vesicle division classification categories: normal division (A), incomplete division (B), no division (C). Midface view of E10.5 embryos (D-G). The lateral and medial nasal processes are pseudocolored in orange and red, respectively, and are surrounded by a dotted line. Medial nasal process (MNP) classification categories: normal separation (D), reduced separation (E), incomplete separation (F), and no separation (G). Scale bars (A, D), 500 $\mu$ m. Telencephalic vesicle (TV) division frequency in E10.5 wildtype (n=23), *Gas1*<sup>-/-</sup> (n=17), *Cdon*<sup>-/-</sup> (n=12), and *Boc*<sup>-/-</sup> (n=36) embryos (H). Medial nasal process (MNP) separation frequency in E10.5 wildtype (n=23), *Gas1*<sup>-/-</sup> (n=17), *Cdon*<sup>-/-</sup> (n=12), and *Boc*<sup>-/-</sup> (n=36) embryos (I).



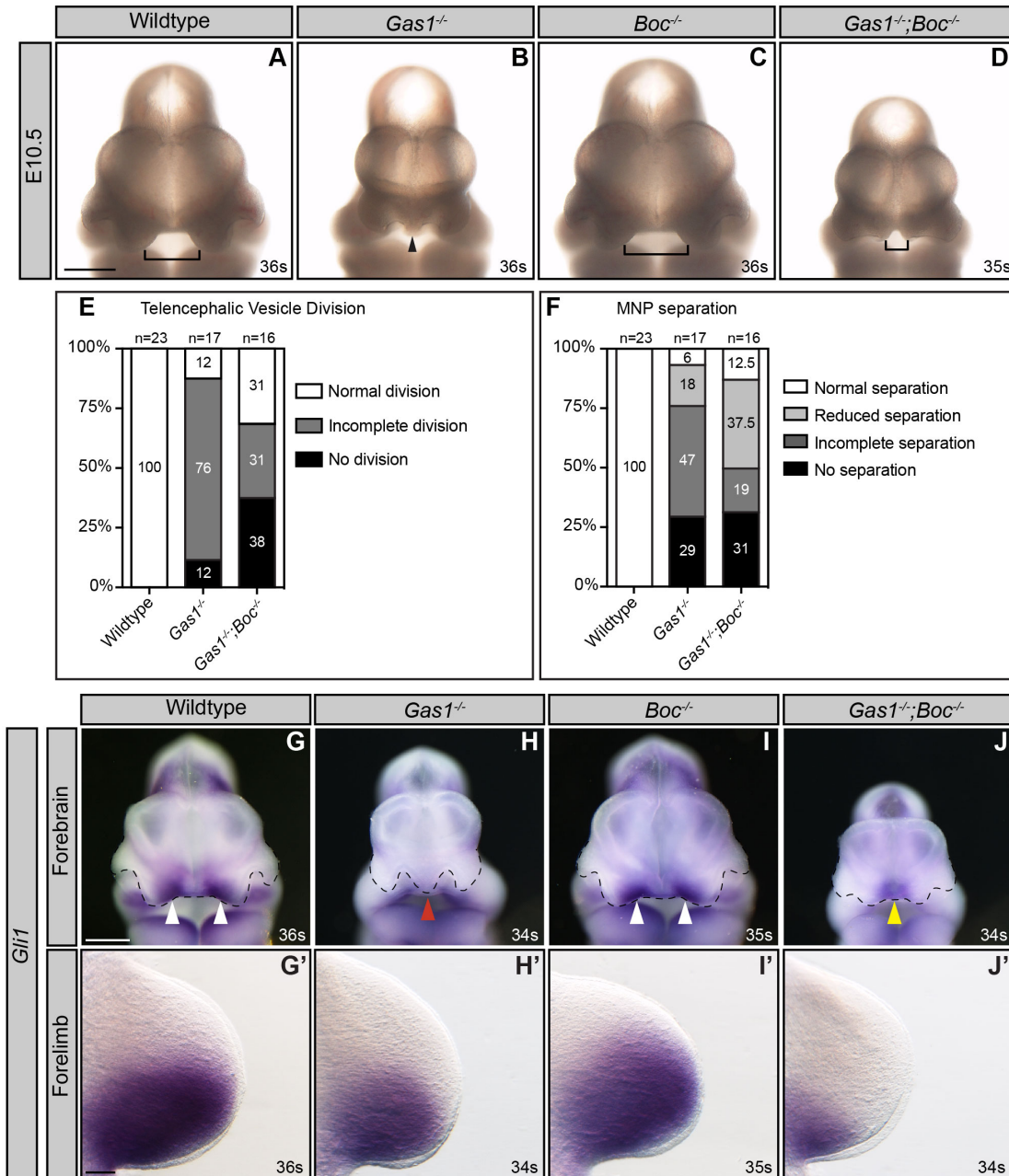
**Figure 2.5** *Gas1*, but not *Cdon* or *Boc*, mutant embryos exhibit decreased embryo size at E10.5.

Sagittal views of E10.5 wildtype (A), *Gas1*<sup>-/-</sup> (B), *Cdon*<sup>-/-</sup> (C), and *Boc*<sup>-/-</sup> (D) embryos. Scale bar (A), 500 µm. Schematic sagittal view of an E10.5 mouse embryo (E); the red diagonal line denotes crown-rump length. Crown-rump length quantitation of E10.5 wildtype (n= 18), *Gas1*<sup>-/-</sup> (n=8), *Cdon*<sup>-/-</sup> (n=7), *Boc*<sup>-/-</sup> (n=27) embryos (F). Quantitation of GLI1 levels in nasal processes isolated from E11.5 wildtype (n=3), *Gas1*<sup>-/-</sup> (n=3) and *Boc*<sup>-/-</sup> (n=3) embryos (G). Data are mean±s.d. P-values were determined by a two-tailed Student's *t*-test. The Bonferroni correction was employed to account for multiple comparisons in each dataset; (F) non-significant (n.s.; p>0.0166), significant (p≤0.0166) and (G) non-significant (n.s.; p>0.0250), significant (p≤0.0250).



**Figure 2.6 The Spectrum of HPE phenotypes correlates with changes in *Gli1* expression.**

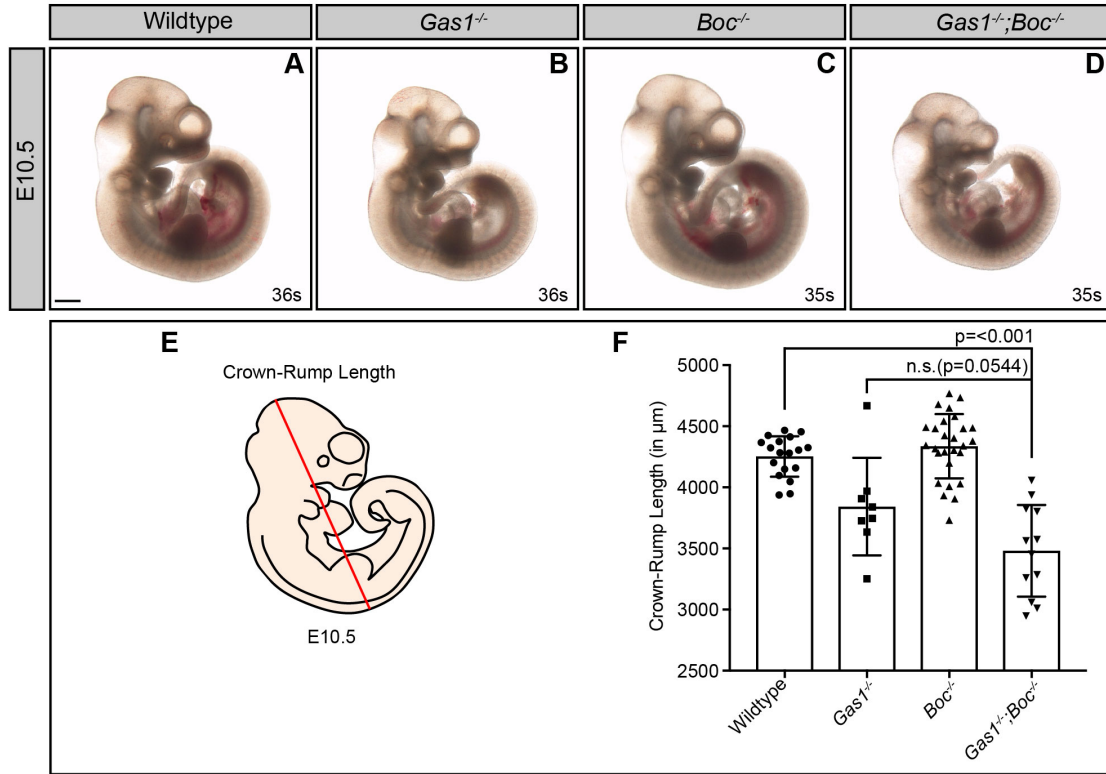
*In situ* hybridization detection of *Gli1* expression in E10.5 forebrains (A-O). *En face* views of E10.5 forebrains from wildtype (A-C), *Gas1*<sup>-/-</sup> (D-F), *Cdon*<sup>-/-</sup> (G-I), *Boc*<sup>-/-</sup> (J-L) and *Gas1*<sup>-/-</sup>;*Boc*<sup>-/-</sup> (M-O) embryos are shown. Somite number (s) is indicated in the lower right corner of each panel. Black dotted lines outline nasal processes. Notice that as the HPE phenotypes worsen (from left to right) in *Gas1* and *Cdon* mutants, the expression of *Gli1* in the MNP is lost. *Boc* mutants display equal levels of *Gli1* in the MNP and do not display any gross craniofacial defects. *Gas1*;*Boc* double mutants with ameliorated craniofacial defects (from left to right) maintain *Gli1* expression in the MNP, while *Gli1* expression is lost in mutants that display severe craniofacial defects. Scale bars (A-O), 500  $\mu$ m.



**Figure 2.7 Tissue-specific rescue of HH signaling in E10.5 *Gas1*;*Boc* double mutant embryos.**

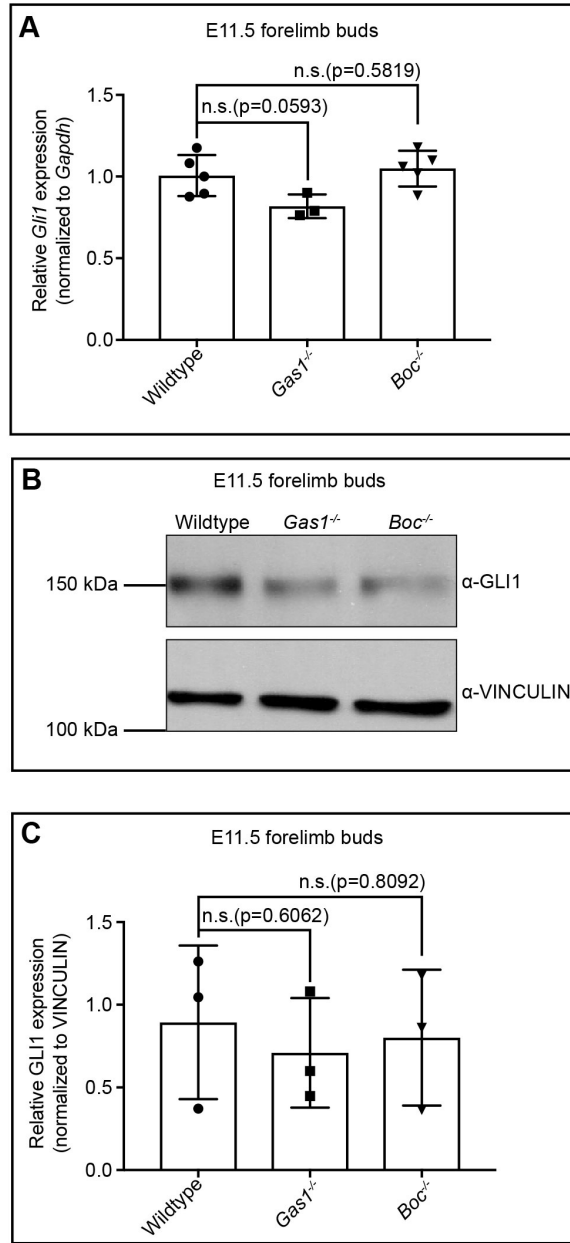
*En face* view of E10.5 embryos (A-D). Somite number (s) is indicated in the lower right corner of each panel. Brackets indicate internasal distance. Black triangles denote fusion of the medial nasal process. E10.5 wildtype (A), *Gas1*<sup>-/-</sup> (B), *Boc*<sup>-/-</sup> (C), and *Gas1*<sup>-/-</sup>;*Boc*<sup>-/-</sup> (D) embryos. Telencephalic vesicle (TV) division frequency in E10.5 wildtype (n=23), *Gas1*<sup>-/-</sup> (n=17) and *Gas1*<sup>-/-</sup>;*Boc*<sup>-/-</sup> (n=16) (E) embryos. TV division was classified according to the following categories: normal division, incomplete division and no division (see Figure 2.4A-C for representative examples of each category). Medial nasal process (MNP) separation frequency in E10.5 wildtype (n=23), *Gas1*<sup>-/-</sup> (n=17) and *Gas1*<sup>-/-</sup>;*Boc*<sup>-/-</sup> (n=16) (E) embryos. MNP separation in each embryo was classified according to the following categories: normal separation, reduced separation, incomplete separation and no separation (see Figure 2.4D-G for representative examples of each category). *In situ* hybridization detection of *Gli1* expression in E10.5 forebrains (G-J) and their corresponding forelimbs (G'-J'). *En face* view of E10.5 forebrains and dorsal view of E10.5 forelimbs in wildtype (G, G'), *Gas1*<sup>-/-</sup> (H, H'), *Boc*<sup>-/-</sup> (I, I'), and *Gas1*<sup>-/-</sup>;*Boc*<sup>-/-</sup> (J, J') embryos. Somite number (s) is indicated in the lower right corner of each panel. Black dotted lines outline nasal processes. Note that *Gli1* is differentially regulated in the MNP and forelimb of *Gas1*;*Boc* mutants. Scale bar in A and G, 500µm; G', 100µm.





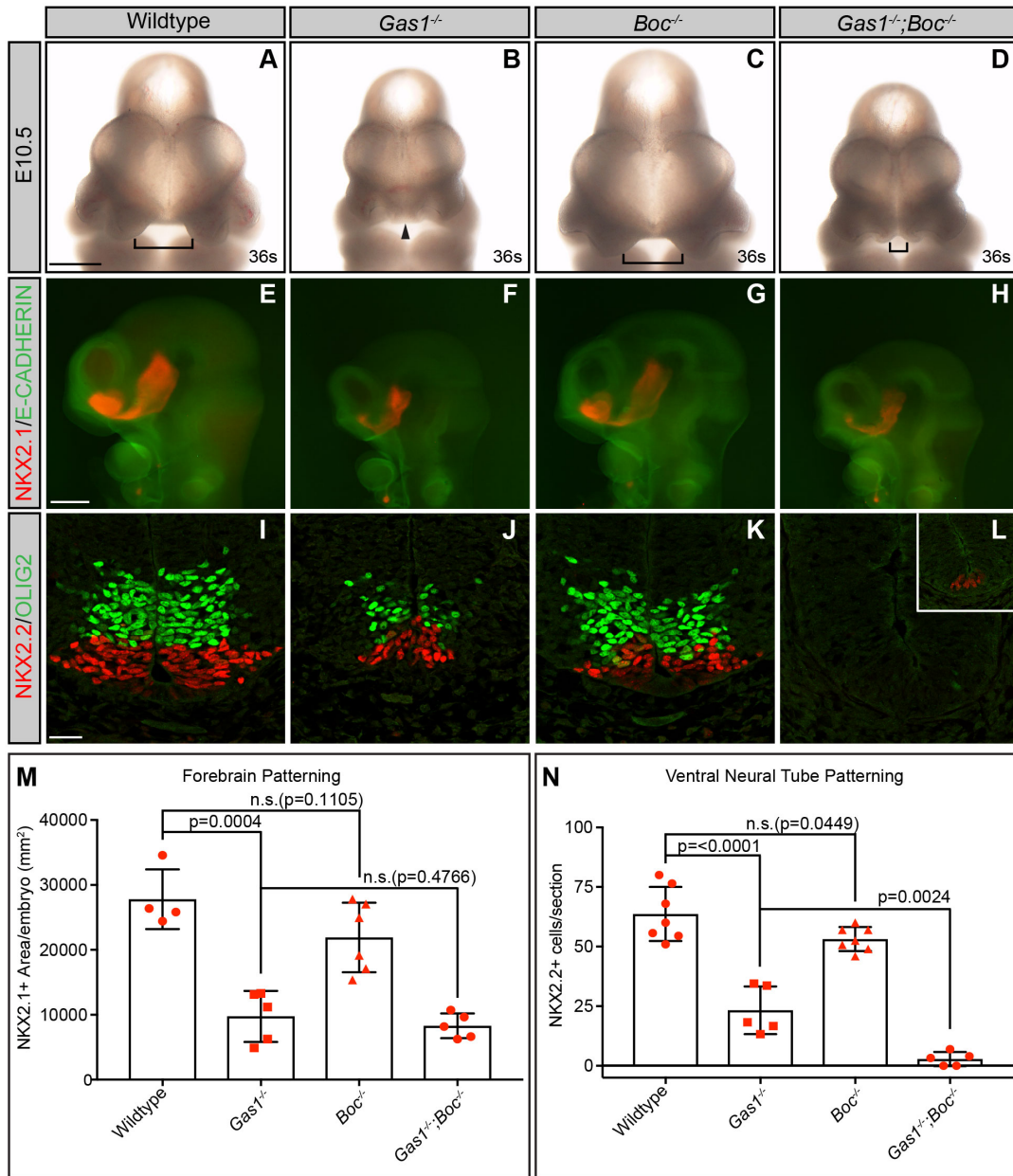
**Figure 2.8 Reduced Crown-Rump Length in E10.5 *Gas1*;*Boc* double mutant embryos.**

Sagittal view of E10.5 wildtype (A), *Gas1*<sup>-/-</sup> (B), *Boc*<sup>-/-</sup> (C), and *Gas1*<sup>-/-</sup>;*Boc*<sup>-/-</sup> (D) embryos. Schematic sagittal view of an E10.5 mouse embryo; the red diagonal line denotes the crown-rump length (E). Crown-rump length quantitation in wildtype (n= 18), *Gas1*<sup>-/-</sup> (n=8), *Boc*<sup>-/-</sup> (n=27), and *Gas1*<sup>-/-</sup>;*Boc*<sup>-/-</sup> (n=12) embryos (F). Scale bar in A, 500μm. Data are mean±s.d. P-values were determined by a two-tailed Student's *t*-test. The Bonferroni correction was employed to account for multiple comparisons in each dataset; (F) non-significant (n.s.; p>0.0250), significant (p≤0.0250).

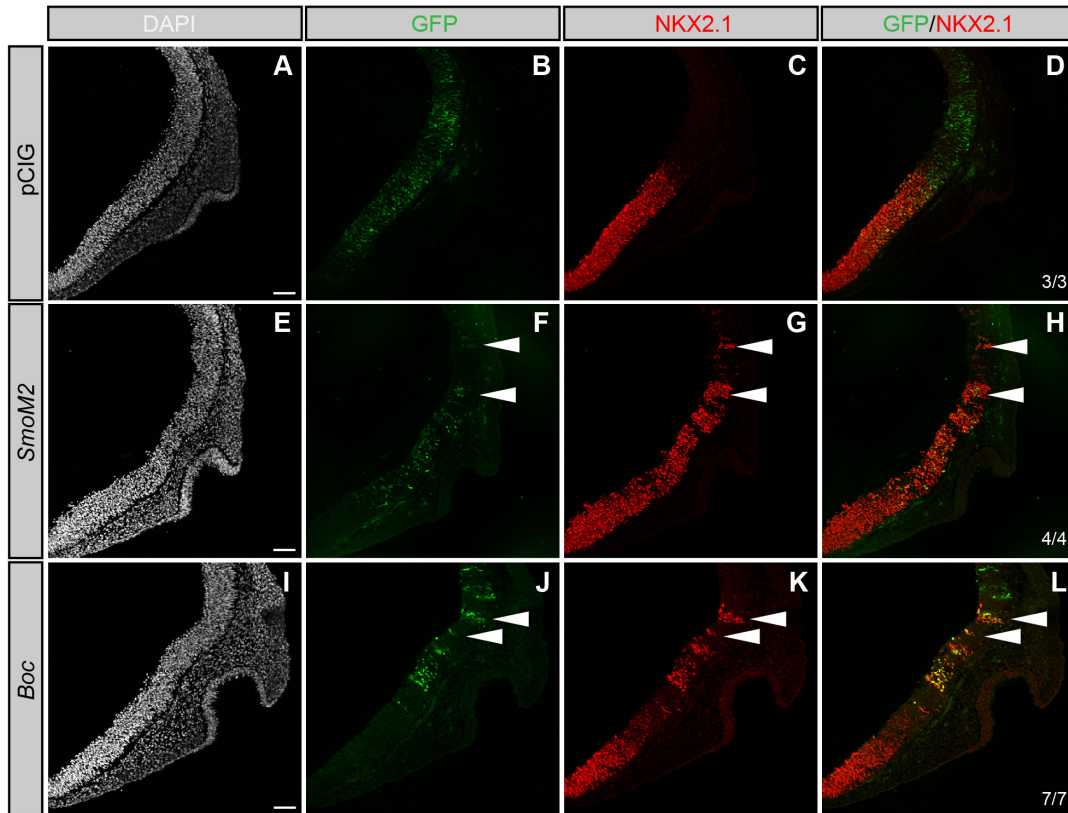


**Figure 2.9 Reduced *Gli1* mRNA and protein levels in E10.5 *Gas1* mutant forelimb buds**

Relative expression of *Gli1* by qRT-PCR in forelimb buds (A) of E11.5 wildtype (n=5), *Gas1*<sup>-/-</sup> (n=3) and *Boc*<sup>-/-</sup> (n=5) embryos normalized to *Gapdh*. Biological replicates were analyzed in triplicate. Western blot analysis of GLI1 endogenous protein in forelimb buds (B). Anti-VINCULIN was used as loading control, three biological replicates were analyzed. Quantitation of GLI1 levels in forelimb buds (C) of E11.5 wildtype (n=3), *Gas1*<sup>-/-</sup> (n=3) and *Boc*<sup>-/-</sup> (n=3) embryos. Data are mean±s.d. P-values were determined by a two-tailed Student's *t*-test. The Bonferroni correction was employed to account for multiple comparisons in each dataset; (A,C) non-significant (n.s.; p>0.0250), significant (p≤0.0250).

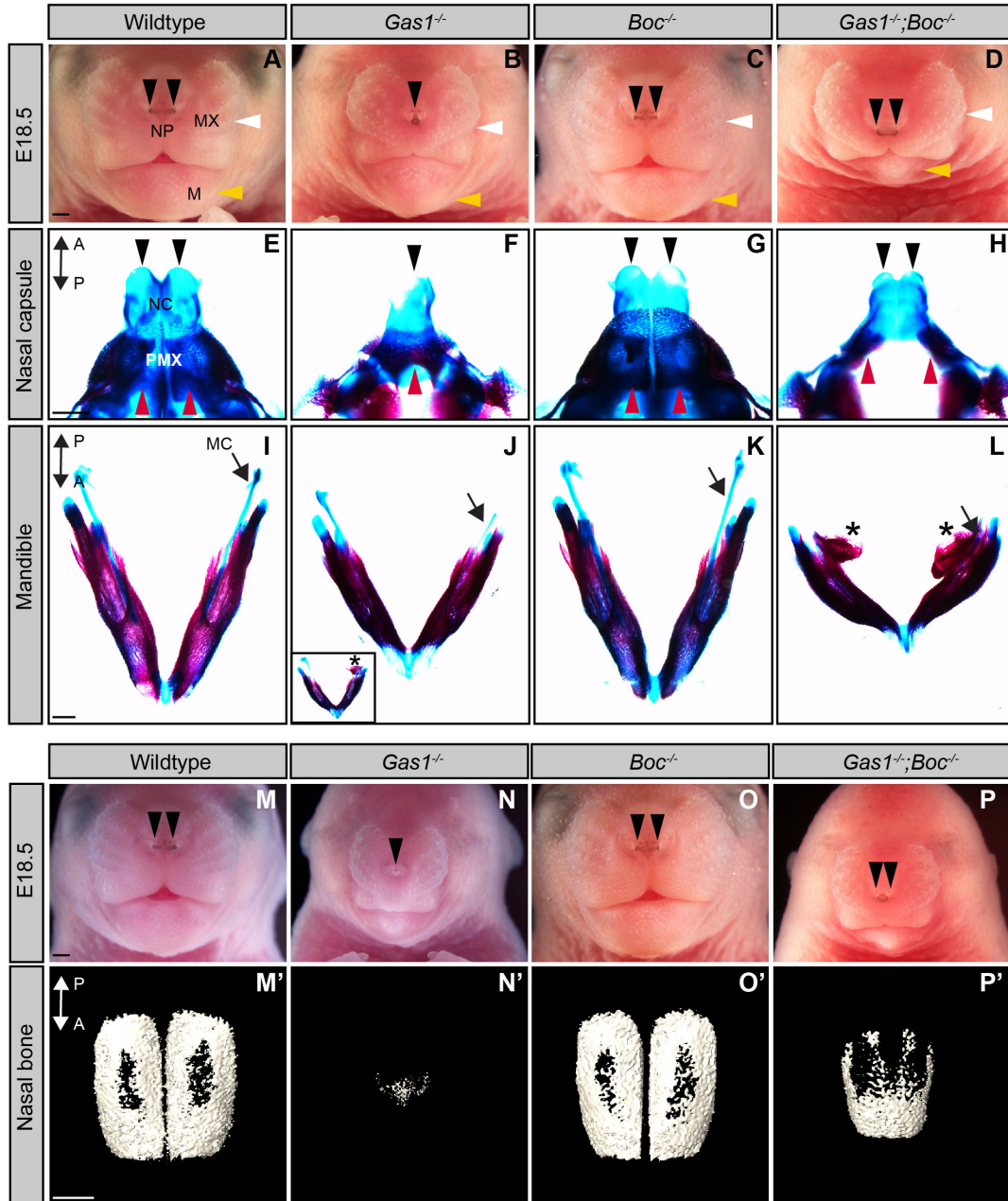


**Figure 2.10 Selective contribution of *Boc* to patterning of the neural tube, but not the forebrain neuroepithelium.** *En face* view of E10.5 embryos (A-D). Somite number (s) is indicated in the lower right corner of each panel. Brackets indicate internasal distance. Black triangles denote fusion of the MNP. E10.5 wildtype (A), *Gas1*<sup>-/-</sup> (B), *Boc*<sup>-/-</sup> (C), and *Gas1*<sup>-/-</sup>;*Boc*<sup>-/-</sup> (D) embryos are shown. Whole-mount immunofluorescent antibody detection of E-CADHERIN (green; E-H) and NKX2.1 (red; E-H) in E10.5 wildtype (E), *Gas1*<sup>-/-</sup> (F), *Boc*<sup>-/-</sup> (G), and *Gas1*<sup>-/-</sup>;*Boc*<sup>-/-</sup> (H) embryos. Antibody detection of OLIG2 (green; I-L) and NKX2.2 (red; I-L) in transverse sections of E10.5 forelimb level neural tubes from wildtype (I), *Gas1*<sup>-/-</sup> (J), *Boc*<sup>-/-</sup> (K), and *Gas1*<sup>-/-</sup>;*Boc*<sup>-/-</sup> (L) embryos. Quantitation of NKX2.1 expression in wildtype (n=4), *Gas1*<sup>-/-</sup> (n=5), *Boc*<sup>-/-</sup> (n=6), and *Gas1*<sup>-/-</sup>;*Boc*<sup>-/-</sup> (n=5) embryos (M). Quantitation of NKX2.2+ cells (2 sections/embryo) for wildtype (n=7), *Gas1*<sup>-/-</sup> (n=5), *Boc*<sup>-/-</sup> (n=7), and *Gas1*<sup>-/-</sup>;*Boc*<sup>-/-</sup> (n=5) embryos (N). Data are represented as the mean ± standard deviation. P-values were determined by a two-tailed Student's *t*-test. The Bonferroni correction was employed to account for multiple comparisons in each dataset; (M,N) non-significant (n.s.; p>0.0166), significant (p≤0.0166). Note that NKX2.2+ cells are only present in a subset of sections from *Gas1*<sup>-/-</sup>;*Boc*<sup>-/-</sup> embryos (inset in M). Scale bars in A and E, 500μm; I, 25 μm.



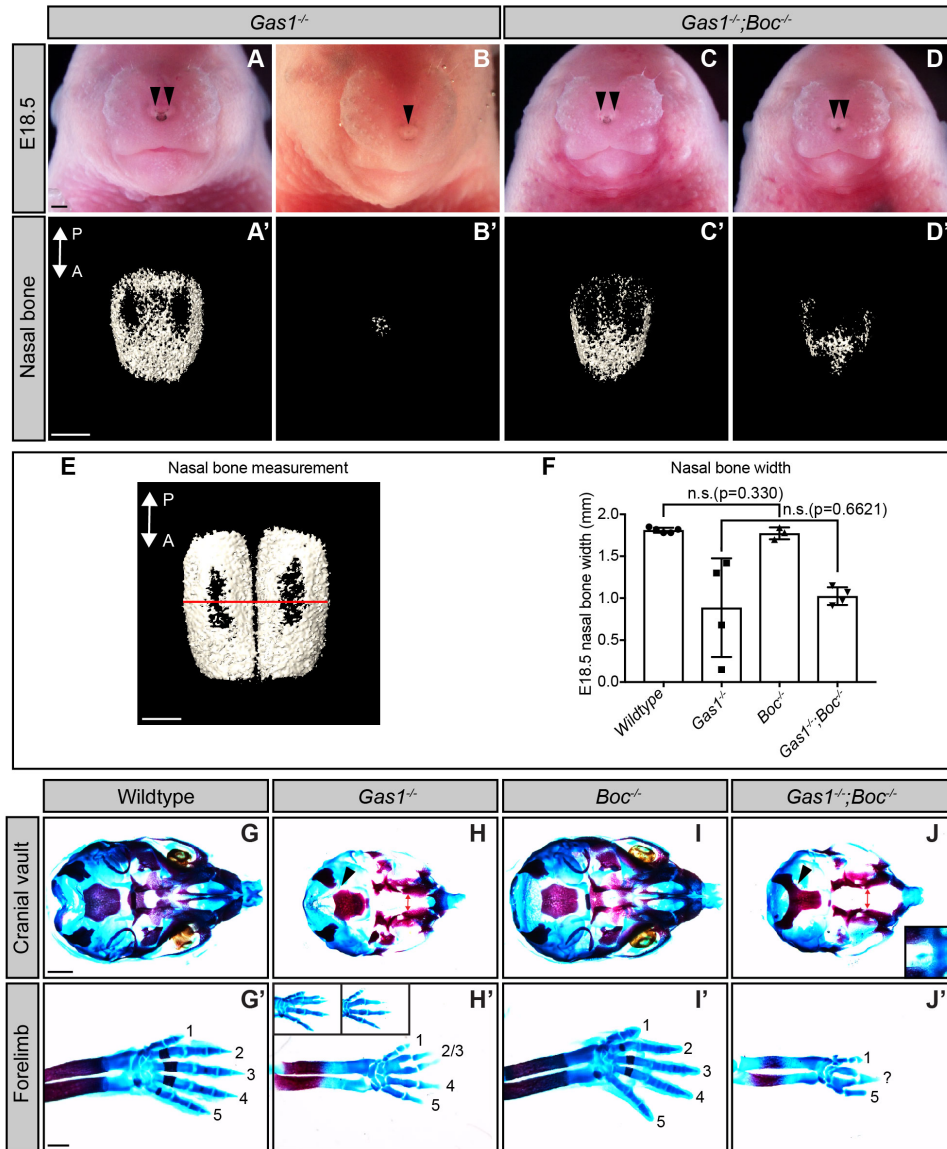
**Figure 2.11 *Boc* promotes HH-dependent neural patterning in the developing chicken**

Coronal sections of Hamburger-Hamilton stage 21-22 chicken forebrains electroporated with empty vector (pCIG; A-D), *SmoM2* (E-H), and *Boc* (I-L). DAPI (grayscale; A,E,I) denotes nuclei. GFP+ cells (green; B,F,J) identify electroporated cells. Antibody detection of NKX2.1 (red; C,G,K) reads out HH pathway activity. Merged images are shown in (D,H,L). The number of electroporated embryos that display ectopic NKX2.1 expression is indicated in the lower right corner (D,H,L). White arrowheads highlight ectopic NKX2.1 expression. Scale bars in A, E, and I, 50 $\mu$ m.



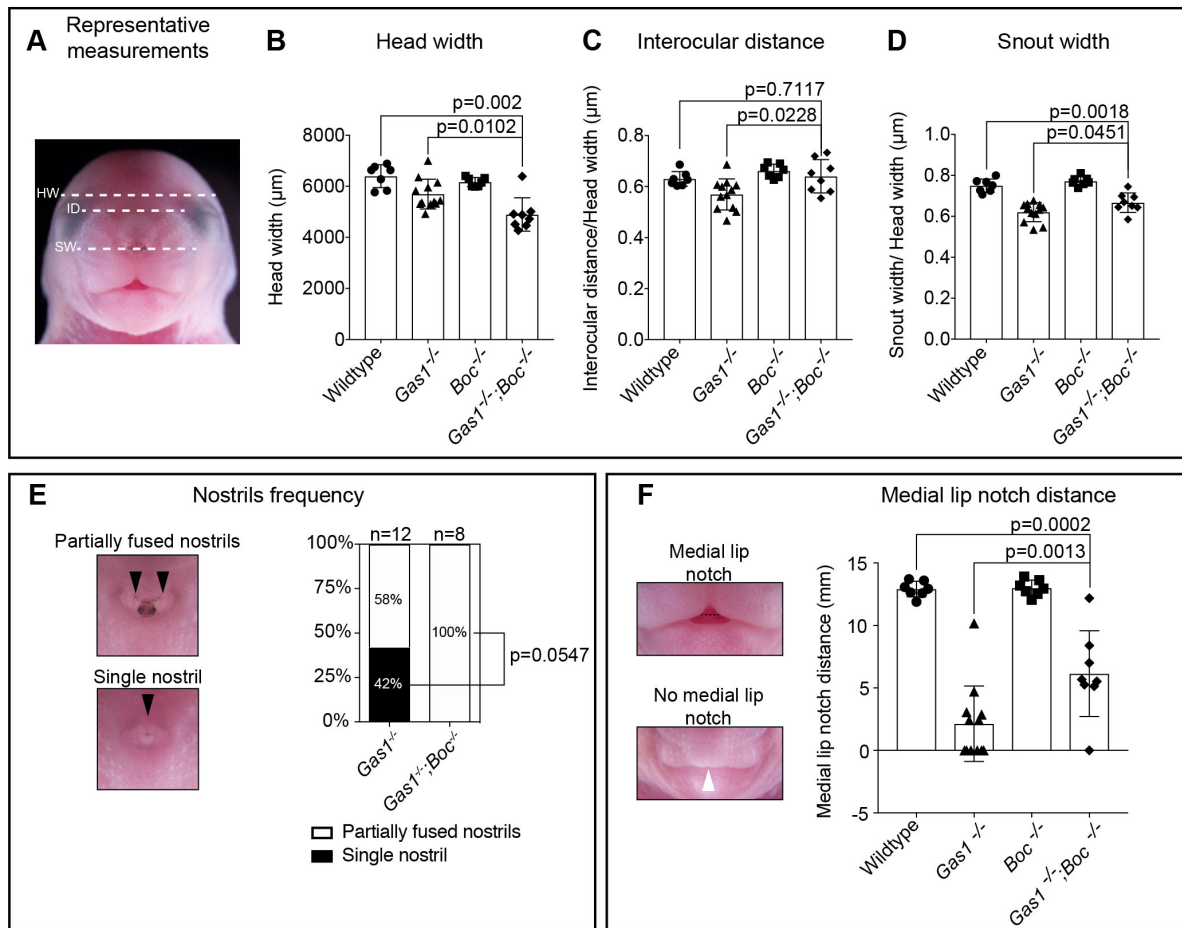
**Figure 2.12 Partial rescue of HPE phenotypes persists through E18.5 in *Gas1*;*Boc* mutant embryos.**

*En face* view of E18.5 wildtype (A,M), *Gas1*<sup>-/-</sup> (B,N), *Boc*<sup>-/-</sup> (C,O), and *Gas1*<sup>-/-</sup>;*Boc*<sup>-/-</sup> (D,P) embryos. Black arrowheads denote the nasal pits (NP), white arrowheads mark the maxilla (MX), and yellow arrowheads identify the mandible (M). E18.5 craniofacial structures stained with Alcian Blue and Alizarin Red to visualize cartilage and bone, respectively (E-L). Dorsal views of the nasal capsule (NC) and premaxilla (PMX) of E18.5 wildtype (E), *Gas1*<sup>-/-</sup> (F), *Boc*<sup>-/-</sup> (G), and *Gas1*<sup>-/-</sup>;*Boc*<sup>-/-</sup> (H) are shown. Black arrowheads indicate the nasal capsule and red arrowheads mark the premaxilla. Dorsal views of the mandible of E18.5, wildtype (I), *Gas1*<sup>-/-</sup> (J), *Boc*<sup>-/-</sup> (K), and *Gas1*<sup>-/-</sup>;*Boc*<sup>-/-</sup> (L) are shown. Asterisks identify ectopic bone duplications in the posterior part of the mandible and black arrows denote Meckel's cartilage (MC). Inset in J, shows ectopic bone in a *Gas1*<sup>-/-</sup> mutant embryo. Three dimensional reconstructions of microCT images of isolated nasal bones from E18.5 wildtype (M'), *Gas1*<sup>-/-</sup> (N'), *Boc*<sup>-/-</sup> (O'), and *Gas1*<sup>-/-</sup>;*Boc*<sup>-/-</sup> (P') embryos. A←→P specifies the anterior to posterior axis in (E-H, I-L, M'-P'). Scale bars (A, E, I, M, M'), 500µm.



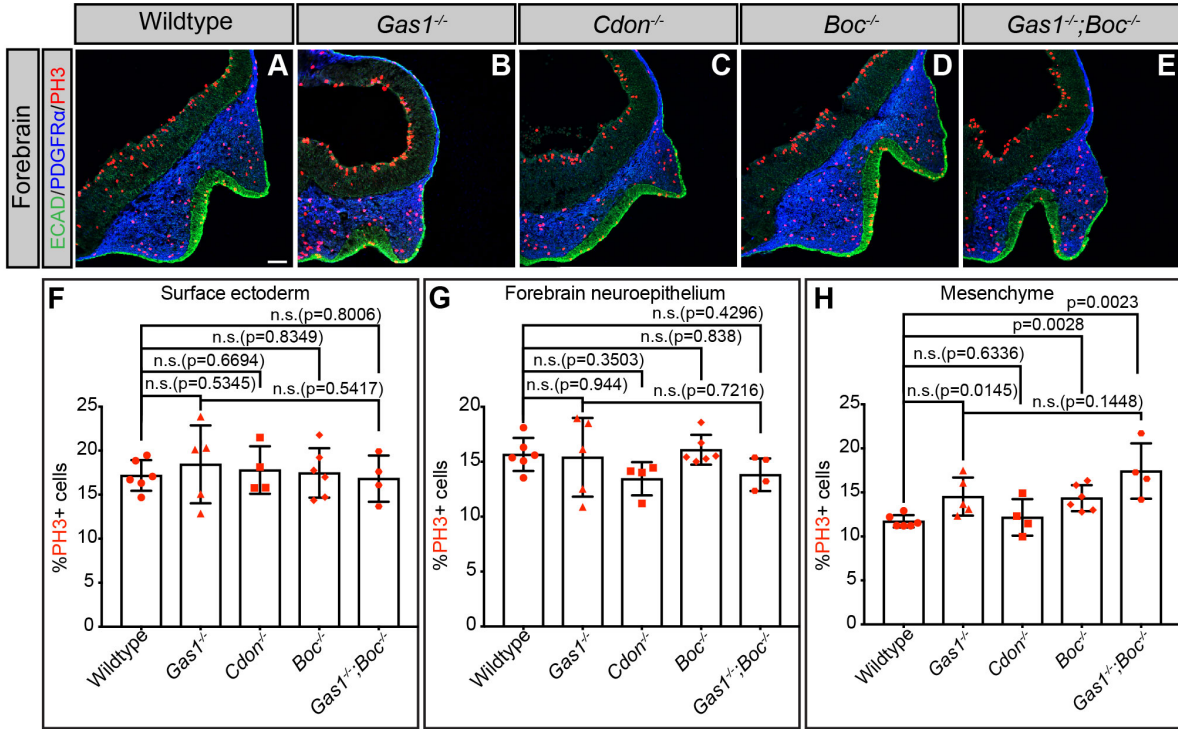
**Figure 2.13 HPE phenotypes and digit specification defects in E18.5 *Gas1;Boc* mutant embryos.**

*En face* view of E18.5 *Gas1<sup>-/-</sup>* (A,B) and *Gas1<sup>-/-</sup>;Boc<sup>-/-</sup>* (C,D) embryos. Black arrowheads denote the nasal pits. Three dimensional reconstructions of microCT images of isolated nasal bones from E18.5 *Gas1<sup>-/-</sup>* (A',B') and *Gas1<sup>-/-</sup>;Boc<sup>-/-</sup>* (C',D') embryos. A $\longleftrightarrow$ P specifies the anterior to posterior axis in (A'-D',E). MicroCT image of an isolated nasal bone from E18.5 wildtype embryo (E); the red horizontal line denotes the nasal bone width. Nasal bone width quantitation in wildtype (n=5), *Gas1<sup>-/-</sup>* (n=4), *Boc<sup>-/-</sup>* (n=3), and *Gas1<sup>-/-</sup>;Boc<sup>-/-</sup>* (n=4) embryos (F). Data are mean $\pm$ s.d. P-values were determined by a two-tailed Student's *t*-test. The Bonferroni correction was employed to account for multiple comparisons in each dataset; (F) non-significant (n.s.;  $p > 0.0250$ ), significant ( $p \leq 0.0250$ ). Ventral views of E18.5 cranial vaults from wildtype (G), *Gas1<sup>-/-</sup>* (H), *Boc<sup>-/-</sup>* (I), and *Gas1<sup>-/-</sup>;Boc<sup>-/-</sup>* (J) embryos, stained with Alcian Blue and Alizarin Red. Red double arrows denote the cleft palate in *Gas1<sup>-/-</sup>* and *Gas1<sup>-/-</sup>;Boc<sup>-/-</sup>* embryos and black arrowheads mark occipital bone. Inset in (J) indicates hypoplastic premaxilla in *Gas1<sup>-/-</sup>;Boc<sup>-/-</sup>* embryos. Forelimbs of E18.5 wildtype (G'), *Gas1<sup>-/-</sup>* (H'), *Boc<sup>-/-</sup>* (I'), and *Gas1<sup>-/-</sup>;Boc<sup>-/-</sup>* (J') embryos, stained with Alcian Blue and Alizarin Red. Numbers denote specific digits where 1 is the most anterior and 5 is the most posterior. Insets in (H') demonstrate variable digit specification phenotypes in *Gas1<sup>-/-</sup>* embryos, which display either partial fusion of digits two and three (left), or the absence of either digit two or three (right). *Gas1<sup>-/-</sup>;Boc<sup>-/-</sup>* embryos exhibit a more severe limb phenotype where only digits 1 and 5 can be clearly identified; a third, unidentified digit is labeled with a question mark (Allen et al., 2011). Scale bars (A,A',E,G',G'), 500  $\mu$ m.

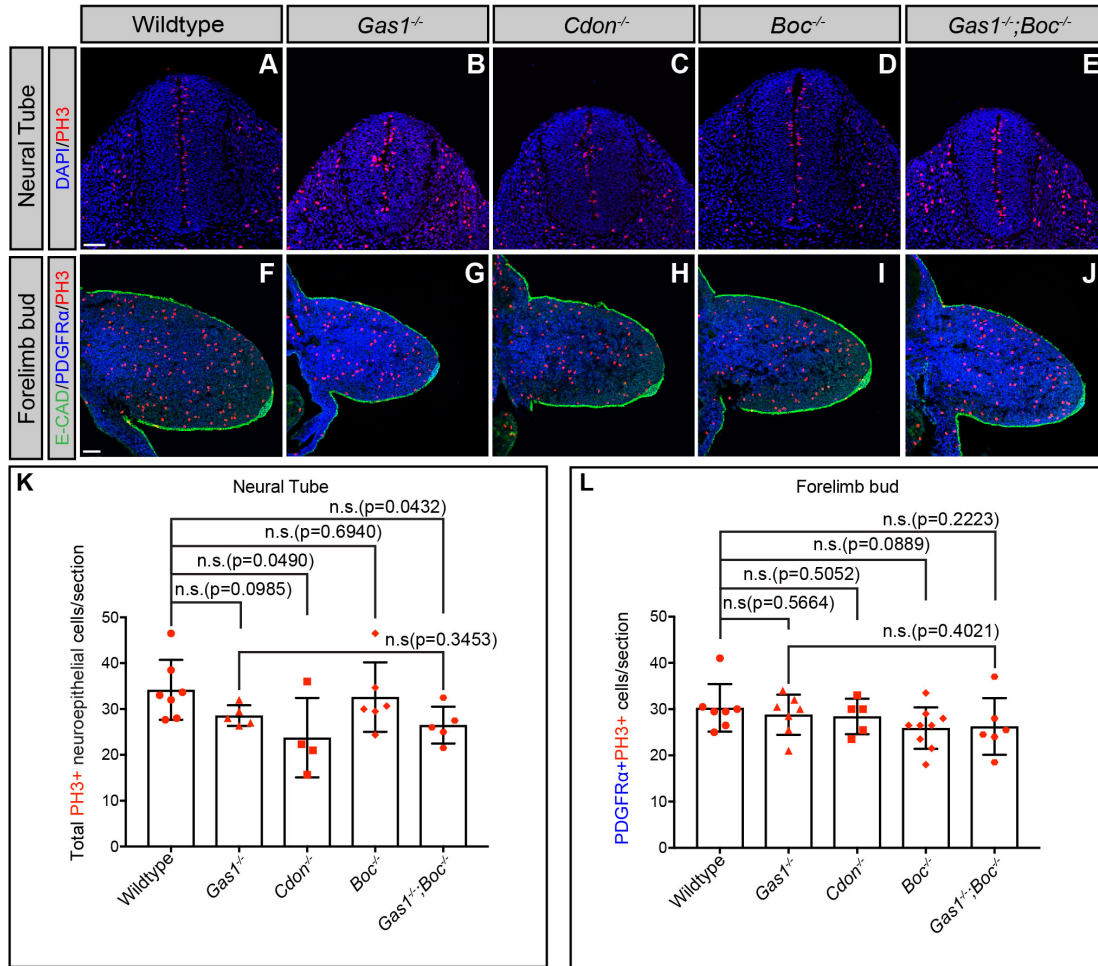


**Figure 2.14 E18.5 *Gas1*;*Boc* mutants display partially ameliorated midfacial defects.**

Quantitation of anatomical landmarks in E18.5 embryos (A-F). Representative measurements of head width (HW), interocular distance (ID), snout width (SW) in E18.5 embryos (A). White dotted lines denote the measured distance. Head width quantitation in wildtype (n=7), *Gas1*<sup>-/-</sup> (n=12), *Boc*<sup>-/-</sup> (n=7) and *Gas1*<sup>-/-</sup>;*Boc*<sup>-/-</sup> (n=8) embryos (B). Interocular distance quantitation, normalized to the head width in wildtype (n=7), *Gas1*<sup>-/-</sup> (n=12), *Boc*<sup>-/-</sup> (n=7) and *Gas1*<sup>-/-</sup>;*Boc*<sup>-/-</sup> (n=8) embryos (C). Snout width quantitation, normalized to the head width in wildtype (n=7), *Gas1*<sup>-/-</sup> (n=12) and *Gas1*<sup>-/-</sup>;*Boc*<sup>-/-</sup> (n=8) embryos (D). Nostril frequency in *Gas1*<sup>-/-</sup> (n=12) and *Gas1*<sup>-/-</sup>;*Boc*<sup>-/-</sup> (n=8) embryos (E). Left panel, representative images of two partially fused nostrils and a single nostril. Black arrowheads denote two nostrils and a single nostril. Right panel, observed nostril frequency. Medial lip notch distance quantitation in wildtype (n=7), *Gas1*<sup>-/-</sup> (n=12), *Boc*<sup>-/-</sup> (n=7) and *Gas1*<sup>-/-</sup>;*Boc*<sup>-/-</sup> (n=8) embryos (F). Left panel, representative images of medial lip notch and no medial lip notch. Right panel, medial lip notch quantitation. White arrowhead denotes the lack of a medial lip notch. Data are mean±s.d. P-values were determined by a two-tailed Student's *t*-test (B-D, F) or a Fisher's Exact test (E). The Bonferroni correction was employed to account for multiple comparisons in (B-D, F); (n.s.;  $p > 0.0250$ ), significant ( $p \leq 0.0250$ ).

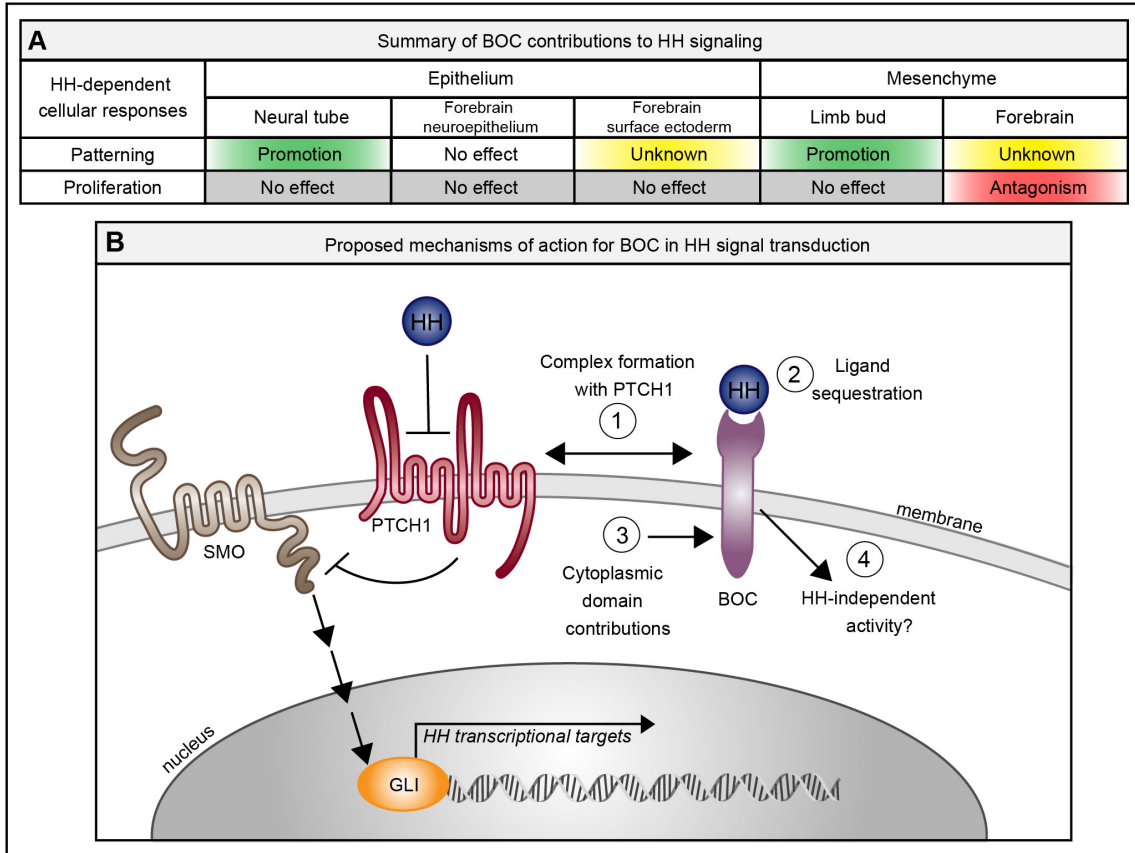






**Figure 2.16 Boc does not contribute to neural tube or forelimb mesenchyme proliferation.**

Immunofluorescent analysis of proliferation in E10.5 neural tube (A-E) and forelimb (F-J) transverse sections from E10.5, wildtype (A,F), *Gas1*<sup>-/-</sup> (B,G), *Cdon*<sup>-/-</sup> (C,H), *Boc*<sup>-/-</sup> (D,I), and *Gas1*<sup>-/-</sup>;*Boc*<sup>-/-</sup> (E,J) embryos. Antibody detection of E-CADHERIN (E-CAD, green, F-J), PDGFRα (blue, F-J), and phospho-histone H3 (PH3, red, A-J). Nuclei are stained with DAPI (blue, A-E). Quantitation of PH3+ cells (2 sections/embryo) in the neural tube (K) from E10.5 wildtype (n=7), *Gas1*<sup>-/-</sup> (n=5), *Cdon*<sup>-/-</sup> (n=4), *Boc*<sup>-/-</sup> (n=6) and *Gas1*<sup>-/-</sup>;*Boc*<sup>-/-</sup> (n=5) embryos. Quantitation of PH3+ cells (2 sections/limb) in forelimb buds (L) from E10.5 wildtype (n=7), *Gas1*<sup>-/-</sup> (n=7), *Cdon*<sup>-/-</sup> (n=5), *Boc*<sup>-/-</sup> (n=9) and *Gas1*<sup>-/-</sup>;*Boc*<sup>-/-</sup> (n=6) embryos. Data are mean±s.d. P-values were determined by a two-tailed Student's *t*-test. The Bonferroni correction was employed to account for multiple comparisons in each dataset; (K-L) non-significant (n.s.; p>0.0125), significant (p≤0.0125). Scale bars (A,F), 50 μm



**Figure 2.17 BOC is a multi-functional regulator of HH signaling.**

Summary of BOC contributions to HH signaling (A). Green indicates promotion of HH signaling, red denotes HH pathway antagonism, gray suggests no effect, and yellow is unknown. Proposed mechanisms of action for BOC in HH signal transduction (B). 1. Complex formation with PTCH1. The interaction of PTCH1 and BOC that allows the formation of a receptor complex that alternately activates or inhibits HH pathway activity. 2. Ligand sequestration. BOC binds HH ligands through its extracellular domain and could antagonize HH signaling by sequestering SHH in areas of low SHH concentration. 3. Cytoplasmic domain contributions. The unique cytoplasmic domain of BOC could regulate additional downstream signaling cascades that enable its tissue-specific functions. 4. HH-independent activity. BOC could mediate yet to be identified HH-independent functions that either augment or counter the HH response.

## 2.10 References

- Allen, B. L., Song, J. Y., Izzi, L., Althaus, I. W., Kang, J. S., Charron, F., Krauss, R. S. and McMahon, A. P.** (2011). Overlapping roles and collective requirement for the coreceptors GAS1, CDO, and BOC in SHH pathway function. *Dev Cell* **20**, 775-787.
- Allen, B. L., Tenzen, T. and McMahon, A. P.** (2007). The Hedgehog-binding proteins Gas1 and Cdo cooperate to positively regulate Shh signaling during mouse development. *Genes Dev* **21**, 1244-1257.
- Aoto, K., Shikata, Y., Imai, H., Matsumaru, D., Tokunaga, T., Shioda, S., Yamada, G. and Motoyama, J.** (2009). Mouse Shh is required for prechordal plate maintenance during brain and craniofacial morphogenesis. *Dev Biol* **327**, 106-120.
- Bae, G. U., Domene, S., Roessler, E., Schachter, K., Kang, J. S., Muenke, M. and Krauss, R. S.** (2011). Mutations in CDON, encoding a hedgehog receptor, result in holoprosencephaly and defective interactions with other hedgehog receptors. *Am J Hum Genet* **89**, 231-240.
- Beachy, P. A., Hymowitz, S. G., Lazarus, R. A., Leahy, D. J. and Siebold, C.** (2010). Interactions between Hedgehog proteins and their binding partners come into view. *Genes Dev* **24**, 2001-2012.
- Bergeron, S. A., Tyurina, O. V., Miller, E., Bagas, A. and Karlstrom, R. O.** (2011). Brother of cdo (umleitung) is cell-autonomously required for Hedgehog-mediated ventral CNS patterning in the zebrafish. *Development* **138**, 75-85.
- Briscoe, J., Pierani, A., Jessell, T. M. and Ericson, J.** (2000). A homeodomain protein code specifies progenitor cell identity and neuronal fate in the ventral neural tube. *Cell* **101**, 435-445.
- Briscoe, J. and Therond, P. P.** (2013). The mechanisms of Hedgehog signalling and its roles in development and disease. *Nat Rev Mol Cell Biol* **14**, 416-429.
- Brugmann, S. A., Allen, N. C., James, A. W., Mekonnen, Z., Madan, E. and Helms, J. A.** (2010). A primary cilia-dependent etiology for midline facial disorders. *Hum Mol Genet* **19**, 1577-1592.
- Cabrera, J. R., Sanchez-Pulido, L., Rojas, A. M., Valencia, A., Manes, S., Naranjo, J. R. and Mellstrom, B.** (2006). Gas1 is related to the glial cell-derived neurotrophic factor family receptors alpha and regulates Ret signaling. *J Biol Chem* **281**, 14330-14339.
- Cardozo, M. J., Sanchez-Arrones, L., Sandonis, A., Sanchez-Camacho, C., Gestri, G., Wilson, S. W., Guerrero, I. and Bovolenta, P.** (2014). Cdon acts as a Hedgehog decoy receptor during proximal-distal patterning of the optic vesicle. *Nat Commun* **5**, 4272.
- Chiang, C., Litingtung, Y., Lee, E., Young, K. E., Corden, J. L., Westphal, H. and Beachy, P. A.** (1996). Cyclopia and defective axial patterning in mice lacking Sonic hedgehog gene function. *Nature* **383**, 407-413.

- Cobourne, M. T., Miletich, I. and Sharpe, P. T.** (2004). Restriction of sonic hedgehog signalling during early tooth development. *Development* **131**, 2875-2885.
- Cole, F. and Krauss, R. S.** (2003). Microform holoprosencephaly in mice that lack the Ig superfamily member Cdon. *Curr Biol* **13**, 411-415.
- Cordero, D., Marcucio, R., Hu, D., Gaffield, W., Tapadia, M. and Helms, J. A.** (2004). Temporal perturbations in sonic hedgehog signaling elicit the spectrum of holoprosencephaly phenotypes. *J Clin Invest* **114**, 485-494.
- Dai, P., Akimaru, H., Tanaka, Y., Maekawa, T., Nakafuku, M. and Ishii, S.** (1999). Sonic Hedgehog-induced activation of the Gli1 promoter is mediated by GLI3. *J Biol Chem* **274**, 8143-8152.
- Dessaud, E., McMahon, A. P. and Briscoe, J.** (2008). Pattern formation in the vertebrate neural tube: a sonic hedgehog morphogen-regulated transcriptional network. *Development* **135**, 2489-2503.
- Han, Y., Xiong, Y., Shi, X., Wu, J., Zhao, Y. and Jiang, J.** (2017). Regulation of Gli ciliary localization and Hedgehog signaling by the PY-NLS/karyopherin-beta2 nuclear import system. *PLoS Biol* **15**, e2002063.
- Ho, T. V., Iwata, J., Ho, H. A., Grimes, W. C., Park, S., Sanchez-Lara, P. A. and Chai, Y.** (2015). Integration of comprehensive 3D microCT and signaling analysis reveals differential regulatory mechanisms of craniofacial bone development. *Dev Biol* **400**, 180-190.
- Holtz, A. M., Peterson, K. A., Nishi, Y., Morin, S., Song, J. Y., Charron, F., McMahon, A. P. and Allen, B. L.** (2013). Essential role for ligand-dependent feedback antagonism of vertebrate hedgehog signaling by PTCH1, PTCH2 and HHIP1 during neural patterning. *Development* **140**, 3423-3434.
- Hong, M. and Krauss, R. S.** (2018). Modeling the complex etiology of holoprosencephaly in mice. *Am J Med Genet C Semin Med Genet* **178**, 140-150.
- Hong, M., Srivastava, K., Kim, S., Allen, B. L., Leahy, D. J., Hu, P., Roessler, E., Krauss, R. S. and Muenke, M.** (2017). BOC is a modifier gene in holoprosencephaly. *Hum Mutat* **38**, 1464-1470.
- Hu, D. and Helms, J. A.** (1999). The role of sonic hedgehog in normal and abnormal craniofacial morphogenesis. *Development* **126**, 4873-4884.
- Hui, C. C. and Angers, S.** (2011). Gli proteins in development and disease. *Annu Rev Cell Dev Biol* **27**, 513-537.
- Izzi, L., Levesque, M., Morin, S., Laniel, D., Wilkes, B. C., Mille, F., Krauss, R. S., McMahon, A. P., Allen, B. L. and Charron, F.** (2011). Boc and Gas1 each form distinct Shh receptor complexes with Ptch1 and are required for Shh-mediated cell proliferation. *Dev Cell* **20**, 788-801.

- Jeong, J., Mao, J., Tenzen, T., Kottmann, A. H. and McMahon, A. P.** (2004). Hedgehog signaling in the neural crest cells regulates the patterning and growth of facial primordia. *Genes Dev* **18**, 937-951.
- Jiang, R., Bush, J. O. and Lidral, A. C.** (2006). Development of the upper lip: morphogenetic and molecular mechanisms. *Dev Dyn* **235**, 1152-1166.
- Kang, J. S., Gao, M., Feinleib, J. L., Cotter, P. D., Guadagno, S. N. and Krauss, R. S.** (1997). CDO: an oncogene-, serum-, and anchorage-regulated member of the Ig/fibronectin type III repeat family. *J Cell Biol* **138**, 203-213.
- Kang, J. S., Mulieri, P. J., Hu, Y., Taliana, L. and Krauss, R. S.** (2002). BOC, an Ig superfamily member, associates with CDO to positively regulate myogenic differentiation. *EMBO J* **21**, 114-124.
- Krauss, R. S.** (2007). Holoprosencephaly: new models, new insights. *Expert Rev Mol Med* **9**, 1-17.
- Kuwajima, T., Sitko, A. A., Bhansali, P., Jurgens, C., Guido, W. and Mason, C.** (2013). ClearT: a detergent- and solvent-free clearing method for neuronal and non-neuronal tissue. *Development* **140**, 1364-1368.
- Lee, C. S., Buttitta, L. and Fan, C. M.** (2001). Evidence that the WNT-inducible growth arrest-specific gene 1 encodes an antagonist of sonic hedgehog signaling in the somite. *Proc Natl Acad Sci U S A* **98**, 11347-11352.
- Lewandowski, J. P., Du, F., Zhang, S., Powell, M. B., Falkenstein, K. N., Ji, H. and Vokes, S. A.** (2015). Spatiotemporal regulation of GLI target genes in the mammalian limb bud. *Dev Biol* **406**, 92-103.
- Lum, L., Yao, S., Mozer, B., Rovescalli, A., Von Kessler, D., Nirenberg, M. and Beachy, P. A.** (2003). Identification of Hedgehog pathway components by RNAi in *Drosophila* cultured cells. *Science* **299**, 2039-2045.
- Makihara, S., Morin, S., Ferent, J., Cote, J. F., Yam, P. T. and Charron, F.** (2018). Polarized Dock Activity Drives Shh-Mediated Axon Guidance. *Dev Cell* **46**, 410-425 e417.
- Marcucio, R. S., Cordero, D. R., Hu, D. and Helms, J. A.** (2005). Molecular interactions coordinating the development of the forebrain and face. *Dev Biol* **284**, 48-61.
- Marigo, V., Davey, R. A., Zuo, Y., Cunningham, J. M. and Tabin, C. J.** (1996). Biochemical evidence that patched is the Hedgehog receptor. *Nature* **384**, 176-179.
- Martinelli, D. C. and Fan, C. M.** (2007). Gas1 extends the range of Hedgehog action by facilitating its signaling. *Genes Dev* **21**, 1231-1243.

- McLellan, J. S., Zheng, X., Hauk, G., Ghirlando, R., Beachy, P. A. and Leahy, D. J.** (2008). The mode of Hedgehog binding to Ihog homologues is not conserved across different phyla. *Nature* **455**, 979-983.
- McMahon, A. P., Ingham, P. W. and Tabin, C. J.** (2003). Developmental roles and clinical significance of hedgehog signaling. *Curr Top Dev Biol* **53**, 1-114.
- Muenke, M. and Beachy, P. A.** (2000). Genetics of ventral forebrain development and holoprosencephaly. *Curr Opin Genet Dev* **10**, 262-269.
- Ohazama, A., Haycraft, C. J., Seppala, M., Blackburn, J., Ghafoor, S., Cobourne, M., Martinelli, D. C., Fan, C. M., Peterkova, R., Lesot, H., et al.** (2009). Primary cilia regulate Shh activity in the control of molar tooth number. *Development* **136**, 897-903.
- Okada, A., Charron, F., Morin, S., Shin, D. S., Wong, K., Fabre, P. J., Tessier-Lavigne, M. and McConnell, S. K.** (2006). Boc is a receptor for sonic hedgehog in the guidance of commissural axons. *Nature* **444**, 369-373.
- Pabst, O., Herbrand, H., Takuma, N. and Arnold, H. H.** (2000). NKX2 gene expression in neuroectoderm but not in mesendodermally derived structures depends on sonic hedgehog in mouse embryos. *Dev Genes Evol* **210**, 47-50.
- Ribeiro, L. A., Queizi, R. G., Nascimento, A., Bertolacini, C. P. and Richieri-Costa, A.** (2010). Holoprosencephaly and holoprosencephaly-like phenotype and GAS1 DNA sequence changes: Report of four Brazilian patients. *Am J Med Genet A* **152A**, 1688-1694.
- Roessler, E., El-Jaick, K. B., Dubourg, C., Velez, J. I., Solomon, B. D., Pineda-Alvarez, D. E., Lachawan, F., Zhou, N., Ouspenskaia, M., Paulussen, A., et al.** (2009). The mutational spectrum of holoprosencephaly-associated changes within the SHH gene in humans predicts loss-of-function through either key structural alterations of the ligand or its altered synthesis. *Hum Mutat* **30**, E921-935.
- Roessler, E. and Muenke, M.** (2010). The molecular genetics of holoprosencephaly. *Am J Med Genet C Semin Med Genet* **154C**, 52-61.
- Rubenstein, J. L. and Beachy, P. A.** (1998). Patterning of the embryonic forebrain. *Curr Opin Neurobiol* **8**, 18-26.
- Schachter, K. A. and Krauss, R. S.** (2008). Murine models of holoprosencephaly. In *Curr Top Dev Biol*, pp. 139-170.
- Schneider, C. A., Rasband, W. S. and Eliceiri, K. W.** (2012). NIH Image to ImageJ: 25 years of image analysis. *Nat Methods* **9**, 671-675.
- Seppala, M., Depew, M. J., Martinelli, D. C., Fan, C. M., Sharpe, P. T. and Cobourne, M. T.** (2007). Gas1 is a modifier for holoprosencephaly and genetically interacts with sonic hedgehog. *J Clin Invest* **117**, 1575-1584.

- Seppala, M., Xavier, G. M., Fan, C. M. and Cobourne, M. T.** (2014). Boc modifies the spectrum of holoprosencephaly in the absence of Gas1 function. *Biol Open* **3**, 728-740.
- Tenzen, T., Allen, B. L., Cole, F., Kang, J. S., Krauss, R. S. and McMahon, A. P.** (2006). The cell surface membrane proteins Cdo and Boc are components and targets of the Hedgehog signaling pathway and feedback network in mice. *Dev Cell* **10**, 647-656.
- Vuong, T. A., Leem, Y. E., Kim, B. G., Cho, H., Lee, S. J., Bae, G. U. and Kang, J. S.** (2017). A Sonic hedgehog coreceptor, BOC regulates neuronal differentiation and neurite outgrowth via interaction with ABL and JNK activation. *Cell Signal* **30**, 30-40.
- Wilkinson, D. G.** (1992). *In situ hybridization : a practical approach*. Oxford ; New York: IRL Press at Oxford University Press.
- Xavier, G. M., Seppala, M., Barrell, W., Birjandi, A. A., Geoghegan, F. and Cobourne, M. T.** (2016a). Hedgehog receptor function during craniofacial development. *Dev Biol* **415**, 198-215.
- Xavier, G. M., Seppala, M., Papageorgiou, S. N., Fan, C. M. and Cobourne, M. T.** (2016b). Genetic interactions between the hedgehog co-receptors Gas1 and Boc regulate cell proliferation during murine palatogenesis. *Oncotarget* **7**, 79233-79246.
- Xie, J., Murone, M., Luoh, S. M., Ryan, A., Gu, Q., Zhang, C., Bonifas, J. M., Lam, C. W., Hynes, M., Goddard, A., et al.** (1998). Activating Smoothed mutations in sporadic basal-cell carcinoma. *Nature* **391**, 90-92.
- Xu, J., Liu, H., Lan, Y., Adam, M., Clouthier, D. E., Potter, S. and Jiang, R.** (2019). Hedgehog signaling patterns the oral-aboral axis of the mandibular arch. *Elife* **8**.
- Yao, S., Lum, L. and Beachy, P.** (2006). The ihog cell-surface proteins bind Hedgehog and mediate pathway activation. *Cell* **125**, 343-357.
- Zhang, W., Hong, M., Bae, G. U., Kang, J. S. and Krauss, R. S.** (2011). Boc modifies the holoprosencephaly spectrum of Cdo mutant mice. *Dis Model Mech* **4**, 368-380.
- Zhang, W., Kang, J. S., Cole, F., Yi, M. J. and Krauss, R. S.** (2006). Cdo functions at multiple points in the Sonic Hedgehog pathway, and Cdo-deficient mice accurately model human holoprosencephaly. *Dev Cell* **10**, 657-665.

## Chapter 3 *Cdon* is Required for Proper HH-Dependent Patterning of the Developing Limb

### 3.1 Abstract

The Hedgehog (HH) signaling pathway regulates the patterning, proliferation and differentiation of multiple tissues during development. HH ligands primarily signal through PTCH1 and three co-receptors, GAS1, CDON and BOC. These co-receptors are essential during vertebrate embryogenesis. Interestingly, during limb patterning functional roles for only GAS1 and BOC, but not CDON have been demonstrated during HH-dependent digit specification. A collective role for these co-receptors has not been explored during limb development due to embryonic lethality of *Gas1;Cdon;Boc* mutants at E9.5, prior to the onset of limb development. Here I explore a role for *Cdon* in digit specification by using a *Cdon* conditional allele in combination with a limb-specific *Prx1Cre* driver in a *Gas1;Boc* null background. The limb-specific ablation of *Cdon* in a *Gas1;Boc* null background allows for survival until E18.5, and for the assessment of potential contributions of *Cdon* to HH-dependent digit specification. Combined deletion of *Cdon*, *Gas1* and *Boc* in the limb results in severe digit specification defects, as well as patterning defects in the radius, ulna, tibia, and fibula. Taken together, these data demonstrate a novel role for *Cdon* in proper limb patterning and digit specification.



### 3.2 Introduction

The Hedgehog (HH) signaling pathway is a critical regulator of tissue patterning and growth in both invertebrate and vertebrate embryos (Briscoe and Therond, 2013; McMahon et al., 2003). In mammals, HH signaling contributes to the patterning of multiple tissues including, craniofacial structures, spinal cord and limbs (Briscoe and Therond, 2013; McMahon et al., 2003). Defective HH signaling results in various birth defects such as holoprosencephaly, spina bifida, and polydactyly, as well as numerous cancers including pancreatic cancer, medulloblastoma, and basal cell carcinoma (Roessler et al., 1996; Vortkamp et al., 1992; Vortkamp et al., 1991) (Murdoch and Copp, 2010; Teglund and Toftgard, 2010).

HH ligands are regulated at the cell surface by the twelve-pass transmembrane protein Patched 1 (PTCH1) (Marigo et al., 1996). However, HH ligands are multivalent, and can also signal through three HH co-receptors, growth arrest specific-1 (GAS1), CAM-related/downregulated by oncogenes (CDON) and brother of CDON (BOC) (Allen et al., 2011; Allen et al., 2007; Beachy et al., 2010; Izzi et al., 2011; Lum et al., 2003; McLellan et al., 2008; Tenzen et al., 2006; Yao et al., 2006). CDON and BOC are structurally similar single pass transmembrane proteins from the immunoglobulin superfamily, while GAS1 is a GPI linked protein with resemblance to the GDNF receptors (Cabrera et al., 2006; Kang et al., 2002). In absence of HH ligands, PTCH1 constitutively inhibits the activity of the GPCR-like receptor Smoothed (SMO). HH ligand binding to PTCH1, along with GAS1, CDON and BOC results in the de-repression of SMO, and subsequent modulation of the GLI family of transcription factors (Hui and Angers, 2011). GLIs are comprised of three genes, *Gli1*, *Gli2*, and *Gli3* (Briscoe and Therond, 2013; Hui and Angers, 2011). GLI1 is exclusively a transcriptional activator that is

also a target of the HH pathway and is responsible for amplifying the HH transcriptional response, while GLI2 and GLI3 function primarily as activators and repressors, respectively (Briscoe and Therond, 2013; Dai et al., 1999; Hui and Angers, 2011).

The HH co-receptors, GAS1, CDON and BOC, display similar expression patterns throughout development, they interact with PTCH1 and function in a variety HH-dependent patterning processes (Allen et al., 2011; Bae et al., 2011; Izzi et al., 2011; Lee and Fan, 2001; Mulieri et al., 2002; Mulieri et al., 2000). Their function has been extensively explored during craniofacial development and ventral neural tube patterning, where they are essential for proper HH signal transduction (Allen et al., 2011; Allen et al., 2007; Cole and Krauss, 2003; Seppala et al., 2007; Seppala et al., 2014; Tenzen et al., 2006; Zhang et al., 2011; Zhang et al., 2006). However, their roles in limb development and digit specification remain understudied.

During limb patterning, one of the three mammalian HH ligands, Sonic Hedgehog (SHH) is secreted as a morphogen from the zone of polarizing activity (ZPA) to regulate anterior-posterior patterning (Echelard et al., 1993; Riddle et al., 1993; Saunders, 1968). Importantly, SHH not only regulates anterior-posterior patterning, but also cell survival and proliferation in the limb bud (Bastida et al., 2004). Specifically, SHH dictates the specification of digits in the limbs, 1 to 5, or thumb to pinky (Harfe et al., 2004). Multiple detailed studies in chicken embryos and mice, have demonstrated that digit specification is dictated both by the concentration of SHH ligand and time of exposure that HH-responding cells receive. [reviewed by (Tickle, 2006)]. The SHH morphogen gradient establishes digit identity by autocrine (digits 5, 4, and part of 3) and paracrine (part of digit 3 and digit 2) signaling (Harfe et al., 2004). Additionally, this process is influenced by a GLI3 repressor anterior-posterior gradient, which maintains proper levels of HH signaling in the developing limb (te Welscher et al., 2002; Wang

et al., 2000). Genetic deletion of *Shh* results in the complete absence of digits 2-5 and fusion of the tibia and the fibula in the hindlimb (Chiang et al., 1996). Digit 1, the most anterior digit in these mutants is unaffected, as its patterning is SHH-independent (Chiang et al., 1996).

Genetic ablation of HH co-receptors results in variable digit specification phenotypes. Interestingly, Only *Gas1*<sup>-/-</sup> and *Gas1*<sup>-/-</sup>;*Boc*<sup>-/-</sup> embryos display digit specification defects (Allen et al., 2011). In contrast, *Boc*<sup>-/-</sup>, *Cdon*<sup>-/-</sup>, and *Cdon*<sup>-/-</sup>;*Boc*<sup>-/-</sup> embryos exhibit normal digit specification (Allen et al., 2011). These data suggest that GAS1 is a major contributor to HH-dependent digit specification, with a smaller, redundant role for *Boc* in this process. Strikingly, despite a requirement for *Cdon* in multiple other SHH-responsive tissues such as craniofacial structures and the ventral neural tube, its function appears dispensable in SHH-dependent digit specification (Allen et al., 2011; Allen et al., 2007; Cole and Krauss, 2003; Tenzen et al., 2006; Zhang et al., 2011). However, a redundant function for CDON could be masked by the collective overlapping roles of GAS1 and BOC during SHH-dependent digit specification. Unfortunately, the simultaneous deletion of *Gas1*, *Cdon* and *Boc* results in near complete loss of HH signaling and embryonic lethality at E9.5, thus precluding a definitive analysis of a role for CDON in HH-dependent digit specification and limb patterning (Allen et al., 2011).

In this study I investigate the role of CDON in SHH-dependent digit specification during limb patterning. Specifically, I utilized a novel *Cdon*<sup>fl/fl</sup> conditional allele in combination with the *Prx1-Cre* transgene in a *Gas1*;*Boc* null background (Bae et al., 2020; Logan et al., 2002) to assess the consequences of combined GAS1, CDON and BOC removal on limb development. I find that limb-specific *Cdon* deletion in a *Gas1*;*Boc* null background results in severe digit specification defects and patterning defects in the radius, ulna, tibia, and fibula in the forelimbs

and hindlimbs. Overall these data reveal a novel role for CDON during limb patterning and digit specification.

### 3.3 Results

To assess a potential role for CDON during limb development, I first examined the expression of *Gas1*, *Cdon* and *Boc* in E10.5 forelimb buds using *lacZ* (*Gas1* and *Cdon*) and *Alkaline phosphatase* (*AP*; *Boc*) reporter alleles (Figure 3.1) (Cole and Krauss, 2003; Martinelli and Fan, 2007; Zhang et al., 2011). As previously shown, *Gas1*, *Cdon* and *Boc* are all expressed in the E10.5 limb bud, although their expression is confined to the anterior part of the E10.5 forelimb buds (Figure 3.1B-D) (Allen et al., 2011; Allen et al., 2007; Tenzen et al., 2006). Interestingly, the expression domain of *Cdon* is more anteriorly and proximally restricted in the forelimb bud (Figure 3.1C) than either *Gas1* or *Boc* expression (Figure 3.1B, D). Overall, the expression of the HH co-receptors is similar, but not identical in the forelimb buds and is consistent with their general negative transcriptional regulation by the HH signaling pathway, as observed in other tissues (Allen et al., 2011; Allen et al., 2007; Tenzen et al., 2006). However, it is yet to be determined if *Cdon* expression remains restricted to the most proximal region of the developing limb over time, and whether there might be differences in forelimb and hindlimb expression.

The individual deletion of HH co-receptors results in phenotypes of variable severity across HH-responsive tissues, including the craniofacial structures and the ventral neural tube (Allen et al., 2011; Allen et al., 2007; Cole and Krauss, 2003; Seppala et al., 2007; Tenzen et al., 2006). To determine the individual contribution of the HH co-receptors to SHH-digit specification and to assess variability across different mutants, we examined the levels of the

general HH target *Gli1* by *in situ* hybridization. *Gas1*<sup>-/-</sup> embryos display decreased variable expression levels of *Gli1* in the developing forelimb bud (Figure 3.1F-H). These data suggest that variable digit specification defects observed in E18.5 *Gas1* mutants could arise from differences in HH pathway activity (Allen et al., 2011; Martinelli and Fan, 2007). *Cdon*<sup>-/-</sup> embryos also display variable reduced *Gli1* levels, but to a lesser extent than *Gas1*<sup>-/-</sup> embryos (Figure 3.1J-L). Conversely, *Boc*<sup>-/-</sup> embryos, exhibit normal and consistent levels of *Gli1* when compared to wildtype embryos (Figure 3.1N-P). These data suggest that GAS1 is the primary co-receptor that functions in SHH-dependent digit specification. However, further examination of *Gli1* levels in of double co-receptor mutants revealed that the deletion of *Boc* or *Cdon* in a *Gas1* null background, significantly reduces *Gli1* expression in the developing forelimb bud (Figure 3.2B-D). Interestingly, *Cdon*<sup>-/-</sup>;*Boc*<sup>-/-</sup> mutants do not display any changes in *Gli1* expression (Figure 3.2D). Thus, these data suggested that GAS1 appears to be playing a more significant role, based in its broad expression when compared to *Cdon* and *Boc*.

Analysis of skeletal patterning and digit specification in E18.5 *Gas1*, *Cdon* and *Boc* single and compound mutants performed by (Allen et al., 2011) (Reprinted here as Figure 3.3, with permission of (Allen et al., 2011)) is consistent with the reduced *Gli1* levels observed at E10.5. *Gas1*<sup>-/-</sup> embryos display a loss of digits 2 or 3 in both forelimbs and hindlimbs (Allen et al., 2011; Martinelli and Fan, 2007) (Figure 3.3A,G). However, despite the subtle variability of *Gli1* levels in *Cdon* mutant embryos, this does not result in any digit specification defects (Figure 3.3B,H). In contrast, *Boc*<sup>-/-</sup> embryos do not exhibit any digit specification abnormalities (Figure 3.3C,I) (Allen et al., 2011; Cole and Krauss, 2003). These data are consistent with the notion that *Gas1* is the primary co-receptor contributor to HH signaling in the limb bud, while *Cdon* and *Boc* appear to play smaller roles, if at all. However, the deletion of *Boc* in a *Gas1* null

background enhances the severity of the phenotypes observed in *Gas1*<sup>-/-</sup> embryos, resulting in the formation of digits 1 and 5, along with an unidentified digit that could be a fusion of digits 3 and 4 (Figure 3.3D,J) (Allen et al., 2011). In contrast, the deletion of *Cdon* in a *Gas1* background does not enhance the digit specification defects, instead phenocopying *Gas1*<sup>-/-</sup> embryos (Figure 3.3E,K) (Allen et al., 2011). Further, *Cdon*<sup>-/-</sup>;*Boc*<sup>-/-</sup> embryos display overtly normal digit specification in both forelimbs and hindlimbs (Figure 3.3F,L ) (Allen et al., 2011). The lack of phenotypes observed at E18.5 in *Cdon* single mutants and lack of enhanced severity in *Cdon*;*Boc* and *Gas*;*Cdon* mutants, suggests that CDON does not play a role during digit specification. However, the reduction in *Gli1* expression in *Cdon* and *Gas1*;*Cdon* mutants, along with the clear contribution of *Boc* to digit specification in a *Gas1* null background, suggests a potential role for *Cdon* that could be masked by functional compensation by *Gas1* and/or *Boc*.

*Gas1*;*Cdon*;*Boc* triple mutants exhibit severe developmental defects such as cyclopia, heart looping defects and complete loss of ventral neural patterning (Allen et al., 2011). These striking developmental defects result in embryonic lethality at E9.5, which precludes the analysis of digit specification at later embryonic stages (Allen et al., 2011). To define the role of *Cdon* in SHH-dependent digit specification and to circumvent the embryonic lethality observed in *Gas1*;*Cdon*;*Boc* triple mutants, we utilized a novel floxed allele of *Cdon* (*Cdon*<sup>fl/fl</sup>) (Figure 3.4B). This allele was generated by (Bae et al., 2020), and is a targeted trap allele with a *lacZ* reporter-tagged insertion. In the presence of Cre, the *Cdon*<sup>fl/fl</sup> allele deletes exon 9, which truncates the CDON protein (Figure 3.4C). This allele has been previously crossed with two different Cre lines, *Pax7*<sup>CreERT2</sup> and *Meox2*-Cre, both of which resulted in efficient deletion of *Cdon* (Bae et al., 2020). To conditionally delete *Cdon* in the developing limb, we utilized the *Prx1*-Cre transgene (Logan et al., 2002). To define which cell types are labeled by the *Prx1*-Cre,

I examined *Prx1-Cre;tdTomato* embryos at E10.5 (Figure 3.5). At this stage, *Prx1-Cre* induces recombination in a variety of tissues including the midbrain, the heart and the limbs (Figure 3.5D,F,H), while no recombination is detected in the neural tube, another HH-responsive tissue (Figure 3.5J). Specifically, *Prx1-Cre* drives recombination through the forelimb and the hindlimb bud by E9.5 (Logan et al., 2002). The expression of *Prx1-Cre* is restricted to the lateral plate-derived mesoderm, which gives rise to the limb bones, tendons and muscle connective tissue (Figure 3.6 B,C,E) and is excluded from the forelimb bud epithelium (Figure 3.6B,D,E) (Logan et al., 2002). Furthermore, *Prx1-Cre* recombination is not detected in the HH-responsive paraxial mesoderm surrounding the neural tube (Figure 3.6G-I).

To investigate the combined contributions of *Gas1*, *Cdon* and *Boc* to limb development, I generated *Prx1-Cre;Gas1<sup>+/-</sup>;Cdon<sup>fl/fl</sup>;Boc<sup>-/-</sup>*, which display normal limb patterning (Figure 3.7E-F), and are viable and fertile. These data are consistent with a primary role for *Gas1* in HH-dependent digit specification. I then crossed *Prx1-Cre;Gas1<sup>+/-</sup>;Cdon<sup>fl/fl</sup>;Boc<sup>-/-</sup>* animals with *Gas1<sup>+/-</sup>;Cdon<sup>fl/fl</sup>;Boc<sup>-/-</sup>* mice to generate *Prx1-Cre;Gas1<sup>-/-</sup>;Cdon<sup>fl/fl</sup>;Boc<sup>-/-</sup>* embryos. At E18.5, the deletion of *Cdon* in a *Gas1;Boc* null background, results in severe limb patterning defects. Grossly, these mutants display a forelimb that resembles a bird wing or a small fish fin (Figure 3.7A), while the hindlimb resembles *Gas1;Boc* mutants hindlimbs (Figure 3.7B and Figure 3.3D,J). Skeletal preparation from these mutants reveal variable phenotypes in the digit specification in the forelimbs. Specifically, these mutants display digit 1 and another digit with unidentifiable identity (Figure 3.7C). In some cases, I observe digit 1 and 5, and a middle digit with unknown identity (Figure 3.7C inset); which we also observe in the hindlimb (Figure 3.7D). Notably, even in mutants where we detect a similar number of digits as observed in *Gas1;Boc* mutants, the long bone morphology is dramatically different. Along these lines, *Prx1-Cre;Gas1<sup>-/-</sup>*

; *Cdon*<sup>fl/fl</sup>; *Boc*<sup>-/-</sup> embryos exhibit severe patterning defects and bone shortening in the radius, ulna, tibia and fibula of both forelimb and hindlimb (Figure 3.7C,D); a severe phenotype that is not observed in any previously published single or compound HH co-receptor mutant. Notably, these mutants also display severe patterning defects in the carpals, metacarpals, tarsal and metatarsal bones in both forelimb and hindlimbs (Figure 3.7C,D). Overall these data demonstrate that *Cdon* does play a role in limb patterning and digit specification. However, further experiments will be required to elucidate the mechanism by which it regulates HH signaling during digit specification and long bone patterning.

### 3.4 Discussion

In this study I defined a novel role for *Cdon* in SHH-dependent digit specification and limb patterning. *Cdon* is expressed in the E10.5 forelimb bud, where it is primarily confined to a more anterior and proximal domain of mesenchyme compared to the other HH co-receptors, *Gas1* and *Boc*. Limb-specific deletion of *Cdon* with *Prx1-Cre* in a *Gas1*; *Boc* null background results in severe digit specification defects and shortening and patterning defects in the radius, ulna, tibia and fibula. Notably, these phenotypes arise only in the absence of *Gas1* and *Boc*, suggesting that these proteins share redundant functions. Taken together, these data demonstrate that *Cdon* plays a role in the promotion of SHH signal transduction during digit specification and limb patterning. In addition to their role in digit specification, I have also identified a new role for the HH co-receptors in the development of the radius, ulna, tibia and fibula.



### 3.4.1 Novel role for CDON during digit specification and limb development

During vertebrate embryogenesis *Cdon* regulates a variety of HH-dependent processes including, the patterning of the craniofacial structures and the ventral neural tube (Allen et al., 2011; Cole and Krauss, 2003; Zhang et al., 2011; Zhang et al., 2006). The lack of limb patterning and digit specification defects in *Cdon* mutants suggested that this co-receptor was not required for SHH-dependent digit specification (Allen et al., 2011; Cole and Krauss, 2003). However, these data are also consistent with a redundant function of CDON, along with the other HH co-receptors, GAS1 and BOC, which play redundant roles in certain tissues, such as in the mouse neural tube and in the developing cerebellum (Izzi et al., 2011) (Allen et al., 2011). Here I provide evidence that *Cdon* has a role in digit specification and limb development, as demonstrated by the limb-specific deletion of *Cdon* in a *Gas1;Boc* null background. Compared to *Gas1;Boc* mutants, which display the most severe limb phenotype of the different double co-receptor mutants (cf. *Gas1;Cdon* and *Cdon;Boc* mutants), the *Prx1-Cre;Gas<sup>-/-</sup>;Cdon<sup>fl/fl</sup>;Boc<sup>-/-</sup>* embryos exhibit an even more severe digit specification defect, although with incomplete penetrance, and restricted to the forelimb. Interestingly, the morphology of the remaining digits and limb bones in *Prx1-Cre;Gas<sup>-/-</sup>;Cdon<sup>fl/fl</sup>;Boc<sup>-/-</sup>* is different from *Gas1<sup>-/-</sup>;Boc<sup>-/-</sup>* mutants, even when they have the same number of digits. Specifically, the digits in *Prx1-Cre;Gas<sup>-/-</sup>;Cdon<sup>fl/fl</sup>;Boc<sup>-/-</sup>* look like uninterrupted cartilaginous elements, lacking the joints between the phalanges. This characteristic phenotype has also been reported in *Indian Hedgehog (Ihh)* mutants, which regulates joint formation (Koyama et al., 2007).

To properly interpret these results, it will be imperative to validate the efficiency of the deletion of *Cdon* by qPCR and western blot. Additionally, examining the levels of *Gli1* and other

transcriptional targets associated with digit specification in the developing limb buds of *Prx1-Cre;Gas<sup>-/-</sup>;Cdon<sup>fl/fl</sup>;Boc<sup>-/-</sup>* embryos. To further define the role of *Cdon* in limb patterning it will be useful to investigate the consequences of *Cdon* deletion on proliferation and apoptosis, which are both regulated by SHH (Bastida et al., 2004; Zhu et al., 2008). The patterning defects in the radius, ulna, tibia and fibula of *Prx1-Cre;Gas<sup>-/-</sup>;Cdon<sup>fl/fl</sup>;Boc<sup>-/-</sup>* mutants, revealed a novel role for *Gas1*, *Cdon* and *Boc* in the patterning of long bones. Since this severe phenotype is not observed in any of the double mutants, these data suggested that the HH co-receptor play redundant roles during the development of the long bones of the limb. Interestingly, long bone defects are also observed in *Ihh* mutants (St-Jacques et al., 1999). *Ihh* is critical for proper skeleton development, where it regulates proliferation and differentiation of chondrocytes and long bone formation (Amano et al., 2015; St-Jacques et al., 1999). Although the interactions of *Cdon* and *Ihh* are currently unexplored, based on the defects observed in *Prx1-Cre;Gas<sup>-/-</sup>;Cdon<sup>fl/fl</sup>;Boc<sup>-/-</sup>* it will be essential to define their interactions during limb development. The characteristic restriction of *Cdon* expression to the proximal limb bud in comparison to *Gas1* and *Boc* suggests a more limited function in the developing limb; which can be compensated by the broad expression and function of *Gas1* and *Boc*. Overall, these data demonstrate novel roles for *Cdon* in both SHH-dependent digit specification and IHH-dependent long bone growth.

#### 3.4.2 Forelimb and hindlimb phenotypic differences

The differences observed in digit specification of forelimbs and hindlimbs of *Prx1-Cre;Gas<sup>-/-</sup>;Cdon<sup>fl/fl</sup>;Boc<sup>-/-</sup>* embryos could have multiple explanations. One technical explanation is that to achieve limb-specific deletion of *Cdon* we utilized the *Prx1-Cre* transgene, which exhibits mosaic recombination in the hindlimb at E9.5 (Logan et al., 2002). This could result in

variability in the timing of recombination, altering the levels of *Cdon* and subsequently impacting the levels of HH signaling in the developing hindlimb. Alternatively, this could also be explained by differences in the recombination efficiency of the *Prx1-Cre* allele. However, despite the differences observed in the digit specification defects in the forelimbs and hindlimbs of the *Prx1-Cre;Gas1<sup>-/-</sup>;Cdon<sup>fl/fl</sup>;Boc<sup>-/-</sup>* embryos, we consistently observe defects in the patterning of the radius, ulna, tibia and fibula. These phenotypes suggest that *Prx1-Cre* mediates similar recombination efficiency in both forelimb and hindlimb. Interestingly, (Amano et al., 2015) utilized the *Prx1-Cre* transgene to perform the conditional deletion of *Ihh*, which resulted in the same phenotype in both forelimb and hindlimb, and it was similar to *Ihh* germline mutants. (St-Jacques et al., 1999). These data suggest the possibility that *Cdon* could differentially regulate digit specification in the hindlimb. This could be achieved by functioning independently of HH signaling or by the function of additional HH co-receptors that function to promote HH signaling in the hindlimb. Another possibility is that *Cdon* is differentially expressed between the forelimb and the hindlimb. Further analyses using different Cre drivers (*Hoxb6-CreER*; (Schughart et al., 1991)) and a careful characterization of *Cdon* expression in the developing limb will be essential to understand the differences between forelimb and hindlimb phenotypes.

### 3.4.3 Role of *Gas1*, *Cdon* and *Boc* in SHH-dependent digit specification

The mechanism by which SHH digit specification occurs in the developing limb is still unclear. Several studies have proposed multiple models which integrate SHH levels, time of exposure, cell survival and proliferation [reviewed by (Tickle, 2006)]. Even though the HH co-receptor mutants display digit specification and limb pattern defects the mechanisms by which they regulate HH signaling in this process are unknown. The differences in digit identity in the

HH co-receptor mutants suggest that GAS1, CDON and BOC could transduce different levels of HH signaling in the developing limb. Additionally, their subtle expression differences suggest different spatiotemporal functions that can explain their contribution to both the anterior-posterior and proximo-distal axis of the developing limb. Finally, another major question is whether the interaction of GAS1, CDON and BOC with PTCH1 leads to the formation of different individual complexes, which could mediate different cellular responses during limb development and vertebrate embryogenesis.

### 3.5 Materials and methods

#### Reagents

General reagents (Table 3.1) and primary antibodies for immunofluorescence (Table 3.2).

#### Animal Models

*Gas1<sup>lacZ</sup>* (Martinelli and Fan, 2007), *Cdon<sup>lacZ-1</sup>*, *Cdon<sup>lacZ-2</sup>* (Cole and Krauss, 2003), *Boc<sup>AP</sup>* (Zhang et al., 2011), *Cdon<sup>fl/fl</sup>* (Bae et al., 2020), *Prx1;Cre* (Logan et al., 2002), *tdTomato* (Madisen et al., 2010) mice have been all described previously. *Gas1*, *Cdon*, and *Boc* mice were maintained on a C57BL/6J background. *Cdon<sup>lacZ-1</sup>* mice (Cole and Krauss, 2003) were maintained on a mixed 129S4/SvJaeJ/C57BL/6 background for expression analysis.

*Prx1Cre;tdTomato* and *Prx1;Cre;Gas1<sup>+/-</sup>;Cdon<sup>fl/fl</sup>;Boc<sup>-/-</sup>* mice were maintained in a mixed background FVB/NJ/C57BL/6. For embryonic dissections, noon of the day on which a vaginal plug was detected was considered as E0.5. For precise staging, somites were counted during the dissection. Embryos with 34-38 somites were considered E10.5 embryos. All animal procedures

were reviewed and approved by the Institutional Animal Care and Use Committee (IACUC) at the University of Michigan.

#### X-gal staining

Embryos were dissected in 1X PBS, pH 7.4, and fixed (1% formaldehyde, 0.2% glutaraldehyde, 2mM MgCl<sub>2</sub>, 5mM EGTA, 0.02% NP-40) on ice for 10-60 minutes depending on the embryonic stage. Subsequently, the embryos were washed 3 x 5 minutes with 1X PBS, pH 7.4 + 0.02% NP-40 for permeabilization. B-Galactosidase activity was detected with X-Gal staining solution (5mM K<sub>3</sub>Fe(CN)<sub>6</sub>, 5mM K<sub>4</sub>Fe(CN)<sub>6</sub>, 2mM MgCl<sub>2</sub>, 0.01% Na deoxycholate, 0.02% NP-40, 1mg/mL X-gal). The signal was developed from 25 minutes to 24 hours at 37° C depending on the *lacZ* allele. After staining, the embryos were washed 3 x 5 minutes with 1X PBS, pH 7.4 at 4°C, and post-fixed in 4% paraformaldehyde for 20 minutes at room temperature, followed by 3 x 5 minute washes in 1X PBS, pH 7.4. Finally, embryos were stored and photographed in 1X PBS, pH 7.4 + 50% glycerol. X-gal staining of sections (20µm) was performed as described above for whole mount embryos. After staining, sections were washed 3 x 5 minutes with 1X PBS, pH 7.4, counterstained with nuclear fast red for 5 minutes and dehydrated in an ethanol series (70% ethanol, 95% ethanol, 100% ethanol and 100% Xylenes) followed by application of coverslips with permount mounting media.

#### Alkaline Phosphatase Staining

Embryos were dissected on 1X PBS, pH 7.4, and fixed (1% formaldehyde, 0.2% glutaraldehyde, 2mM MgCl<sub>2</sub>, 5mM EGTA, 0.02% NP-40) on ice for 10-60 minutes depending on the embryonic stage on ice. Subsequently, the embryos were washed 3 x 5 minutes with 1X PBS, pH 7.4. To

deactivate endogenous alkaline phosphatases, embryos were incubated in 1X PBS, pH 7.4 at 70°C for 30 minutes. Then the embryos were rinsed with 1X PBS, pH 7.4 and washed for 10 minutes in alkaline phosphatase buffer (100mM NaCl, 100mM Tris-HCl pH9.5, 50mM MgCl<sub>2</sub>, 1% Tween-20) at room temperature. Embryos were stained with BM purple from 2 to 3 hours at 37°C depending on the embryonic stage. After staining, the embryos were washed 3 x 5 minutes with 1X PBS, pH 7.4 at 4°C, and post-fixed in 4% paraformaldehyde for 20 minutes at room temperature, followed by 3 x 5 minute washes with 1X PBS, pH 7.4. Finally, embryos were stored and photographed in 1X PBS, pH 7.4 + 50% glycerol. Alkaline phosphatase staining of sections (20µm) was performed as described above for whole mount embryos. After staining, sections were washed 3 x 5 minutes with 1X PBS, pH7.4, counterstained with nuclear fast red for 5 minutes and dehydrated in an ethanol series (70% ethanol, 95% ethanol, 100% ethanol and 100% xylenes for five minutes each) followed by application of coverslips with permount mounting media.

#### Whole-Mount Digoxigenin *in situ* Hybridization

Whole-mount digoxigenin *in situ* hybridization was performed as previously described in (Allen et al., 2011; Wilkinson, 1992). In brief, embryos were dissected in 1X PBS, pH 7.4 and fixed in 4% paraformaldehyde overnight on a rocking platform. After fixation, embryos were dehydrated in a methanol/PBST (1X PBS, pH 7.4 + 0.1 % Tween) series (25% methanol, 50 %methanol, 75% methanol) and stored in 100% methanol at -20°C until the experiment was performed for up to 6 months. Embryos were digested with 10µg/mL proteinase K at RT for 2 minutes.

Hybridization was performed with the indicated digoxigenin probe with a concentration of 1ng/µL for 16-19 hours at 70°C. The embryos were incubated in alkaline phosphatase-

conjugated anti-DIG antibody at a dilution of 1:4,000. AP-anti-DIG was detected with BM purple, and signal was developed for 3.5 hours at room temperature. Embryos were cleared in 50% glycerol in 1XPBST and were photographed using a Nikon SMZ1500 microscope.

### Immunofluorescence

Section immunofluorescence was performed as in (Allen et al., 2011). Embryos were dissected in 1X PBS, pH 7.4 and fixed for 1 hour in 4% paraformaldehyde on ice, followed by 3 x 5 minutes washes with 1X PBS, pH 7.4 and cryoprotected for 24-48 hours in 1X PBS + 30% sucrose. Embryos were embedded in OCT compound and sectioned on a Leica cryostat (12  $\mu$ m thick forebrain and forelimb neural tube sections). Sections were blocked in blocking buffer (3% bovine serum albumin, 1% heat-inactivated sheep serum, 0.1% TritonX-100 in 1X PBS, pH 7.4) for 1 hour. Primary antibodies were diluted in blocking buffer incubated overnight at 4 °C in a humidified chamber. A list of all the primary antibodies used in this study is provided in (Table 3.2). Secondary antibodies were diluted in blocking solution and incubated for 1 hour at room temperature, followed by 3 x 5 minutes washes with 1X PBS, pH 7.4. All Alexa Fluor Dyes secondary antibodies were used at a 1:500 dilution. Nuclei were labeled with DAPI for 10 minutes at room temperature and slides were mounted with coverslips using Immu-mount aqueous mounting medium. Sections were visualized on a Leica upright SP5X confocal microscope.

### Skeletal Preparation

Skeletons were prepared as previously described before in (Allen et al., 2011). E18.5 embryos were skinned and eviscerated. Subsequently, embryos were fixed in 100% ethanol, followed by

100% acetone for 24 hours respectively at room temperature. Cartilage and bone were stained with alcian blue/alizarin red staining solution (5% alcian blue, 5% alizarin red, 5% glacial acetic acid and 70% ethanol) for 4 days at room temperature. The remaining tissue was digested with several washes of 1% potassium hydroxide. The skeletons were cleared by 24 hour washes of a gradient of glycerol (20%, 50%, and 80%) in 1% potassium hydroxide, and photographed in 80% glycerol.

### **3.6 Acknowledgments**

We thank all the current members of the Allen lab for discussions and experiment suggestions. In particular, we thank Nicole Franks and Savannah Strubble for technical assistance with genotyping and mouse colony maintenance. We also thank Dr. Robert Krauss (Icahn School of Medicine at Mount Sinai) and Dr. Enerstina Schipani (University of Michigan) for their generosity by providing the *Cdon* conditional and *Prx1-Cre* alleles, respectively. We also gratefully acknowledge the Department of Cell and Developmental Biology for providing access to research equipment. Finally, we acknowledge the Biomedical Research Core Facilities Microscopy Core for providing access to confocal microscopy equipment, which is supported by the Rogel Cancer Center.

### **3.7 Author contributions**

Conceptualization, M.L.E.A. and B.L.A.; Methodology, M.L.E.A. and B.L.A.; Validation, M.L.E.A. and B.L.A.; Formal Analysis, M.L.E.A.; Investigation, M.L.E.A. Resources, B.L.A.; Writing – Original Draft, M.L.E.A. and B.L.A.; Writing – Review & Editing, M.L.E.A. and



B.L.A.; Visualization, M.L.E.A. and B.L.A.; Supervision, B.L.A.; Project Administration, B.L.A.; Funding Acquisition, B.L.A.

### 3.8 Tables

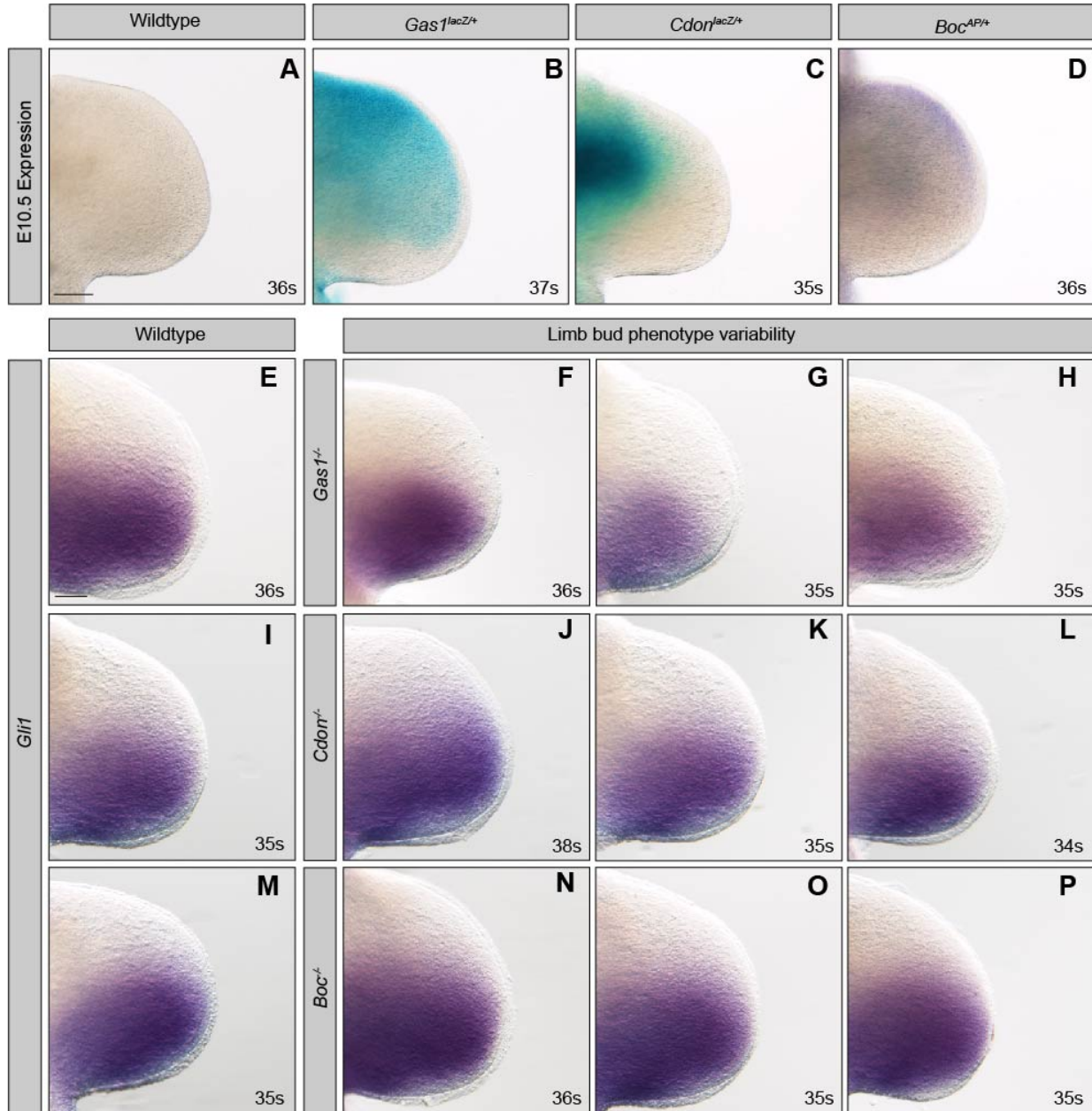
**Table 3.1 General reagents II**

Reagent	Vendor	Catalog number
Alcian blue	Millipore Sigma	A5268
Alizarin red	Millipore Sigma	A5533
Alexa Fluor Dyes	Thermo Fisher Scientific	A21428, A21131 and A21240
Anti-Digoxigenin-Ap, Fab fragments	Roche	11 093 274 910
BM purple	Roche	11442074001
BSA	Millipore Sigma	A7906
DAPI	Thermo Fisher Scientific	D1306
EGTA	Millipore Sigma	E3889
EDTA	Thermo Fisher Scientific	S311-500
Formaldehyde	VWR	EMD-FX0410-5
Formamide	Millipore Sigma	4650-500ML
Glacial Acetic Acid	Thermo Fisher Scientific	BP2401-500
Glutaraldehyde	Millipore Sigma	G5882
Glycerol	VWR	EMGX0185-5
Igepal (NP-40)	Millipore Sigma	I8896
Immu-mount	Thermo Fisher Scientific	9990412
K <sub>3</sub> Fe(CN) <sub>6</sub>	Millipore Sigma	PX1455
K <sub>4</sub> Fe(CN) <sub>6</sub>	Millipore Sigma	P9387
MgCl <sub>2</sub>	VWR	0288-500G
NaCl	Millipore Sigma	SX0420-3
Na deoxycholate	VWR	SX0480-2
OCT	Thermo Fisher Scientific	23730571
Paraformaldehyde	Thermo Fisher Scientific	50980489
Permount	Thermo Fisher Scientific	SP15100
Potassium hydroxide	VWR	PX1490-1
Proteinase K	Roche	03115836001
Sheep serum	Bioworld	30611168-1
Tris	VWR	JT4109-2
Triton X-100	VWR	9410
Tween-20	VWR	9480
X-gal	Goldbio	X4281C
Xylenes	VWR	XX00555

**Table 3.2 Primary antibodies used for immunofluorescence II**

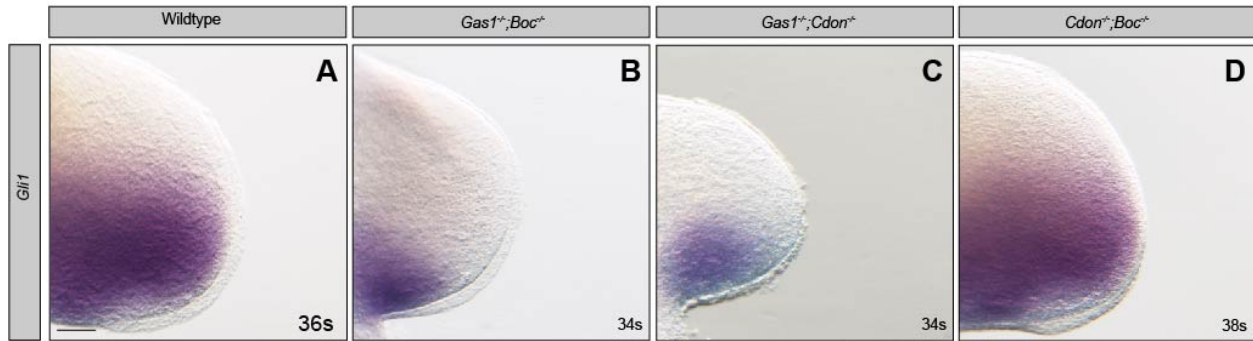
Antibody	Vendor	Catalog number	Dilution
PDGFR $\alpha$ (rabbit IgG)	Cell Signaling	3174S	1:100
E-CADHERIN (mouseIgG2a)	BD-biosciences	610181	1:500
TUJ-1 (mouse IgG1)	Promega	G7121	1:2,000

### 3.9 Figures



**Figure 3.1 Analysis of HH-coreceptor expression and function in the developing forelimb bud.**

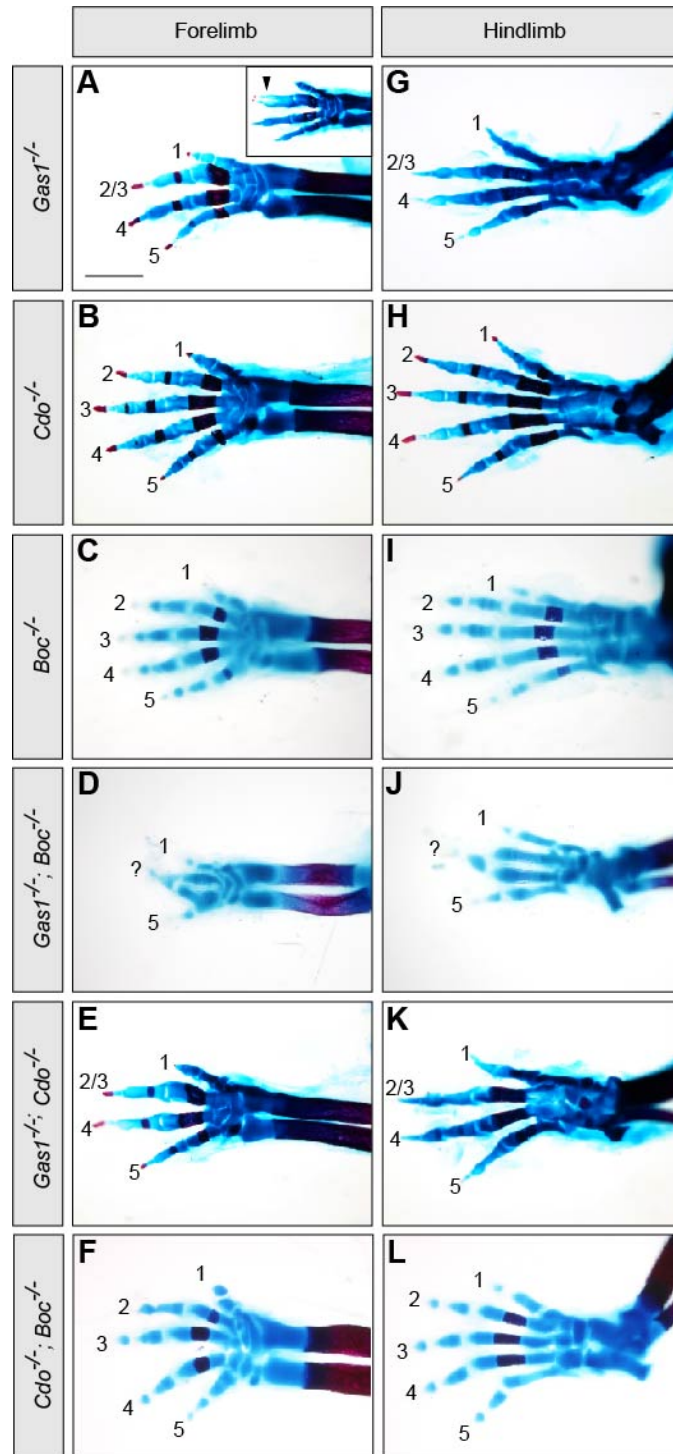
Whole mount X-Gal and Alkaline Phosphatase staining of E10.5 forelimb buds (A-D), wildtype (A), *Gas1<sup>lacZ/+</sup>* (B), *Cdon<sup>lacZ/+</sup>* (C), and *Boc<sup>AP/+</sup>* (D). Panel (A-D), was also shown in Supplemental Figure 2.1) *In situ* hybridization detection of *Gli1* expression in E10.5 forelimb buds (E-P). Dorsal views of E10.5 forelimb buds of wildtype (E,I,M), *Gas1<sup>-/-</sup>* (F-H), *Cdon<sup>-/-</sup>* (J-L), *Boc<sup>-/-</sup>* (N-P) embryos are shown. Somite number (s) is indicated in the lower right corner of each panel. Scale bars in A, 200µm and E, 100µm.



**Figure 3.2 *Gas1;Boc* and *Gas1;Cdon* but not *Cdon;Boc* mutant embryos exhibit significant reduction of *Gli1* in the developing forelimb bud.**

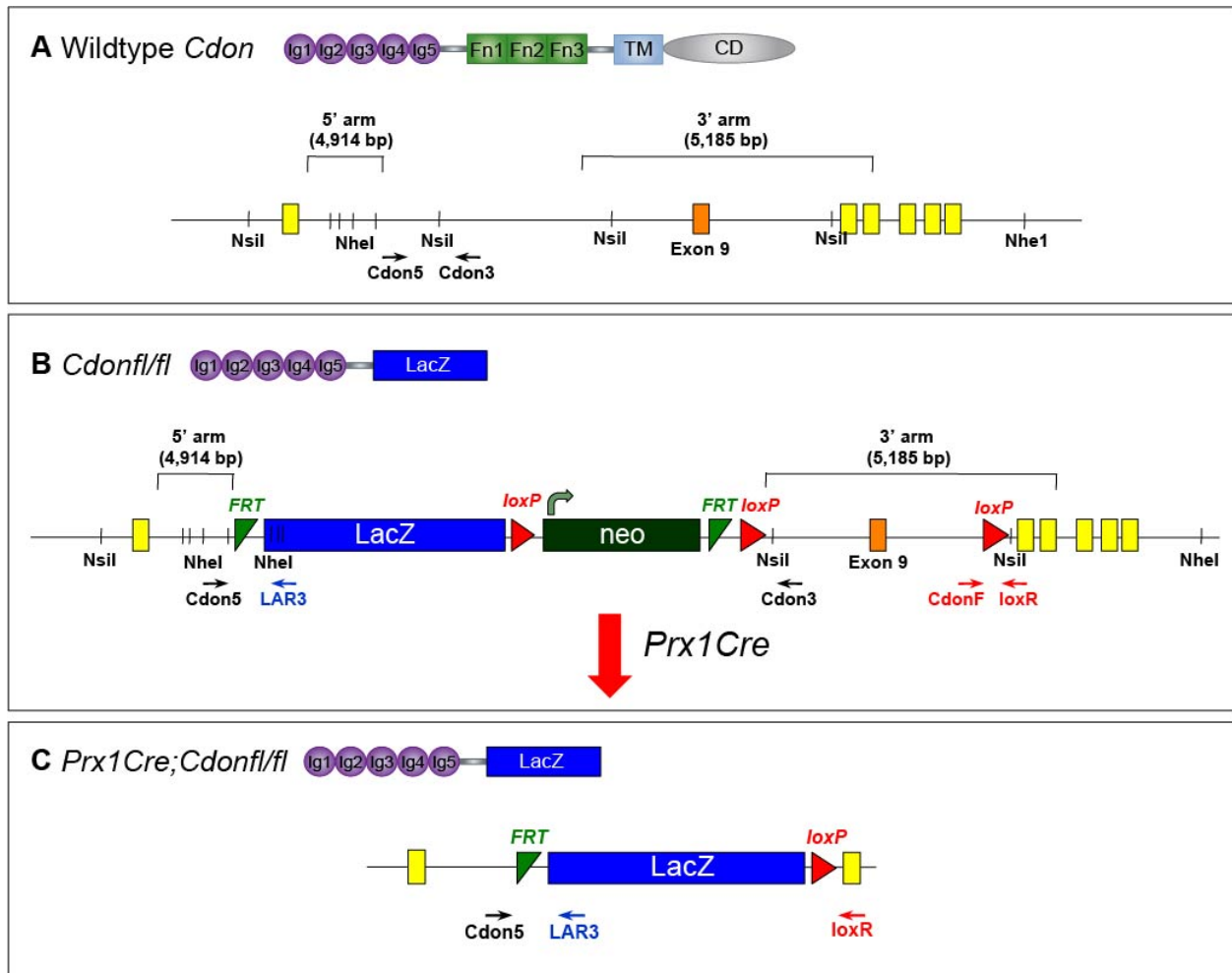
Analysis of collective co-receptor function in E10.5 forelimb buds.

*In situ* hybridization detection of *Gli1* expression in E10.5 forelimb buds (A-D). Dorsal views of E10.5 forelimb buds of wildtype (A; also showed in Figure 3.1) *Gas1<sup>-/-</sup>;Boc<sup>-/-</sup>* (B), *Gas1<sup>-/-</sup>;Cdon<sup>-/-</sup>* (C), *Cdon<sup>-/-</sup>;Boc<sup>-/-</sup>* (D) embryos are shown. Note that the levels of *Gli1* in *Cdon<sup>-/-</sup>;Boc<sup>-/-</sup>* embryos is not significantly reduced as in the other double HH co-receptor mutants. Somite number (s) is indicated in the lower right corner of each panel. Scale bar in A, 100µm.



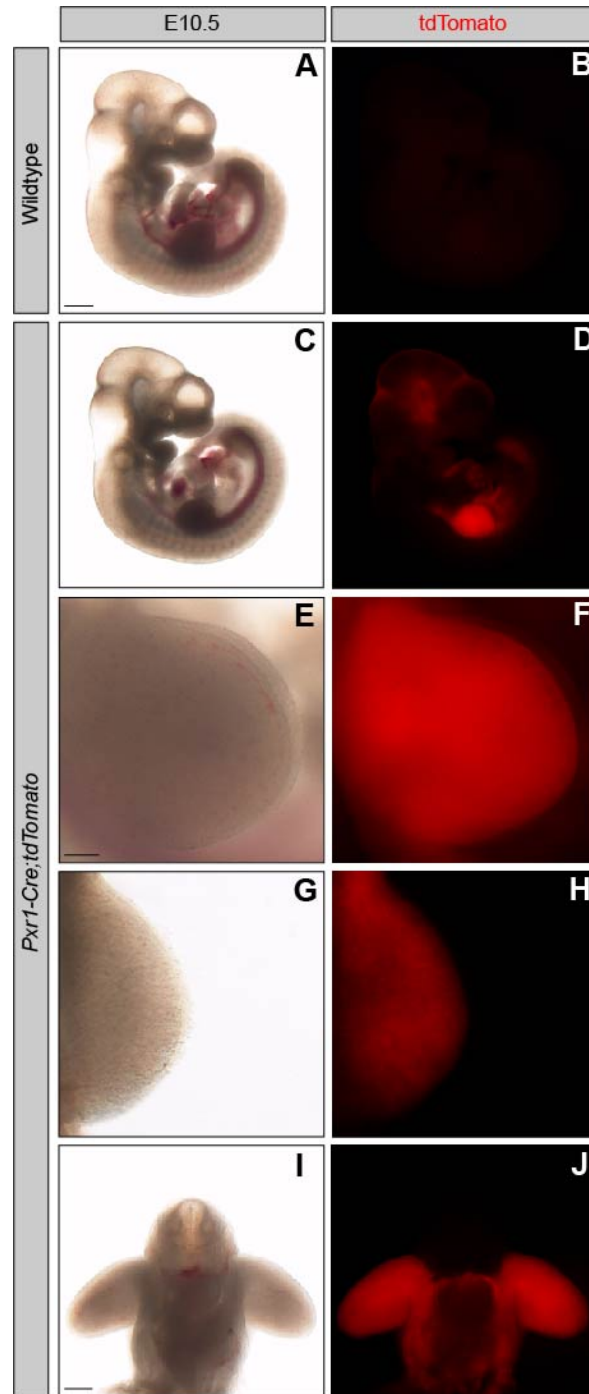
**Figure 3.3 Analysis of limb development in single and double HH co-receptors mutants.**

Forelimbs (A-F) and hindlimbs (G-L) of E18.5 embryos stained with alcian blue and alizarin red. *Gas1*<sup>-/-</sup> (A,G), *Cdo*<sup>-/-</sup> (B,H), *Boc*<sup>-/-</sup> (C,I), *Gas1*<sup>-/-</sup>; *Boc*<sup>-/-</sup> (D,J), *Gas1*<sup>-/-</sup>; *Cdo*<sup>-/-</sup> (E, K), *Cdo*<sup>-/-</sup>; *Boc*<sup>-/-</sup> (F, L). Numbers denote specific digits where 1 is the most anterior and 5 is the most posterior. Arrow denotes fusion and loss of digits 2 and 3 in *Gas1*<sup>-/-</sup> (A, G, inset in A), and *Gas1*<sup>-/-</sup>; *Cdo*<sup>-/-</sup> (E,K) forelimbs and hindlimbs. *Gas1*<sup>-/-</sup>; *Boc*<sup>-/-</sup> (D,J) mutants exhibit the most severe phenotype in the forelimbs and hindlimbs, where only digits 1 and 5 identifiable and the third digit is unidentifiable (denoted as ?). Note that *Cdo*<sup>-/-</sup>; *Boc*<sup>-/-</sup> (F,L) embryos display normal limb development. Scale bar in A, 1000  $\mu$ m. Reprinted with permission from (Allen et al., 2011).



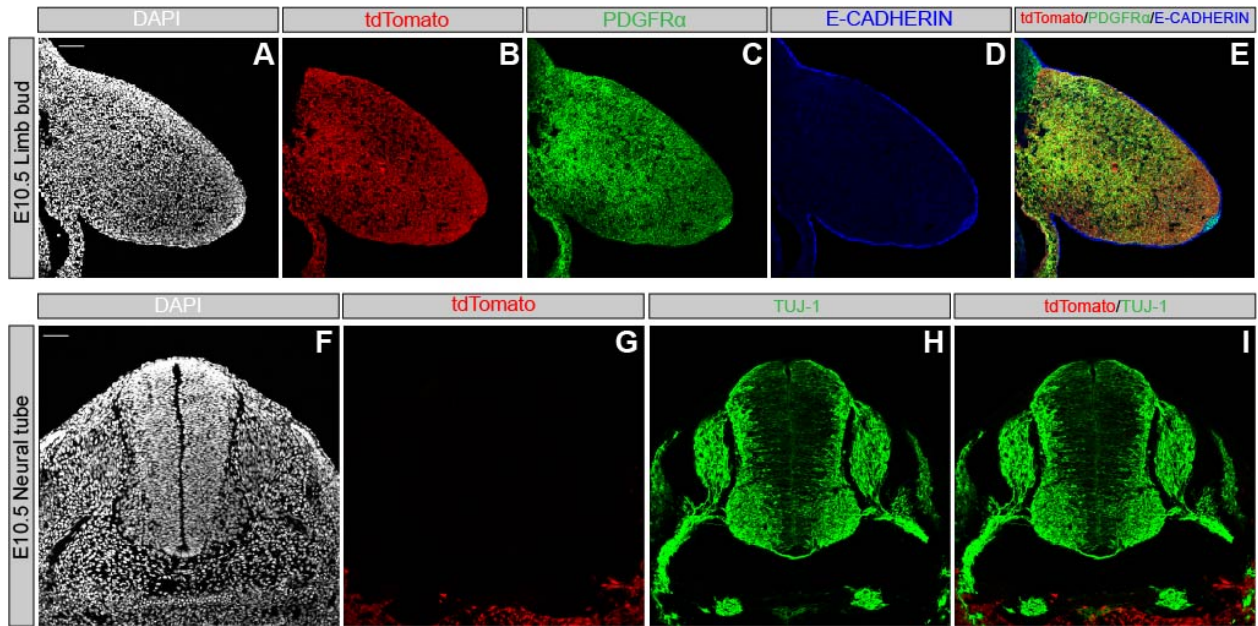
**Figure 3.4 Conditional *Cdon* knockout allele.**

Diagram of the *Cdon<sup>fl/fl</sup>* allele. The following shapes depict different structures, yellow boxes (exons), orange box (floxed exon 9), green triangles (flippase recognition target site; *FRT*), red triangles (*loxP* sites), blue box (*LacZ*), dark green box (neomycin cassette). Enzyme restriction sites are represented by black vertical lines. Arrows below the alleles denote primers for screening and genotyping. The predicted CDON protein is represented by its structure next to each allele. Wildtype *Cdon* allele (panel A), *Cdon<sup>fl/fl</sup>* allele (panel B; before Cre mediated recombination), *Prx1Cre; Cdon<sup>fl/fl</sup>* allele (panel C; after Cre mediated recombination). Schematic adapted and reprinted with permission from Robert S. Krauss and (Bae et al., 2020).



**Figure 3.5 *Prx1-Cre* recombination activity in E10.5 embryos.**

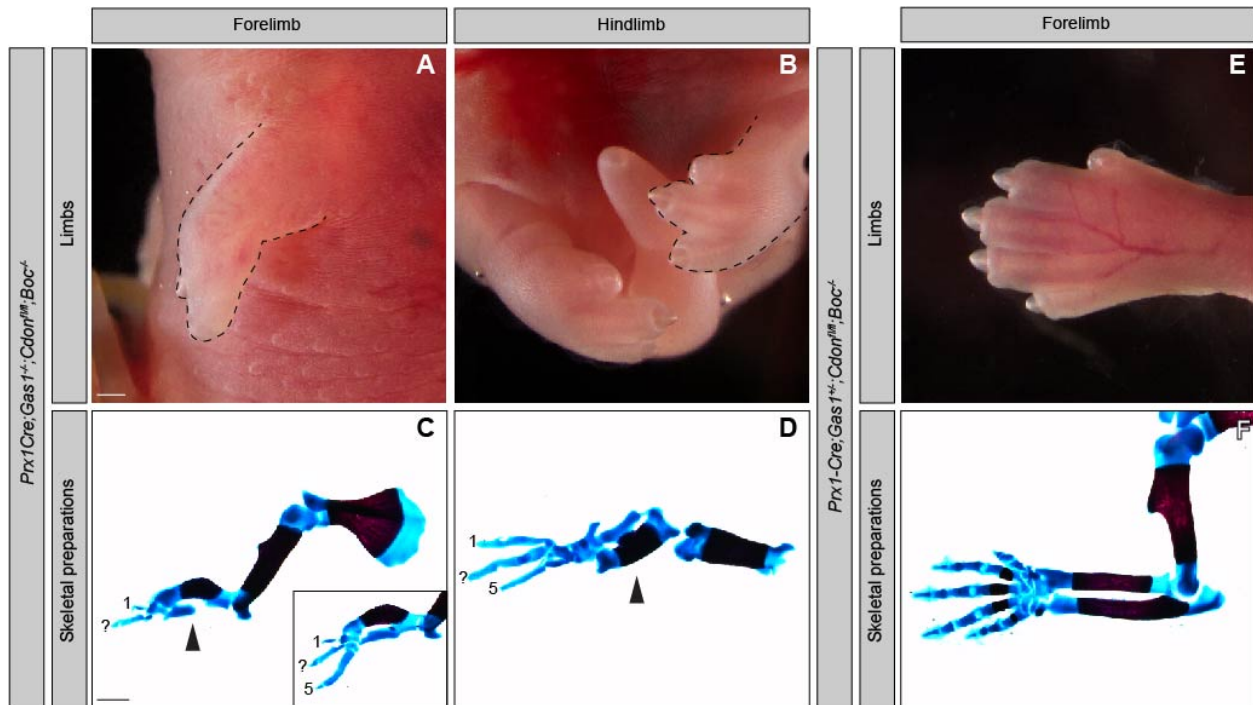
Whole-mount immunofluorescence visualization of Cre activity in E10.5 *Prx1-Cre;tdTomato* mouse embryos. Left panel, brightfield images of E10.5 wildtype (A) and *Prx1-Cre;tdTomato* (C, E, G, I) embryos. Right panel, *tdTomato* expression labeling Cre recombinase activity in 10.5 wildtype (B) and *Prx1-Cre;tdTomato* (D, F, H, J) embryos. Note the lack of *tdTomato* (indicating no Cre activity) expression in wildtype embryos (B), while in *Prx1-Cre;tdTomato* embryos *tdTomato* is expressed in multiple structures (indicating Cre activity) (D). Expression of *tdTomato* in the forelimb bud (F), hindlimb bud (H), neural tube (J; at the forelimb level). Scale bars in A-D, 500  $\mu$ m; E-H, 200  $\mu$ m and I-J, 250  $\mu$ m.



**Figure 3.6 Tissue-specific expression of Cre recombinase in the developing forelimb bud and spinal cord of *Prx1-Cre;tdTomato* E10.5 embryos.**

Co-expression of Cre activity by visualization of *tdTomato* and tissue-specific markers including, PDGFR $\alpha$  (mesenchyme), E-CADHERIN (epithelium), and TUJ-1 (neurons) in E10.5 *Prx1-Cre;tdTomato* embryos. Antibody detection of PDGFR $\alpha$  (green; C, E), E-CADHERIN (blue; D, E) and TUJ-1 (green; H, I). Scale bars in A-I, 50  $\mu$ m.





**Figure 3.7 Digit specification and long bone defects in E18.5 *Prx1-Cre; Gas1<sup>-/-</sup>; Cdon<sup>fl/fl</sup>; Boc<sup>-/-</sup>*.**

Analysis of forelimb and hindlimb patterning in E18.5 embryos stained with alcian blue and alizarin red. Brightfield images of forelimb (A) and hindlimb (B) of E18.5 *Prx1-Cre; Gas1<sup>-/-</sup>; Cdon<sup>fl/fl</sup>; Boc<sup>-/-</sup>* and forelimb (E) of *Prx1-Cre; Gas1<sup>+/-</sup>; Cdon<sup>fl/fl</sup>; Boc<sup>-/-</sup>*. Skeletal preparations of forelimbs (C) and hindlimbs (D) of *Prx1-Cre; Gas1<sup>-/-</sup>; Cdon<sup>fl/fl</sup>; Boc<sup>-/-</sup>* and forelimb (F) of *Prx1-Cre; Gas1<sup>+/-</sup>; Cdon<sup>fl/fl</sup>; Boc<sup>-/-</sup>*. Note the severe defects in digit specification in the forelimb and hindlimbs of *Prx1-Cre; Gas1<sup>-/-</sup>; Cdon<sup>fl/fl</sup>; Boc<sup>-/-</sup>*, where digit 1 and 5 are specified (inset in C) and the rest of the digits are fused or absent in both limbs (denoted with a ?). In more severe *Prx1-Cre; Gas1<sup>-/-</sup>; Cdon<sup>fl/fl</sup>; Boc<sup>-/-</sup>* forelimbs only digit 1 and an unidentifiable digit forms (denoted with a ?). Black arrowhead denotes severe defects in the radius and ulna of the *Prx1-Cre; Gas1<sup>-/-</sup>; Cdon<sup>fl/fl</sup>; Boc<sup>-/-</sup>*. Note that *Prx1-Cre; Gas1<sup>+/-</sup>; Cdon<sup>fl/fl</sup>; Boc<sup>-/-</sup>* embryos display normal digit specification and limb patterning (E-F). Scale bars in A-F, 1000  $\mu$ m.

### 3.10 References

- Allen, B. L., Song, J. Y., Izzi, L., Althaus, I. W., Kang, J. S., Charron, F., Krauss, R. S. and McMahon, A. P.** (2011). Overlapping roles and collective requirement for the coreceptors GAS1, CDO, and BOC in SHH pathway function. *Dev Cell* **20**, 775-787.
- Allen, B. L., Tenzen, T. and McMahon, A. P.** (2007). The Hedgehog-binding proteins Gas1 and Cdo cooperate to positively regulate Shh signaling during mouse development. *Genes Dev* **21**, 1244-1257.
- Amano, K., Densmore, M. J. and Lanske, B.** (2015). Conditional Deletion of Indian Hedgehog in Limb Mesenchyme Results in Complete Loss of Growth Plate Formation but Allows Mature Osteoblast Differentiation. *J Bone Miner Res* **30**, 2262-2272.
- Bae, G. U., Domene, S., Roessler, E., Schachter, K., Kang, J. S., Muenke, M. and Krauss, R. S.** (2011). Mutations in CDON, encoding a hedgehog receptor, result in holoprosencephaly and defective interactions with other hedgehog receptors. *Am J Hum Genet* **89**, 231-240.
- Bae, J. H., Hong, M., Jeong, H. J., Kim, H., Lee, S. J., Ryu, D., Bae, G. U., Cho, S. C., Lee, Y. S., Krauss, R. S., et al.** (2020). Satellite cell-specific ablation of Cdon impairs integrin activation, FGF signalling, and muscle regeneration. *J Cachexia Sarcopenia Muscle*.
- Bastida, M. F., Delgado, M. D., Wang, B., Fallon, J. F., Fernandez-Teran, M. and Ros, M. A.** (2004). Levels of Gli3 repressor correlate with Bmp4 expression and apoptosis during limb development. *Dev Dyn* **231**, 148-160.
- Beachy, P. A., Hymowitz, S. G., Lazarus, R. A., Leahy, D. J. and Siebold, C.** (2010). Interactions between Hedgehog proteins and their binding partners come into view. *Genes Dev* **24**, 2001-2012.
- Briscoe, J. and Therond, P. P.** (2013). The mechanisms of Hedgehog signalling and its roles in development and disease. *Nat Rev Mol Cell Biol* **14**, 416-429.
- Cabrera, J. R., Sanchez-Pulido, L., Rojas, A. M., Valencia, A., Manes, S., Naranjo, J. R. and Mellstrom, B.** (2006). Gas1 is related to the glial cell-derived neurotrophic factor family receptors alpha and regulates Ret signaling. *J Biol Chem* **281**, 14330-14339.
- Chiang, C., Litingtung, Y., Lee, E., Young, K. E., Corden, J. L., Westphal, H. and Beachy, P. A.** (1996). Cyclopia and defective axial patterning in mice lacking Sonic hedgehog gene function. *Nature* **383**, 407-413.
- Cole, F. and Krauss, R. S.** (2003). Microform holoprosencephaly in mice that lack the Ig superfamily member Cdon. *Curr Biol* **13**, 411-415.
- Dai, P., Akimaru, H., Tanaka, Y., Maekawa, T., Nakafuku, M. and Ishii, S.** (1999). Sonic Hedgehog-induced activation of the Gli1 promoter is mediated by GLI3. *J Biol Chem* **274**, 8143-8152.

**Echelard, Y., Epstein, D. J., St-Jacques, B., Shen, L., Mohler, J., McMahon, J. A. and McMahon, A. P.** (1993). Sonic hedgehog, a member of a family of putative signaling molecules, is implicated in the regulation of CNS polarity. *Cell* **75**, 1417-1430.

**Harfe, B. D., Scherz, P. J., Nissim, S., Tian, H., McMahon, A. P. and Tabin, C. J.** (2004). Evidence for an expansion-based temporal Shh gradient in specifying vertebrate digit identities. *Cell* **118**, 517-528.

**Hui, C. C. and Angers, S.** (2011). Gli proteins in development and disease. *Annu Rev Cell Dev Biol* **27**, 513-537.

**Izzi, L., Levesque, M., Morin, S., Laniel, D., Wilkes, B. C., Mille, F., Krauss, R. S., McMahon, A. P., Allen, B. L. and Charron, F.** (2011). Boc and Gas1 each form distinct Shh receptor complexes with Ptch1 and are required for Shh-mediated cell proliferation. *Dev Cell* **20**, 788-801.

**Kang, J. S., Mulieri, P. J., Hu, Y., Taliana, L. and Krauss, R. S.** (2002). BOC, an Ig superfamily member, associates with CDO to positively regulate myogenic differentiation. *EMBO J* **21**, 114-124.

**Koyama, E., Ochiai, T., Rountree, R. B., Kingsley, D. M., Enomoto-Iwamoto, M., Iwamoto, M. and Pacifici, M.** (2007). Synovial joint formation during mouse limb skeletogenesis: roles of Indian hedgehog signaling. *Ann N Y Acad Sci* **1116**, 100-112.

**Lee, C. S. and Fan, C. M.** (2001). Embryonic expression patterns of the mouse and chick Gas1 genes. *Mech Dev* **101**, 293-297.

**Logan, M., Martin, J. F., Nagy, A., Lobe, C., Olson, E. N. and Tabin, C. J.** (2002). Expression of Cre Recombinase in the developing mouse limb bud driven by a Prxl enhancer. *Genesis* **33**, 77-80.

**Lum, L., Yao, S., Mozer, B., Rovescalli, A., Von Kessler, D., Nirenberg, M. and Beachy, P. A.** (2003). Identification of Hedgehog pathway components by RNAi in Drosophila cultured cells. *Science* **299**, 2039-2045.

**Madisen, L., Zwingman, T. A., Sunkin, S. M., Oh, S. W., Zariwala, H. A., Gu, H., Ng, L. L., Palmiter, R. D., Hawrylycz, M. J., Jones, A. R., et al.** (2010). A robust and high-throughput Cre reporting and characterization system for the whole mouse brain. *Nat Neurosci* **13**, 133-140.

**Marigo, V., Davey, R. A., Zuo, Y., Cunningham, J. M. and Tabin, C. J.** (1996). Biochemical evidence that patched is the Hedgehog receptor. *Nature* **384**, 176-179.

**Martinelli, D. C. and Fan, C. M.** (2007). Gas1 extends the range of Hedgehog action by facilitating its signaling. *Genes Dev* **21**, 1231-1243.

**McLellan, J. S., Zheng, X., Hauk, G., Ghirlando, R., Beachy, P. A. and Leahy, D. J.** (2008). The mode of Hedgehog binding to Ihog homologues is not conserved across different phyla. *Nature* **455**, 979-983.

- McMahon, A. P., Ingham, P. W. and Tabin, C. J.** (2003). Developmental roles and clinical significance of hedgehog signaling. *Curr Top Dev Biol* **53**, 1-114.
- Mulieri, P. J., Kang, J. S., Sassoon, D. A. and Krauss, R. S.** (2002). Expression of the boc gene during murine embryogenesis. *Dev Dyn* **223**, 379-388.
- Mulieri, P. J., Okada, A., Sassoon, D. A., McConnell, S. K. and Krauss, R. S.** (2000). Developmental expression pattern of the cdo gene. *Dev Dyn* **219**, 40-49.
- Murdoch, J. N. and Copp, A. J.** (2010). The relationship between sonic Hedgehog signaling, cilia, and neural tube defects. *Birth Defects Res A Clin Mol Teratol* **88**, 633-652.
- Riddle, R. D., Johnson, R. L., Laufer, E. and Tabin, C.** (1993). Sonic hedgehog mediates the polarizing activity of the ZPA. *Cell* **75**, 1401-1416.
- Roessler, E., Belloni, E., Gaudenz, K., Jay, P., Berta, P., Scherer, S. W., Tsui, L. C. and Muenke, M.** (1996). Mutations in the human Sonic Hedgehog gene cause holoprosencephaly. *Nat Genet* **14**, 357-360.
- Saunders, J. W., Jr. and M. T. Gasseling** (1968). *Ectodermal-mesodermal interactions in the origin of limb symmetry*. Baltimore: Williams & Wilkins.
- Schughart, K., Bieberich, C. J., Eid, R. and Ruddle, F. H.** (1991). A regulatory region from the mouse Hox-2.2 promoter directs gene expression into developing limbs. *Development* **112**, 807-811.
- Seppala, M., Depew, M. J., Martinelli, D. C., Fan, C. M., Sharpe, P. T. and Cobourne, M. T.** (2007). Gas1 is a modifier for holoprosencephaly and genetically interacts with sonic hedgehog. *J Clin Invest* **117**, 1575-1584.
- Seppala, M., Xavier, G. M., Fan, C. M. and Cobourne, M. T.** (2014). Boc modifies the spectrum of holoprosencephaly in the absence of Gas1 function. *Biol Open* **3**, 728-740.
- St-Jacques, B., Hammerschmidt, M. and McMahon, A. P.** (1999). Indian hedgehog signaling regulates proliferation and differentiation of chondrocytes and is essential for bone formation. *Genes Dev* **13**, 2072-2086.
- te Welscher, P., Zuniga, A., Kuijper, S., Drenth, T., Goedemans, H. J., Meijlink, F. and Zeller, R.** (2002). Progression of Vertebrate Limb Development Through SHH-Mediated Counteraction of GLI3. *Science* **298**, 827-830.
- Teglund, S. and Toftgard, R.** (2010). Hedgehog beyond medulloblastoma and basal cell carcinoma. *Biochim Biophys Acta* **1805**, 181-208.
- Tenzen, T., Allen, B. L., Cole, F., Kang, J. S., Krauss, R. S. and McMahon, A. P.** (2006). The cell surface membrane proteins Cdo and Boc are components and targets of the Hedgehog signaling pathway and feedback network in mice. *Dev Cell* **10**, 647-656.

**Tickle, C.** (2006). Making digit patterns in the vertebrate limb. *Nat Rev Mol Cell Biol* **7**, 45-53.

**Vortkamp, A., Franz, T., Gessler, M. and Grzeschik, K. H.** (1992). Deletion of GLI3 supports the homology of the human Greig cephalopolysyndactyly syndrome (GCPS) and the mouse mutant extra toes (Xt). *Mamm Genome* **3**, 461-463.

**Vortkamp, A., Gessler, M. and Grzeschik, K. H.** (1991). GLI3 zinc-finger gene interrupted by translocations in Greig syndrome families. *Nature* **352**, 539-540.

**Wang, B., Fallon, J. F. and Beachy, P. A.** (2000). Hedgehog-regulated processing of Gli3 produces an anterior/posterior repressor gradient in the developing vertebrate limb. *Cell* **100**, 423-434.

**Wilkinson, D. G.** (1992). *In situ hybridization : a practical approach*. Oxford ; New York: IRL Press at Oxford University Press.

**Yao, S., Lum, L. and Beachy, P.** (2006). The ihog cell-surface proteins bind Hedgehog and mediate pathway activation. *Cell* **125**, 343-357.

**Zhang, W., Hong, M., Bae, G. U., Kang, J. S. and Krauss, R. S.** (2011). Boc modifies the holoprosencephaly spectrum of Cdo mutant mice. *Dis Model Mech* **4**, 368-380.

**Zhang, W., Kang, J. S., Cole, F., Yi, M. J. and Krauss, R. S.** (2006). Cdo functions at multiple points in the Sonic Hedgehog pathway, and Cdo-deficient mice accurately model human holoprosencephaly. *Dev Cell* **10**, 657-665.

**Zhu, J., Nakamura, E., Nguyen, M. T., Bao, X., Akiyama, H. and Mackem, S.** (2008). Uncoupling Sonic hedgehog control of pattern and expansion of the developing limb bud. *Dev Cell* **14**, 624-632.

## Chapter 4 Discussion and Future Directions

### 4.1 Summary of findings

The focus of this thesis is the investigation of novel tissue-specific roles for GAS1, CDON and BOC during vertebrate embryogenesis. These HH co-receptors bind to HH ligands, interact with PTCH1 and display similar expression patterns (Bae et al., 2011; Izzi et al., 2011; Lee et al., 2001; Lee and Fan, 2001; Mulieri et al., 2002; Mulieri et al., 2000; Tenzen et al., 2006). Further, their combined deletion results in a complete loss of HH signaling, leading to a model where these proteins play essential, but redundant roles as positive regulators of the HH signaling pathway (Allen et al., 2011; Allen et al., 2007; Cole and Krauss, 2003; Seppala et al., 2007; Seppala et al., 2014; Zhang et al., 2011). However, in certain tissues these proteins can function to restrain HH pathway function (Bergeron et al., 2011; Cardozo et al., 2014; Cobourne et al., 2004; Ohazama et al., 2009). The ability of these HH co-receptors to alternately promote or antagonize HH signaling in a tissue-specific manner has been understudied (Figure 4.1). My work provides an extensive characterization of single and compound HH co-receptor mutants across multiple tissues; uncovering novel roles. Specifically, my analyses revealed a novel antagonistic role for *Boc* during craniofacial development (Chapter Two) and a novel positive role for *Cdon* in limb development (Chapter Three).

A particularly exciting result was the discovery that *Boc* differentially regulates HH signaling during craniofacial development. Previous studies concluded that *Boc*<sup>-/-</sup> embryos did not display any HPE phenotypes, but its deletion in a *Gas1* or *Cdon* null background enhanced the severity of the HPE defects (Seppala et al., 2014; Zhang et al., 2011). However, in mouse models the severity of the craniofacial defects depends on the genetic background of the mouse model (Hong and Krauss, 2018). Generally, in a mixed (129/Sv/CD-1/C57Bl/6J) background the craniofacial defects associated to HPE are mild, while in C57Bl/6J background the phenotypes are extremely severe (Hong and Krauss, 2018). The differences in the severity of the craniofacial defects is attributed to silent modifier genes in each genetic background (Hong and Krauss, 2018). Mutations in silent modifier genes do not produce craniofacial defects but can alter the phenotype of another mutation that exhibit a phenotype (Hong and Krauss, 2018). One of the major caveats of some of the previous studies was their lack of control of the genetic background of the HH co-receptor mouse models (Seppala et al., 2014). My research addressed this caveat by examining all the HH co-receptor mutants on a congenic C57BL/6J background. In addition, I performed an extensive examination of HH transcriptional targets within the craniofacial structures and in other HH-responsive tissues to establish tissue-specific differences. Surprisingly, loss of *Boc* in a C57BL/6J resulted in internasal distance widening, increased levels of *Gli1* in the nasal processes, and increased proliferation in the cranial neural crest-derived mesenchyme. Other HH-responsive tissues such as the limbs and the ventral neural tube had normal levels of HH transcriptional targets. In contrast, the deletion of *Gas1* and *Cdon* results in severe HPE defects and decreased *Gli1* transcript. These data suggest that *Boc* works in opposition to *Gas1* and *Cdon* in the craniofacial structures by antagonizing HH signaling. Moreover, I also demonstrated that deletion of *Boc* in a *Gas1* null background ameliorates the

craniofacial defects observed in *Gas1* single mutants. Interestingly, the rescue of the craniofacial defects in *Gas1;Boc* mutants is restricted to certain craniofacial structures, including the nostrils, nasal bone and snout, further confirming that *Boc* functions in a tissue-specific manner. Thus, these data demonstrate that *Boc* functions as a tissue-specific antagonist of HH signaling during craniofacial development and opens a series of mechanistic questions about how it interacts with SHH ligand to regulate HH signaling.

My thesis research also revealed a novel role for *Cdon* during limb development. Interestingly, previous studies determined that *Gas1* and *Boc*, but not *Cdon* had a role in digit specification during limb patterning (Cole and Krauss, 2003). This conclusion was based in the lack of phenotypes in *Cdon* mutants and its inability to enhance the severity of the limb defects in a *Gas1* or *Cdon* null background. However, in some tissues these co-receptors are functionally redundant. To define a role for *Cdon* during limb development, I wanted to analyze triple HH-coreceptor mutants. To generate this mutant I utilized a novel *Cdon* conditional allele in combination with a *Prx1-Cre* driver in a *Gas1;Boc* null background (Logan et al., 2002). My data indicate that *Prx1-Cre;Gas1<sup>-/-</sup>;Cdon<sup>fl/fl</sup>;Boc<sup>-/-</sup>* mutants exhibit severe digit specification defects and patterning defects in the radius, ulna, tibia and fibula. These data indicate that *Cdon* does contribute to proper HH-dependent limb development. Overall the findings of my thesis research demonstrate that HH co-receptors are tissue-specific, multi-functional regulators of HH signaling during vertebrate embryogenesis.

## 4.2 Future directions

The data presented in Chapters Two and Three have generated a series of open questions about HH co-receptor function during vertebrate embryogenesis. In this section I highlight



several interesting questions based on my data and propose a series of experiments that will address these questions.

*What is the consequence of *Boc* deletion on HH signaling across different genetic backgrounds?*

My data demonstrate that on a C57BL/6J background E10.5 *Boc*<sup>-/-</sup> embryos display internasal distance widening and increased levels of HH signaling. However, in mouse models the severity of the craniofacial defects can be influenced by the genetic background (Hong and Krauss, 2018; Schachter and Krauss, 2008). To investigate whether these phenotypes persist on a different genetic background, I would examine *Boc*<sup>-/-</sup> embryos on a congenic 129S4/SVJaeJ background. On a 129 background the craniofacial defects are less sensitive to be altered by modifier genes (Hong and Krauss, 2018; Schachter and Krauss, 2008). I have been working to backcross mice carrying the *Boc* mutant allele from a C57BL/6J to a 129S4/SVJaeJ background. After ten generations of backcrossing, I now have *Boc* mutant animals maintained on a congenic 129 S4/SVJaeJ background. In the future, I would examine *Boc*<sup>-/-</sup> embryos to quantify the internasal distance, determine the levels of *Gli1* by qPCR and whole mount *in situ* hybridization, and the levels of GLI1 protein by western blot. With this experiment I would be able determine if the gain-of-function phenotype and antagonistic function of *Boc* is dependent on genetic background. If *Boc*<sup>-/-</sup> embryos do not display similar phenotypes on a 129S4/SVJaeJ background, this would suggest that the function of *Boc* is influenced by strain-specific silent modifier genes. If this is the case, I could use the *Boc* mouse models maintained on the separate 129S4/SVJaeJ and C57BL/6J backgrounds to identify the modifier genes that dictate its function. To analyze modifier genes, I could analyze the transcriptome of the heads of E9.5 and E10.5 *Boc*<sup>-/-</sup> embryos by RNA deep sequencing and subsequently performing gene expression analyses. This

experiment could also be performed with *Gas1* and *Cdon* mutants which display variable HPE phenotypes in 129S4/SVJaeJ and C57BL/6J backgrounds. This approach is currently being utilized to analyze the variable HPE phenotypes in *Lrp2* mutant mice in two different backgrounds, where 138 genes were differentially regulated when the C57BL/6N and FVB/N strains were compared (Mecklenburga, 2017). Understanding how genetic background influences the function of HH co-receptors such as *Boc* will be critical to understand the variability in the craniofacial defects in mice and human HPE patients.

*What are the effects of mesenchyme-specific deletion of Boc on craniofacial development?*

The increased levels of *Gli1* in the mesenchyme of the nasal processes and the increased proliferation in the cranial neural crest-derived mesenchyme of *Boc*<sup>-/-</sup> embryos suggests a tissue-specific antagonistic function for *Boc* during craniofacial development. To further investigate a potential antagonistic function for *Boc*, I propose to conditionally delete this gene specifically in the mesenchyme. To perform this experiment, I would utilize a *Boc* conditional allele (*Boc*<sup>tm1a(KOMP)Wtsi</sup>) that is available from the Knockout Mouse Project ([www.komp.org](http://www.komp.org)). This allele would be used in combination with either *Pdgfra-CreER* or *Wnt-1-Cre2* drivers to specifically delete *Boc* in the mesenchyme of the developing craniofacial structures and in neural crest cells respectively (Chung et al., 2018; Lewis et al., 2013). Using this approach, I expect to compare the effects of the ubiquitous deletion of *Boc* with mesenchyme- or neural crest cell-specific deletion. I could expect several different scenarios when comparing these animals: 1) mesenchymal deletion of *Boc* phenocopies the germline mutants, confirming that *Boc* acts as a tissue-specific HH pathway antagonist; 2) mesenchymal deletion of *Boc* results in a more severe phenotype, suggesting that upon *Boc* deletion, the HH signaling pathway compensates

this loss by increasing the levels of HH activity; 3) mesenchymal deletion of *Boc* results in a less severe phenotype, suggesting that the increase HH signaling in the craniofacial mesenchyme is an indirect or cell-non-autonomous result of *Boc* deletion in a different craniofacial tissue compartment like the surface ectoderm (which was not explored in Chapter 2). In this case, I could use the *Foxg1-Cre* which drives Cre-mediated recombination in the cranial epithelium and telencephalon (Hebert and McConnell, 2000). To extend these genetic experiments and investigate the mechanism of a putative antagonistic function for *Boc* in the mesenchyme, I could use FACS to isolate recombined mesenchymal cells (based on either PDGFR $\alpha$  expression or by *tdTomato* expression using a reporter allele) and perform bulk RNA-Seq. This would allow for the identification of target genes that are upregulated or downregulated after the mesenchymal or neural crest ablation of *Boc*, providing mechanistic insight into specific genes that might act downstream of BOC to antagonize HH signaling. Additionally, I could utilize the *Boc* conditional allele to delete *Boc* during different stages of craniofacial development, to more precisely assess when and where BOC is critical for HH-dependent craniofacial patterning. By performing this experiment, I could define if *Boc* functions as an antagonist throughout craniofacial development or just at specific stages. For example, I would be interested to investigate *Boc* function during both early craniofacial development around E7.5 when *Boc* expression initiates, and at later stages at E10.5 when the facial prominences begin to form the craniofacial structures.

*Is the antagonistic function of Boc partially masked by redundancy with other HH pathway antagonists?*

Multiple proteins at the cell surface have the ability to antagonize HH pathway activity including PTCH1, PTCH2, HHIP, LRP2, GPR161, and a subset of GPCs (Carpenter et al., 1998; Christ et al., 2015; Holtz et al., 2015; Holtz et al., 2013; Marigo et al., 1996; Mukhopadhyay et al., 2013; Nieuwenhuis et al., 2006; Williams et al., 2010). Previous studies have demonstrated that these proteins function redundantly and compensate for the absence of each other (Holtz et al., 2013; Jeong and McMahon, 2005). Even though *Boc*<sup>-/-</sup> embryos display widening of the internasal distance in the craniofacial structures, it is a subtle phenotype that was overlooked by previous studies. One possibility is that the antagonistic function of *Boc* is masked by the redundant activity of other HH pathway antagonists. To test this hypothesis, I propose to generate different compound mutants lacking HH pathway antagonists. Specifically, I plan to examine *Boc*<sup>-/-</sup>;*Hhip*<sup>-/-</sup>, *Boc*<sup>-/-</sup>;*Ptch2*<sup>-/-</sup> and *Boc*<sup>-/-</sup>;*Hhip*<sup>-/-</sup>;*Ptch2*<sup>-/-</sup> E10.5 embryos. In these mutants I would examine the gross morphology of the embryo and analyze patterning in the craniofacial structures, ventral neural tube and the limb bud by examining the expression of different HH pathway targets. If I do not observe any apparent phenotypes, I could also perform similar experiments by targeting *Ptch1*. Previous studies from our lab by (Holtz et al., 2013) to address possible redundancy between HH pathway antagonists, utilized an *MT-Ptch1* transgene which produces low levels of HH signaling that largely rescue the gain-of-function HH phenotypes observed in *Ptch1* mutants (Milenkovic et al., 1999). Taking advantage of this tool (Holtz et al., 2015) performed the double and the triple deletion of *Hhip*, *Ptch2*, *MT-Ptch1*;*Ptch*<sup>-/-</sup>, revealing a collective requirement for HH inhibition in the neural tube. Based on this study I could generate *Boc*<sup>-/-</sup>;*MT-Ptch1*;*Ptch*<sup>-/-</sup> animals and also integrate the deletion of *Hhip* and *Ptch2* to reveal if *Boc* function can be masked by the redundant function of these proteins.

*Are the structural requirements for the HH co-receptors similar in the spinal cord and in the forebrain?*

Previous studies from our lab have shown that CDON and BOC employ distinct structural domains to promote HH signaling in the developing spinal cord (Song et al., 2015). This study performed a gain-of-function approach by overexpressing different CDON and BOC constructs in the developing spinal cord by chicken *in ovo* electroporations. However, the artificial nature of overexpression studies could affect the interpretations of the results. To circumvent this issue, I propose to perform this type of experiment but in mutant mouse embryos lacking different HH co-receptors. To perform this experiment, I would take advantage of the whole mouse embryo roller bottle culture system (Sakai and Trainor, 2014), which would allow me to culture mouse embryos lacking *Gas1*, *Cdon* and *Boc* from E8.5-E11.0. The Allen lab has an entire series of GAS1, CDON and BOC constructs that lack specific domains of each protein. These constructs would be injected into the lumen of the spinal cord, and in the forebrain mesenchyme and subsequently electroporated. If the overexpression of the constructs is inefficient, alternatively we can deliver the constructs by viral infection. With this technique I would be able to define which domains are required for the promotion of HH signaling in the spinal cord and in the developing forebrain in the same embryos. Analysis of HH pathway targets in both tissues can be examined by immunofluorescence or RNAscope. Specifically, I would like to test the requirements for membrane attachment, the cytoplasmic domain, and extracellular interactions with PTCH1 in these two tissues. Additionally, this system could be also used to overexpress constructs with mutations identified in human birth defects associated SHH, like HPE, where mutations have been identified in *Gas1*, *Cdon* and *Boc* (Bae et al., 2011; Hong et al., 2017; Ribeiro et al., 2010).

*Does the cytoplasmic domain of Boc contribute to its tissue-specific functions?*

CDON and BOC are two very similar proteins from the Ig superfamily (Kang et al., 2002). These co-receptors share significant amino acid identity and structural motifs in their extracellular domains (Kang et al., 2002). Interestingly, their cytoplasmic domains are unique and do not share any homology with each other or with any other proteins (Kang et al., 2002). Recently, studies have identified proteins that bind to the BOC cytoplasmic domain: the non-receptor tyrosine kinase ABL and the adaptor protein ELMO1 (Makihara et al., 2018; Vuong et al., 2017). These data suggest that the cytoplasmic domain could be essential to mediate tissue-specific HH-dependent functions, or HH-independent functions that could lead to the activation of distinct intracellular signaling cascades. To test a potential role for the BOC cytoplasmic domain, I propose to generate a *Boc* mouse mutant lacking this region. This mouse model could be generated by taking advantage of CRISPR/CAS9 technology (Hsu et al., 2014). This region is comprised by 238 amino acids, and previous studies have shown that it is dispensable for HH signal transduction in the neural tube and during myogenic differentiation (Kang et al., 2002; Song et al., 2015). Next, I could define the effects of the deletion by examination of defects in multiple HH-responsive tissues such as craniofacial structures, the spinal cord and the limb bud. In addition, I could also exchange the cytoplasmic domain of BOC with that of CDON. Distinct from BOC, the cytoplasmic domain of CDON is required for myogenic differentiation and dispensable for HH signal transduction in the neural tube (Kang et al., 2002; Song et al., 2015). The generation of these mouse models would allow for the assessment of the contribution of the BOC cytoplasmic domain in HH signal transduction in vivo. Lastly, we could knock in *Cdon* into the *Boc* locus, and *Boc* into the *Cdon* locus to investigate whether the differential

contributions of these genes are due to differences in protein function or due to differences in expression.

### *How does BOC interact with HH ligands?*

Previous studies have demonstrated that the HH ligand binds to the third FNIII domain of BOC (McLellan et al., 2008; Tenzen et al., 2006). The current paradigm is that SHH ligand also binds to PTCH1 through a different interface, forming an active complex of BOC-SHH-PTCH1 (Qi et al., 2018a; Qi et al., 2018b). However, its unknown if this co-receptor-ligand-receptor complex exists *in vivo*, and if so, where it is localized within a cell, and whether this localization may vary from one tissue to the next. Recent studies of commissural axon guidance *in vivo* suggest that SHH induces BOC internalization into early endosomes through an endocytic adaptor NUMB (Ferent et al., 2019). This internalization event is required for proper SHH-mediated axon guidance (Ferent et al., 2019). Another example of a receptor that regulates endocytosis and cellular trafficking of the SHH-PTCH1 receptor complex is LRP2, which controls SHH ligand concentration (Christ et al., 2012). I propose that understanding the localization of SHH-BOC complexes *in vivo* can help to elucidate the mechanism by which BOC regulates HH signaling.

To address this question, I propose two different approaches. First, I could perform proximity ligation assays to detect *in situ* physical interactions between SHH and BOC in tissue sections that express SHH (Fredriksson et al., 2002). I would be particularly interested, but not limited, to examine these interactions in tissue sections of craniofacial structures, where SHH is expressed in the ventral forebrain and in the medial nasal process. A second approach to visualize the interactions *in vivo* would be to generate alleles of *Shh* and *Boc* that contain split

GFP domains. Specifically, this technique is called bimolecular fluorescence complementation (BiFC) (Foglieni et al., 2017). This technique requires the splitting of a GFP protein into two different fragments of different sizes (Foglieni et al., 2017). The first fragment is comprised of 216 amino acids and has the first ten  $\beta$  strands of GFP (GFP<sub>1-10</sub>), while the second fragment contains 16 amino acids and has the eleventh  $\beta$  strand of GFP (GFP<sub>S11</sub>), which is a very small protein tag (Foglieni et al., 2017). Ideally, I would utilize CRISPR/CAS9 technology to perform a targeted insertion of the GFP fragments in the *Boc* and *Shh* loci (Hsu et al., 2014). The GFP<sub>1-10</sub> fragment will be inserted after the signal peptide of the *Boc* locus and the GFP<sub>S11</sub> fragment in the *Shh* locus before the cholesterol attachment site (a new intein cleave-cholesterol site will have to be engineered to ensure proper ligand processing). Following the successful generation of these alleles and subsequent mouse breeding to generate *Boc:GFP<sub>1-10</sub>; Shh;GFP<sub>S11</sub>* animals, I would be able to use GFP expression to visualize sites of interaction between SHH and BOC. Importantly, a related approach has been previously used by (Chamberlain et al., 2008), in which they generated mice that produce SHH ligand fused to a GFP protein instead of wildtype SHH. This study demonstrated that this modified version of SHH undergoes regular processing but is less efficient, and heterozygous mice were normal while homozygous mice displayed reduced levels of SHH and were stillborn (Chamberlain et al., 2008). Notably, for these proposed experiments, I would not need to generate homozygous animals; *Boc:GFP<sub>1-10</sub>; Shh;GFP<sub>S11</sub>* compound animals should suffice to visualize GFP. Further, it is possible that the use of a smaller GFP fusion (16 amino acids instead of 238) will allow for normal SHH function such that homozygous animals will be viable. Even with these caveats, these will be useful tools to directly observe and localize the interaction of SHH and BOC during embryogenesis. Specifically, I will be able to visualize the *in vivo* interactions of SHH and BOC in multiple tissues and define the subcellular



localization of these interaction as well as temporal changes in these interactions. If successful, this approach could be extended to investigate SHH interactions with other HH co-receptors (i.e., GAS1 and CDON) as well as with the canonical receptor, PTCH1. Finally, I could perform analogous experiments to generate split GFP alleles of *Ihh* and *Dhh* to examine potential differences in the localization and dynamics of ligand-receptor interactions between different HH ligand and HH receptor pairs.

*Could Gas1, Cdon and Boc differentially regulate gene expression during craniofacial development?*

The deletion of the HH co-receptors results in variable craniofacial defects. Specifically, *Gas1* and *Cdon* mutants display highly variable HPE defects, while *Boc* mutants display facial widening at E10.5. Interestingly, the severity of the HPE defects and the facial widening in these mutants, correlate with the downregulation and upregulation of *Gli1* respectively. These data suggest that the HH co-receptors differentially regulate *Gli1* expression during craniofacial development. Also, it raises the possibility that the HH co-receptors could differentially regulate the expression of other genes during craniofacial development. To address this question, I propose to assess the changes in gene expression in E10.5 heads of *Gas1*<sup>-/-</sup>, *Cdon*<sup>-/-</sup> and *Boc*<sup>-/-</sup> embryos by single cell RNA-seq (Kolodziejczyk et al., 2015). This method would allow me to examine changes in gene expression at a single cell resolution and throughout the different populations that comprise the craniofacial tissues in the same embryo. Specifically, I would like to examine, 1) overall changes in gene expression and 2) changes in specific tissue compartments (mesenchyme, surface ectoderm and forebrain neuroepithelium) and 3) changes in the distinct facial prominences. Particularly, I would like to examine the expression levels of

the *Fox* genes, which are HH transcriptional targets in the craniofacial structures (Jeong et al., 2004). Additionally, I would like to determine if there are any gene expression differences that correlate with the variable severity in the phenotypes of *Gas1* and *Cdon* mutants and the widening of *Boc* mutant embryos. Finally, I will be able to determine if there are any stochastic changes in expression that correlate with the variable phenotypes in the craniofacial structures.


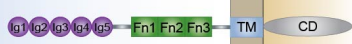
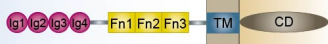
*What roles do HH co-receptors play in postnatal development, adult tissue homeostasis, and tissue regeneration?*

To date the available knockout alleles for *Gas1*, *Cdon* and *Boc* have provided numerous insights about their role in HH signal transduction (Allen et al., 2011; Allen et al., 2007; Cole and Krauss, 2003; Martinelli and Fan, 2007; Seppala et al., 2007; Seppala et al., 2014; Tenzen et al., 2006; Zhang et al., 2011; Zhang et al., 2006). However, the redundancy of these cell surface regulators of HH signaling requires the generation of triple mutant embryos to reveal their full contribution (Allen et al., 2011). Unfortunately, these embryos die around E9.5, which precludes a complete analysis of co-receptor function during later developmental stages, not to mention during postnatal development and in adult tissue function. Therefore, new tools are required to understand HH co-receptor function in different tissues at later developmental stages. One solution is to generate triple HH co-receptor conditional mice to define their contribution to postnatal development, adult tissue homeostasis and tissue regeneration. Conditional alleles for *Gas1*, and *Cdon* are already available, and in a previous section I described the existence of a conditional *Boc* allele that is available through the Knockout Mouse Project (Bae et al., 2020; Jin et al., 2015). Having these alleles available will provide a great opportunity to explore the individual and collective roles for the HH co-receptors in different tissues. To explore the

function of the HH co-receptors in multiple adult tissues, I would perform the triple conditional ablation of the HH co-receptors using the ubiquitous Cre, *ROSA26-CreER<sup>fl2</sup>* (Ventura et al., 2007). With this approach I will be able to examine all adult tissues and screen for potential phenotypes. Notably, HH signaling plays key roles in several tissues such as the skin and the lingual epithelium in which I could explore HH co-receptor function (Abe and Tanaka, 2017; Mistretta and Kumari, 2019).

Taken together, the data presented in this dissertation demonstrates that the HH co-receptors are tissue-specific regulators of HH signaling during vertebrate embryogenesis. Specifically, I provide evidence that shows that BOC antagonizes HH signaling in the craniofacial structures. Also, I uncovered a role for CDON in digit specification and limb patterning. These results provide novel insights about the mechanisms by which the HH co-receptors regulate HH signal transduction during vertebrate embryogenesis. The future directions proposed in this section provides a strong foundation for further experiments that will elucidate the role of the HH co-receptors in HH pathway function during development, adult tissue homeostasis and disease. Expanding the genetic tools available to study the HH co-receptors will be essential to broaden our understanding about their mechanistic function in different tissues. Furthermore, the careful and detailed simultaneous examination of single and compound HH co-receptor mutants will provide insights into their collective and distinct functions in HH signal transduction during development, postnatal development and adulthood.

### 4.3 Figures

Tissue Specific Roles of the HH Co-Receptors		
HH Co-Receptors	Positive regulation	Negative regulation
<p><b>GAS1</b></p>  <p>extracellular</p> <p>intracellular</p>	<p><b>Ventral neural patterning</b>-(Martinelli et al., 2007; Allen et al., 2007; Allen et al., 2011)</p> <p><b>Digit specification</b>- (Martinelli et al., 2007; Allen et al., 2011)</p> <p><b>Craniofacial development</b>- (Seppala et al., 2007; Allen et al., 2007; Seppala et al., 2014, Echevarria-Andino, <i>in review</i>)</p> <p><b>Cerebellar development</b>-(Izzi et al., 2011)</p>	<p><b>Tooth bud</b>-(Cobourne et al., 2004; Ohazama et al., 2009)</p> <p><b>Somite</b>-(Lee et al., 2001)</p>
<p><b>CDON</b></p>  <p>extracellular</p> <p>intracellular</p>	<p><b>Ventral neural patterning</b>-(Tenzen et al., 2006; Allen et al., 2007; Allen et al., 2011; Song et al., 2015)</p> <p><b>Digit specification</b>-(Echevarria-Andino, <i>in prep</i>)</p> <p><b>Craniofacial development</b>-(Cole et al., 2003; Zhang., et al 2006; Zhang et al., 2011)</p>	<p><b>Eye development</b>-(Cardozo et al.,2014)</p>
<p><b>BOC</b></p>  <p>extracellular</p> <p>intracellular</p>	<p><b>Ventral neural patterning</b>-(Tenzen et al., 2006; Allen et al., 2011; Song et al., 2015)</p> <p><b>Digit Specification</b>-(Allen et al., 2011)</p> <p><b>Cerebellar development</b>-(Izzi et al., 2011)</p> <p><b>Axon guidance</b>-(Okada et al., 2006)</p>	<p><b>Zebrafish lower jaw</b>-(Bergeron et al., 2011)</p> <p><b>Craniofacial Mesenchyme</b>-(Echevarria-Andino, <i>in review</i>)</p>

**Figure 4.1 Summary of the tissue-specific roles of the HH co-receptors**

(Left panel) Schematic of the HH co-receptor structure. (Middle panel) Tissues in which the HH co-receptors positively regulate HH signaling. (Right panel) Tissues in which the HH co-receptors negatively regulate HH signaling.

#### 4.4 References

**Abe, Y. and Tanaka, N.** (2017). Roles of the Hedgehog Signaling Pathway in Epidermal and Hair Follicle Development, Homeostasis, and Cancer. *J Dev Biol* **5**.

**Allen, B. L., Song, J. Y., Izzi, L., Althaus, I. W., Kang, J. S., Charron, F., Krauss, R. S. and McMahon, A. P.** (2011). Overlapping roles and collective requirement for the coreceptors GAS1, CDO, and BOC in SHH pathway function. *Dev Cell* **20**, 775-787.

**Allen, B. L., Tenzen, T. and McMahon, A. P.** (2007). The Hedgehog-binding proteins Gas1 and Cdo cooperate to positively regulate Shh signaling during mouse development. *Genes Dev* **21**, 1244-1257.

**Bae, G. U., Domene, S., Roessler, E., Schachter, K., Kang, J. S., Muenke, M. and Krauss, R. S.** (2011). Mutations in CDON, encoding a hedgehog receptor, result in holoprosencephaly and defective interactions with other hedgehog receptors. *Am J Hum Genet* **89**, 231-240.

**Bae, J. H., Hong, M., Jeong, H. J., Kim, H., Lee, S. J., Ryu, D., Bae, G. U., Cho, S. C., Lee, Y. S., Krauss, R. S., et al.** (2020). Satellite cell-specific ablation of Cdon impairs integrin activation, FGF signalling, and muscle regeneration. *J Cachexia Sarcopenia Muscle*.

**Bergeron, S. A., Tyurina, O. V., Miller, E., Bagas, A. and Karlstrom, R. O.** (2011). Brother of cdo (umleitung) is cell-autonomously required for Hedgehog-mediated ventral CNS patterning in the zebrafish. *Development* **138**, 75-85.

**Cardozo, M. J., Sanchez-Arrones, L., Sandonis, A., Sanchez-Camacho, C., Gestri, G., Wilson, S. W., Guerrero, I. and Bovolenta, P.** (2014). Cdon acts as a Hedgehog decoy receptor during proximal-distal patterning of the optic vesicle. *Nat Commun* **5**, 4272.

**Carpenter, D., Stone, D. M., Brush, J., Ryan, A., Armanini, M., Frantz, G., Rosenthal, A. and de Sauvage, F. J.** (1998). Characterization of two patched receptors for the vertebrate hedgehog protein family. *Proc Natl Acad Sci U S A* **95**, 13630-13634.

**Chamberlain, C. E., Jeong, J., Guo, C., Allen, B. L. and McMahon, A. P.** (2008). Notochord-derived Shh concentrates in close association with the apically positioned basal body in neural target cells and forms a dynamic gradient during neural patterning. *Development* **135**, 1097-1106.

**Christ, A., Christa, A., Klippert, J., Eule, J. C., Bachmann, S., Wallace, V. A., Hammes, A. and Willnow, T. E.** (2015). LRP2 Acts as SHH Clearance Receptor to Protect the Retinal Margin from Mitogenic Stimuli. *Dev Cell* **35**, 36-48.

**Christ, A., Christa, A., Kur, E., Lioubinski, O., Bachmann, S., Willnow, T. E. and Hammes, A.** (2012). LRP2 is an auxiliary SHH receptor required to condition the forebrain ventral midline for inductive signals. *Dev Cell* **22**, 268-278.

**Chung, M. I., Bujnis, M., Barkauskas, C. E., Kobayashi, Y. and Hogan, B. L. M.** (2018). Niche-mediated BMP/SMAD signaling regulates lung alveolar stem cell proliferation and differentiation. *Development* **145**.

**Cobourne, M. T., Miletich, I. and Sharpe, P. T.** (2004). Restriction of sonic hedgehog signalling during early tooth development. *Development* **131**, 2875-2885.

**Cole, F. and Krauss, R. S.** (2003). Microform holoprosencephaly in mice that lack the Ig superfamily member Cdon. *Curr Biol* **13**, 411-415.

**Ferent, J., Giguere, F., Jolicoeur, C., Morin, S., Michaud, J. F., Makihara, S., Yam, P. T., Cayouette, M. and Charron, F.** (2019). Boc Acts via Numb as a Shh-Dependent Endocytic Platform for Ptch1 Internalization and Shh-Mediated Axon Guidance. *Neuron* **102**, 1157-1171 e1155.

**Foglieni, C., Papin, S., Salvade, A., Afroz, T., Pinton, S., Pedrioli, G., Ulrich, G., Polymenidou, M. and Paganetti, P.** (2017). Split GFP technologies to structurally characterize and quantify functional biomolecular interactions of FTD-related proteins. *Sci Rep* **7**, 14013.

**Fredriksson, S., Gullberg, M., Jarvius, J., Olsson, C., Pietras, K., Gustafsdottir, S. M., Ostman, A. and Landegren, U.** (2002). Protein detection using proximity-dependent DNA ligation assays. *Nat Biotechnol* **20**, 473-477.

**Hebert, J. M. and McConnell, S. K.** (2000). Targeting of cre to the Foxg1 (BF-1) locus mediates loxP recombination in the telencephalon and other developing head structures. *Dev Biol* **222**, 296-306.

**Holtz, A. M., Griffiths, S. C., Davis, S. J., Bishop, B., Siebold, C. and Allen, B. L.** (2015). Secreted HHIP1 interacts with heparan sulfate and regulates Hedgehog ligand localization and function. *J Cell Biol* **209**, 739-757.

**Holtz, A. M., Peterson, K. A., Nishi, Y., Morin, S., Song, J. Y., Charron, F., McMahon, A. P. and Allen, B. L.** (2013). Essential role for ligand-dependent feedback antagonism of vertebrate hedgehog signaling by PTCH1, PTCH2 and HHIP1 during neural patterning. *Development* **140**, 3423-3434.

**Hong, M. and Krauss, R. S.** (2018). Modeling the complex etiology of holoprosencephaly in mice. *Am J Med Genet C Semin Med Genet* **178**, 140-150.

**Hong, M., Srivastava, K., Kim, S., Allen, B. L., Leahy, D. J., Hu, P., Roessler, E., Krauss, R. S. and Muenke, M.** (2017). BOC is a modifier gene in holoprosencephaly. *Hum Mutat* **38**, 1464-1470.

**Hsu, P. D., Lander, E. S. and Zhang, F.** (2014). Development and applications of CRISPR-Cas9 for genome engineering. *Cell* **157**, 1262-1278.

**Izzi, L., Levesque, M., Morin, S., Laniel, D., Wilkes, B. C., Mille, F., Krauss, R. S., McMahon, A. P., Allen, B. L. and Charron, F.** (2011). Boc and Gas1 each form distinct Shh

receptor complexes with Ptch1 and are required for Shh-mediated cell proliferation. *Dev Cell* **20**, 788-801.

**Jeong, J., Mao, J., Tenzen, T., Kottmann, A. H. and McMahon, A. P.** (2004). Hedgehog signaling in the neural crest cells regulates the patterning and growth of facial primordia. *Genes Dev* **18**, 937-951.

**Jeong, J. and McMahon, A. P.** (2005). Growth and pattern of the mammalian neural tube are governed by partially overlapping feedback activities of the hedgehog antagonists patched 1 and Hhip1. *Development* **132**, 143-154.

**Jin, S., Martinelli, D. C., Zheng, X., Tessier-Lavigne, M. and Fan, C. M.** (2015). Gas1 is a receptor for sonic hedgehog to repel enteric axons. *Proc Natl Acad Sci U S A* **112**, E73-80.

**Kang, J. S., Mulieri, P. J., Hu, Y., Taliana, L. and Krauss, R. S.** (2002). BOC, an Ig superfamily member, associates with CDO to positively regulate myogenic differentiation. *EMBO J* **21**, 114-124.

**Kolodziejczyk, A. A., Kim, J. K., Svensson, V., Marioni, J. C. and Teichmann, S. A.** (2015). The technology and biology of single-cell RNA sequencing. *Mol Cell* **58**, 610-620.

**Lee, C. S., Buttitta, L. and Fan, C. M.** (2001). Evidence that the WNT-inducible growth arrest-specific gene 1 encodes an antagonist of sonic hedgehog signaling in the somite. *Proc Natl Acad Sci U S A* **98**, 11347-11352.

**Lee, C. S. and Fan, C. M.** (2001). Embryonic expression patterns of the mouse and chick Gas1 genes. *Mech Dev* **101**, 293-297.

**Lewis, A. E., Vasudevan, H. N., O'Neill, A. K., Soriano, P. and Bush, J. O.** (2013). The widely used Wnt1-Cre transgene causes developmental phenotypes by ectopic activation of Wnt signaling. *Dev Biol* **379**, 229-234.

**Logan, M., Martin, J. F., Nagy, A., Lobe, C., Olson, E. N. and Tabin, C. J.** (2002). Expression of Cre Recombinase in the developing mouse limb bud driven by a Prxl enhancer. *Genesis* **33**, 77-80.

**Makihara, S., Morin, S., Ferent, J., Cote, J. F., Yam, P. T. and Charron, F.** (2018). Polarized Dock Activity Drives Shh-Mediated Axon Guidance. *Dev Cell* **46**, 410-425 e417.

**Marigo, V., Davey, R. A., Zuo, Y., Cunningham, J. M. and Tabin, C. J.** (1996). Biochemical evidence that patched is the Hedgehog receptor. *Nature* **384**, 176-179.

**Martinelli, D. C. and Fan, C. M.** (2007). Gas1 extends the range of Hedgehog action by facilitating its signaling. *Genes Dev* **21**, 1231-1243.

**McLellan, J. S., Zheng, X., Hauk, G., Ghirlando, R., Beachy, P. A. and Leahy, D. J.** (2008). The mode of Hedgehog binding to Ihog homologues is not conserved across different phyla. *Nature* **455**, 979-983.

**Mecklenburga, N.** (2017). Holoprosencephaly phenotypes in LRP2 deficient mouse models are strongly modified by genetic background. In *18th International Congress of Developmental Biology* University Cultural Centre, National University of Singapore.

**Milenkovic, L., Goodrich, L. V., Higgins, K. M. and Scott, M. P.** (1999). Mouse patched1 controls body size determination and limb patterning. *Development* **126**, 4431-4440.

**Mistretta, C. M. and Kumari, A.** (2019). Hedgehog Signaling Regulates Taste Organs and Oral Sensation: Distinctive Roles in the Epithelium, Stroma, and Innervation. *Int J Mol Sci* **20**.

**Mukhopadhyay, S., Wen, X., Ratti, N., Loktev, A., Rangell, L., Scales, S. J. and Jackson, P. K.** (2013). The ciliary G-protein-coupled receptor Gpr161 negatively regulates the Sonic hedgehog pathway via cAMP signaling. *Cell* **152**, 210-223.

**Mulieri, P. J., Kang, J. S., Sassoon, D. A. and Krauss, R. S.** (2002). Expression of the boc gene during murine embryogenesis. *Dev Dyn* **223**, 379-388.

**Mulieri, P. J., Okada, A., Sassoon, D. A., McConnell, S. K. and Krauss, R. S.** (2000). Developmental expression pattern of the cdo gene. *Dev Dyn* **219**, 40-49.

**Nieuwenhuis, E., Motoyama, J., Barnfield, P. C., Yoshikawa, Y., Zhang, X., Mo, R., Crackower, M. A. and Hui, C. C.** (2006). Mice with a targeted mutation of patched2 are viable but develop alopecia and epidermal hyperplasia. *Mol Cell Biol* **26**, 6609-6622.

**Ohazama, A., Haycraft, C. J., Seppala, M., Blackburn, J., Ghafoor, S., Cobourne, M., Martinelli, D. C., Fan, C. M., Peterkova, R., Lesot, H., et al.** (2009). Primary cilia regulate Shh activity in the control of molar tooth number. *Development* **136**, 897-903.

**Qi, X., Schmiede, P., Coutavas, E. and Li, X.** (2018a). Two Patched molecules engage distinct sites on Hedgehog yielding a signaling-competent complex. *Science* **362**.

**Qi, X., Schmiede, P., Coutavas, E., Wang, J. and Li, X.** (2018b). Structures of human Patched and its complex with native palmitoylated sonic hedgehog. *Nature* **560**, 128-132.

**Ribeiro, L. A., Queizi, R. G., Nascimento, A., Bertolacini, C. P. and Richieri-Costa, A.** (2010). Holoprosencephaly and holoprosencephaly-like phenotype and GAS1 DNA sequence changes: Report of four Brazilian patients. *Am J Med Genet A* **152A**, 1688-1694.

**Sakai, D. and Trainor, P. A.** (2014). Gene transfer techniques in whole embryo cultured post-implantation mouse embryos. *Methods Mol Biol* **1092**, 227-234.

**Schachter, K. A. and Krauss, R. S.** (2008). Murine models of holoprosencephaly. In *Curr Top Dev Biol*, pp. 139-170.

**Seppala, M., Depew, M. J., Martinelli, D. C., Fan, C. M., Sharpe, P. T. and Cobourne, M. T.** (2007). Gas1 is a modifier for holoprosencephaly and genetically interacts with sonic hedgehog. *J Clin Invest* **117**, 1575-1584.



**Seppala, M., Xavier, G. M., Fan, C. M. and Cobourne, M. T.** (2014). Boc modifies the spectrum of holoprosencephaly in the absence of Gas1 function. *Biol Open* **3**, 728-740.

**Song, J. Y., Holtz, A. M., Pinskey, J. M. and Allen, B. L.** (2015). Distinct structural requirements for CDON and BOC in the promotion of Hedgehog signaling. *Dev Biol* **402**, 239-252.

**Tenzen, T., Allen, B. L., Cole, F., Kang, J. S., Krauss, R. S. and McMahon, A. P.** (2006). The cell surface membrane proteins Cdo and Boc are components and targets of the Hedgehog signaling pathway and feedback network in mice. *Dev Cell* **10**, 647-656.

**Ventura, A., Kirsch, D. G., McLaughlin, M. E., Tuveson, D. A., Grimm, J., Lintault, L., Newman, J., Reczek, E. E., Weissleder, R. and Jacks, T.** (2007). Restoration of p53 function leads to tumour regression in vivo. *Nature* **445**, 661-665.

**Vuong, T. A., Leem, Y. E., Kim, B. G., Cho, H., Lee, S. J., Bae, G. U. and Kang, J. S.** (2017). A Sonic hedgehog coreceptor, BOC regulates neuronal differentiation and neurite outgrowth via interaction with ABL and JNK activation. *Cell Signal* **30**, 30-40.

**Williams, E. H., Pappano, W. N., Saunders, A. M., Kim, M. S., Leahy, D. J. and Beachy, P. A.** (2010). Dally-like core protein and its mammalian homologues mediate stimulatory and inhibitory effects on Hedgehog signal response. *Proc Natl Acad Sci U S A* **107**, 5869-5874.

**Zhang, W., Hong, M., Bae, G. U., Kang, J. S. and Krauss, R. S.** (2011). Boc modifies the holoprosencephaly spectrum of Cdo mutant mice. *Dis Model Mech* **4**, 368-380.

**Zhang, W., Kang, J. S., Cole, F., Yi, M. J. and Krauss, R. S.** (2006). Cdo functions at multiple points in the Sonic Hedgehog pathway, and Cdo-deficient mice accurately model human holoprosencephaly. *Dev Cell* **10**, 657-665.